Influence of dam operation on water resources management under different scenarios in the Zambezi River Basin considering environmental objectives and hydropower

PAR

Théodora COHEN LIECHTI

EPFL

ÉCOLE POLYTECHNIQUE
FÉDÉRALE DE LAUSANNE

Suisse
2013

Influence of dam operation on water resources management under different scenarios in the Zambezi River Basin considering environmental objectives and hydropower

Abstract

Worldwide, almost 50,000 dams over 15 m height have been built during the last six decades with an aggregated storage capacity of 6,000 km^3. The fact that large dams, by increasing irrigation and hydroelectricity production, can sustain development and reduce poverty has led developing countries to undertake major investment in dam construction. However, scientific progress is required in order to design and manage the future complex hydrologic/hydraulic systems in sustainable ways.

The African Dams project (ADAPT) aimed at enhancing the scientific basis of integrated water resource management. New models for the real-time control and multi-objective optimization of large hydraulic structures were created and data resources enhanced through field survey. The case study considered to apply this new knowledge is the Zambezi River basin located in southern Africa. It contains many of southern Africa's largest and most intact freshwater and estuarine wetlands, e. g. the Kafue flats, the Mana Pools and the Zambezi delta as well as several free-flowing yet unprotected river reaches. Three of Africa's largest dams (Kariba, Cahora Bassa and Kafue) inundate hundreds of square kilometers of river habitat and modify the natural flow patterns that sustain floodplains. Increasing human activity by cities and industry is causing a regional energy shortage, leading governments and investors to plan yet more dams in the basin.

In the framework of the ADAPT project, the major contribution of the present research is to set-up a hydrologic-hydraulic model of the whole catchment area which includes all relevant elements as hydraulic structures and schemes as well as floodplains. The multi-objective modelling and simulation define how dam operation can be adapted to get the highest environmental results under highest energy production. Three main steps structure the project: (1) the evaluation of the quality of available input data, (2) the definition of the specific hydrological processes needed for hydraulic-hydrological modeling of the Zambezi Basin along with the establishment of a calibration outline, (3) the assessment of the impacts of the planned new hydraulic structures and the refurbishment of the existing hydropower plants on the flow regime at critical points of the basin.

At first, three operational and acknowledged satellite derived precipitation products (the Tropical Rainfall Measuring Mission product 3B42 -TRMM 3B42-, the Famine Early Warning System product 2.0 -FEWS RFE2.0- and the National Oceanic and Atmospheric Administration/Climate Prediction Centre (NOAA/CPC) morphing technique -CMORPH-) are analyzed in terms of spatial and temporal distribution of the precipitation. They are compared to ground data at daily, 10-daily and monthly time steps. Based on the results, TRMM 3B42 was chosen as input data for the hydrological modeling.

Secondly, the Soil and Water Assessment Tool (SWAT 2009), a semi-distributed physically based continuous time model, was selected to simulate the hydrology of the basin. Due to the specificities of the Zambezi River basin, two main additional functions were developed. (1) A floodplain sub-model based on a reservoir approach was implemented. The model separates the outflow of the reservoir simulating the floodplain into main channel flow and flow over the floodplain area. (2) The hydropower plant operations are simulated based on the rule curve and the technical characteristics of the dams. The pertinence of the implemented approach was verified by modeling the existing hydropower plants. Given the complexity and the size of the basin, an automated calibration procedure based on A Multi-ALgorithm Genetically Adaptive Multi-objective method (AMALGAM) was applied to optimize the relative error and the volume ratio at multiple discharge stations. The observed volume at the artificial reservoir derived from the measured water level was included in the calibration.

Thirdly, scenarios combining different levels of environmental requirements as well as multiple hydropower development schemes were simulated at a daily time step with the hydraulic-hydrological model. The hydropower operation rules are simulated in detail. The mean annual energy produced, the firm power and the spilled volume during flood season are computed for each scenario. The impact on flow regime is characterized by Pardé coefficients, a set of indicators based on the Range of Variability Approach (RVA) and duration curves. In a global perspective, the analysis shows that it is possible to reach a compromise between energy production and environmental sustainability.

Finally, the data of two Global Circulation Models (GFDL-CM2.0 and CCCma-CGCM3) for the emission scenario SRES A2 of the IPCC report were used to simulate the hydrological input during 2045-2065 and 2080-2100 periods. The prediction of the climate models diverge in terms of precipitation as GFDL-CM2.0 forecasts an increase while CCCma-CGCM3 a diminution but agree on the increase of temperature. The impacts of climate change were assessed both on energy production and flow pattern changes.

The development and application of a hydraulic-hydrological model to a large river basin in a context of data scarcity and particular hydrologic units is particularly important for water resource management. The use of open source data and adapted calibration tools allows operators, authorities and researchers to assess together the impacts of hydropower development.

Keywords: satellite derived precipitation, hydrological modeling, floodplain, water resources management, hydropower plant operations, development scenarios, climate change.

Influence de l'exploitation des barrages sur la gestion des ressources en eaux dans le bassin versant du Zambèze par différents scénarios considérant des objectifs environnementaux et la production d'électricité

Résumé

Dans le monde, près de 50,000 barrages de plus de 15 m de hauteur ont été construits au cours des six dernières décennies, avec une capacité de stockage cumulée de 6,000 km^3. Le fait que les grands barrages puissent participer au développement et réduire la pauvreté en produisant de l'électricité et en facilitant l'irrigation, a conduit les pays en développement à entreprendre d'importants investissements dans ce domaine. Cependant, il est nécessaire d'intégrer le progrès scientifique dans la conception et la gestion durable de ces futurs systèmes hydrologiques / hydrauliques complexes.

Le projet Barrages Africains (ADAPT) vise à renforcer les connaissances scientifiques en gestion intégrée des eaux. De nouveaux modèles ont été créés pour le contrôle en temps réel et l'optimisation à objectifs multiples des grands ouvrages hydrauliques. En outre, les bases de données ont été améliorées grâce à des campagnes de terrain. Le bassin du Zambèze, situé en Afrique australe, a été choisi comme étude de cas pour appliquer ces nouvelles idées. Il contient certaines des zones humides les plus grandes encore intactes d'Afrique australe (les Kafue flats, les Mana Pools et le delta du Zambèze) ainsi que plusieurs cours d'eau entièrement naturels. Trois des plus grands barrages d'Afrique (Kariba, Cahora Bassa et Kafue) inondent des centaines de kilomètres carrés de zones riveraines et modifient le régime hydrologique naturel essentiel aux zones humides. L'augmentation de l'activité humaine dans les villes et l'industrie est à l'origine d'une pénurie énergétique régionale, forçant les gouvernements et les investisseurs à planifier de nouveaux barrages.

Dans le cadre du projet ADAPT, la contribution majeure de cette étude est de mettre en place un modèle hydrologique-hydraulique de l'ensemble du bassin hydrographique comprenant les éléments particuliers tels que les barrages et les plaines inondables. La modélisation et la simulation à objectifs multiples définissent la façon dont l'exploitation des barrages peut être adaptée pour diminuer l'impact sur l'environnement tout en produisant le plus d'énergie possible. Trois étapes principales structurent le projet: (1) l'évaluation de la qualité des données d'entrée disponibles, (2) la définition des processus hydrologiques spécifiques nécessaires pour la modélisation hydraulique-hydrologique du bassin du Zambèze avec la mise en place d'une méthode de calage, (3) l'estimation de l'impact des nouvelles structures hydrauliques prévues ainsi que de l'augmentation de la puissance des centrales hydroélectriques existantes sur le régime d'écoulement aux points critiques du bassin.

Dans un premier temps, trois estimations des précipitations basées sur les observations de satellites opérationnels ont été analysées en termes de répartition spatiale et temporelle des précipitations (le *Tropical Rainfall Measuring Mission product 3B42* -TRMM 3B42-, le *Famine Early Warning System product* 2.0 -FEWS RFE2.0- et le *National Oceanic and Atmospheric Administration/Climate Prediction Centre (NOAA/CPC) morphing technique* -

CMORPH-). Ces estimations ont été comparées aux données de terrain pour des pas de temps quotidiens, de 10 jours et mensuels. Basé sur les résultats, TRMM 2B42 a été choisi comme donnée d'entrée pour la modélisation hydrologique.

Deuxièmement, le logiciel *Soil and Water Assessemnt Tool* (SWAT 2009), un modèle semi-distribué basé sur les processus physiques, a été sélectionné pour simuler l'hydrologie du bassin. En raison des spécificités du Zambèze, deux sous-modèles ont été développés: (1) un modèle de réservoir pour les zones inondables séparant le débit sortant en un débit de base et un débit de débordement, (2) un modèle calculant la production hydroélectrique basé sur les caractéristiques techniques et les règles d'exploitation des barrages. La pertinence de la démarche a été vérifiée par la modélisation des centrales hydroélectriques existantes. Compte tenu de la complexité et de la taille du bassin, une procédure de calage automatique a été appliquée basée sur un algorithme génétique adaptatif à objectifs multiples (AMALGAM). L'erreur relative et le rapport de volume ont été optimisés à plusieurs stations de débit et les variations de volume observées dans les réservoirs artificiels ont été incluses dans la procédure.

Troisièmement, des scénarios combinant différents niveaux d'exigences environnementales ainsi que plusieurs schémas de développement hydroélectriques ont été simulés à un pas de temps journalier avec le modèle hydraulique-hydrologique développé. Pour chaque scénario, l'énergie moyenne produite annuellement, la puissance et le volume déversé pendant la saison des crues sont calculés. L'impact sur le régime d'écoulement est caractérisé par les coefficients de Pardé, une série d'indicateurs basés sur l'approche de la variabilité (RVA) et les courbes de débits classés. Dans une perspective globale, l'analyse montre qu'il est possible de parvenir à un compromis entre la production énergétique et la durabilité environnementale.

Finalement, les données de deux modèles de circulation générale (GFDL-CM2.0 et CCCma-CGCM3) pour le scénario d'émissions SRES A2 du rapport de l'IPCC ont été utilisées pour simuler l'hydrologie au cours des périodes 2045-2065 et 2080-2100. Les résultats des modèles climatiques divergent en termes de précipitations (GFDL-CM2.0 prédit une augmentation alors que CCCma-CGCM3 une diminution) mais s'accordent sur l'augmentation de la température. Les impacts de ces changements climatiques ont été évalués à la fois sur la production d'énergie et sur les modifications du régime d'écoulement.

Le développement et l'application d'un modèle hydraulique-hydrologique à un grand bassin versant, dans un contexte de rareté des données et d'éléments hydrographiques particuliers, est particulièrement important pour la gestion des ressources en eau. L'utilisation de données et de logiciels en libre accès ainsi que d'outils de calage adaptés permet aux opérateurs, aux autorités et aux chercheurs d'évaluer ensemble les impacts du développement hydroélectrique.

Mots-clés : précipitations dérivées d'observations satellite, modélisation hydrologique, plaine inondable, gestion des ressources en eau, exploitation des centrales hydroélectriques, scénarios de développement, changement climatique.

Table of contents

I

LIST OF SYMBOLS AND ACRONYMS

Roman capitals

ALPHA_B	Baseflow recession constant	[day]
CANMAX	Maximum canopy storage	[mm]
Cd	Discharge constant for the weir	[-]
CH_KII	Effective hydraulic conductivity in main channel alluvium	[mm hr-1]
CN	Curve Number	[-]
CN_F	SCS curve number for moisture condition	[%]
$\overline{COR}_{p(I,j),r}$	Mean temporal correlation for each pixel at a distance r	[-]
$\overline{COR}_{p(i,j)(k,l)}$	Pearson correlation between pixel I,j and pixel k,l	[-]
COR_r	Global mean correlation at a distance r	[-]
D	Hydrological alteration indicator	[-]
D_{dateQ}	Hydrological alteration for the flood timing	[-]
D_{Q1}	Hydrological alteration for annual 1-day maximum flow	[-]
D_{Q3}	Hydrological alteration for annual 3-days maximum flow	[-]
D_{Q30}	Hydrological alteration for annual 30-days maximum flow	[-]
D_{Q7}	Hydrological alteration for annual 7-days maximum flow	[-]
D_{Qthres}	Hydrological alteration for the flood duration	[-]
D_{mean}	Overall degree of alteration	[-]
D_{var}	Variation ratio	[-]
D_{volQ30}	Hydrological alteration for the flood volume	[-]

E	Potential evapotranspiration	[mm d^{-1}]
E$_o$	Evapotranspiration	[mm]
EPCO	Plant uptake compensation factor	[-]
ESCO	Soil evaporation compensation factor	[-]
F(x)	Set of objective functions	[-]
FAR	False alarm ratio	[-]
F$_{inf}$	Cumulative infiltration at time t	[mm]
G	Heat flux density to the ground	[MJ m^{-2} d^{-1}]
GW_DELA	Groundwater delay	[day]
GW_REVA	Groundwater revap coefficient	[-]
GWQMN	Threshold depth of water for return flow to occur	[mm]
H	Water depth in the reservoir	[m]
Head	Available head	[m]
H$_{min}$	Minimum water depth for upper flow to occur	[m]
H$_{net}$	Net radiation	[MJ m^{-2} d^{-1}]
H$_o$	Extraterrestrial radiation	[MJ m^{-2} d^{-1}]
IA	Index of agreement	[-]
Ia	Initial abstractions prior to runoff	[mm]
LAI	Leaf area index	[-]
N$_e$	Expected number of years in which the indicator value falls within the RVA target range (75th and 25th percentiles)	[-]
N$_o$	Observed number of years in which the indicator value falls within the RVA target range (75th and 25th percentiles)	[-]
NS	Nash-Sutcliffe coefficient	[-]
Obs	Ground observed rainfall data	[mm]
PC	Pardé coefficient	[-]
POD	Probability of detection	[-]

Q_{base}	Base flow from the reservoir	$[m^3s^{-1}]$
Q_{gw}	Return flow	[mm]
Q_{out}	Reservoir outflow	$[m^3s^{-1}]$
Q_{spil}:	Spilled discharge at time t	$[m^3s^{-1}]$
$Q_{spilmax}$	Maximum spillage discharge	$[m^3s^{-1}]$
$Q_{stor,i-1}$	Surface runoff stored or lagged from the previous day	[mm]
Q_{surf}	Surface runoff	[mm]
$Q_{surf'}$	Surface runoff generated in the subbasin on a given day	[mm]
Q_{turb}	Turbinated discharge at time t	$[m^3s^{-1}]$
$Q_{turbmax}$:	Maximum turbinated discharge	$[m^3s^{-1}]$
Q_{up}	Upper flow from the reservoir	$[m^3s^{-1}]$
R	Pearson correlation coefficient	[-]
R_{day}	Precipitation	[mm]
RE	Relative error	[-]
REVAPMN	Threshold depth of water for revap to occur	[mm]
RRMSE	Relative Root Mean Square Error	[-]
RVol	Volume Ratio	[-]
S	Retention parameter	[mm]
SA	Reservoir surface area	$[m^3]$
Sat	Satellite rainfall data	[mm]
SC	Storage coefficient	[-]
SOL_AWC	Available water capacity of the soil layer	[%]
SOL_Z	Depth from soil surface to bottom of the layer	[%]
SURLAG	Surface runoff lag time	[day]
SW	Soil water content	[mm]
$SW_{ly,excess}$	Drainable volume of water in the soil layer on a given day	[mm]
Tail	Tailwater level	[m a.s.l.]

T_{av}	Mean air temperature	[°C]
T_{max}	Maximum air temperature	[°C]
T_{min}	Minimum air temperature	[°C]
TT_{perc}	Travel time for percolation	[hrs]
V	Volume of water in the reservoir	[m^3]
V_{evap}	Evaporation from the reservoir	[m^3]
V_{flowin}	Reservoir inflow volume	[m^3]
$V_{flowout}$	Reservoir outflow volume	[m^3]
V_{in}	Inflow volume in the reach	[m^3]
V_{max}	Maximum capacity of the natural reservoir	[m^3]
V_{min}	Volume of water permanently stored in the main channel	[m^3]
Vol	Reservoir volume at time t	[m^3]
Vol_{max}	Maximum operation volume for hydropower reservoir	[m^3]
Vol_{min}	Minimum operation volume for hydropower reservoir	[m^3]
Vol_{targ}	Reservoir target volume	[m^3]
V_{out}	Outflow volume from the reach	[m^3]
V_{pcp}	Rainfall falling on the reservoir	[m^3]
VR	Volume ratio	[-]
V_{seep}	Seepage from the reservoir bottom	[m^3]
V_{stored}	Volume of water stored in the reservoir	[m^3]
WL	Reservoir water level	[m a.s.l.]
X	Parameter space	[-]
ΔV_{stored}	Change in stored volume in the reach	[m^3]

Roman lower cases

a	Reservoir overflow coefficient	[m$^{3/2}$ s^{-1}]
b	Reservoir overflow exponent	[-]

can_{day}	Water that can be trapped in the canopy on a day	[mm]
e_{0z}	Saturation vapour pressure of air at height z	[kPa]
e_z	Vapour pressure of air at height z	[kPa]
f	False alarm (estimated rain/observed no rain)	[-]
$f_{inf,t}$	Infiltration rate at time t	[mm hr^{-1}]
g	Gravitational acceleration	[m s^{-2}]
h	Hit (estimated rain/observed rain)	[-]
k	Reservoir release coefficient	[m^{2}s^{-1}]
m	Miss (estimated no rain/observed rain	[-]
ndtarg	Number of days required to reach target storage	[s]
P	Atmospheric pressure	[kPa]
q_{75} and q_{25}	75th and 25th quartiles	[-]
q_{rel}	Average daily release rate	[m^{3}s^{-1}]
r_a	Diffusion resistance of air layer	[s m^{-1}]
r_o	Plant canopy resistance	[s m^{-1}]
surlag	Surface runoff lag coefficient	[-]
targ	Monthly target reservoir water volume	[m^3]
t_{conc}	Time of concentration for the subbasin	[hrs]
w	Weir width	[m]
$w_{perc,ly}$	Water percolating to the underlying soil layer	[mm]
$w_{rchrg,i}$	Water recharge entering the aquifers on day i	[mm]
$w_{revap,max}$	Maximum amount of 'revap' water	[mm]
w_{seep}	Water entering the vadose zone	[mm]

Greek symbols

K	Dimension coefficient	[-]
K_e	Effective hydraulic conductivity	[mm hr^{-1}]

y	Psychometric constant	[kPa °C^{-1}]
α	Adjustment constant linking reservoir volume and surface	[-]
β	Adjustment exponent linking reservoir volume and surface	[-]
β$_{rev}$	Revap coefficient	[-]
γ	Adjustment exponent linking reservoir volume and depth	[-]
δ	Adjustment constant linking reservoir volume and depth	[-]
Δ	Slope of the saturation vapour pressure-temperature curve	[-]
Δθ$_v$	Change in volumetric moisture content	[-]
ε	Adjustment exponent linking tailwater and outflow	[-]
η	Turbine efficiency	[-]
κ	Adjustment exponent linking tailwater and outflow	[-]
λ$_{ev}$	Latent heat of vaporization	[MJ kg^{-1}]
μ	Adjustment exponent linking spillway outflow and level	[-]
ν	Adjustment exponent linking spillway outflow and level	[-]
ρ	Water density	[kg m^{-3}]
ρ$_{air}$	Air density	[kg m^{-3}]
ψ$_{wf}$	Wetting front matric potential	[mm]

Acronyms

ADAPT	African DAms ProjecT
AMALGAM	Multi-ALgorithm Genetically Adaptive Multi-objective method
AMS	Adaptive Metropolis Search
AMSR-E	Advanced Microwave Scanning Radiometer-Earth Observing System
AMSU-B	Advanced Microwave Sounding Unit-B
ARA-Zambeze	Regional Administration of Zambezi Water
CCCma-CGCM3	Canadian Centre for Climate modeling and analysis Coupled Global Climate Model (version 3)

CCES	Competence Centre Environment and Sustainability
CMORPH	NOAA/CPC morphing technique
CPC	Climate Prediction Centre
DE	Differential Evolution
DEM	Digital Elevation Model
DMSP	Defense Meteorological Satellite Program
DWA	Department of Water Affairs of Zambia
EAWAG	Swiss Federal Institute of Aquatic Science and Technology
E-flow	Environmental flow
EPFL	Ecole Polytechnique Fédérale de Lausanne
ETH	Swiss Federal Institute of Technology in Zurich
FAO	Food and Agriculture Organisation
FAST	Fourier Amplitude Sensitivity Test
FEWS	Famine Early Warning System
FNS	Fast Nondominated Sorting
GCM	General Circulation Model
GFDL-CM2.0	US Geophysical Fluid Dynamic Laboratory Climate Model (version 2)
GIS	Geographic Information System
GLCC	Global Land Cover Characterization
GLUE	Generalized Likelihood Uncertainty Estimation
GPCC	Global Precipitation Climatology Centre
GRDC	Global Runoff Data Centre
GSOD	Global Summary Of the Day
GTS	Global Telecommunication System
HCB	Hidroelectrica de Cahora Bassa
HP	Hydropower Plant
HRU	Hydrologic Response Units

IPCC	Intergovernmental Panel on Climate Change
IPWG	International Precipitation Working Group
IR	Infrared Radiance
ITCZ	Inter-Tropical Convergence Zone
ITT	Itezhi Tezhi
IWRM	Integrated Water Resources Management
JAXA	Japan Aerospace Exploration Agency
LCH	Laboratory of Hydraulic Constructions
LEO	Low Earth-Orbiting
LEW	Lumped Elementary Watershed
LH	Latin Hypercube sampling
MW	Microwave
NASA	National Aeronautics and Space Administration
NCDC	National Climatic Data Centre
NCEP	National Centers for Environmental Prediction
NGO	Non Governmental Organizations
NOAA	National Oceanic and Atmospheric Administration
NSGA-II	Non-dominated Sorted Genetic Algorithm-II)
OAT	One-factor-At-a-Time sampling
PET	Potential evapotranspiration
PM	Passive Microwave
PR	Precipitation Radar
PSO	Particle Swarm Optimization
RT	Real Time
RVA	Range of Variability Approach
SCS	Soil Conservation Service
SSM/I	Special Sensor Microwave Imager

STREAM	Spatial Tools for River basin Environmental Analysis and Management
SWAT	Soil and Water Assessment Tool
SYNOP	Synoptic weather observation data
TEDPAS	Temporal dynamics of parameter sensitivity
TMI	TRMM Microwave Imager
TMPA	TRMM Multisatellite Precipitation Analysis
TRMM	Tropical Rainfall Measuring Mission
USDA	US Department of Agriculture
VIS	Visible and Radiance
WMO	World Meteorological Organization
ZESCO	Zambian Electricity Supply Corporation
ZRA	Zambezi River Authorities

1 INTRODUCTION

This chapter presents the general context of the project and state the research objectives. It also provides the applied methodology and describes the structure of the thesis report.

1.1 GENERAL CONTEXT

Based on the information collected by the World Commission on Dam [2000], the following statistics should be considered. Worldwide, almost 50,000 dams over 15 m height have been built during the last six decades with an aggregated storage capacity of 6,000 km^3 [*International Commission On Large Dams*, 2007]. The belief that large dams by increasing irrigation and hydroelectricity production can sustain development and reduce poverty has led developing countries to undertake major investment in dam construction. During the 1990s, an estimated USD 32 – 46 billion was spent annually on large dams, four-fifth of it in developing countries. By the year 2000, dams generated 19 percent of the world's total electricity supply and irrigated over 30 percent of the 271 million hectares irrigated worldwide. However, 60 percent of the world's largest rivers are severely fragmented by dams, diversions and canals leading to the degradation of ecosystems. Despite the huge economic benefits provided by large dams, the environmental and social costs have been poorly accounted for in economic terms so that the wider long-term cost/benefit analysis to determine the true profitability of these schemes remains elusive. As the needs for further water services are increasing, the challenges for the future are to avoid past mistakes; that is, to operate existing large hydraulic systems in more sustainable ways; to develop future water resource schemes that achieve a better balance between ecological and socioeconomic demands; and to improve the institutional settings for transboundary water management [*International Commission On Large Dams*, 2012; *United Nations Development Programme*, 2006].

Africa is the continent with the smallest proportion of irrigated agriculture, the lowest degree of electrification and water storage capacity per capita worldwide. Dams offer solutions to these problems and could thereby contribute to socio-economic progress. However, the urgent need for expanding water storage capacity in Africa conflicts with the negative social and ecological impacts of large dams that have been identified in some of the past international projects. In exploiting the potential of African rivers, major challenges will be to improve the operation of existing dams and to avoid past mistakes when designing new ones. Meeting these challenges requires scientific progress in order to design and manage complex hydrologic/hydraulic systems in sustainable ways.

The Zambezi River Basin contains many of southern Africa's largest and most intact freshwater and estuarine wetlands, e. g. the Kafue flats, the Mana Pools and the Zambezi delta as well as several free-flowing yet unprotected river reaches. The basin supports some of the world's largest remaining elephant herds and serves as a refuge for many other large animals, including African buffalo, hippopotamus and crocodile. Three of Africa's largest dams (Kariba dam, Cahora Bassa dam and Kafue scheme) inundate hundreds of square kilometers of river habitat and modify the natural flow patterns that sustain floodplains. Increasing electricity demand by cities and industry is causing a regional energy shortage, and governments and investors are planning yet more dams in the Zambezi Basin. The Southern African Power Pool (SAPP) integrated expansion plans include more than 6,300 MW of new

large scale hydropower between 2010 and 2015. At least another 6,500 MW are under discussion within the Zambezi River basin alone. Climate change promises to reduce annual average river flow and increase between-year variability, putting even greater stresses on a regional energy network that relies heavily on hydropower. Therefore, the Zambezi Basin constitutes a particularly interesting and important system for further developing existing approaches of integrated water resources management.

1.2 PROJECT CONSORTIUM AND COLLABORATIONS

The African Dams project (ADAPT) aims at enhancing the scientific basis of integrated water resource management in the Zambezi River Basin. New models for the real-time control and multi-objective optimization of large hydraulic structure should be created and data resources enhanced through field survey. The improvement of the conceptual framework driving and integrating these models is also included in the project task along with coupled models. The final outcome should allow identifying operation modes that improve the balance between ecological and socioeconomic demands, and will be useful not only for optimizing the operation of existing structures but also for designing new ones. Therefore, the project focuses mainly on the large reservoirs and wetlands on a basin wide scale and on a regional scale (Kafue subbasin) [*Mertens et al.*, 2013]. To reach this goal, ADAPT combines expertise from biogeochemistry, aquatic physics, ecology, economy, political sciences, hydraulic engineering, and hydrology (Figure 1-1).
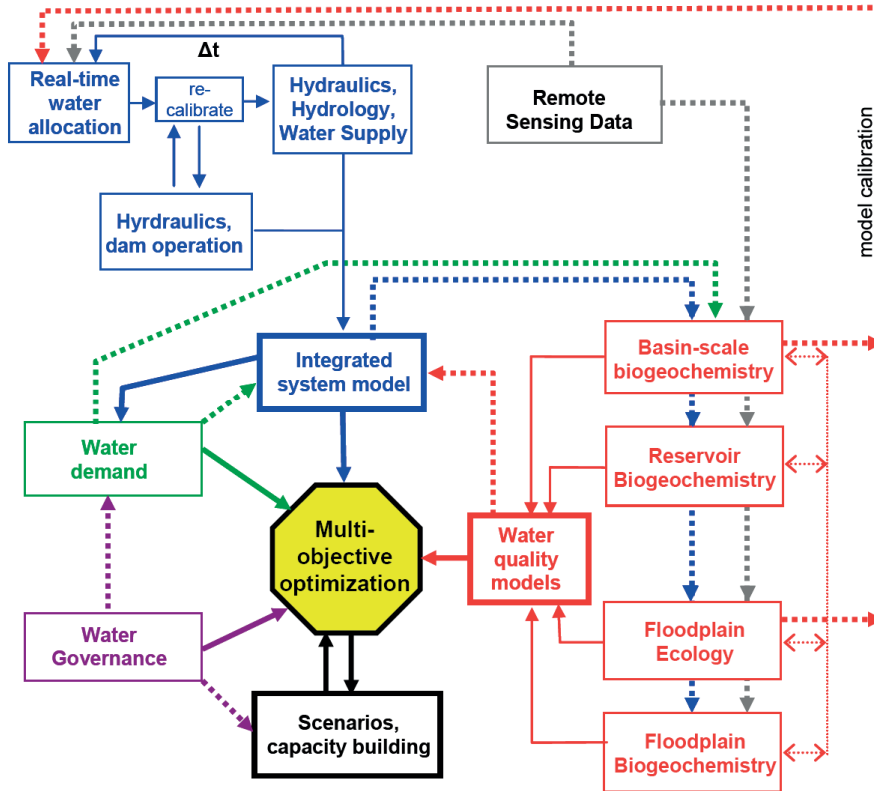

Figure 1-1 : Organization of the ADAPT project (solid lines represent main workflow; dashed lines indicate information exchange between projects) [*ADAPT*, 2008]

The close collaboration with African partners including exchanges and joint supervision of students, training activities, and systematic involvement of governmental agencies and NGOs throughout the research process ensure the dissemination of models and data and maximizes exchange and synergies.

ADAPT project is constituted of an interdisciplinary consortium of different research institutes in Switzerland (Table 1-1) and mainly funded by the Competence Centre Environment and Sustainability (CCES) of the ETH Domain.

Table 1-1 : Consortium partners of the CCES-project

Partner	Field of expertise
Center for Comparative and International Studies (CIS-ETH)	Economics, political and environmental sciences, conflict/cooperation in managing natural resources, …
Institute of Integrative Biology (IBZ-ETH)	Floodplain ecology, plant-herbivore interaction, wetland plant nutrition, plant invasion, field work…
Institute of environmental Engineering (IfU-ETH)	Sustainable water management, hydrological-hydraulic modeling, use of satellite imagery…
Postgrade Studies on Developing Countries (NADEL-ETH)	Economic policies, environment and resource policies, applied econometrics and modeling…
Institute of Biogeochemistry and Pollutant Dynamics (ETH-EAWAG)	Biogeochemical processes in river and lakes, field methods…
Surface waters (EAWAG)	Field instrumentation, simulation of reservoir internal processes, …
Laboratory of Hydraulic Constructions (LCH-EPFL)	Civil engineering, hydrological-hydraulic modeling including dams and reservoirs, decision support system, multipurpose optimization…

During its main phase (2008-2011) this interdisciplinary project developed new models that can be used to improve the operation of existing large hydraulic structures and to design future water use schemes at the basin-scale.

More precisely, in the biogeochemistry research area, Kariba reservoir was studied through field campaigns and modelling to characterize the processes happening in a tropical reservoir [*Kunz et al.*, 2011a; *Kunz et al.*, 2011b]. The floodplain biogeochemistry was also investigated regarding the dam effect [*Wamulume et al.*, 2011; *Zurbrügg et al.*, 2013]. In terms of hydrological modelling, a real time model was applied to the Kafue flat region [*Meier et al.*, 2011]. The water governance was studied on the Kafue basin [*Uhlendahl et al.*, 2011] including extensive field survey and multi-objective modelling. At the basin scale, the effect of coordinated dam operations as well as the optimization of water resources management was globally assessed by applying a statistical model with different scenarios [*Tilmant and Kinzelbach*, 2012; *Tilmant et al.*, 2010a; *Tilmant et al.*, 2010b; *Tilmant et al.*, 2012].

Capacity building has been included through exchanges and joint supervision of master students and involvement of governmental agencies and NGOs in the research process. A stakeholder meeting has been organized by ADAPT on January 2011 in Lusaka where

representatives of governmental, non-governmental, and educational institutions have identified critical research needs to address problems of water demands for agriculture, hydropower, and the environment (Figure 1-2).

Figure 1-2. ADAPT stakeholder meeting held on 24th January 2011 in Lusaka.

1.3 RESEARCH OBJECTIVES

In the framework of the ADAPT project, the major contribution of the presented research project was to set-up a hydrologic-hydraulic model of the whole catchment area which includes all relevant elements as hydraulic structures and schemes as well as floodplains. The task included a simulation of the possibilities and ranges of influencing water flow regime downstream of dams by joint reservoir operations [*ADAPT*, 2008; *CCES*, 2008]. The multi-objective modelling and simulation should define how dam operation can be adapted to get the highest environmental results under highest energy production. A refinement of these objectives has lead to the definition of three research steps:

1. Evaluate thoroughly the quality of available input data for hydrological modelling on the Zambezi River Basin.

2. Define the specific hydrological processes needed for hydraulic-hydrological modelling of the Zambezi Basin and establish a calibration outline.

3. Assess the impact of the planned new hydraulic structures as well as the refurbishment of the existing hydropower plants on the flow regime at critical points of the basin.

The substantial originality of the resulting contribution lies in the development and application of a hydraulic-hydrological model to a large river basin in a context of data scarcity and particular hydrologic units. The use of open source data and adapted calibration tools lead to the definition of an innovative methodology. The development strategy defined based on the model allows a multi-purpose assessment of the existing dams and reservoirs and the future projects.

1.4   APPROACH AND OUTLINE

The present thesis consists of nine chapters. The *Introduction* and *State of the art* present the context of the study as well as an overall literature review of the concerned research fields: satellite derived precipitation, hydrological modeling, water resources management and climate change. More specific information can be found in the corresponding main chapters. In Chapter 3, the case study is presented, revealing geographical and hydrological characteristics of the Zambezi River Basin along with the main features of the hydraulic-hydrological model including dams and reservoirs under operation and planned in future.

The main chapters 4 to 8 have been prepared as individual manuscripts in international peer-reviewed journals that have already been published (Chapter 4: Cohen Liechti, T., Matos, J. P., Boillat, J.-L., and Schleiss, A. J.: *Comparison and evaluation of satellite derived precipitation products for hydrological modeling of the Zambezi River Basin*, Hydrology and Earth System Sciences, 16(2): 489-500, 2012) or accepted for publication (Chapter 6: Cohen Liechti, T., Matos, J. P., Ferras, D., Boillat, J.-L., and Schleiss, A. J.: *Modeling floodplain hydrology in an African catchment using a modified reservoir approach*, Journal of River Basin Management).

Major repetitions in these 4 main chapters have been eliminated compared to the journal papers. Nevertheless some repetitions could not be avoided in the introduction of the chapters as well as in case studies due to coherence of the text.

A short outline of each chapter is given in the following.

Chapter 4: *Comparison and evaluation of satellite derived precipitation products*

Three operational and acknowledged satellite derived precipitation products (the Tropical Rainfall Measuring Mission product 3B42 -TRMM 3B42-, the Famine Early Warning System product 2.0 -FEWS RFE2.0- and the National Oceanic and Atmospheric Administration/Climate Prediction Centre (NOAA/CPC) morphing technique –CMORPH-) are analyzed in terms of spatial and temporal distribution of the precipitation. They are compared to ground data for the wet seasons of the years 2003 to 2009 on a point to pixel basis at daily, 10-daily and monthly time steps and on a pixel to pixel basis for the wet seasons of the years 2003 to 2007 at monthly time steps.

Chapter 5: *Hydraulic-hydrological modeling framework*

The Soil and Water Assessment Tool (SWAT 2009), a semi-distributed physically based continuous time model, is chosen to simulate the hydrology of the basin. Given the complexity and the size of the basin, an automated calibration procedure based on A Multi-ALgorithm Genetically Adaptive Multi-objective method (AMALGAM) is applied to optimize the relative error and the volume ratio at multiple discharge stations. The observed volume at the artificial reservoir is derived from the measured water level and included in the

calibration. The final calibrated model along with intermediate results of the calibration process is presented.

Chapter 6: *Modeling floodplain hydrology using a modified reservoir approach*

An adapted version of SWAT 2009 reservoir model is proposed with the intention of adequately modeling floodplain behavior. The model simulating the floodplain separates the outflow of the reservoir into a main channel flow and a flow over the floodplain area. The improved solution is compared with the original model regarding its potential to simulate observed discharges. A sensitivity analysis is carried out at two geographical levels namely at the outlet of a floodplain and at the outlet of the entire basin.

Chapter 7: *Analysis of hydropower development scenarios in view of sustainable ecological catchment development*

Different hydropower development scenarios are defined combined with three levels of environmental flows requirements. The results are presented in terms of energy production and environmental satisfaction by a set of indicators.

Chapter 8: *Impacts of climate change on future energy production*

The emission scenario A2 of the IPCC report is applied to the Zambezi basin based on the results of two different global climate models. The impact of climate change is assessed both on energy production and flow pattern changes.

A synthesis of the research is presented in the Chapter 9 along with recommendations and an outlook on further research.

2 STATE OF THE ART

This chapter contains a general introduction to the main topics of the research project. The specific scientific questions and the corresponding literature are more detailed and discussed in the main chapters. At first, the theoretical bases of the methodology used to the derivation of precipitation based on satellite data are explained. Secondly, an overview of the relevant modeling approaches applied to hydrology is given. Thirdly, the problematic of hydropower and environmental flows is briefly presented, along with the different multi-objective optimization models used. The impact of climate change in Africa is summarized. Finally, the methodology and the results obtained by the existing studies of the Zambezi Basin water resources are listed. The content should allow general understanding of the concerned fields.

2.1 SATELLITE DERIVED PRECIPITATION DATA

In view of the sparse available gauging network for rainfall monitoring on the African continent, the observations from spaceborne instrumentation currently produce the only measured data for a large part of the territory. Two types of sensors are commonly used in the satellite rainfall estimation algorithms: Passive Microwave (PM) and Visible and Infrared Radiance (VIS/IR).

The PM sensors identify the precipitation particles by the scattering due to large ice particles present in the clouds. Early systems focused on the detection of rainfall over oceans allowed by the clear contrast between the radiometrically cold background of the low-emissivity ocean surface and radiometrically warm emission from falling rain at low frequencies [*Wilheit et al.*, 1977]. More recently, the Special Sensor Microwave/Imager (SSM/I) which measures vertically and horizontally surface/atmospheric microwave brightness temperatures at four frequencies remains the primary source of information regarding precipitation over land surface [*Munchak and Skofronick-Jackson*, 2013]. These instruments and algorithms generally perform well for moderate to heavy rainfall during the warm season [*Ebert et al.*, 2007]. Unfortunately, these sensors are installed on Low Earth-Orbiting (LEO) satellites which offer only intermittent coverage of a given region of interest (currently about ten observations per day).

Therefore, the estimation of precipitation from proxy parameters such as cloud top temperature that can be inferred from geo-stationary satellites with high spatial and temporal resolutions has been developed. The algorithms based on IR data relate rainfall to cloud top temperature and cloud optical properties through a precipitation index. The indexing method assigns a fixed rain rate to each identified cloud type [*Kidd*, 2001]. This assumption is most effective for convective conditions but can yield crude estimates because of the weak link between cloud properties and precipitation. Current approaches use rain rates estimated from coincident microwave observations to derive regional calibrations of Global-IR techniques [*Anagnostou*, 2004]. However, both kinds of sensors have difficulties in capturing non-convective rainfall and shallow "warm" rain events [*Ebert et al.*, 2007].

The Tropical Rainfall Measuring Mission (TRMM) is a collaborative science project sponsored by the National Aeronautics and Space Administration (NASA) and the Japan Aerospace Exploration Agency (JAXA), particularly designed to monitor tropical and subtropical rainfall [*Prakash and Gairola*, 2013]. The satellite launched in this framework includes two microwave (MW) precipitation sensors, the TRMM Microwave Imager (TMI), a passive microwave radiometer with nine linearly polarized channels, and the Precipitation Radar (PR), the first space-borne active MW sensor [*Kummerow et al.*, 1998]. Abundant valuable data have been archived since the mission was initiated in the late 1997. Among them, the TRMM Multisatellite Precipitation Analysis (TMPA) product is developed by the synergistic use of MW and IR measurements combined with available rain gauge data [*Huffman et al.*, 2007]. The released precipitation estimates is available in a global belt extending from 50° S to 50° N at 0.25° × 0.25° spatial resolution and 3-h temporal resolution.

It combines precipitation estimates from the various satellite systems as well as feasible land surface rain gauge analyses. The LEO satellites sensors included are the following: Microwave Imager (TMI) on TRMM, Special Sensor Microwave Imager (SSM/I) on Defense Meteorological Satellite Program (DMSP) satellites, Advanced Microwave Scanning Radiometer-Earth Observing System (AMSR-E) on *Aqua*, and the Advanced Microwave Sounding Unit-B (AMSU-B) on the National Oceanic and Atmospheric Administration (NOAA) satellite. The snapshot for a particular 3-hourly period covers about 80% of the earth's surface in the latitude band 50°N–S (Figure 2-1).
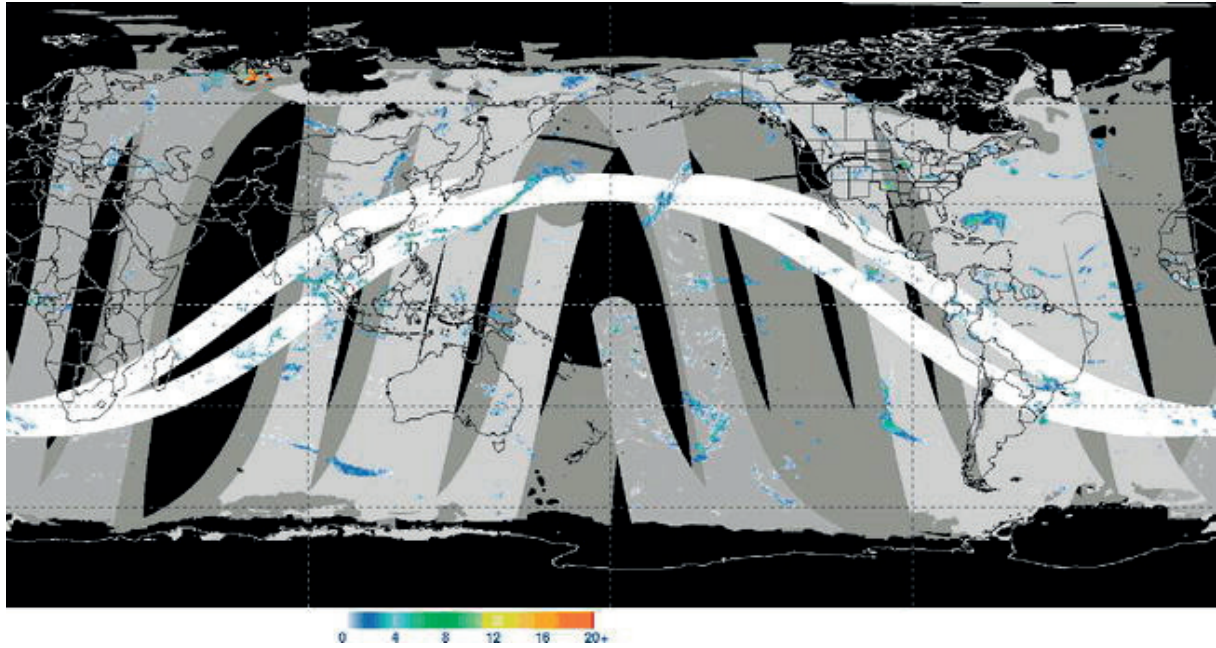
Figure 2-1. Combined microwave precipitation estimate for the 3-h period centered at 0000 UTC 25 May 2004 in mm h^{-1}. Blacked-out areas denote regions that lack reliable estimates, while the zero values in the remaining areas are color-coded to depict the coverage by the various sensors. The order of precedence for display and corresponding zero color are TMI (white), SSM/I (light gray), AMSR-E (medium gray), and AMSU-B (dark gray). (In the TMPA the TMI, SSM/I, and AMSR-E are averaged where overlaps occur) [from *Huffman et al.*, 2007]

In the present study the TMPA-3B42 research product was used as input data for the hydrological model. At first, the version 6 was implemented and then updated to the version 7a (released in December 2012) during model calibration. The TMPA-3B42 estimates are produced in four stages (Figure 2-2): (1) the MW precipitation estimates are calibrated and combined, (2) the IR precipitation estimates are created using the calibrated MW precipitation, (3) the MW and IR estimates are combined, and (4) rescaling to monthly data is applied. A real-time (RT) version of the product is released which does not include ground data rescaling.
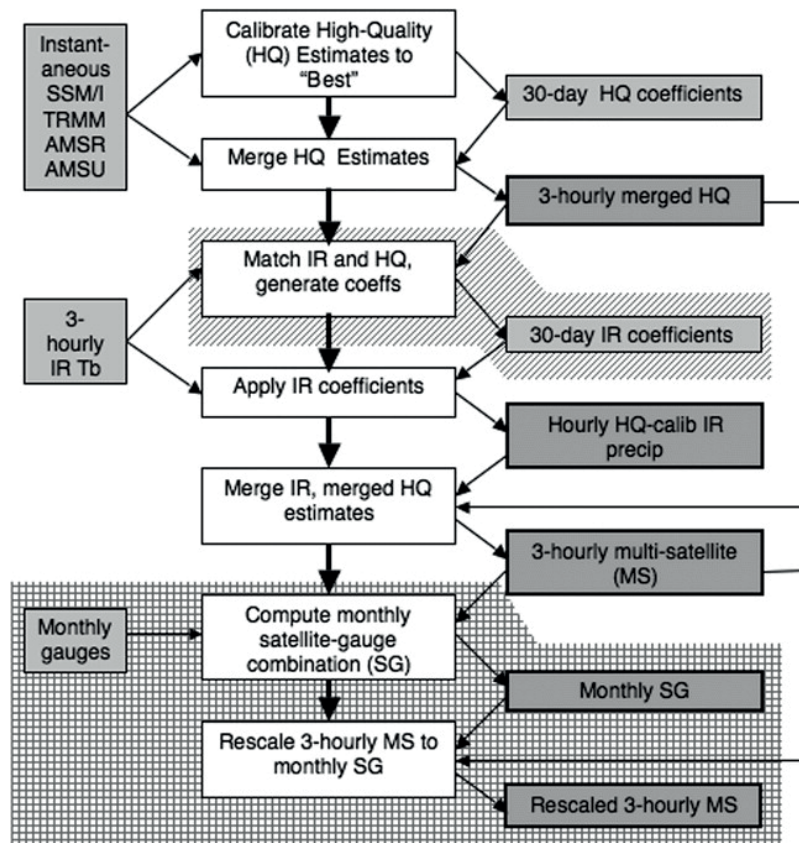
Figure 2-2. Block diagram for both the RT and research product algorithms, showing input data (left side), processing (center), output data (right side), data flow (thin arrows), and processing control (thick arrows). The items on the slanted shading run asynchronously for the RT algorithm, and the items on the grid shading are only performed for the research product. "Best" in the top center shaded box is the TMI GPROF precipitation estimate for the RT algorithm and the TMI–PR combined algorithm precipitation estimate for the research product. [from *Huffman et al.*, 2007]

2.2 HYDROLOGICAL MODELLING WITH FOCUS ON SOUTHERN AFRICA

2.2.1 Overview

The development of water resources models in Southern Africa is greatly challenging. Several factors contributing to the present situation can be highlighted. Firstly, the order of relevance of hydrologic processes in catchments below the Sahara Desert does not necessarily match what has been extensively observed in temperate catchments [*Pilgrim et al.*, 1988]. For example, evaporation is the dominant hydrological process and no glaciers are present. Secondly, there is a constraining and prevalent lack of hydrological data within most countries in this area. Although data scarcity usually appears as a ubiquitous problem to water resources modelers, in Southern African catchments has to be explicitly taken into account during hydrological model choice, calibration and validation phases.

The model choice, set-up and calibration must therefore be based on equilibrium between the model complexity required and supported by the system, depending on the data availability and the purpose of the modeling process (Figure 2-3).
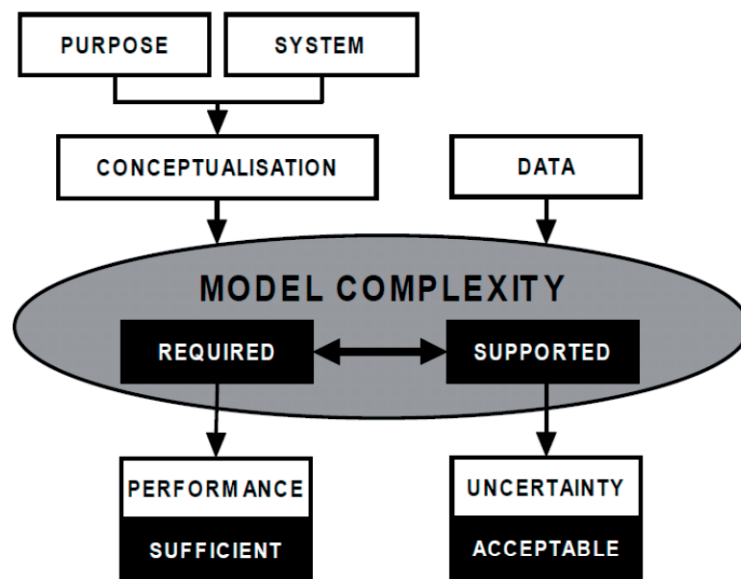
Figure 2-3. Framework for development and application of hydrological models [from *Wagener et al.*, 2001]

2.2.2 Types of model

The definition of a model is a "simplified representation of a real world system" [*Wheater et al.*, 2008]. It uses parameters as numerical measurement of a property or characteristic which is constant under specified conditions for simulation of one or many processes.

Depending on the character of the results obtained, hydrological models can be classified as *deterministic* or *stochastic*. If one or more of the variables in a mathematical model are regarded as random variables whose values can change unpredictably over time, then the model is stochastic. This random character is usually based on fluctuations observed in historical time series. With a large number of simulations, it is possible to derive distributions of potential outcomes for example by the help of Monte-Carlo simulation. If all the variables are considered to be free from random variation, the model is deterministic.

The models can be used to simulate single events or sequences of time periods, designed respectively as *event-based* or *continuous-time*. In an event-base simulation, the accuracy of the output depends on the reliability of the initial conditions which have to be assumed or determined by other means and supplied as input data for each event. In a continuous-time simulation, the effect of any assumed initial conditions decreases rapidly as time advances [*Loucks et al.*, 2005].

The most usual classification of the models is regarding the process description (Table 2-1). Three main categories are distinguished. The "black box" model is based on empirical descriptions of the hydrological processes. The "conceptual model" or "semi-distributed model" simulates the hydrological behaviour applying physically based functions to geographical units. The "distributed model" takes into account the physical variability of the catchment characteristics for computing the run-off at each grid point.

Table 2-1 : Classification of hydrological models according to process description

	Empirical models (black box)	**Conceptual models (grey box)**	**Distributed models (white box)**
Spatial description	No discretization	Lumped/semi-distributed	Distributed
Hydrological-hydraulic description	Empirical, statistical	Physically based (conceptual)	Physically based

2.2.2.1 "Black box" models

Purely empirical or statistical models omit the physics and are in reality representations of the observed data.

Ex: Neural network techniques have been applied to estimate runoff based on rainfall [*Rajurkar et al.*, 2004; *Shamseldin*, 1997].

2.2.2.2 Conceptual models

Semi-distributed models are defined as lumped since they assume homogenous or average conditions over portions of a watershed. This model form originated in the 1960s, when computing power allowed generating continuous flow sequences. To apply these models to a particular catchment, the model must be calibrated using either manual or automatic procedure. The model parameters can be fitted using generalized likelihood

uncertainty estimation (GLUE) procedure [*Beven and Binley*, 1992] in order to keep only the consistent simulation (based on prior information and pre-selected threshold value). The goal is to relate the parameters to catchment characteristics.

Ex: The Soil and Water Assessment Toll (SWAT) [*J G Arnold et al.*, 1998] simulates physically based processes at the subbasin scale taking into account different soil and land use types. Routing System [*Garcia Hernandez et al.*, 2007] models snow and glacier melt as well as infiltration, runoff and flow routing on each subbasin.

2.2.2.3 *Distributed models*

Distributed models require more detailed data than the other types. They are explicitly based on the best available understanding of the physics of hydrological processes. The equations of the constituent processes are solved numerically using a grid. They appeared in the 1970s, when the computing power became sufficient to solve coupled partial differential equations. The parameters are measurable and have a direct physical significance.

Ex: The Système Hydrologique Européen (SHE) [*Abbott et al.*, 1986] models the processes by finite difference representations of the partial differential equations of mass, momentum and energy conservation in an orthogonal grid network and in the vertical by a column of horizontal layers at each grid square. MODFLOW is a three-dimensional finite-difference ground-water model [*Harbaugh*, 2005].

In the case of a large watershed with limited data accessible, the choice of a semi-distributed model is admitted in order to balance the need of detailed results and the information available [*Notter et al.*, 2012; *Yu et al.*, 2011].

2.2.3 Calibration

Most of the hydrological models have to be calibrated in order to obtain reliable results. The calibration consists of an estimation of the model parameters values that enable the model to match as closely as possible the behaviour of the system. In few cases, the values can be defined through direct field measurements but in most of the situations, the parameters are conceptual, even if physically based, and must be determined by a trial-and-error process that adjust the parameter values to match the model response to historical data [*Gupta et al.*, 1998; *Madsen*, 2000]. Manual calibration attempt is important to learn the behaviour of the model. Nevertheless, it largely depends on the experience of the modeller along with his knowledge of the model and is time consuming [*Confesor Jr and Whittaker*, 2007]. Automatic calibration overcomes these shortcomings but requires a large amount of computation.

The traditional single-objective calibration schemes are limited in terms of the number of parameter that can be identified. Therefore, they are often replace by multi-objective calibration framework, introduced by Gupta *et al*. [1998], the choice of the objective functions being dependent of the model goals. Multiple objectives are often transformed into a single objective function by the weighted sum principle where the objectives are defined by user-defined weights. To avoid this conversion, the use of Pareto optimization has gained use

and popularity in hydrologic modelling. More precisely, the general form of a multi-objective calibration problem can be stated as follows:

$$\hat{\mathbf{x}}_{opt} = \arg\min_{\mathbf{x}} \mathbf{F}(\mathbf{x}) = \arg\min_{\mathbf{x}} \left[F_1(\mathbf{x}), F_2(\mathbf{x}), ..., F_p(\mathbf{x}) \right], \quad \mathbf{x} = (x_1, ..., x_i), \mathbf{x} \in X \qquad [2\text{-}1]$$

where X is the parameter space, $\mathbf{x}$ the parameter vector and $\mathbf{F}(\mathbf{x})$ the set of associated objective functions.

The solution of Eq. [2-1] is not likely to be a unique set of parameters but rather a Pareto front of optimal non-dominated solutions. Formally, any member of the Pareto set has the properties [*Gupta et al.*, 1998]:

1. For all non-members x_j there exists at least one member x_{opt} where $F_k(x_{opt}) < F_k(x_j)$ for all $k = 1, 2, ..., p$.

2. It is not possible to find x_i within the Pareto set such that $F_k(x_i) < F_k(x_{opt})$ for all $k = 1, 2, ..., p$.

In other words, according to the first statement, the feasible parameter set can be divided into optimum solutions and non-optimum solutions and, according to the second statement there is no uniquely best solution among the Pareto solutions.

In general, optimization problems can be categorized as local and global search methods. Local search algorithm may be further divided into direct and gradient-based methods [*Madsen*, 2000]. Popular global search methods are the population-evolution based search strategies.

Among them, the multi-algorithm genetically adaptive multi-objective method (AMALGAM) [*Vrugt and Robinson*, 2007; *Vrugt et al.*, 2009] is distinguished by its capacity to combined two concepts, simultaneous multimethod search, and self-adaptive offspring creation. Since AMALGAM has already been documented as a high performance solution compared to other evolutionary multi-objective algorithms for hydrological model calibration [*Zhang et al.*, 2010; *Zhang et al.*, 2011], it was applied in the presented research project. The algorithm is initiated by using a random initial population, generated by using Latin hypercube sampling. A rank is assigned to each parent using the fast nondominated sorting (FNS) algorithm [*Deb et al.*, 2002]. The multimethod search concept, the heart of AMALGAM, is then used to create a population of offspring, each candidate algorithm generating a pre-specified number of offspring points. Four optimization methods are included: (i) non-dominated sorted genetic algorithm-II (NSGA-II) [*Deb et al.*, 2002], (ii) particle swarm optimization (PSO) [*Kennedy and Eberhart*, 1995], (iii) adaptive Metropolis search (AMS) [*Haario et al.*, 2001], and (iv) differential evolution (DE) [*Storn and Price*, 1997]. The best solutions of the offspring generated are selected using the FNS operator. By comparing the current offspring with the previous generation, elitism is ensured as all previous nondominated members will be included in the new population. Typically, the algorithm is stopped when it has reached a satisfying value of the objective function or the convergence rate falls consistently below a certain threshold.

2.2.4 Uncertainty

To assess the reliability and the applicability of a model to support decisions about water resources management under development or climate change scenarios, it is necessary to consider uncertainty. Three main sources are defined: input data, model structure and parameter, and output uncertainty.

Input data are subject to systematic and random errors, *e. g.* bias in the satellite derived rainfall data or misreading from a ground gauge measurement of precipitation. The uncertainty arising from this source have often only a limited impact on model predictions [*Butts et al.*, 2004] but should be considered when assessing the model quality.

In terms of model structure and parameter uncertainty, the theory of equifinality can be cited. The principle of equifinality is used '*in the sense that the same end, in this case an acceptable model prediction, might be achieved in many different ways, i. e. different model structures or parameter sets'* [*Beven*, 1993]. Each of these model structure/parameter sets will produce different results when apply to predict the behaviour of the system which can be used to assess to uncertainty in the predictions. The parameter uncertainty is often taken into account during the calibration process and is the easiest category of uncertainty to assess. Many different techniques have been developed and applied. One possible implementation of the concept is the Generalised Likelihood Uncertainty Estimation (GLUE) [*Beven and Binley*, 1992] using Monte Carlo sampling which explicitly recognises the equivalence of different parameter sets / model structure in the representation of the hydrological response.

The uncertainty arising from error in data used for model calibration, *e. g.* observed discharge, has been recently included in the analysis. Errors in the rating curve estimations results in uncertainties in the range of 2 to 19% using velocity-area methods [*Di Baldassarre and Montanari*, 2009; *McMillan et al.*, 2012]. When the flow is low or high, the uncertainty increases as the rating curves are extrapolated.

In the case of the Zambezi River, the large flow variation and the variable channel geometry in the floodplains results in low reliability of the discharge observations. Errors in observed outflow at the dams also come from various sources. First, the turbine flow is not directly measured; it is estimated from the electricity production. Secondly, during high flows, the outlet outflow is estimated based on the reservoir level and the outlet capacity but not directly measured either. Moreover, a small error in the water level can cause a significant divergence in the corresponding volume as the reservoirs are very large and without knowing precisely the reservoir geometry, the water level-volume relation is only estimated.

2.3 HYDROPOWER AND MULTI-OBJECTIVE ASSESSMENT OF ENVIRONMENTAL FLOWS

Hydroelectric power dams currently provide 19% of the world's electricity supply; one in three nations depends on hydropower to meet at least half of its electricity demands [*World Commission on Dams*, 2000]. At the end of the 20th century, the number of large dams (more than 15 m height) has climbed to more than 50,000 and the water demand is exponentially increasing, especially in developing countries [*International Commission On Large Dams*, 2007; *World Commission on Dams*, 2000]. However, the modification of water flow regimes caused by dams is one of the primary causes of the degradation of freshwater ecosystems worldwide [*D Harrison et al.*, 2007]. More precisely, dam induced changes affect water temperature and chemistry, sediment transport, floodplain vegetation communities and downstream deltas [*Richter and Thomas*, 2007]. Hydropeaking resulting from peak energy production, affects fish habitat [*Person et al.*, 2013]. Water diversion for hydropower production often leaves only a minimum flow for the ecosystem with a resulting hydrograph very different from the natural one [*Perona et al.*, 2013].

'*The concept of environmental flows (e-flows) has been advanced to meet ecosystem demands for water. E-flows are defined as the volume of water that should flow in a river and its variation over time to maintain specific indicators of ecosystem health*' [*Yin et al.*, 2012]. Historically, the e-flows were defined as a single minimum 'compensation' or 'reserved' flow. Nowadays, experts has reached a consensus: e-flows should represent the full range of natural flow variations, taking into consideration the magnitude, frequency, timing, duration and rate of change of the flow event [*Arthington et al.*, 2006; *Yin et al.*, 2012]. However, it results a loss in terms of energy production.

Multiple methodologies for evaluating natural flows and quantifying the effect of dam on flow alteration are available. They are mainly based on aquatic ecology theory and require as starting point either measurements or synthesized daily streamflows from a period with no human perturbations on the hydrological regime. The Range of Variability Approach (RVA) [*Richter et al.*, 1997] characterizes the flows using 32 different parameters derived from long term (> 20 years) daily streamflow records defining the timing, magnitude, duration, frequency and rate of change of the regime. The targets for flow management are then defined by the range of variation in each of the parameter. Homa *et al.* [2005] developed one indicator for instream flow alteration called the 'Ecodeficit' consisting in the area below the unregulated and above the regulated flow duration curves.

A multi-objective optimization algorithm was applied to a reservoir in Taiwan to determine the trade-offs between human and ecosystem needs [*Suen and Eheart*, 2006]. A set of six indicators characterizing the difference to the natural hydrographs was defined to determine the ecosystem needs objective (coefficient of efficiency of the yearly trend of the hydrograph, dry season 10-days minimum, wet season 3-days maximum, number of high flows events, mean duration of low flow events and rising rate during wet season). For the human needs objective, three usages were considered: domestic and industrial water supply,

agricultural water and power generation. The conclusion of the authors was that finding the Pareto front of optimal solutions enables water managers to identify operating rules that balance the water needs between human and ecosystem.

Richter and Thomas [2007] described a framework for planning and implementing a dam re-operation project. They separated the approach in six steps: (1) assess dam-induced hydrological alteration based on the RVA approach [*Richter et al.*, 1997], (2) describe ecological and social consequences, (3) specify goals for dam re-operation, (4) design dam re-operation strategies, (5) implement the strategies and (6) assess the results against the goals. For the hydropower systems, they proposed the solution of building a re-regulation reservoir downstream of the dam or use one of the dam already constructed in a cascade as the re-regulation reservoir. In the case of a multi-dam hydropower system, they stated that a computer-based decision support system is one of the most cost-effective ways to optimize the performance by balancing the impact of environmental flow release among the dams.

A reservoir operating approach combining reservoir operating rule curves and e-flow strategy was developed to optimize e-flow provision under given water supply constraints [*Yin et al.*, 2011; 2012]. The flows were divided into four functional components (floods, high-flow pulses, base flows and extreme low flows) and the flow regime alteration was quantified by the range of variability approach (RVA) [*Richter et al.*, 1997], deriving the range of variation for each hydraulic indicator from the natural hydrograph. The case study chosen was the Tanghe reservoir in China's Tang River Basin.

In the first paper [*Yin et al.*, 2011], three e-flow management strategies were defined: (1) a preferred e-flow regime which maintains flow variability as natural as possible applied during wet years, (2) an acceptable e-flow regime for normal years maintaining seasonal base flows with a planned number of high-flow events and (3) a basic regime for dry years concentrating only on the seasonal base flow. The reservoir water level was used as trigger for the different strategies and the reservoir inflow as trigger for different e-flow rules. The planned water supply reliability was fixed to different levels. Only the indicators related to floods and high flow pulses were taken into account for the optimization as including the indicators related to low and extreme low flows would mask the impacts upon high flows events. In the second paper [*Yin et al.*, 2012], multiple water supply reliabilities were fixed and the reservoir operations optimized for each case taking into account both high and low flow indicators. The developed methodology was compared to conventional methods achieving a significant lower degree of flow alteration. The result of the case study showed the tradeoffs between water supply reliability and riverine ecosystem needs.

Ecological and economical profits of dynamic release policies within a diverted river reach were evaluated by Perona *et al.* [2013]. The hydrological differences from the natural flow regime were used as a proxy to assess environmental benefits and the mean of the ratio of the allocated net flows between environment and hydropower was implemented as a suitable engineering parameter to represent their relative value.

A summary of the research done to support possible re-operation of dams in Southern Africa is presented by Brown and King [2012]. For the Zambezi Delta, they stated that there is no e-flow requirement at this stage and that recreating a flood would generate costs in terms of hydropower loss. Discussions are ongoing on the future operating rules of Cahora Bassa, including the new dam projected downstream but they will have little effect as Kariba sited upstream Cahora Bassa is mainly controlling the flooding pattern of the Zambezi. Their conclusion was that implementation of e-flow is still in its infancy in Southern Africa and will take one or two decades to be part of the national legislation.

2.4   CLIMATE CHANGE IN SOUTHERN AFRICA

The Fourth assessment report if the Intergovernmental Panel on Climate Change [*IPCC*, 2007] is the largest and most detailed summary of climate change situation over the world. The climate predictions are based on illustrative emission scenarios based on four groups: (1) the A1 storyline describes a future work of very rapid economic growth with rapid introduction of new and more efficient technology, (2) the A2 storyline describes a very heterogeneous world with a slow economic growth, (3) the B1 storyline describes a convergent world with rapid change in economic structures, (4) the B2 storyline describes an intermediate level of economic development. In Africa, the regional models estimates a larger warming than the global annual mean throughout the continent and in all seasons, with drier subtropical regions warming more than the moister tropics. Rainfall in southern Africa is likely to decrease in much of the winter rainfall region and western margins.

Specific studies about climate change in Southern Africa showed an increase in the severity of dry extremes along with a significant decrease in mean precipitation during austral summer months [*Shongwe et al.*, 2009]. A delay in the onset of the rainy season is found in almost the entire region. The observed and projected changes in the climate of southern Africa in the period 1900–2100 were analyzed by Jury [2013]. Ten observed reanalyzed and model-simulated climate data sets were explored for changes in surface air temperature, rainfall, air pressure, winds, ocean currents and sea surface height. Surface air temperature trends were positive and larger in recent periods leading to a +2 °C anomaly by the end of the 21st century. Rainfall trends were mixed and generally negative across marine latitudes (35–40°S) decreasing from south to north with a deficit of -0.3 mm/day by the end of the 21st century.

Comparing the results from a high-resolution climate change simulation over Southern Africa to those of forcing global model (GCM), Haensler et al. [2011] found that for temperature, the magnitude of the projected changes of the regional model only slightly differs from the GCM and that for precipitation, the regional model showed a more intense drying toward the end of the 21st century than it is simulated by the global model.

Long term hydrological cycles on the Zambezi have been analyzed. Based on recreated rainfall records extending back 200 years to 1800, Mason [2013] identified four separate cycles of 70, 130, 35 and 44 years accounting respectively for approximately 50% of the rainfall variability, 25%, 12.5% and 12.5%. Between 1924 and 2004, the duration of the main

runoff cycle was estimated at about 40 years by spectral analysis but secondary cycles of 10 to 20 years are also present [*Mazvimavi and Wolski*, 2006]. The same analysis conducted between 1950 and 1995 results in a dominant runoff cycle of 5.6 years [*Jury*, 2003]. Finally, an extensive analysis of southern African climate reveals variability patterns with main components of 80 and 18 years [*Tyson et al.*, 2002]. These cycles should be taken into account when evaluating the impact of climate change.

2.5 WATER RESOURCES MODELLING IN THE ZAMBEZI RIVER BASIN

2.5.1 Overview

The Zambezi River Basin is an interesting area to analyze water resources management. Four large dams (Kariba, Kafue Gorge, Itezhi Tezhi and Cahora Bassa) have already extensively change the flow regime in the downstream part of the basin and the extension of the existing infrastructures as well as the construction of new hydropower plants will occur in the near future. Moreover, the development of irrigated agriculture is also foreseen. Several studies have assessed the impact of this economic development on the management of the water resources at monthly time step based on historical flow records.

2.5.2 Kariba operations

Kariba operations have been analysed by Gandolfi and Salewicz [1991]. The management problem is described as a balance between two conflicting objectives: maximize hydropower output and leave a safe capacity at the beginning of the flood season to avoid release through the floodgates. They conclude that a highly reliable firm energy output (firm energy target of 600 GWh/month) can be maintained while keeping low discharge through the floodgates and that an inflow forecasting system would results in significant improvement of the performance of the hydropower plant.

2.5.3 Hydropower optimization model

The entire Zambezi River system performance was evaluated for selected development alternatives [*Gandolfi et al.*, 1997]. The management problem was formulated as a network optimization problem. The energy production was assumed to be a function only of the turbine flow and the hydropower plants were assumed to operate in a cooperative way. The goal of the management was to guarantee the highest firm energy output and achieve the best long-term performance. The model was run at a monthly time step for the period from October 1930 to September 1942 based on available flow records and continuity equations. A dry period from October 1907 to September 1919 was also considered to evaluate the system under extreme conditions. The firm generation power for the reference case reached 3,855 MW and the mean annual output 34,100 GWh/yr. Constraints at the reservoir were set as a minimum flow of 300 m^3/s in March at Itezhi Tezhi and 15 m^3/s spilled from Kafue

Gorge. For the scenarios, the power plant upgrades at Kariba (+534MW), Cahora Bassa (+1200 MW) and at Kafue Gorge (+450 MW) have been considered. The firm power increased to 4,355 MW and the mean yearly output to 39,700 GWh/yr mostly due to the upgrade at Kafue Gorge. By considering new irrigation projects (an increase of the diverted flow in the Kafue flats to 50 m^3/s) the firm power was reduced by 3.5% and the mean yearly output by 2.6%. A greater consideration of the paludal environments was also considered, increasing the constraint on the maximum flow rate at Itezhi Tezhi in March to 600 m^3/s and introducing a constraint of 300 m^3/s in February and April. Furthermore, a minimal flow of 1,800 m^3/s in March downstream Kariba was introduced to preserve Mana Pool ecosystem. The resulting firm power was reduced by 6% compared to the reference case and the mean annual power by 6.5%. They also implemented a constraint on the lake level fluctuation to enable navigation and fishery, which reduces considerably the firm power (84% of the reference case) while keeping the mean yearly output high (97% of the reference case).

An inventory of available water resources was carried out based on available hydro-meteorological data over the year 1956 to 1960 and 1990-1991 selecting a typical dry year and a typical wet year for specific analysis [*Matondo and Mortensen*, 1998a]. The conclusions were that for a typical dry year, the mean annual flow entering the Indian Ocean is 1,812 m^3/s while for a typical wet year it is 6,908 m^3/s.

2.5.4   Hydro-economical optimization model

A trade-off relationship between hydropower generation and ecological preservation was illustrated with the Zambezi River Basin [*Tilmant et al.*, 2010a]. The reservoir operating policies are optimized for three different scenarios: the first focussing on hydropower generation, the second giving a low value to environmental flow release and the third giving a high value to environmental flow release. The optimization problem is solved using stochastic dual dynamic programming. Only the flows in the Zambezi Delta are considered for environmental flow release, fixing a target pulse of 7,000 m^3/s in February and March. The model determines reservoir release, spills and end-of-period storage maximising the economic net benefit over a planning period of 120 months with 50 optimization sequences. The inflows were calculated based on historical data available. The difference to the model used by Gandolfi et al. [1997] reside in the stochastic approach, the economic objective function and the insertion of environmental flow in the objective function instead of defining them as constraints. The demand curve for the environmental flow is defined in two blocks: positive value from 0 to 7,000 m^3/s (3.4 USD/m^3 and 34 USD/m^3) and no value beyond. Energy prices are assumed to be stable at 80 USD/MWh. The results showed that increasing peak discharge in the delta is only possible through larger spills from Cahora Bassa as the turbine are already discharging at maximum capacity and that this reduces the turbine outflow during the dry season in order to refill the reservoir. The need for a basin-wide approach is emphasized as Kariba dam should compensate for Cahora Bassa spills during dry years. The average annual energy output without environmental flows consideration is 30,828 GWh/yr. It is reduced by 6% in the case of high economic value attributed to environmental floods and by 1.4% in the case of low valuation of environmental floods.

The same hydro-economic model was used to assess two questions: the cost of noncooperation in the Zambezi basin [*Tilmant and Kinzelbach*, 2012] and the economic valuation of coordinated development in the basin [*Tilmant et al.*, 2012]. Both studies used the same 50 hydrologic sequences of 120 month generated based on 30 years of monthly historical natural discharge. The simulation results were analyzed for year five only. The modeling framework captures the spatial and seasonal variability of river discharge but not the presence of multi-year cycles or climate change.

The cost of noncooperation was estimated by modeling two development scenarios with the future infrastructures (irrigation and hydropower plants) in an advanced stage. In the first scenario, the irrigation withdrawals were imposed to the system; a fixed volume of water is diverted to the irrigation schemes independently of both their productivity and the hydrologic status of the system. In the second scenario, the model determines the optimal allocation policies according to the productivity of the users. The average energy price was assumed to be 60 USD/MWh and the net agricultural margin was estimated to 300 USD/ha. The simulation results gave the turbine outflow, spills, storage levels, irrigation withdrawals (for the second scenario) and marginal water values. The comparison between total benefits obtained with the two scenarios showed that the upstream countries will have little incentive to move toward a cooperative framework as they would lose their irrigated agriculture to increase energy generated downstream. In conclusion, developing irrigation projects unilaterally would cost 10% of the total benefits in the Zambezi Basin [*Tilmant and Kinzelbach*, 2012].

The model structure with the largest existing and planned hydraulic infrastructure and irrigation schemes was used to derive basin wide allocation policies [*Tilmant et al.*, 2012]. The question answered were: what would be the economically efficient balance between irrigated agriculture and hydropower generation in the Zambezi, what is the economic value of the three largest existing dams on the basin and where should water be withdrawn for irrigation taking into account the planned hydropower projects and the productivity of the wetland. Four scenarios were tested: (1) energy security (no value to environmental flow, dynamic water allocation for irrigation and new hydropower plants), (2) food security (environmental flows valued, static water allocation for irrigation and new hydropower plants), (3) balanced situation (environmental flows valued, dynamic water allocation for irrigation and new hydropower plants) (4) environmental integrity (no value to environmental flows, dynamic water allocation for agriculture, run-of-river hydropower plants). The energy generated value was estimated at 40 USD/MWh. The value assigned to irrigation water was 50 USD/1,000 m^3 and the value attached to the wetland was 10 USD/1,000 m^3 up to the target flow and zero beyond as excess water is valueless. The results of the simulation showed that (1) the maximum potential hydropower generation can be achieved only if the riparian countries agree to lose 28% of the benefits from irrigation, (2) the maximum productivity of irrigated agriculture would reduce by 10% the maximum energy production, (3) the presence of reservoirs increases by 24% (to 63,000 MWh) the average annual energy produced. In terms of spatial distribution, upstream farmers must be highly productive in order to compete with the cascade of power stations.

2.5.5   Simulation model

Another simulation model using 97 years of historical flow series was developed to assess the trade-offs between environmental flows and hydropower generation in the Lower Zambezi Basin [*Beilfuss*, 2010]. HEC-5 model version 8 (a multi-purpose multi-reservoir routing program) was selected to model water availability. The period from 1907 to 2004 was simulated at a monthly time step and a range of scenarios for environmental flow release from Cahora Bassa were tested. The results showed a decrease in average annual energy production of more than 10% to reproduce environmental flow over four or five months. To limit the influence on energy production (less than 3% reduction in average annual power), the environmental flow can only be defined for a two-month period. The options to recreate flood pulse without affecting the energy production would be to release an early flood (December-January instead of March), to change the operating rule curve to a flat rule curve or to operate Kariba and Cahora Bassa conjunctively.

2.5.6   Multi-sector investment opportunities analysis

The World Bank led a multi-sector investment opportunities analysis for the Zambezi Basin [*The World Bank*, 2010]. A set of development scenarios (Table 2-2) was tested in a coupled hydro-economic model. HEC-3 modeling package was adopted for the analysis at a monthly time step. The simulation period goes from October 1962 to September 2002. The results showed that the implementation of all presently identified irrigation projects without further development of hydropower would reduce the firm energy produced by 21% and the average energy by 9%. If both new irrigation projects and new hydropower projects are developed, the reduction would be about 8% for firm energy and 4% for average energy. Coordinated basin-wide operation of existing hydropower would increase the firm energy production by 7% and the same principle applied to the new projects would generate a gain of 23%. Restoring natural flooding in the delta would cause a reduction in hydropower production varying from 3 to 33% for Cahora Bassa dam and from 4 to 34% for the planned Mphanda Nkuwa dam.

Table 2-2. List of the scenarios tested by the World Bank based on [*The World Bank*, 2010]

Scenario	Hydropower development	Irrigation development	Natural flooding in the lower delta (7'000 m^3/s in February)	Climate change	Flood protection in Tete (max of 10'000 m^3/s)
Current situation	No	No	No	No	No
Coordinated operation of key existing HP	No	No	No	No	No
Development of HP (up to 2025)	Yes Yes Yes (with coordination)	No No No	No Yes No	No	No
Existing HP + irrigation projects + e-flows	No	Yes (two levels of development)	Yes	No	No
Development of HP + irrigation projects + e-flows	Yes	Yes (two levels of development) (with or without cooperation)	Yes	No	No
Development of HP + development of irrigation + e-flows + climate change	Yes	Yes	Yes	Yes	Yes
Restoring natural flooding in the delta + Flood protection	Yes	No	• 4'500, 7'000 and 10'000 m^3/s in February • 4'500, 7'000 and 10'000 m^3/s in December	No	With and without flood protection

2.5.7   Water demand and climate change

A comprehensive set of water demand and climate change scenario until 2050 was combined to a hydrological model in order to estimate freshwater availability in key parts of the Zambezi Basin [*Beck and Bernauer*, 2011]. Three scenarios were implemented: the first consisting in minor change in demand, the second combining moderate demand to moderate climate change and the third combining strong demand and large climate change. Four sector of water demand were simulated varying spatially and temporally: agriculture, hydropower production, domestic sector and industrial sector. The potential new hydropower production sites were included in terms of increased water consumption through evaporation from reservoirs but their influence on flow was not modeled. The projects taken into account were Cahora Bassa extension, Mependa Uncua and Lower Kafue for the moderate growth scenario, Cahora Bassa extension, Mependa Uncua, Lower Kafue, Boroma, Lower Fufu, Rumukali,

Revubue projects, Kapache and Angola projects for the medium growth scenario and Cahora Bassa extension, Mependa Uncua, Lower Kafue, Chemba, Batoka Gorge, Devils Gorge, Luapata, Mupata Gorge for the accelerated growth scenario. The results showed a mean annual flow reduction across all sub-basins of respectively 4%, 31% and 77% for the three scenarios. The impact of Victoria Falls for the third scenario implies no discharge during eight months per year. For hydropower production, the most dramatic changes would be at Kariba dam (no production for the third scenario). The wetlands would experience flow reduction up to 85%, the Barotse plain being the most affected since no regulation structure is present upstream.

2.5.8   Synthesis

To synthesise the presented studies (Table 2-3), a wide range of environmental flows have been defined and tested for the Zambezi delta. The Kafue flat and the Mana Pool have also been taken into account in some of the studies but less extensively. The most advanced hydropower plant projects have been included in the analysis as well as the new irrigation projects. Optimal flow allocation was assessed by pricing the irrigated land and the energy generated, considering the environmental flow as constraints [*Gandolfi et al.*, 1997] or setting a value for the flooded area [*Tilmant et al.*, 2010a; *Tilmant et al.*, 2012]. Different economic development scenarios including environmental flows and irrigated area as constraints were simulated and their impact on energy production was assessed [*Beilfuss*, 2010; *The World Bank*, 2010]. However, none of the study has assessed the state of the basin at a daily time step which is of relatively high importance considering that the future hydropower production will be more fluctuating following the energy prices. The presented research work combines a detailed simulation of the hydropower production at the existing and future sites to an assessment of their impact on environmental flow based on documented indicators. The multi-objective analysis is based on the simulation of scenario at daily time step at a finer spatial resolution than the previous studies.

Table 2-3. Summary of the main results of the previous study concerning water resources management in the Zambezi basin

Title of the study	Period	Scenarios	Firm power MW]	Mean annual power [GWh/year]
Optimal flow allocation in the Zambezi River System [*Gandolfi et al.*, 1997]	1930-1942	Reference case	3,855	34,100
		Upgrade at Cahora Bassa, Kariba and Kafue	4,355 (+13.0%)	39,700 (+16.4%)
		Irrigation from the Kafue river	3,719 (−3.5%)	33,200 (−2.6%)
		E- flows in the Kafue flats and the Mana Pools	3,626 (−5.9%)	31,940 (−6.3%)
Restoring a flow regime through the coordinated operation of a multireservoir system: the case of the Zambezi River basin [*Tilmant et al.*, 2010a]	50 hydrologic sequences of 10 years based on time series of historical natural discharge	Reference case	-	30,928
		High value for e-flows (delta)		28,966 (−6%)
		Low value for e- flows (delta)		30,392 (−1.4%)
Modeling trade-offs between hydropower generation and environmental flow scenarios: a case study of the Lower Zambezi River basin [*Beilfuss*, 2010]	1907-2004	Reference case	-	14,393
		10 scenarios mimicking unregulated mean monthly flows over 5 month		12,552-14,225 (−1.2%-−13.6%)
		Release of 2000 to 8000 m^3/s between December and March		12,873-14,336 (−0.4%-−10.6%)
The Zambezi River basin a multi-sector investment opportunity analysis [*The World Bank*, 2010]	1962-2002	Current situation	2,609	30,298
		New hydropower plants	4,452 (+71.2%)	60,760 (+100.5%)
		New hydropower plants and e- flows	4,030 (+55.0%)	59,304 (+95.7%)
		Existing hydropower plants, new irrigation projects and e- flows	2,061 (−20.7%)	27,629 (−8.8%)
		New hydropower plants, new irrigation projects and e- flows	3,694 (+42.1%)	56,993 (+88.1%)
Economic valuation of benefits and costs associated with the coordinated development of the basin [*Tilmant et al.*, 2012]	50 hydrologic sequences of 10 years based on time series of historical natural discharge	Reference case (existing and planned hydraulic structures)	-	63,000
		Priority given to irrigated agriculture		57,140 (−9.3%)
		Taking the value of wetland into account		60,390 (−4.1%)
The cost of non cooperation in international river basins [*Tilmant and Kinzelbach*, 2012]	50 hydrologic sequences of 10 years based on time series of historical natural discharge	Existing and planned hydraulic structures with priority given to the agricultural sector	-	53,050
		Existing and planned hydraulic structures with optimization of water allocation		58,820

3 CASE STUDY AND MODEL DESCRIPTION

This chapter provides a general description of the studied river basin. The existing and planned hydropower schemes are presented as well as the other water demands over the basin. The results of the past attempt to model the hydrology of the Zambezi River Basin are discussed. Finally, the hydrological model used is introduced. At first, the general equations are described and then the specific modules developed in the frame of the presented study are detailed. At last, the input data and the model set-up are presented.

3.1 INTRODUCTION

The Zambezi river basin, located in the South of the African continent, is shared by eight countries, making it a particularly interesting system to further investigate the implementation of IWRM's (Integrated Water Resources Management) principles. From its headwaters in Angola to the delta in Mozambique, the Zambezi River runs over 2600 km and connects eight African nations that share different portions of its 1.4 M km^2 large drainage basin (Figure 3-1): Angola (18.3%), Namibia (1.2%), Botswana (2.8%), Zambia (40.7%), Zimbabwe (15.9%), Malawi (7.7%), Tanzania (2.0%) and Mozambique (11.4%) [*Vörösmarty and Moore III*, 1991]. The basin lies fully within the tropics between 10° and 20°S encompassing humid, semi-arid and arid regions dominated by seasonal rainfall patterns associated with the Inter-Tropical Convergence Zone (ITCZ). The ITCZ is a convective front oscillating along the equator. It moves from 6°N to 15°S from July to January and back North from February to June. Associated with it, the peak rainy season occurs during the Southern hemisphere summer (from October to April) and the winter months are dry. Rainfall varies considerably from year to year. The diurnal cycle of precipitation depends also on the ITCZ. Usually, clouds form in the late morning and early afternoon hours and then by the end of the afternoon, convectional short thunderstorms form and precipitation begins. The yearly cumulated rainfall over the entire basin is about 1000 mm yr^{-1} and the potential evaporation reaches 2000 mm yr^{-1}. The mean annual discharge at the delta is of 3800 m^3/s [*Tilmant et al.*, 2010a].

The annual flow series registered at Victoria Falls (from 1907 to present) reveals long-term (inter-annual) cycles of high, medium, and low runoff. More precisely, the flow was below average from 1907 to 1924, above average from 1947 to 1981, and finally below average from 1981 to date [The World Bank, 2010]. Between 1924 and 2004, the duration of the main runoff cycle was estimated at about 40 years by spectral analysis but secondary cycles of 10 to 20 years are also present [*Mazvimavi and Wolski*, 2006]. The same analysis conducted between 1950 and 1995 results in a dominant runoff cycle of 5.6 years [*Jury*, 2003]. Finally, an extensive analysis of southern African climate reveals variability patterns with main components of 80 and 18 years [*Tyson et al.*, 2002]. It is therefore very difficult to get a time series of observed data which covers the whole cycles. Since in the Zambezi area the runoff cycles have been reported to be primarily explained by rainfall cycles [*Beilfuss and Dos Santos*, 2001; *Farquharson and Sutcliffe*, 1998], the hypothesis adopted in this study is that the model is able to reproduce the observed cycles even if it is not calibrated over the entire range of conditions.
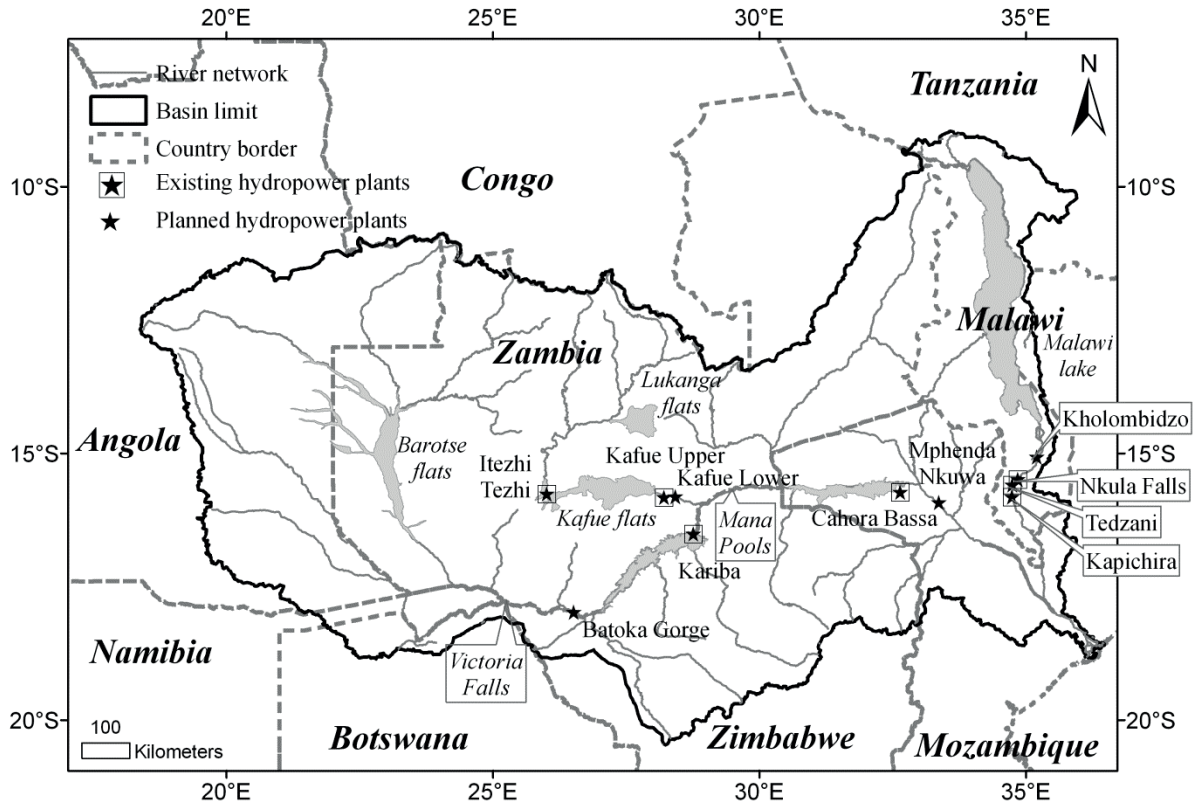
Figure 3-1. Basin map with the river network, the principal flats and lakes, the country borders and the main existing hydropower plants as well as the planned schemes.

The river can be separated in three distinct stretches: the Upper Zambezi, the Middle Zambezi and the Lower Zambezi [*Beilfuss and Dos Santos*, 2001; *Moore et al.*, 2007]. The upper Zambezi is characterized by the Northern Highlands where the river rises and the Central Plains constituted by two major wetlands attenuating the runoff: the Barotse and the Chobe Flats (Figure 3-1).

Between Victoria Falls and Cahora Bassa reservoir, the river drains the middle Zambezi catchment. The main impoundment is the Kariba reservoir, regulating more than 50% of the catchment. Downstream of Kariba and before Cahora Bassa two large tributaries flow into the Zambezi River: the Kafue and the Luangwa Rivers. The hydrological processes in the Kafue Basin are particularly complex with the influence of massive floodplains (the Lukanga and the Kafue flats) and two large dams (Itezhi-Tezhi and Kafue Gorge) (Figure 3-1). The Itezhi-Tezhi reservoir controls about 70% of the total Kafue catchment.

The lower Zambezi is a complex physical system with narrow gorges and a large delta of mobile reaches. The major tributary is the Shire River originating as outflow from the Malawi Lake, the only large natural lake of relevant proportions in the Zambezi Basin.

41

3.2 HYDROPOWER PRODUCTION

The use of the potential of Zambezi River is currently mainly limited to hydropower production through a series of large impoundments: Kariba Dam, between Zambia and Zimbabwe; the Kafue hydropower scheme in Zambia; and Cahora Bassa Dam in Mozambique.

The hydropower sector is by far the highest water user because of the evaporation from hydropower reservoirs [*Euroconsult Mott MacDonald*, 2007]. The total annual evaporation from the existing reservoirs has been estimated at approximately 17 billion m^3 from what 85% is lost by Kariba and Cahora Bassa reservoirs [*Denconsult*, 1998].

The characteristics of the existing and the projected hydropower plants included in the model are presented in the Table 3-1. All new projects as well as the existing dams are illustrated on the Figure 3-2.

To determine the actual operation rules of the existing hydropower plants, the observed data (water level and outflow) have been analysed and compared to the flood rule curve as defined in the World Bank report [*The World Bank*, 2010].
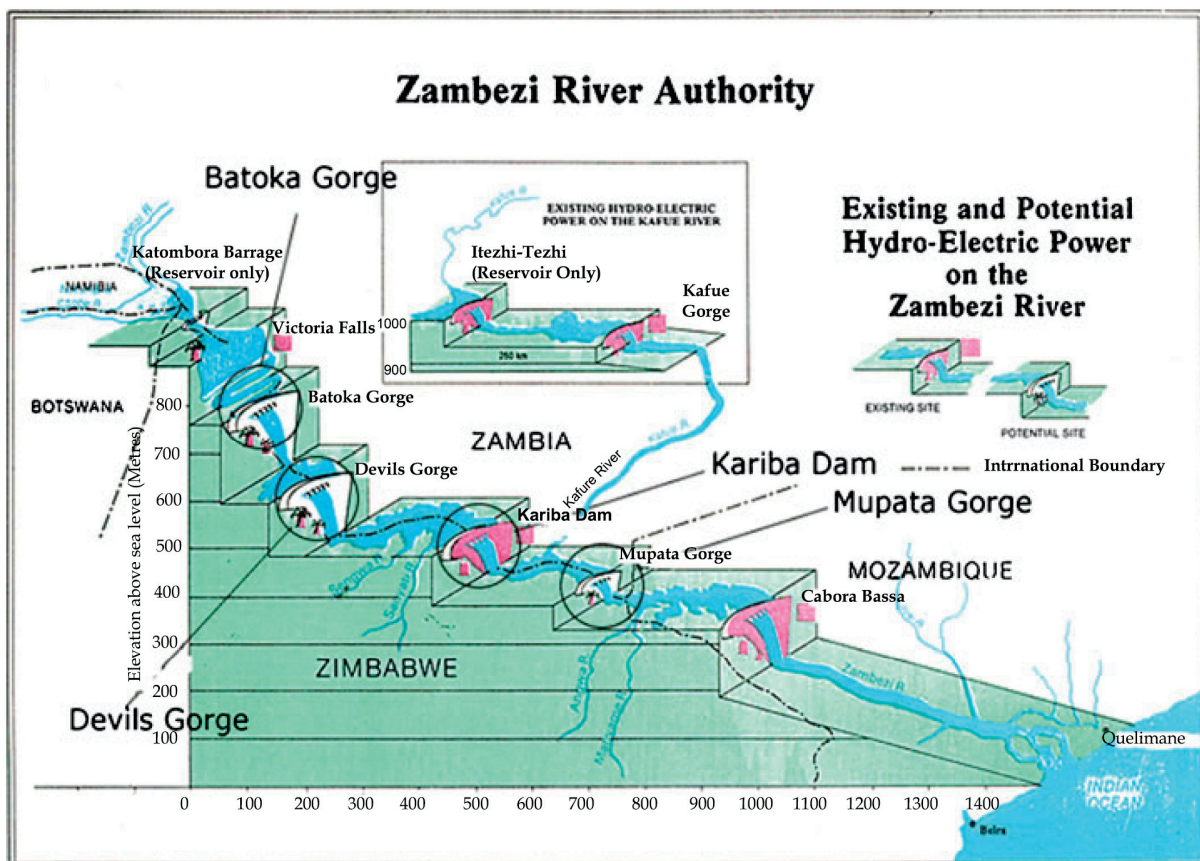

Figure 3-2. Schematic layout of the actual proposed and existing hydroelectric power schemes on the Zambezi River Basin [from *Yamba et al.*, 2011]

3.2.1   Kariba dam

Kariba dam was built in 1955-59. With a storage capacity of 180km^3, extending over a length of about 300km, and having a surface area of some 5500km^2 at full supply level, is one of the largest reservoirs in the world [*Soils Incorporated (Pty) Ltd and Chalo Environmental and Sustainable Development Consultants*, 2000]. It is currently owned by two countries: Zimbabwe and Zambia and provide hydropower to both of the countries. The two power stations located on the left and right banks were originally constructed with a combined generating capacity of 1200 MW and recently undergone plant refurbishment that increased the capacity to 1450 MW. The spillway capacity was designed at 9500 m^3/s.

The downstream hydrological impacts of Kariba Dam extend all the way to the Indian Ocean. The seasonal high and low floods do not occurs as much as they did before Kariba and the delta floodplain ecology has been negatively affected (decrease of shrimp catches, invasion by upland vegetation and decrease of productivity in the fisheries,...) [*Magadza*, 2010; *Soils Incorporated (Pty) Ltd and Chalo Environmental and Sustainable Development Consultants*, 2000]. The impressive plunge pool scour hole of almost 90 m beneath the tailwater level developed just below the dam arch is known worldwide since it is an unprecedented value in dam history [*Bollaert et al.*, 2013].

For Kariba dam (Figure 3-3), the observed outflow is available only at monthly time step. The upgraded turbine capacity is of 1800 m^3/s but has rarely been reached. The turbine discharge seems to be around 1200 m^3/s and constant trough the year. In terms of water level, the dam is operated below the flood rule curve following the design as the level is reduced before the flooding season (minimum level in January). The spillways have been rarely used during the period from 1998 to 2006 and never to their full capacity (9,500 m^3/s). Due to the problem of the plunge pool erosion, the operations planning aims to reduce the use of the spillway to the minimum possible.
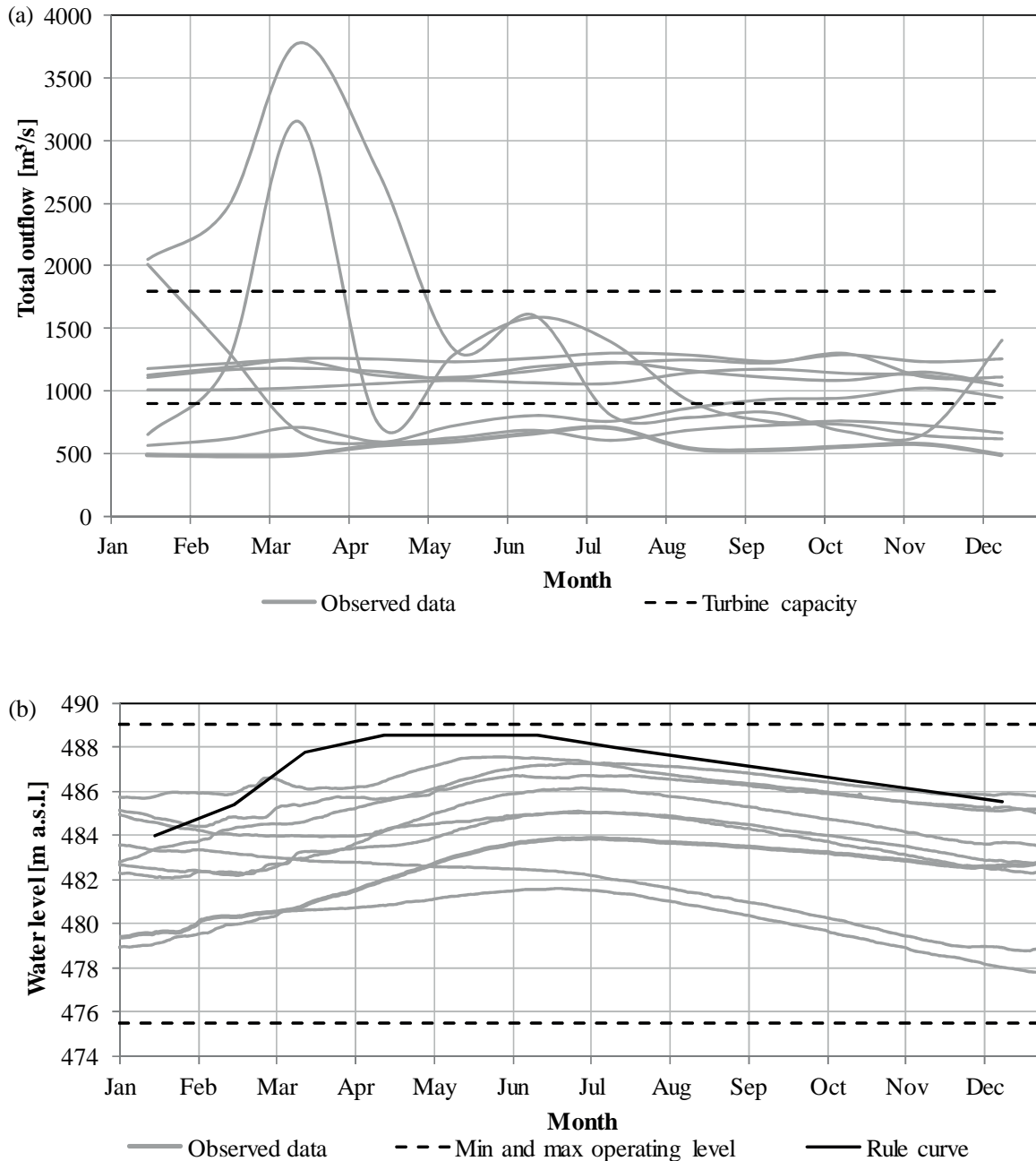
Figure 3-3. Observed outflow (a) and water level (b) at Kariba dam for the years 1998 to 2006.

3.2.2   Kafue hydropower scheme

The Kafue Gorge dam was built in 1971 on the Kafue River downstream the Kafue flats. Its power plant capacity is of 900 MW. However, due to the low topography of the reservoir, a second dam, the Itezhi Tezhi dam, was necessary to guaranty the minimum flow of 120 m³/s corresponding to a firm energy target of 430 MW [*McCartney and Houghton-Carr*, 1998; *Obrdlik et al.*, 1989].

The Itezhi Tezhi (ITT) dam was therefore built in 1977 upstream the Kafue flats on the Kafue River for the main purpose of providing additional discharge during the dry season to

the downstream Kafue Gorge Dam, both dams being operated by the Zambian Electricity Supply Corporation (ZESCO). The spillway has a design discharge capacity of about 4500 m³/s. Regulating the flow of the Kafue River had a huge impact on the Kafue flats in terms of nutrient transport and flooding extension [*Kunz et al.*, 2011a; *Wamulume et al.*, 2011].

Itezhi Tezhi dam was designed to produce routed outflow for the Kafue Gorge dam located below. Consequently, it releases a constant flow of about 100 m³/s through the year and uses its storage capacity to transfer a part of the flood volume to the dry season (Figure 3-4). The water levels show that the flood rule curve is approximately followed by the operations.
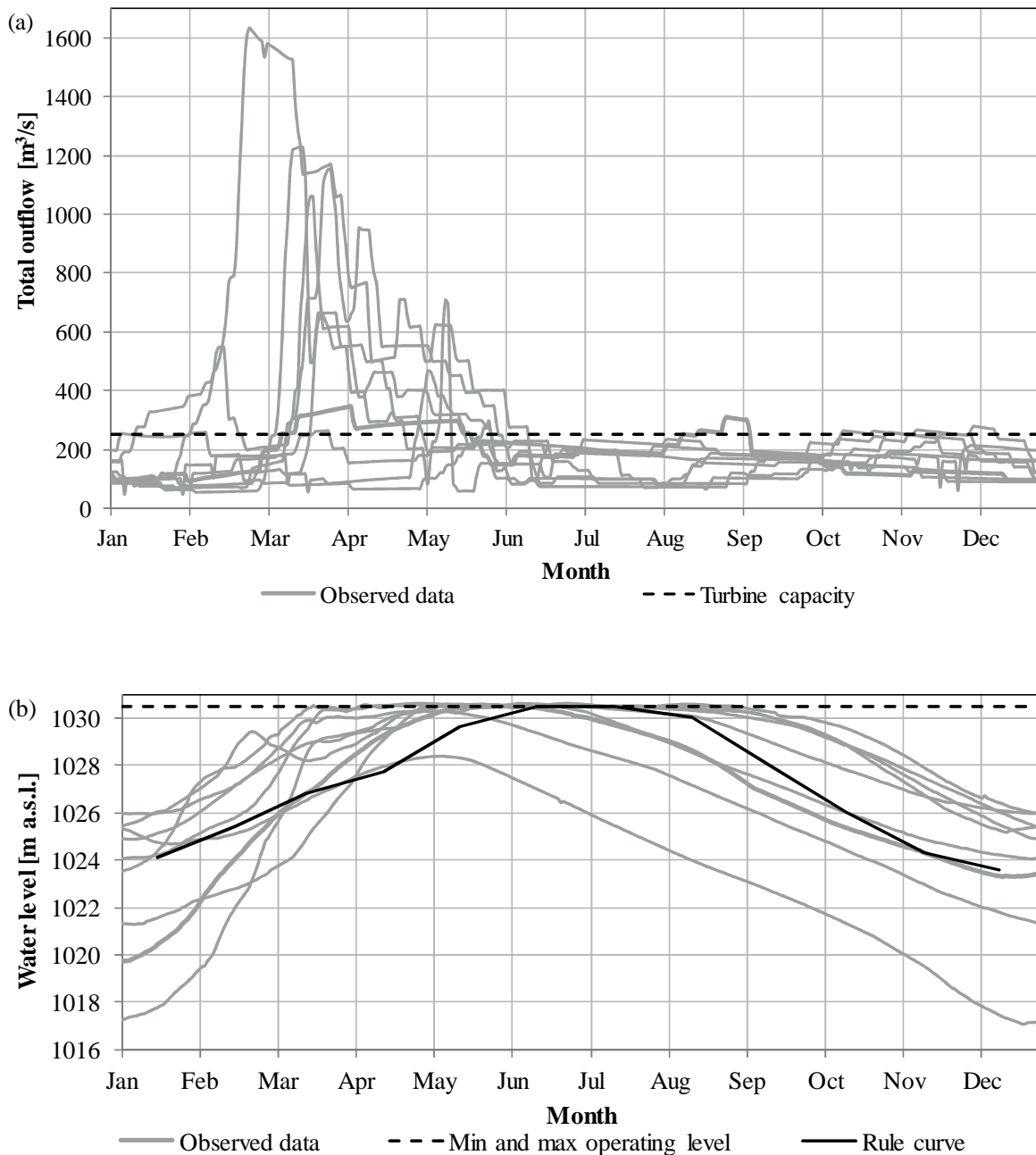
Figure 3-4. Observed outflow (a) and water level (b) at Itezhi Tezhi dam for the years 1998 to 2006.

At Kafue Gorge dam (Figure 3-5), the turbinated outflow seems to be around 170 m^3/s and the flood rule curve is not followed for the operation.
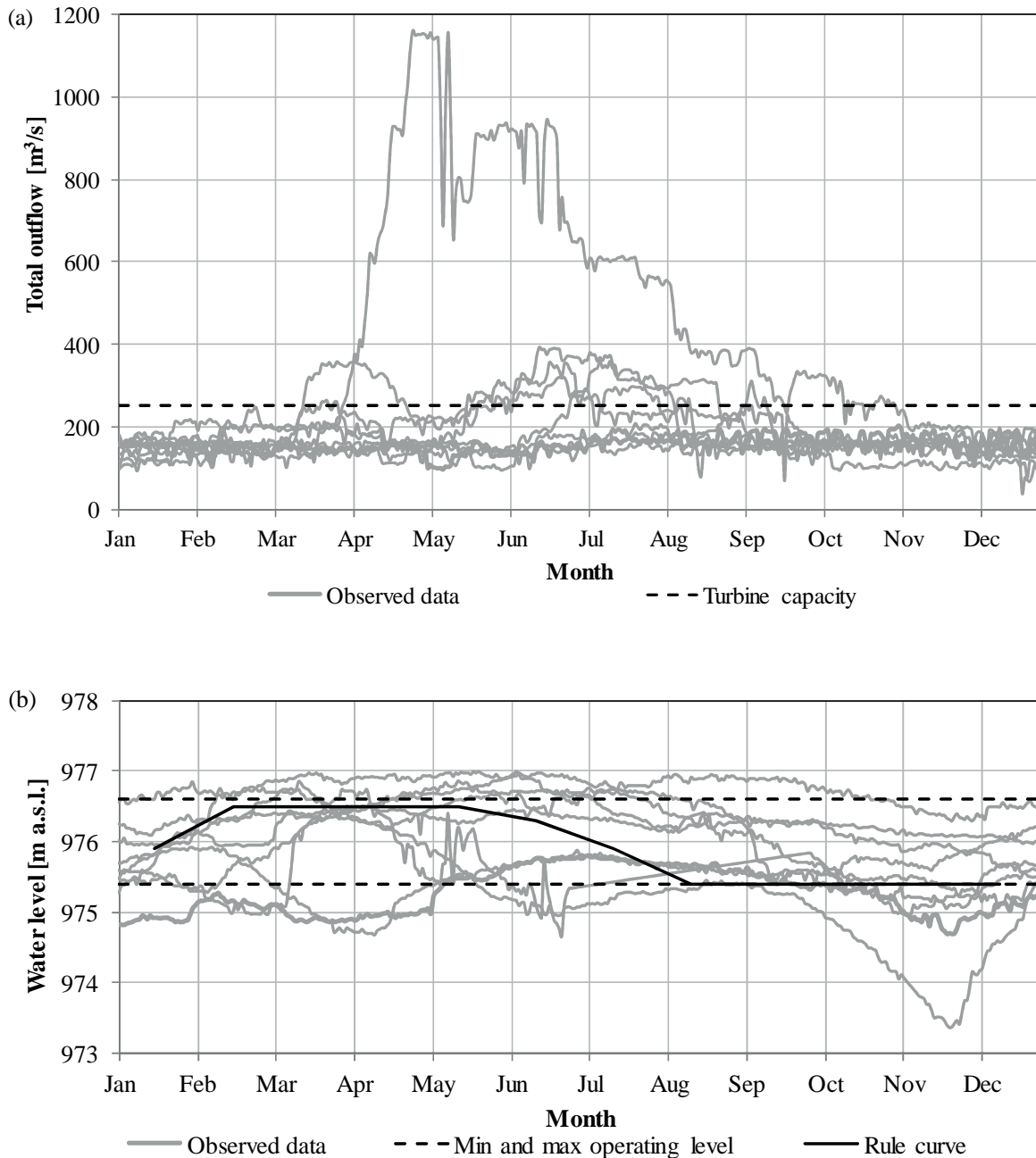
Figure 3-5. Observed outflow (a) and water level (b) at Kafue Gorge dam for the years 1998 to 2006

3.2.3   Cahora Bassa dam

The Cahora Bassa Dam was completed in 1974 with the primary objective to export power to South Africa. However, due to the civil war, the transmission line was destroyed and for 20 years, almost no electricity was produced. The hydropower station was reoperated from 2000 and nowadays delivers about 2000 MW power to South Africa operated by the Mozambican Hydroelectric Company Hidroelectrica de Cahora Bassa (HCB). Its spillways

capacity of about 16,000 m^3/s is inadequate to handle extreme floods so the reservoir level has to be drawn down before the flooding season [*The World Bank*, 2010].

The data received from the operator of Cahora Bassa dam separated the turbine and the spilled outflow (Figure 3-6). It is therefore clearly visible that the five turbines are never operated at the same time (Figure 3-6, a). The averaged discharge at the turbines is about 1,600 m^3/s whereas the full turbine capacity would reach 2,250 m^3/s. The flood rule curve is globally followed by the operators. The year 2001 was characterized by an extreme high level in the reservoir and the opening of all spillways in emergency to lower the level.
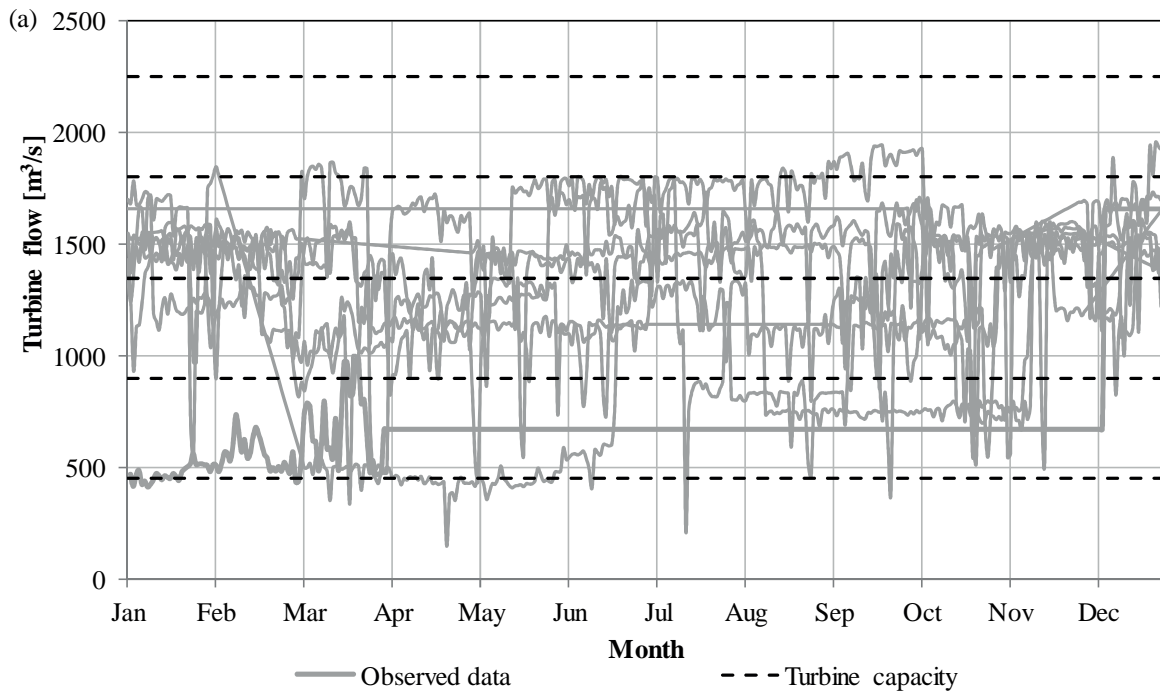
Figure 3-6. Observed turbine outflow (a), spilled outflow (b) and water level (c) at Cahora Bassa dam for the years 1998 to 2006.
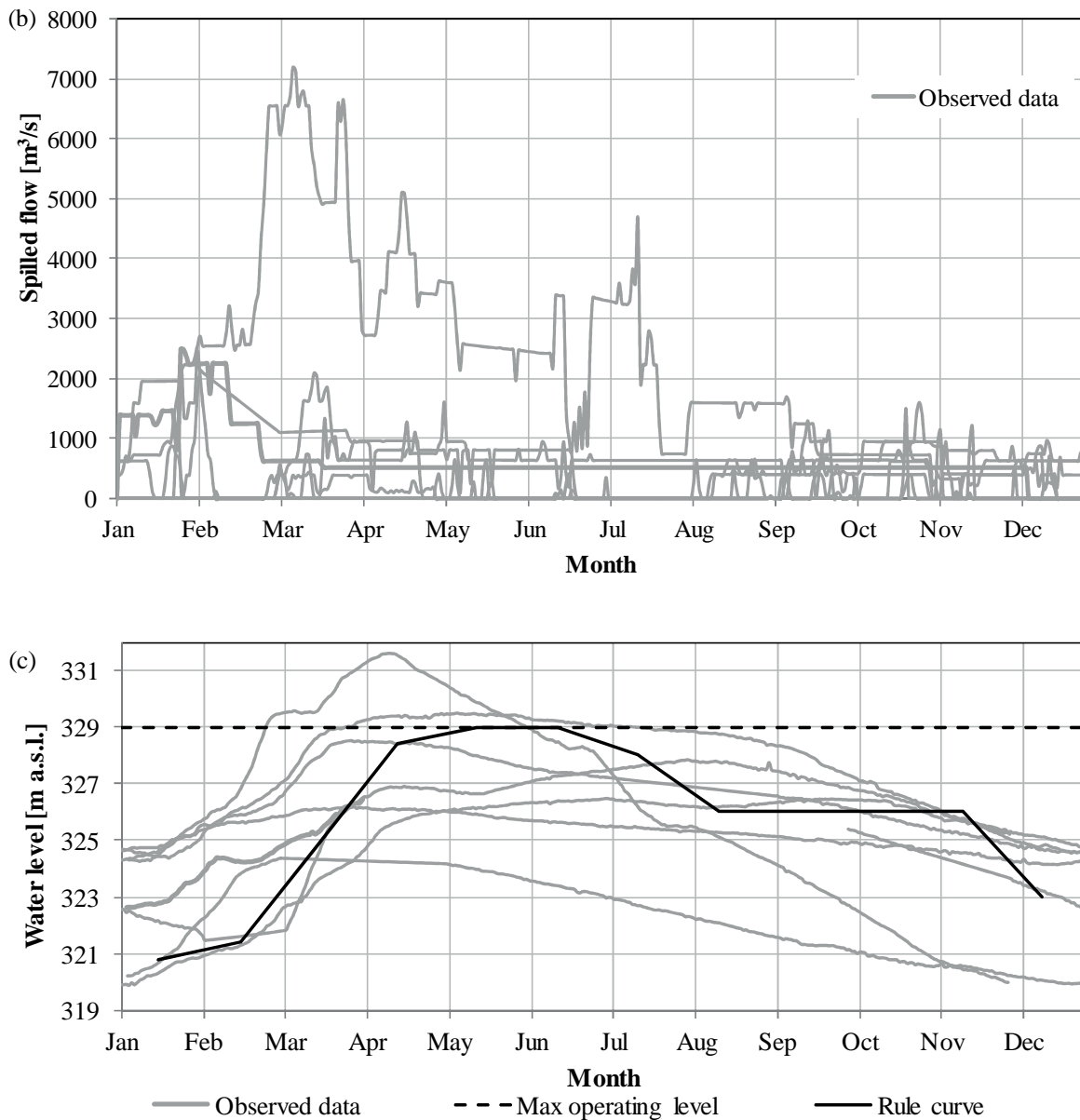
Figure 3-6 (following). Observed turbine outflow (a), spilled outflow (b) and water level (c) at Cahora Bassa dam for the years 1998 to 2006.

3.2.4 New hydropower plants and extensions

The new hydropower projects included are the following: the Batoka Gorge dam, the Kafue Gorge Lower dam and the Mphanda Nkuwa dam. Moreover, four extensions of existing hydropower plants are considered: the Kariba North and South bank extensions, the Itezhi Tezhi power extension, the Cahora Bassa North Bank extension and the Kapichira extension.

The **Batoka Gorge** hydropower project, bilateral between Zambia and Zimbabwe, is considered for development in the medium term. The relatively small storage means that the

plant is intended to operate as a run-of-river plant maximising firm power delivery on a system level [*G P Harrison and Whittington*, 2002].

Two **extensions** have been developed for **Kariba** in both banks. On the North bank (Zambian side), the new powerhouse of about 360 MW is actually under construction by Sinhydro. On the South bank (Zimbabwean side), the extension is planned for the medium term.

The **Itezhi Tezhi power extension** would not be operated to firm up energy but rather to generate available energy in accordance with reservoir variation as the reservoir is used for regulation of the Kafue Gorge Upper dam [*The World Bank*, 2010]. As Zambia has a large power deficit, the project is on fast-track for development. In the medium term, the construction of **Kafue Gorge Lower** is also foreseen.

The **Cahora Bassa North Bank extension** consists in a new underground powerhouse. Combined with a new spillway, it would allow operation of the Cahora Bassa reservoir without lowering the lake level before the high flow period (flat rule curve) [*The World Bank*, 2010]. The impact of using a flat rule curve (at 326 m a.s.l.) for hydropower generation would result in an increase of nearly 6% of the firm power generated in the actual state [*Beilfuss*, 2010].

The **Mphanda Nkuwa** project is located 70 km downstream Cahora Bassa. Two options of operation have been proposed, a run-of-river plant or a peaking mode plant which would necessitate a reservoir downstream for reregulation [*The World Bank*, 2010].

Table 3-1. Characteristics of the existing and projected hydropower plants included in the model.

Reservoir name		Commissioning year	Operation level	Volume	Reservoir area	Turbine capacity planned (observed)		Spillway capacity and associated water level		Tailwater level and associated discharge	
			[m a.s.l.]	[10^9m^3]	[10^6m^2]	[m^3/s]	[MW]	[m^3/s]	[m a.s.l.]	[m a.s.l.]	[m^3/s]
Itezhi Tezhi	Max	1977	1030.5	6.00	380	160	-	4425	1030.5	-	-
	Min		1006.0	0.78	90			402	1020.0	-	-
Itezhi Tezhi power extension		*2013*				*312*	*120*			*1003.3*	-
Kafue Gorge (upper)	Max	1972	976.6	0.90	750	252 (170)	900	3600	978.0	572,1	-
	Min		975.4	0.13	180			780	972.3		
Kafue Gorge (lower)	*Max*	*2017-2022*	*582.0*	*0.06*	*1.5*	*442*	*750*	*5200*	*582.0*	*389.6-*	-
	Min		*530.0*	*0.01*	*0.5*			*780*	*560.0*		
Batoka Gorge	*Max*	*2023-2024*	*762.0*	*1.68*	*26*	*1100*	*1600*	*20000*	*765.0*	*597.2*	-
	Min		*746.0*	*1.29*	*22*			*7200*	*762.0*		
Kariba	Max	1961	489.0	191.0	5627	1800 (1200)	1470	9402	488.6	403.0	10100
	Min		475.5	116.0	5300			8502	484.0	392.0	400
Kariba North bank extension		*2012-2014*				*+430*	*+360*				
Kariba South bank extension		*2014-2016*				*+370*	*+300*				
Cahora Bassa	Max	1974	329.0	63.0	2974	2250 (1600)	2075	15683	331.0	232.0	22000
	Min		295.0	12.2	838			6760	295.0	221.0	500
Cahora Bassa extension		*2013*				*3200*	*2925*	*18700*	*331*		
Mphanda Nkuwa	*Max*	*2024*	*210.0*	*2.5*	*100*	*2450*	*1500*	*33000*	*207.0*	*137.7*	-
	Min		*195.0*	*2.0*	*80*			*10000*	*195.0*		
Kholombidzo	*Max*	*2025*	*475.3*	*0.9*	*152*	*372*	*240*	*5000*	*475.3*	*402.2*	-
	Min		*471.0*	*0.4*	*92*			*1000*	*471.0*		
Nkula Falls	Max	1966	378.5	7.0	0.4	246	124	5000	378.0	319.9	-
	Min		377.0	4.0	0.3						
Tedzani	Max	1973	320.0	5.0	0.8	276	92	5000	320.0	282.4	-
	Min		315.0	3.0	0.6						
Kapichira	Max	2000	147.0	20.0	2.0	134	64	5000	146.5	92.3	-
	Min		144.6	9.0	1.5						
Kapichira extension		*2010*				*268*	*128*				

3.3 OTHER WATER DEMANDS

3.3.1 Irrigation demand

Agriculture in the Zambezi Basin is largely rain-fed or flood-dependent [*Euroconsult Mott MacDonald*, 2007]. The combined water use for irrigation in 1995 was estimated at 1'472 Mm^3 corresponding to an area of 171'600 ha [*Denconsult*, 1998]. According to the Food and Agriculture Organisation (FAO), the irrigation potential in the Zambezi River Basin is more than 7 million ha, of which only 5% is already developed. The additional water demand for 2025 is projected to 4'635 Mm^3 at maximum development [*Euroconsult Mott MacDonald*, 2007].

To test the influence of irrigation on development scenario, an irrigation intensity of 1.3 m^3/m^2 per year can be assumed for the new projected irrigated area [*Beck and Bernauer*, 2011]. A finer alternative is to used typical crop water requirements calculated for the different countries [*Denconsult*, 1998] based on CROPWAT/CLIWAT [*Allen et al.*, 1998] as did Tilmant and Kinzelbach [2012]. In the Kafue basin, a discharge of 15 m^3/s is actually released from Kafue Gorge for agricultural uses. An increase of the diverted flow to 50 m^3/s would allow the irrigation of about 30'000 ha [*Gandolfi et al.*, 1997].

3.3.2 Domestic and industrial water demand

The total number of people living in the Zambezi Basin was close to 30 million in 2005/6 [*Euroconsult Mott MacDonald*, 2007] based on the Gridded Population of the World version 3 (GPWv3). In terms of spatial distribution, more than 85% of the basin population live in Malawi close to the Shire River, in Mozambique, in the Kafue sub-basin (Zambia) and in Zimbabwe. The population density in the upper sub-basins is very low.

Part of the water used by domestic and urban user is derived from groundwater sources. As such it does not directly affect the Zambezi. Reliable data on this water use is not readily available. Estimation has been made for 2005 based on multiple assumptions of less than 200 Mm^3 with a consumption of 85 litres/day/capita in the cities and 20 litres/day/capita in the rural area.

The basin population is forecasted as about 47 million by 2025 with a trend toward urbanization. Taking into account an increase in living standards, the total annual consumption is projected to be about 700 Mm^3 [*Euroconsult Mott MacDonald*, 2007].

Industrial water use is rather insignificant as part of the total supply [*Euroconsult Mott MacDonald*, 2007]. In 2025, the industrial water use is projected to 500 Mm^3.

3.3.3 Navigation minimum flow

The section of the Zambezi from the Indian Ocean to Mphanda Nkuwa was traditionally used for navigation. There is a scope to improve a part of it which would require higher releases from Cahora Bassa (minimum flow of 2'000 m^3/s to maintain a water depth of 3 m) [*Euroconsult Mott MacDonald*, 2007].

3.4 PAST HYDROLOGICAL MODELLING OF THE BASIN

Modeling the hydrology of the Zambezi River Basin has been attempted in global studies with poor performance on the timing and amplitude of peak flows [*Yates*, 1997]. For example, Schuol et al. [2008b] calibrated the Soil and Water Assessment Tool (SWAT) model over the whole African continent with monthly river discharges from 1971 to 1995 on a minimum of three years of data available splitting data in two, the more recent half used for calibration and the prior half for validation. Over the Zambezi catchment, the Nash-Sutcliffe coefficient was below zero for both periods.

Specific studies over the entire Zambezi catchment showed better results but illustrated also the difficulties related to model calibration. A water balance coupled with a water transport model was implemented operating at 0.5° spatial scale and at a monthly time step [*Vorosmarty et al.*, 1991; *Vörösmarty and Moore III*, 1991]. The result of the global calibration was a systematic and substantial overestimation of the mean annual runoff. By adjusting the precipitation, the evaporation and the available soil water capacity at each sub-basin, the final index of agreement reached 0.8 over 1 with a mean error of nearly 50% [*Vorosmarty et al.*, 1991]. More recently, Michailovsky [2008] and Landert [2008] implemented Soil and Water Assessment Tool (SWAT) at monthly time steps, calibrating it respectively manually and automatically using the SWAT-CUP2 software [*Abbaspour et al.*, 2007]. Both calibrations led to poor results in terms of hydrograph comparison. No validations were undertaken in any of the models.

A lumped rainfall-runoff model including surface and base flow, regulated dams for hydropower production and water storage dams for consumptive water use was calibrated on long-term mean annual water flow for the period 1900 to 2002 using re-aggregated monthly precipitation data [*Beck and Bernauer*, 2011]. The results of the calibration were correlation coefficients varying from 0.6 to 0.98 without any validation for another period.

In order to study the hydrology of a sub-basin un-influenced by the large artificial reservoir, the Upper Zambezi Basin (up to Victoria Falls) was modeled at a monthly time step for the period 1961 to 1990 as a single storage bucket with three parameters [*G P Harrison and Whittington*, 2002] and calibrated and validated using 15 years for each phase with a resulting correlation coefficient of 0.8. However, due to the poor high flow performance, a manual adjustment of the parameter was necessary leading to correlation coefficients of 0.6 and 0.5 respectively for calibration and validation periods. The Spatial Tools for River basin Environmental Analysis and Management (STREAM) [*Aerts et al.*, 1999] and a Lumped

Elementary Watershed (LEW) model were calibrated on the same sub-basin for the period 1960 to 1972 at a monthly time step [*Winsemius et al.*, 2006a]. The NS coefficient was about 0.8; similar to the results obtained by Gerrits [2005] for the period 1978 to 2004. Again, no validation was undertaken.

More recently, a forecasting framework for the discharge prediction on three different sub-basins of the Zambezi (Upper Zambezi, Luangwa and Kafue) for the period from July 1995 to January 2002 at 10-daily time step was developed by Meier et al. [2011]. A soil moisture runoff model was compared to a regression model in terms of performance simulating the observed discharge. The NS coefficients were around 0.8 but no validation was implemented as the 6 years of data were used for calibration.

In all cases, calibration was difficult and a major concern regarding future model use. Reasons pointed out are not only the scarce data but, mostly the uneven distribution of the existing gauging stations and hydrological particularities of the wetlands. Several studies addressed the problem of lack of data by using novel satellite derived data sources in addition to rainfall, such as terrestrial water storage change [*Winsemius et al.*, 2006b] and soil moisture [*Meier et al.*, 2011]. An alternative consists to condition the model parameters based on alternative hydrological information such as remotely sensed evaporation [*Winsemius et al.*, 2008], soil moisture, water levels [*Michailovsky et al.*, 2012] or old discharge time series [*Winsemius et al.*, 2009].

In the presented research project, an original approach has been developed to simulate the hydrology of the wetlands and a comprehensive calibration framework was implemented to include all available discharge data as well as the registered water level at the main reservoirs. The model validation was part of the methodology leading to a robust result.

3.5 HYDROLOGICAL MODEL (SWAT 2009)

3.5.1 General description

SWAT is a semi-distributed deterministic model which operates on a daily time step [*J G Arnold et al.*, 1998; *Neitsch et al.*, 2005]. Its main components include weather, hydrology, sedimentation, crop growth, nutrients, pesticides, agricultural management and stream routing. The hydrologic model is based on the water balance for the four storage volumes snow, soil profile, shallow aquifer, and deep aquifer, and considers precipitation, interception, evapotranspiration, surface runoff, infiltration, percolation, and subsurface runoff. The pre-processing of input data can be performed within ESRI ArcGIS by using the ArcSWAT interface [*Winchell et al.*, 2007]. The SWAT model has proved to be successful for many applications and a wide variety of hydrologic conditions [*Gassman et al.*, 2007].

The main equations as well as the concept of the model are presented here based on the information available in the user manual of the SWAT 2009 version [*Neitsch et al.*, 2009].

For modelling purpose, the watershed is partitioned into a number of subbasins defined based on the topography. Input information for each subbasin is grouped into the following categories: climate, hydrologic response units (HRU), pond/wetland, groundwater and the main channel or reach draining the subbasin. Hydrologic response units are lumped land areas within the subbasin that are comprised of unique land cover, soil and management conditions.

The simulation of the hydrology of the watershed is separated into two major divisions: the land phase and the routing phase.

3.5.1.1 Land phase

In the land phase, the hydrological cycle simulation is based on the water balance equation:

$$SW_t = SW_o + \sum_{i=1}^{t} (R_{day} - Q_{surf} - E_a - w_{seep} - Q_{gw})$$

[3-1]

where SW_t is the final soil water content (mm H_2O), SW_o is the initial soil water content on day i (mm H_2O), t is the time (days), R_{day} is the amount of precipitation on day i (mm H_2O), Q_{surf} is the amount of surface runoff on day i (mm H_2O), E_o is the amount of evapotranspiration on day i (mm H_2O), w_{seep} is the amount of water entering the vadose zone from the soil profile on day i (mm H_2O) and Q_{gw} is the amount of return flow on day i (mm H_2O). The Figure 3-7 summarizes the sequence of processes used by SWAT.

The difference in evapotranspiration for various crops and soils is reflected by the watershed subdivision and the runoff is computed separately for each HRU and routed which increases accuracy.
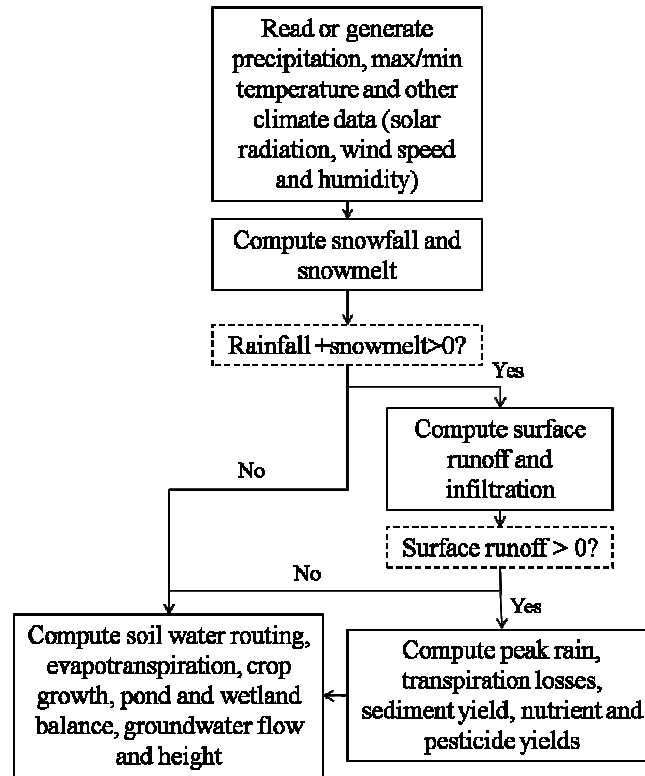
Figure 3-7. General sequence of processes used by SWAT to model the land phase of the hydrological cycle [based on *Neitsch et al.*, 2009]

The climatic variables required by SWAT are mainly used to calculate potential evapotranspiration (PET) and separate snowfall from rainfall. Depending on data availability, the PET can be computed using three methods: Hargreaves [*Hargreaves and Samani*, 1985] [3-2], Priestley-Taylor [*Priestley and Taylor*, 1972] [3-3] and Penman-Monteith [*Monteith*, 1965] [3-4].

$$\lambda_{ev} E = 0.0023 \cdot H_o \cdot (T_{max} - T_{min})^{0.5} \cdot (T_{av} + 17.8) \qquad [3\text{-}2]$$

where λ_{ev} is the latent heat of vaporization (MJ kg^{-1}), E is the potential evaporation (mm d^{-1}), H_o is the extraterrestrial radiation (MJ m^{-2} d^{-1}), T_{max} is the maximum air temperature for a given day (°C), T_{min} is the minimum air temperature for a given day (°C) and T_{av} is the mean air temperature for a given day (°C).

$$\lambda_{ev} E = a_{pet} \cdot \frac{\Delta}{\Delta + y} \cdot (H_{net} - G) \qquad [3\text{-}3]$$

where λ_{ev} is the latent heat of vaporization (MJ kg^{-1}), E is the potential evaporation (mm d^{-1}), a_{pet} is a coefficient, Δ is the slope of the saturation vapour pressure-temperature curve, y is the psychometric constant (kPa °C^{-1}), H_{net} is the net radiation (MJ m^{-2} d^{-1}) and G is the heat flux density to the ground (MJ m^{-2} d^{-1}).

$$\lambda_{ev} E = \frac{\Delta \cdot (H_{net} - G) + y \cdot K \cdot (0.622 \cdot \lambda \cdot \rho_{air} / P) \cdot (e_z^0 - e_z) / r_a}{\Delta + y \cdot (1 + r_c / r_{a)}} \qquad [3\text{-}4]$$

where λ_{ev} is the latent heat of vaporization (MJ kg^{-1}), E is the potential evaporation (mm d^{-1}), Δ is the slope of the saturation vapour pressure-temperature curve, H_{net} is the net radiation (MJ m^{-2} d^{-1}), G is the heat flux density to the ground (MJ m^{-2} d^{-1}), y is the psychometric constant (kPa °C^{-1}), K is a dimension coefficient needed to ensure the two terms in the numerator have the same units, ρ_{air} is the air density (kg m^{-3}), P is the atmospheric pressure (kPa), e^0_z is the saturation vapour pressure of air at height z (kPa), e_z is the vapour pressure of air at height z (kPa), r_o is the plant canopy resistance (s m^{-1}) and r_a is the diffusion resistance of air layer (s m^{-1}).

The inputs required for the Priestley-Taylor and Penman-Monteith methods are quite substantial: solar radiation, surface air temperature, relative humidity and wind (only for Penman-Monteith method) whereas the Hargreaves method estimates PET based only on maximum and minimum surface air temperature. Based on the PET and additional soil and landuse parameters, the actual plant transpiration and the actual soil evaporation are estimated separately.

As precipitation descends, it may be held in the vegetation canopy [3-5] or fall to the soil surface.

$$can_{day} = can_{max} \cdot \frac{LAI}{LAI_{max}}$$ [3-5]

where can_{day} is the amount of water that can be trapped in the canopy on a given day (mm H$_2$O), can_{max} is the maximum amount of water that can be trapped in the canopy when the canopy is fully developed (mm H$_2$O), LAI is the leaf area index for a given day and LAI$_{max}$ is the maximum leaf area index for the plant.

Water on the soil surface can infiltrate into the soil or flow overland. Two methods for estimating surface runoff are available: the Green and Ampt infiltration method, which requires precipitation input in sub-daily scale [*Green and Ampt*, 1911] and the Soil Conservation Service (SCS) curve number procedure [*USDA Soil Conservation Service*, 1972] which uses daily precipitation.

The Green and Ampt infiltration rate is defined by the following equation [3-6]:

$$f_{\text{inf},t} = K_e \cdot \left(1 + \frac{\Psi_{wf} \cdot \Delta\theta_v}{F_{\text{inf},t}}\right)$$ [3-6]

where $f_{inf,\text{t}}$ is the infiltration rate at time t (mm/hr), K_e is the effective hydraulic conductivity (mm/hr), ψ_{wf} is the wetting front matric potential (mm) $\Delta\theta_v$ is the change in volumetric moisture content across the wetting front (mm/mm) and F_{inf} is the cumulative infiltration at time t (mm H$_2$O).

With the SCS procedure, the surface runoff in calculated based on the retention capability of the soil [3-7] and the infiltration is computed as the difference between the amount of rainfall and the amount of surface runoff. The retention parameter (S) is very

significant in SCS method, being defined by the Curve Number (*CN*) which is a sensitive function of the soil's permeability, land use and antecedent soil water conditions [3-8].

$$Q_{surf} = \frac{(R_{day} - I_a)^2}{(R_{day} - I_a + S)}$$ [3-7]

where Q_{surf} is the accumulated runoff or rainfall excess (mm H_2O), R_{day} is the rainfall depth for the day (mm H_2O), I_a is the initial abstractions which included surface storage and infiltration prior to runoff (mm H_2O) and *S* is the retention parameter (mm H_2O) [3-8].

$$S = 25.4 \cdot \left(\frac{1000}{CN} - 10 \right)$$ [3-8]

where *CN* is the curve number varying in function of soil, land use and slope.

Once surface runoff is calculated, the amount of total runoff released to the main channel is computed using the following equation [3-9].

$$Q_{surf} = (Q'_{surf} + Q_{stor,i-1}) \cdot \left(1 - \exp\left[\frac{-surlag}{t_{conc}} \right] \right)$$ [3-9]

where Q_{surf} is the amount of surface runoff discharged to the main channel on a given day (mm H_2O), Q_{surf}' is the amount of surface runoff generated in the subbasin on a given day (mm H_2O), $Q_{stor,i-1}$ is the surface runoff stored or lagged from the previous day (mm H_2O),, *surlag* is the surface runoff lag coefficient and t_{conc} is the time of concentration for the subbasin (hrs).

The water entering the soil may be removed from the soil by plant uptake or evaporation, percolate past the bottom of the soil profile [3-10] or move laterally in the profile and contribute to streamflow.

$$w_{perc,ly} = SW_{ly,excess} \cdot \left(1 - \exp\left[\frac{-\Delta t}{TT_{perc}} \right] \right)$$ [3-10]

where $w_{perc,ly}$ is the amount of water percolating to the underlying soil layer on a given day (mm H_2O), $SW_{ly,excess}$ is the drainable volume of water in the soil layer on a given day (mm H_2O), Δt is the length of the time step (hrs) and TT_{perc} is the travel time for percolation (hrs).

The soil profile can be subdivided into multiple layers and the model considers infiltration, evaporation, plant uptake, interflow as well as up- and downward redistribution processes for each layer.

Water enters groundwater storage mainly by percolation [3-11] and leaves by discharge into the rivers or lakes.

$$w_{rchrg,i} = \left(1 - \exp\left[-1/\delta_{gw} \right] \right) \cdot w_{perc,ly=n} + \exp\left[-1/\delta_{gw} \right] \cdot w_{rchrg,i-1}$$ [3-11]

where $w_{rchrg,i}$ is the amount of recharge entering the aquifers on day i (mm H$_2$O), δ_{gw} is the groundwater delay time (days) $w_{perc,ly=n}$ is the total amount of water exiting the bottom of the lowest soil layer on day i (mm H$_2$O) and $w_{rchrg,i-1}$ is the amount of discharge entering the aquifer on day i -*1* (mm H$_2$O).

It is also possible for water to move upward from the water table into the soil layer [3-12].

$$w_{revap,\max} = \beta_{rev} \cdot E_o \qquad\qquad [3\text{-}12]$$

where $w_{revap,max}$ is the maximum amount of water moving into the soil zone in response to water deficit (mm H$_2$O), β_{rev} is the revap coefficient and E_o is the potential evaporation for the day (mm H$_2$O).

3.5.1.2 Routing phase

The routing phase simulates the movement of the mass flow in the channel. Flow may be loss due to evaporation, transmission through main channel or removal for human use. Two methods are implemented to route the flow: a variable storage coefficient method or the Muskingum routing method, both methods being variations are the kinematic wave model. SWAT assumes the reaches to have a trapezoidal shape.

The variable storage routing method is based on the continuity equation:

$$V_{in} - V_{out} = \Delta V_{stored} \qquad\qquad [3\text{-}13]$$

where V_{in} is the volume of inflow during the time step (m^3 H$_2$O), V_{out} is the volume of outflow during the time step (m^3 H$_2$O), and ΔV_{stored} is the change in volume of storage during the time step (m^3 H$_2$O).

The outflow volume at the end of the time step can therefore be computed as:

$$V_{out} = SC \cdot (V_{in} + V_{stored}) \qquad\qquad [3\text{-}14]$$

where SC is the storage coefficient defined as $SC = \dfrac{2 \cdot \Delta t}{2 \cdot TT + \Delta t}$ and TT is the travel time (s).

3.5.2 Reservoir model

3.5.2.1 Original reservoir model

In the original SWAT 2009 code (revision number 477) [*Neitsch et al.*, 2009], two types of reservoir model exist: (1) a reservoir placed out of the main channel, receiving water only through runoff from the subbasin in which it is located and not from the upstream parts of the basin through main channel and (2) a reservoir located on the main channel, receiving water from the upstream parts of the basin as well as from its own subbasin. In the literature [*Ndomba and Van Griensven*, 2011; *Schuol et al.*, 2008a; *Schuol et al.*, 2008b; *Van Griensven*

et al., 2012], the floodplains located on the main channel were simulated using the latter alternative, which is described below.

The reservoir model includes in the daily water balance inflow (V_{flowin}), outflow ($V_{flowout}$), seepage from the reservoir bottom (V_{seep}), rainfall (V_{pcp}) and evaporation (V_{evap}) [3-15].

$$V = V_{stored} + V_{flowin} - V_{flowout} + V_{pcp} - V_{evap} - V_{seep} \qquad [3\text{-}15]$$

where V is the volume of water in the impoundment at the end of the day and V_{stored} is the volume of water stored in the water body at the beginning of the day.

The amount of precipitation and evaporation is calculated based on the area of the reservoir's surface. To relate this surface area (SA) to the volume stored in the reservoir [3-16], two surface-volume couples need to be defined: one corresponding to the volume of water permanently stored in the main channel during low flow (V_{min}) and one corresponding to the maximum capacity of the reservoir simulating the floodplain (V_{max}). Both values can be fixed based on a literature review or field survey.

$$SA = \beta \cdot V^{\alpha} \qquad [3\text{-}16]$$

where β and α are adjustment coefficients relating the volume and the surface of a reservoir by a power law.

The daily outflow volume may be determined using four different methods: (1) measured daily outflow, (2) measured monthly outflow, (3) average annual release rate (recommended for uncontrolled reservoirs) and (4) controlled outflow with targeted release (developed for artificial reservoirs). Among these, the average annual release rate is the best candidate to model floodplains.

The volume at the beginning of the time step is calculated by [3-17]:

$$V' = V_{stored} + V_{flowin} + V_{pcp} - V_{evap} - V_{seep} \qquad [3\text{-}17]$$

When the average annual release rate method is chosen to calculate the reservoir outflow, the reservoir releases water whenever its volume exceeds the minimum. While the volume is between the minimum (V_{min}) and the maximum (V_{max}), the outflow depends on the average daily release rate (q_{rel}):

$$V_{flowout} = V' - V_{min} \qquad \text{if} \quad V' - V_{min} \leq q_{rel} \cdot \Delta t \qquad [3\text{-}18]$$

$$V_{flowout} = q_{rel} \cdot \Delta t \qquad \text{if} \quad V' - V_{min} > q_{rel} \cdot \Delta t \qquad [3\text{-}19]$$

If the volume exceeds the maximum, the outflow increases in order to maintain it within bounds:

$$V_{flowout} = (V' - V_{max}) + (V_{max} - V_{min}) \qquad \text{if} \quad V_{max} - V_{min} \leq q_{rel} \cdot \Delta t \qquad [3\text{-}20]$$

$$V_{flowout} = (V' - V_{max}) + q_{rel} \cdot \Delta t \qquad \text{if} \quad V_{max} - V_{min} > q_{rel} \cdot \Delta t \qquad [3\text{-}21]$$

The average daily release rate (q_{rel}) has to be defined by the user based on his knowledge of the reservoir.

The volume at the end of the time step is finally defined as:

$$V = V' - V_{flowout} \qquad [3\text{-}22]$$

The main disadvantages of this method when modeling floodplains are that the outflow does not always depend on the volume of stored water and that there will be no outflow if the volume decreases below the minimum.

Additionally, even if the surface area of the reservoir is computed at each time step, it has no influence on the subbasin surface area where it is located. Therefore, the water balance of the subbasin does not take into account the surface reduction/increase caused by the extension/reduction of the reservoir. In the case of floodplains, with highly variable surface and with large extents compared to the subbasins where they are located, this may cause substantial deviations in the subbasins' water balances.

3.5.2.2 *Modified reservoir model*

The original SWAT reservoir model has been used to simulate the African floodplains [*Schuol et al.*, 2008b]. However, the results on Zambezi Basin reached a Nash-Sutcliffe coefficient below zero, which was justified by the authors with the difficulty of simulating outflow from the wetlands. The authors believe that there was, indeed, an inadequacy with the original SWAT reservoir model. Despite this, and overlooking the secondary effect of reservoir surface evaporation, a tendency to delay (or rush) flows in reservoirs will not contribute appreciably to a large bias (as over a sufficiently large number of years roughly what goes in the reservoir must come out). Large floodplains attenuate runoff, reducing and delaying flood peaks downstream [*Beilfuss and Dos Santos*, 2001; The World Bank, 2010], and are characterized by significant evaporation losses and seasonal fluctuations. During high flow periods, water spreads over bank and inundates the floodplains whereas during low flows, it runs only along the main channel. It has been observed that such floodplains have a great impact on the water storage capacity of the subbasins [*Meier et al.*, 2011].

Modeling floodplains as natural reservoirs with specific storage and outlet characteristics proved to be a successful approach for hydrological simulation [The World Bank, 2010]. As such, a set of two equations to reproduce the outflow from the floodplains [6-9] was developed and appended to the original SWAT reservoir model. The base flow (Q_{base}) is defined by a release coefficient and depends on the water depth (H) in the reservoir simulating the floodplain [3-24]. The additional inflow is stored in the reservoir and released as an upper flow (Q_{up}) if the water depth exceeds a fixed threshold (H_{min}), corresponding to the minimum water level in the main channel, as from a free crest weir [3-25].

$$Q_{outflow} = Q_{base} + Q_{up} \qquad [3\text{-}23]$$

$$Q_{base} = k \cdot H \tag{3-24}$$

$$Q_{up} = \begin{cases} 0 & \text{if } H \leq H_{min} \\ a \cdot (H - H_{min})^b & \text{if } H > H_{min} \end{cases} \tag{3-25}$$

where *k* (release coefficient), *a* (overflow coefficient) and *b* (overflow exponent) are the model parameters used in the calibration process.

The overflow coefficient is an aggregate of the constants for weir flow rate definition and the weir width [3-26]. The weir width corresponds to the mean width of the floodplain; it is assumed to be different for each floodplain but constant through time.

$$a = C_d \cdot \sqrt{2 \cdot g} \cdot w \tag{3-26}$$

where C_d is the discharge constant for the weir, *g* is the gravitational acceleration and *w* is the weir width in meters.

The bounds for the overflow coefficient depend on the geometrical characteristics of the floodplain. The calibration process could be done on the discharge constant (C_d) alternatively to the overflow coefficient (*a*) if enough data were available to define the weir width (*w*). However, in the present case study, in light of insufficient information on the geometry of the floodplains, the overflow coefficient (*a*) was used as a calibration parameter.

The standard value for the overflow exponent is 1.5, but in order to account for specificity of the floodplains, it was assumed that it can vary from 1 to 3.5. Accordingly, the units of the discharge constant (C_d) will vary to provide a discharge result in m^3/s.

The release coefficient controlling the base flow (*k*) varies on a wide range as it allows the simulation of the main channel flow and can be very different between floodplains.

The daily water depth in the reservoir is calculated based on its volume [3-27]. As for the surface-volume relation, two depth-volume couples need to be defined: one corresponding to the volume of water permanently stored into the main channel during low flow (V_{min}) and one corresponding to the maximum capacity of the reservoir simulating the floodplain (V_{max}). Such parameters can be derived from a Digital Elevation Model analysis if the data are available at a scale corresponding to the floodplain characteristics or defined based on literature review or field survey. The parameters can also be adapted by the user depending on the simulation results. For example, if V_{min} is too low, the downstream base flow will be too high and if V_{min} is too high the downstream baseflow will be too low. Vmax will not affect the simulation results.

$$H_t = \gamma \cdot V_t^{\delta} \tag{3-27}$$

where δ and γ are adjustment coefficients linking the volume and the water depth of a reservoir assumedly by a power law.

Finally, an improvement has been made to the original model concerning the relation between subbasin and reservoir surface. Because the reservoir surface can be large relatively to the subbasin surface and can be subject to substantial fluctuations in time, it is subtracted at every time step from the subbasin surface to compute an accurate water balance.

The initial volume of water inside the floodplain should be defined by the user. If no data are available, it is recommended to run the model starting from a period with minimum flow so that the floodplain would be as empty as possible and that the initial conditions would have a limited influence on the simulation results.

3.5.3   Hydropower model

In the original SWAT model, the method available for calculating the outflow from a controlled reservoir consists in a target release approach [*Neitsch et al.*, 2009]. The model requires the beginning and the ending month of the flood season, the principal spillway volume which corresponds to the maximum flood control reservation and the emergency spillway volume which corresponds to no flood control reservation. During the non-flood season, the target storage is set to the emergency volume as no flood control reservation is needed and during the flood season, the flood control reservation is calculated as a function of the soil water content in the subbasin. The target storage may be specified by the user on a monthly basis. The user defines also the number of days required for the reservoir to reach target storage ($ndtarg$). The outflow (Q_{out}) at each time step is calculated as:

$$Q_{out} = \frac{Vol - Vol_{targ}}{ndtarg}$$
[3-28]

where Vol is the reservoir volume at time t (m^3) and Vol_{targ} is the target volume (m^3).

To allow a more precise simulation of the hydropower operations, a new routine has been developed for outflow calculation based on the flood rule curve and the maximum and minimum exploitation levels. The total outflow is separated into turbine outflow and spillway outflow. A calculation of the energy generated at each time step has been added based on the turbine capacity as well as the water head available.

More precisely, the inputs of the hydropower model are:

- the minimum and the maximum exploitation level with their associated volumes and surface area,
- the minimum and maximum tailwater level with the associated discharge,
- the maximum spillway discharge at each reservoir level $Qspil_{max}$,
- the turbine maximum capacity $Qturb_{max}$,
- the monthly target level $targ$,
- the number of day needed to reach target storage $ndtarg$.

Based on the value given, the following relations are adjusted to be able to calculate the reservoir characteristics at each time step:

$$Surf = \alpha \cdot Vol^{\beta} \qquad\qquad [3\text{-}29]$$

where *Surf* is the reservoir surface area (m^2), *Vol* is the reservoir volume and α and β are coefficients.

$$Vol = \gamma \cdot WL^{\delta} \qquad\qquad [3\text{-}30]$$

where *WL* is the reservoir water level (m a.s.l.) and γ and δ are coefficients,

$$Tail = \varepsilon \cdot Qout^{\kappa} \qquad\qquad [3\text{-}31]$$

where *Tail* is the tailwater level (m a.s.l.), *Qout* is the reservoir outflow (m^3/s) and ε and κ are coefficients.

$$Qspil_{max} = \mu \cdot WL^{\nu} \qquad\qquad [3\text{-}32]$$

where *Qspil$_{max}$* is the maximum spillage discharge (m^3/s) and μ and ν are coefficients.

At each time step *t*, the reservoir surface area is computed based on the reservoir volume at time *t-1*. The evaporated (*V$_{evap}$*) and precipitated (*V$_{pcp}$*) volumes are calculated based on this surface. The reservoir volume at time *t* is then derived as:

$$Vol(t) = Vol(t-1) - V_{evap} + V_{pcp} + V_{flowin} \qquad\qquad [3\text{-}33]$$

The reservoir water level (*WL*) and the corresponding maximum spillway discharge (*Qspil$_{max}$*) are then computed based on equations [3-30] and [3-32]. The model works with volume instead of water level inside the reservoir as it calculates spilled and turbine flow volumes.

For each reservoir, a target rule curve is defined in terms of monthly water volume inside the reservoir (*targ*). A set of operation rules is then defined based on the difference between the reservoir volume (*Vol(t)*), the target volume (*targ*), the reservoir minimum operation volume (*Vol$_{min}$*) and the reservoir maximum operation volume (*Vol$_{max}$*).

The user can choose between two sets of operation rules depending if the target rule curve should be used as a constraint or not.

3.5.3.1 *Operation rules without taking into account target volume as a constraint*

In the first option, the operation rules are taking into account the target volume only as maximum volume constraints and allow the volume to decrease below as long as it stays above the minimum operation volume (Table 3-2). The range of variability around the target volume depends on the number of days to reach the target volume defined by the user.

(1) The reservoir volume is lower than the target volume

Rule 1. If the reservoir volume is lower than the minimum exploitation volume, there is no turbine flow and no spillage.

Rule 2. If the difference between the reservoir volume and the minimum exploitation volume is higher than the number of days required for the reservoir to reach target storage (*ndtarg*) multiplied by the turbine flow volume, the turbine flow is at maximum. It means that the turbine will continue working at full capacity if there is a reserve before reaching the minimum exploitation volume.

Rule 3. If the difference between the reservoir volume and the target volume is lower than the number of days required for the reservoir to reach target storage (*ndtarg*) multiplied by the turbine flow, the turbine flow depends on the volume available before reaching the minimum exploitation volume. This rule allows a progressive decrease of the turbine flow when the reservoir volume approaches the minimum exploitation volume.

(2) The reservoir volume is higher than the target volume

Rule 4. If the reservoir volume is higher than the maximum exploitation volume, the turbine flow will be at maximum and the spillage will depend on the reservoir volume. For small reservoirs, it is important to check whether the turbine flow at maximum capacity would empty the reservoir below the minimum volume and if it is the case, to adapt the turbine flow. In rule 4, the turbine are not able to empty the reservoir in the given time step but are sufficient to decrease the reservoir volume to the maximum exploitation volume so no spillage is needed.

Rule 5. If the reservoir volume is higher than the maximum exploitation volume, the turbine flow will be at maximum and the spillage will depends on the reservoir volume. If the turbines are not able to decrease the volume to the maximum exploitation volume, the remaining volume needs to be evacuated by the spillways, taking into account their maximum capacity.

Rule 6. If the reservoir volume is higher than the maximum exploitation volume, the turbine flow will be at maximum and the spillage will depends on the reservoir volume. For small reservoirs, it is important to check whether the turbine flow at maximum capacity would empty the reservoir below the minimum volume and if it is the case, to adapt the turbine flow. In rule 6, the turbines are able to empty the reservoir in the given time step. Therefore, the turbine flow is set to the difference of volume between the reservoir volume and the minimum exploitation volume.

Rule 7. If the reservoir volume is lower than the maximum exploitation volume, there will be no spillage. For small reservoirs, it is important to check whether the turbine flow at maximum capacity would empty the reservoir below the minimum volume and if it is the case, to adapt the turbine flow. In rule 7, the turbines are not able to empty the reservoir in the given time step. Therefore, the turbine flow is set to the maximum.

Rule 8. If the reservoir volume is lower than the maximum exploitation volume, there will be no spillage. For small reservoirs, it is important to check whether the turbine flow at maximum capacity would empty the reservoir below the minimum volume and if it is the case, to adapt the turbine flow. In rule 8, the turbines are able to empty the reservoir in the given time step. Therefore, the turbine flow is set to the difference of volume between the reservoir volume and the minimum exploitation volume.

Table 3-2. Reservoir operating rules without constraints on the lower volume (*Vol*: volume at time t (m³), *targ*: target volume (m³), *Vol_min*: minimum operating volume (m³), *Vol_max*: maximum operating volume (m³), *Qspil*: spilled discharge at time t (m³/s), *Qspil_max*: maximum spilled discharge (m³/s), *Qturb_max*: maximum turbinated discharge (m³/s), *Qturb*: turbinated discharge at time t (m³/s), *ndtarg*: number of days to reach target storage (s))

Rule #	Reservoir volume	Turbine flow volume	Spill flow volume
1	$Vol(t) < targ$ $Vol(t) < Vol_{min}$	$Qspil = 0$	$Qturb = 0$
2	$Vol(t) < targ$ $Vol(t) > Vol_{min}$ $Vol(t) - Vol_{min} > ndtarg \cdot Qturb_{max}$	$Qspil = 0$	$Qturb = Qturb_{max}$
3	$Vol(t) < targ$ $Vol(t) > Vol_{min}$ $Vol(t) - Vol_{min} < ndtarg \cdot Qturb_{max}$	$Qspil = 0$	$Qturb = \cdot \dfrac{Vol(t) - Vol_{min}}{ndtarg}$
4	$Vol(t) > targ$ $Vol(t) > Vol_{max}$ $Vol_{max} > Vol(t) - Qturb_{max} \cdot dt > Vol_{min}$	$Qspil = 0$	$Qturb = Qturb_{max}$
5	$Vol(t) > targ$ $Vol(t) > Vol_{max}$ $Vol(t) - Qturb_{max} \cdot dt > Vol_{max}$	$Qspil = \dfrac{Vol(t) - Qturb_{max} \cdot dt - Vol_{max}}{dt}$ if $Qspil < Qspil_{max}$, $Qspil = Qspil$ if $Qspil \geq Qspil_{max}$, $Qspil = Qspil_{max}$	$Qturb = Qturb_{max}$
6	$Vol(t) > targ$ $Vol(t) > Vol_{max}$ $Vol(t) - Qturb_{max} \cdot dt < Vol_{min}$	$Qspil = 0$	$Qturb = \dfrac{Vol(t) - Vol_{min}}{dt}$
7	$Vol(t) > targ$ $Vol(t) < Vol_{max}$ $Vol(t) - Qturb_{max} \cdot dt > Vol_{min}$	$Qspil = 0$	$Qturb = Qturb_{max}$
8	$Vol(t) > targ$ $Vol(t) < Vol_{max}$ $Vol(t) - Qturb_{max} \cdot dt < Vol_{min}$	$Qspil = 0$	$Qturb = \dfrac{Vol(t) - Vol_{min}}{dt}$

3.5.3.2 *Operation rules taking into account target volume as a constraint*

As an alternative, the second set of operation rules takes into account the target volume as the objective volume at each time step (Table 3-3), the fluctuations around the defined volume depending on the number of days to reach the target volume defined by the user.

(1) The reservoir volume is lower than the target volume

Rule 1. If the reservoir volume is lower than the minimum exploitation volume, there is no turbine flow and no spillage.

Rule 2. If the difference between the reservoir volume and the target volume is higher than the number of days required for the reservoir to reach target storage (*ndtarg*) multiplied by the turbine flow volume, the turbine flow is 20% of the maximum turbine capacity. It means that the reservoir volume reached the critical volume below the rule curve.

Rule 3. If the difference between the reservoir volume and the minimum exploitation volume is lower than the number of days required for the reservoir to reach target storage (*ndtarg*) multiplied by the turbine flow, the turbine flow depends on the volume available before reaching the critical volume. This rule allows a progressive decrease of the turbine flow when the reservoir volume passes below the reservoir target volume. The minimum turbine flow is set to 20% of the maximum turbine capacity.

(2) The reservoir volume is higher than the target volume

Rule 4. If the reservoir volume is higher than the maximum exploitation volume, the turbine flow will be at maximum and the spillage will depend on the reservoir volume. For small reservoirs, it is important to check whether the turbine flow at maximum capacity would empty the reservoir below the target volume reserve and if it is the case, to adapt the turbine flow. In rule 4, the turbines are not able to empty the reservoir below the target volume reserve in the given time step but are sufficient to decrease the reservoir volume to the maximum exploitation volume so no spillage is needed.

Rule 5. If the reservoir volume is higher than the maximum exploitation volume, the turbine flow will be at maximum and the spillage will depend on the reservoir volume. If the turbines are not able to decrease the volume to the maximum exploitation volume, the remaining volume needs to be evacuated by the spillways, taking into account their maximum capacity.

Rule 6. If the reservoir volume is higher than the maximum exploitation volume, the turbine flow will be at maximum and the spillage will depend on the reservoir volume. For small reservoirs, it is important to check whether the turbine flow at maximum capacity would empty the reservoir below the target volume reserve and if it is the case, to adapt the turbine flow. In rule 6, the turbines are able to empty the reservoir below the target volume reserve in the given time step. Therefore, the turbine flow is set to the difference of volume between the reservoir volume and the target volume reserve.

Rule 7. If the reservoir volume is lower than the maximum exploitation volume, there will be no spillage. For small reservoirs, it is important to check whether the turbine flow at maximum capacity would empty the reservoir below the target volume reserve and if it is the case, to adapt the turbine flow. In rule 7, the turbines are not able to empty the reservoir in the given time step. Therefore, the turbine flow is set to the maximum.

Rule 8. If the reservoir volume is lower than the maximum exploitation volume, there will be no spillage. For small reservoirs, it is important to check whether the turbine flow at maximum capacity would empty the reservoir below the minimum volume and if it is the case, to adapt the turbine flow. In rule 8, the turbines are able to empty the reservoir in the given time step. Therefore, the turbine flow is set to the difference of volume between the reservoir volume and the target volume reserve.

Table 3-3. Reservoir operating rules following the rule curve (*Vol*: volume at time t (m^3), *targ*: target volume (m^3), *Vol$_{min}$*: minimum operating volume (m^3), *Vol$_{max}$*: maximum operating volume (m^3), *Qspil*: spilled discharge at time t (m^3/s), *Qspil$_{max}$*: maximum spilled discharge (m^3/s), *Qturb$_{max}$*: maximum turbinated discharge (m^3/s), *Qturb*: turbinated discharge at time t (m^3/s), *ndtarg*: number of days to reach target storage (s))

Rule #	Reservoir volume	Turbine flow volume	Spill flow volume
1	$Vol(t) < targ$ $Vol(t) < Vol_{min}$	$Qspil = 0$	$Qturb = 0$
2	$Vol(t) < targ$ $Vol(t) > Vol_{min}$ $targ - Vol(t) > ndtarg \cdot Qturb_{max}$	$Qspil = 0$	$Qturb = 0.2 \cdot Qturb_{max}$
3	$Vol(t) < targ$ $Vol(t) > Vol_{min}$ $targ - Vol(t) < ndtarg \cdot Qturb_{max}$	$Qspil = 0$	$\max \left(Qturb = 0.2 \cdot Qturb_{max} , \right.$ $\left. Qturb = 1 - \dfrac{Vol(t) - Vol_{min}}{ndtarg} \right)$
4	$Vol(t) > targ$ $Vol(t) > Vol_{max}$ $Vol_{max} > Vol(t) - Qturb_{max} \cdot dt >$ $targ - ndtarg \cdot Qturb_{max}$	$Qspil = 0$	$Qturb = Qturb_{max}$
5	$Vol(t) > targ$ $Vol(t) > Vol_{max}$ $Vol(t) - Qturb_{max} \cdot dt > Vol_{max}$	$Qspil = \dfrac{Vol(t) - Qturb_{max} \cdot dt - Vol_{max}}{dt}$ if $Qspil < Qspil_{max}$, $Qspil = Qspil$ if $Qspil \geq Qspil_{max}$, $Qspil = Qspil_{max}$	$Qturb = Qturb_{max}$
6	$Vol(t) > targ$ $Vol(t) > Vol_{max}$ $Vol(t) - Qturb_{max} \cdot dt <$ $targ - ndtarg \cdot Qturb_{max}$	$Qspil = 0$	$Qturb = \dfrac{Vol(t)}{dt} - \dfrac{(targ - ndtarg \cdot Qturb_{max})}{dt}$
7	$Vol(t) > targ$ $Vol(t) < Vol_{max}$ $Vol(t) - Qturb_{max} \cdot dt >$ $targ - ndtarg \cdot Qturb_{max}$	$Qspil = 0$	$Qturb = Qturb_{max}$
8	$Vol(t) > targ$ $Vol(t) < Vol_{max}$ $Vol(t) - Qturb_{max} \cdot dt <$ $targ - ndtarg \cdot Qturb_{max}$	$Qspil = 0$	$Qturb = \dfrac{Vol(t)}{dt} - \dfrac{(targ - ndtarg \cdot Qturb_{max})}{dt}$

3.5.3.3 Estimation of the power generated

After the turbine and spilled discharges are computed, the tailwater level is calculated. The available head (*Head*) is defined as the difference between the reservoir water level and the tailwater level. The power generated at the time *t* can be approximated by the following equation [3-34].

$$Power = \eta \cdot g \cdot \rho \cdot Head \cdot Qturb \qquad\qquad [3\text{-}34]$$

where η is the turbine efficiency, *g* is the gravitational acceleration [m/s^2] and ρ is the water density [kg/m^3].

3.5.4 Model set-up

3.5.4.1 Topographic and land cover information

The Digital Elevation Model (DEM) chosen was derived from the US Geological Survey's (USGC) public domain geographic database HYDRO1k[1] based on the 30° digital elevation model of the world GTOPO30 completed in 1996. The basis of all of the data layers available in the HYDRO1k database is the hydrologically correct DEM, processed to remove elevation anomalies that can interfere with correct flow. The techniques used to develop this DEM are the following: projection of the DEM, identification of the natural sink features, filling of the DEM and verification (comparison of streamlines generated to existing digitalized data). The horizontal resolution of the HYDRO1k data is 1 km. No specific information about the absolute vertical accuracy is available but GTOPO30 vertical accuracy is of 30 m at 90% confidence level [*Karlsson and Arnberg*, 2011].

The soil map is produced by the Food and Agriculture Organization of the United Nations at a resolution of 10 km [*FAO*, 1995]. About 5,000 soil types are differentiated and some soil properties for two layers 0-30 cm and 30-100 cm) are provided. Further soil characteristics used by the SWAT model (e.g., particle-size distribution, bulk density, organic carbon content, available water capacity, and saturated hydraulic conductivity) are provided by Reynolds *et al.* [2000] or calculated using pedotransfer functions [*Schuol et al.*, 2008a; *Schuol et al.*, 2008b]. A new version of the soil map is now available from the Harmonized World Soil Database of the FAO [*FAO/IIASA/ISRIC/ISSCAS/JRC*, 2012]. After a first comparison the differences on the Zambezi basin are not very big. However, it would be useful to include the refined data in a further version of the model, given that the new soil types can be documented in the SWAT database.

The landuse map was constructed from the Global Land Cover Characterization (GLCC, Version 2, http://edcsns17.cr.usgs.gov/glcc/). It has a 1 km spatial resolution and 24 classes of landuse representation. The parameterization of the landuse classes (e.g., leaf area index, maximum stomatal conductance, maximum root depth, optimal and minimum temperature for plant growth) is based on the characteristics of the classes defined in the

---

[1] http://gcmd.nasa.gov/records/GCMD_HYDRO1k.html

SWAT original database and on literature research [*Schuol et al.*, 2008a; *Schuol et al.*, 2008b] (Figure 3-8).
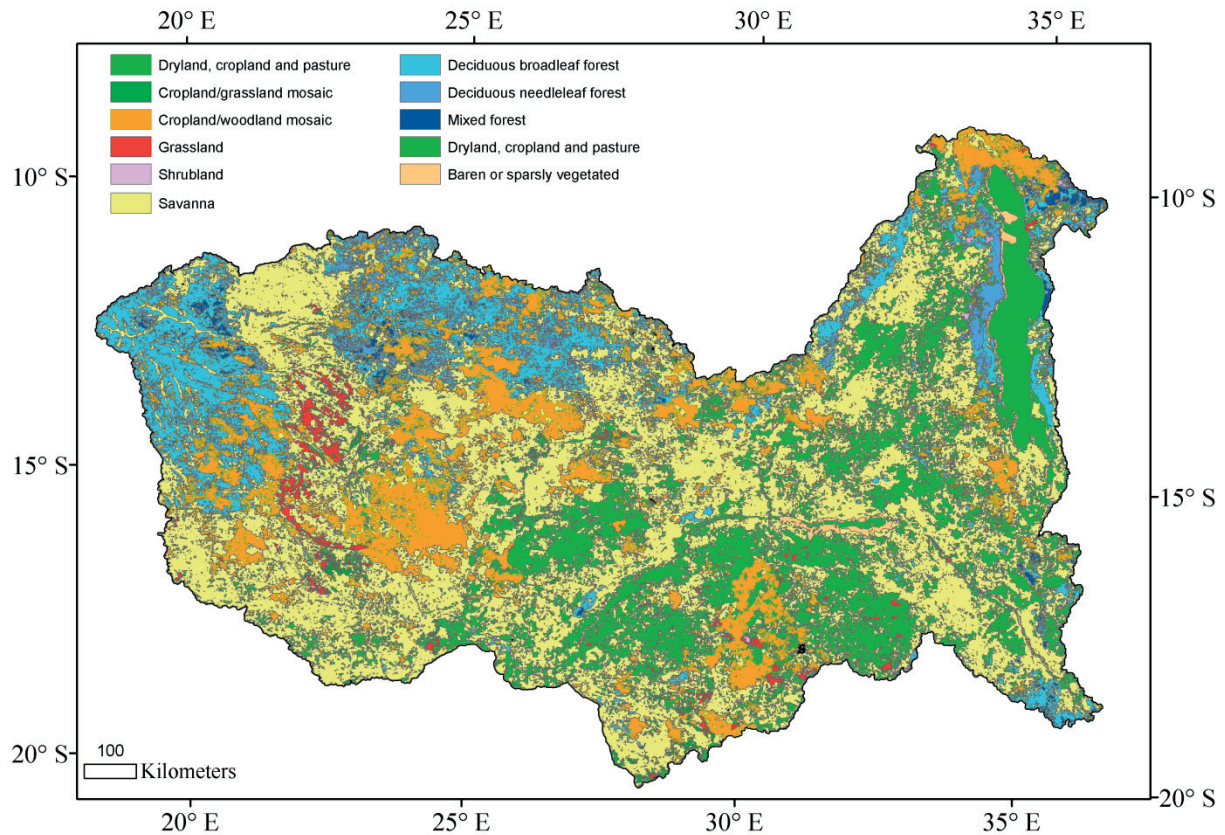
Figure 3-8. Zambezi basin landuse map with the associated SWAT classes.

3.5.4.2 *Precipitation*

TRMM 3B42 version 6, NASA's standard precipitation product, was chosen as precipitation source based on a detailed study of the different satellite products [*Cohen Liechti et al.*, 2012]. It is produced since 1998 in four steps [*Huffman et al.*, 2007]: (1) PM estimates are calibrated and combined, (2) IR estimates are computed using PM estimates for calibration, (3) PM and IR estimates area combined, (4) data are rescaled to monthly total using Global Precipitation Climatology Centre (GPCC) data. The estimates are released on a 0.25° by 0.25° grid at 3-hourly temporal resolution (00:00, 03:00,…, 21:00 UTC) in a global belt extending from 50°N to 50°S. The data have been changed during the calibration process to the version 7 of the same product as it became available and constitutes an improvement in the rainfall estimation.

3.5.4.3 *Temperature*

The temperature grids (daily minimum and maximum) are compiled from the NCEP/DOE 2 Reanalysis data [*Kanamitsu et al.*, 2002] provided by the NOAA/OAR/ESRL PSD, Boulder, Colorado, USA, from their Web site at http://www.esrl.noaa.gov/psd/. The

spatial coverage varies from 88.542°N to 88.542°S and from 0°E to 358.125°E stored on a Gaussian grid of 192 longitudinal bands of 1.875°.

3.5.4.4 Discharge and water level

The critical data set for the reliable hydrologic-hydraulic modeling of a large catchment is the time series of measured discharge which allows for the calibration and validation of the model. The most extensive available database containing historical discharge records in the Zambezi Basin is managed by the Global Runoff Data Centre D - 56002 Koblenz, Germany (GRDC), which operates under the World Meteorological Organization (WMO) [*Fekete et al.*, 1999]. In the global database, 67 daily and 30 monthly stations located within the Zambezi basin are identified. In addition, the Department of Water Affairs of Zambia (DWA, personal communication) provided a list of 34 stations with the associated discharge data over the Zambian part of the basin. The Zambezi River Authority (ZRA), managing the Kariba dam and "Hidroeléctrica de Cahora Bassa" (HCB), which manages the Cahora Bassa dam, shared some of the information recorded at the dams.

Despite these valuable contributions, most of the data series are not continuous and a few stations have not been considered as reliable. As can be seen in the Figure 3-9, most of the available data are distributed in the upper and middle parts of the basin and none downstream of Cahora Bassa.
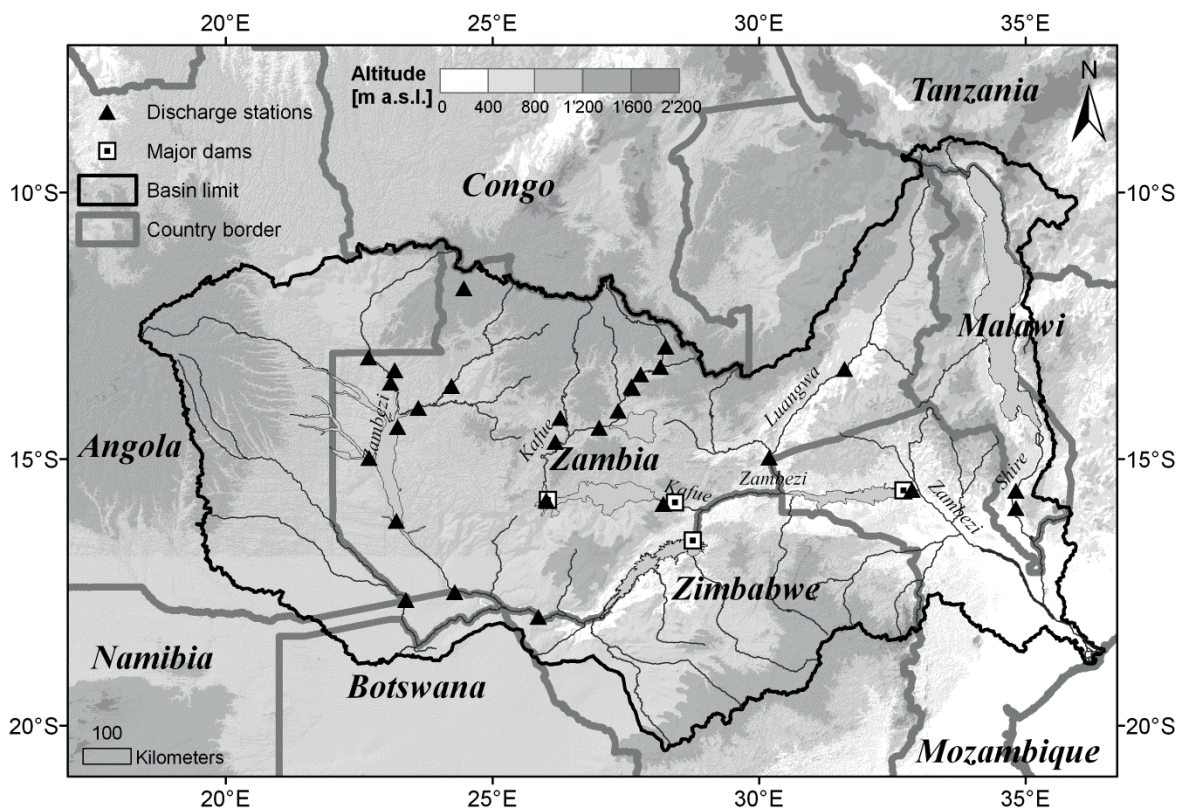
Figure 3-9. Zambezi Basin map with the discharge station producing daily data between 1998 and 2006

The Zambezi River Authority (ZRA) and "Hidroeléctrica de Cahora Bassa" (HCB) transmitted the water levels measured at Itezhi Tezhi, Kafue Gorge, Kariba and Cahora Bassa reservoirs. The water levels were converted to water volumes using a linear relation as the level varies only by small amplitude compared to the respective reservoir height.

3.5.4.5   Subbasin delineation

The preprocessing of the model input was performed within ESRI ArcGIS 9.3.1 using the ArcSWAT interface version 2009.93.7a [*Winchell et al.*, 2007]. Based on the topography, a minimum drainage area of 5,000 km^2 was defined to discretize the watershed in about 200 sub-basins. The sub-basins around the reservoirs, lakes and wetlands were then refined by superposing a GIS layer of lakes and flats of Africa resulting in a total of 405 sub-basins (Figure 3-10). The geomorphology, stream parameterization and overlay of soil and land cover were automatically done within the interface. The Hydrological Response Units (HRU) were delimited using a threshold of 35% for the land use, the soil and the slope resulting in a total of 778 units.
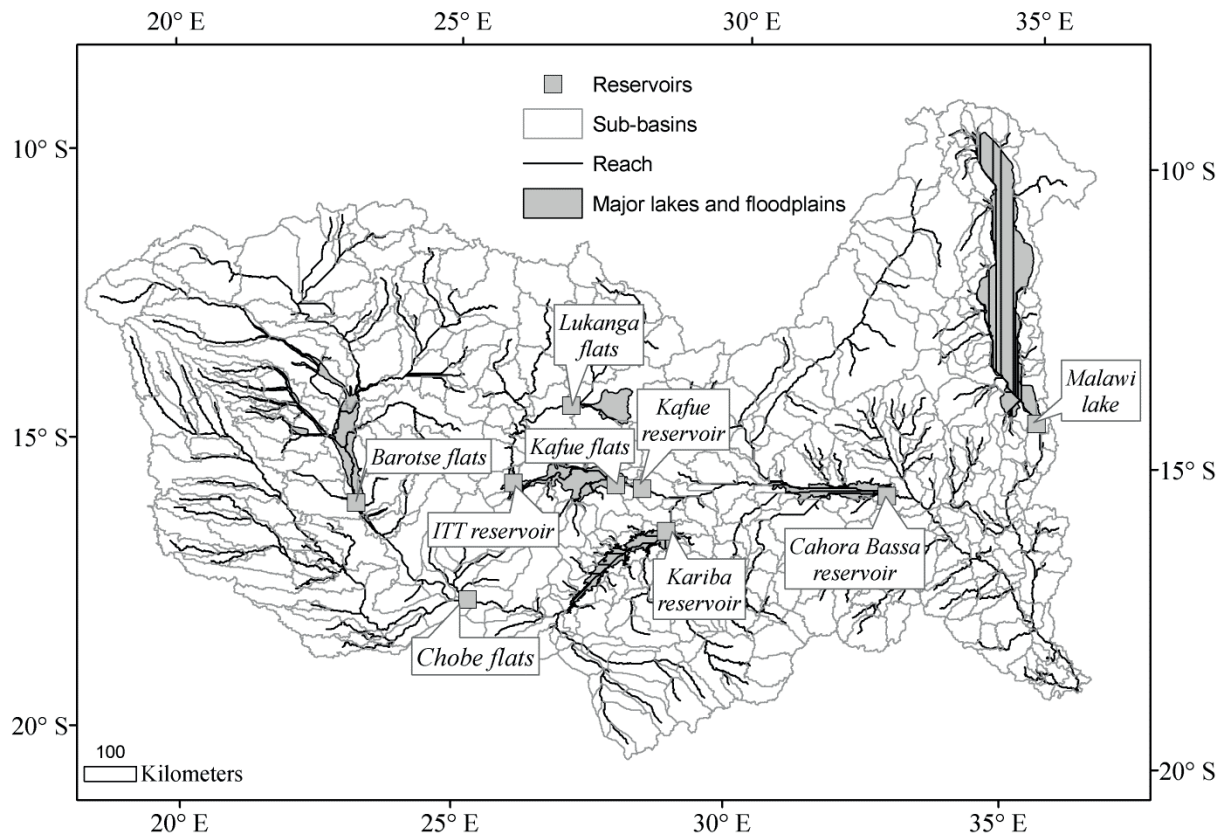
Figure 3-10. Sub-basin delineation with the corresponding reaches and the reservoirs included

The artificial and natural lakes, as well as the main wetlands on the main channel, were modeled as reservoirs. Their main characteristics are derived from literature research and listed in the Table 3-4.

Table 3-4. Reservoirs characteristics

	Barotse flats [1,2]	Chobe flats [1]	Kariba Dam [3,4]	Lukanga flats [2,5]	ITT Dam [3,6]	Kafue flats [2,3,6]	Kafue Gorge Dam [3,6]	Cahora Bassa Dam [3]
Year of operation			1963		1977		1972	1977
Surface during flood / during low flows [10^6 m^3]	11,960 / 1.000	2,800 / 1,000	5,627 / 5,300	2,600 / 2,100	380 / 90	7,000 / 1,850	750 / 180	2,502 / 838
Volume during floods / during low flows [10^9 m^3]	17 / 2	8.4 / 2.5	191 / 116	3.9 / 2.8	6.0 / 0.8	9.5 / 2.2	0.9 / 0.1	57 / 12.2
H_{min} [m]	1.00	2.50	-	1.30	-	1.17	-	-

[1] [*The World Bank*, 2010]
[2] FAO http://www.fao.org/docrep/005/F9051F/F9051F02.htm#ch2.2
[3] [*Beilfuss*, 2001; *Beilfuss and Dos Santos*, 2001]
[4] [*Mhlanga and Goguel*, 2007]
[5] http://en.wikipedia.org/wiki/Lukanga_Swamp
[6] [*Kunz et al.*, 2011a; *McCartney and Houghton-Carr*, 1998; *Obrdlik et al.*, 1989]

3.5.4.6 Model specifications

In the presented research project, the SCS method for surface runoff was selected for model simulations as the time step is daily. For evapotranspiration, as the inputs required for Priestley-Taylor and Penman-Monteith methods are quite substantial and the meteorological data available are limited, the Hargreaves method is chosen. As recommended by the SWAT input/output documentation [*J Arnold et al.*, 2011], the variable storage method was applied to flow routing.

4 COMPARISON AND EVALUATION OF SATELLITE DERIVED PRECIPITATION PRODUCTS

Three operational and acknowledged high resolution satellite derived estimates: the Tropical Rainfall Measuring Mission product 3B42 (TRMM 3B42), the Famine Early Warning System product 2.0 (FEWS RFE2.0) and the National Oceanic and Atmospheric Administration/Climate Prediction Centre (NOAA/CPC) morphing technique (CMORPH) are analyzed in terms of spatial and temporal distribution of the precipitation. They are compared to ground data for the wet seasons of the years 2003 to 2009 on a point to pixel basis at daily, 10-daily and monthly time steps and on a pixel to pixel basis for the wet seasons of the years 2003 to 2007 at monthly time steps.

The general North-South gradient of precipitation is captured by all the analyzed products. Regarding the spatial heterogeneity, FEWS pixels are much more inter-correlated than TRMM and CMORPH pixels. For a rainfall homogeneity threshold criterion of 0.5 global mean correlation coefficient, the area of each subbasin should not exceed a circle of 2.5° latitude/longitude radius for FEWS and a circle of 0.75° latitude/longitude radius for TRMM and CMORPH considering rectangular meshes.

In terms of reliability, the correspondence of all estimates with ground data increases with the time step chosen for the analysis. The volume ratio computation indicates that CMORPH is overestimating the rainfall by nearly 50%. The statistics of TRMM and FEWS estimates show quite similar results.

Due to its lower inter-correlation and longer data set, the TRMM 3B42 product is chosen as input for the hydraulic-hydrologic model of the basin.

4.1 INTRODUCTION

Water resources management in tropical and semi-arid areas of Africa is particularly relevant due to the high temporal and spatial climatic variability that affects the availability of water resources within and between countries and river basins. The overarching goal of the African Dams Project: Adapt planning and operation of large dams to meet social needs and environmental constraints (ADAPT) is to strengthen this interdisciplinary science. A consistent information platform for a large scale river catchment, the Zambezi River basin, is currently under development. Modeling the hydrology of this basin is a challenging task due to its size and heterogeneity, but mostly, due to the lack of reliable input and calibration data. In the past, several studies addressed the problem by using or assessing novel satellite derived data sources in addition to rainfall, such as evaporation [*Winsemius et al.*, 2008], terrestrial water storage change [*Winsemius et al.*, 2006b] and soil moisture [*Meier et al.*, 2011]. However, the satellite derived rainfall data were rarely evaluated even though, concerning model performance, the selection of the type of input precipitation has been considered as equally or even more important than the choice of the hydrological model.

In view of the sparse available gauging network for rainfall monitoring on the African continent, the observations from spaceborne instrumentation currently produce the only measured data for a large part of the territory. Two types of sensors are commonly used in the satellite rainfall estimation algorithms: Passive Microwave (PM) and Visible and Infrared Radiance (VIS/IR). The PM sensors identify the precipitation particles by the scattering due to large ice particles present in the clouds. These sensors are installed on Earth-orbiting satellites which offer only intermittent coverage of a given region of interest (currently about ten observations per day). Therefore, the estimation of precipitation from proxy parameters such as cloud top temperature that can be inferred from geo-stationary observations has been developed. The algorithms based on IR data relate rainfall to cloud top temperature and cloud optical properties through a precipitation index. The indexing method assigns a fixed rain rate to each identified cloud type [*Kidd*, 2001]. This assumption is most effective for convective conditions but can yield crude estimates because of the weak link between cloud properties and precipitation. Current approaches use rain rates estimated from coincident microwave observations to derive regional calibrations of Global-IR techniques [*Anagnostou*, 2004]. However, both kinds of sensors have difficulties in capturing non-convective rainfall and shallow "warm" rain events [*Ebert et al.*, 2007].

With the multiple products currently available, it is important to evaluate their precision and uncertainty, as well as their advantages and drawbacks, before opting for a specific application. Several studies have been conducted with the aim to inter-compare, against locally observed data, rainfall estimates derived from satellite observations. On this issue, the work achieved by the International Precipitation Working Group (IPWG) (information available online at http://www.isac.cnr.it/~ipwg/) appears as a valuable reference. The project started in 2002 over Australia and the United States and an additional verification was undertaken over Europe in 2004. The results showed that PM-IR merged estimates perform

about as well as radar in terms of daily precipitation bias and frequency over the United States [*Ebert et al.*, 2007]. Such elaborated evaluation has not, however, been undertaken over the African continent, as high quality networks of rain gauges and radars are needed in order to assess the performance of the estimates.

Nevertheless, the Tropical Rainfall Measuring Mission (TRMM) monthly estimates have been validated over major climatic regions in Africa [*Adeyewa and Nakamura*, 2003] showing the sensitivity of random and systematic error components to the seasonal and regional differences. Over West Africa, the TRMM-merged product seems to be in excellent agreement with gauge data at monthly time step [*Nicholson et al.*, 2003]: the root mean square error is on the order of 1 mm/day and there is no significant bias. Ten different satellite rainfall products, including TRMM 3B42, the Famine Early Warning System (FEWS) product (RFE2.0) and the National Oceanic and Atmospheric Administration/Climate Prediction Centre (NOAA/CPC) morphing technique (CMORPH), have been evaluated over East Africa's complex topography at monthly and 10-daily spatial resolutions [*Dinku et al.*, 2007]. Their relative root mean square error varies from 45 to 60%, increasing as the time step decreases. FEWS RFE 2.0 performs worse than TRMM 3B42 because of the fixed temperature threshold and fixed rain rate used to compute IR estimates. CMORPH shows superior performance when compared to TRMM 3B42. The performance of seven operational global products, including TRMM 3B42, CMORPH, and FEWS RFE 2.0 was also evaluated during West African monsoon at 10-daily time step [*Jobard et al.*, 2011]. CMORPH exhibited the worst skills (strong positive bias), TRMM 3B42 displayed a moderate aptitude and FEWS RFE 2.0 the best performance in terms of distribution and bias. The Microwave Infra-Red Algorithm (MIRA) has been compared at daily time scale to ground station data over Southern Africa [*Layberry et al.*, 2006] showing better agreement in the wet months than in the drier ones, but overall quite poor skills for rainfall detection. Over the Okavango basin, a monthly dataset at 0.5° based on the TRMM and Special Sensor Microwave Imager (SSM/I) datasets was found to overestimate the rainfall by 20% [*Wilk et al.*, 2006]. The comparison of MIRA and FEWS estimates to in situ stations records over the Zambezi Basin at monthly time scale indicated that MIRA often overestimates (up to 50%) and produces rainfall during dry months whereas FEWS has less bias [*Winsemius et al.*, 2006a]. TRMM 3B42RT and CMORPH were evaluated over Ethiopian river basins [*Bitew and Gebremichael*, 2011; *Romilly and Gebremichael*, 2010] and CMORPH was found to underestimate rainfall by 11% whereas TRMM 3B42RT overestimated it by 5%. However, the results varied depending on the geographical region considered.

Regarding the divergent results obtained from the previous studies and the lack of validation at the daily time step, the objective of this paper is to provide a comparison and an evaluation of the different sources of input data that can be used for hydrological modeling of the Zambezi Basin at daily time step. Therefore, products with long time series were preferred. The aim of the analysis is to determine the appropriate size of sub-basins in terms of rainfall pattern and the reliable time step for modeling. Three operational and acknowledged high resolution (daily time step or smaller and grid not coarser than 0.25° satellite derived estimates (TRMM 3B42, FEWS RFE 2.0 and CMORPH) are analyzed and

compared to ground data for the period from January 2003 to December 2009. The satellite derived datasets are available online without restriction and they fully cover the region of interest. In Chapter 4.2, a brief description of the study area and the data used is given. The methodology applied is presented in Chapter 4.3, before discussing the results in Chapter 4.4. Conclusions are drawn in Chapter 4.5.

4.2 STUDY AREA AND DATA

4.2.1 The Zambezi River Basin

The Zambezi river basin (Figure 4-1), located in the South of the African continent, is shared by eight countries, making it a particularly interesting system to further investigate the implementation of IWRM's (Integrated Water Resources Management) principles. From its headwaters in Angola to the delta in Mozambique, the Zambezi River runs over 2600 km and connects eight African nations that share different portions of its 1.4 Mio km^2 large drainage basin: Angola (18.3%), Namibia (1.2%), Botswana (2.8%), Zambia (40.7%), Zimbabwe (15.9%), Malawi (7.7%), Tanzania (2.0%) and Mozambique (11.4%) [*Vörösmarty and Moore III*, 1991]. The basin lies fully within the tropics between 10° and 20°S encompassing humid, semi-arid and arid regions dominated by seasonal rainfall patterns associated with the Inter-Tropical Convergence Zone (ITCZ). The ITCZ is a convective front oscillating along the equator. It moves from 6°N to 15°S from July to January and back North from February to June. Associated with it, the peak rainy season occurs during the Southern hemisphere summer (from October to April) and the winter months are dry. The diurnal cycle of precipitation depends also on the ITCZ. Usually, clouds form in the late morning and early afternoon hours and then by the end of the afternoon, convectional short thunderstorms form and precipitation begins. In this study, the data from 32 Mozambican national rainfall gauges collected by the Regional Administration of Zambezi Water (ARA-Zambeze) and 48 rainfall gauges from the Global Summary Of the Day (GSOD) international database were collected, resulting in an unequally distributed dataset over the basin (Figure 4-1).

The use of the potential of Zambezi River is currently mainly limited to hydropower production through a series of large impoundments: Kariba Dam, between Zambia and Zimbabwe; the Kafue hydropower scheme in Zambia; and Cahora Bassa Dam in Mozambique.
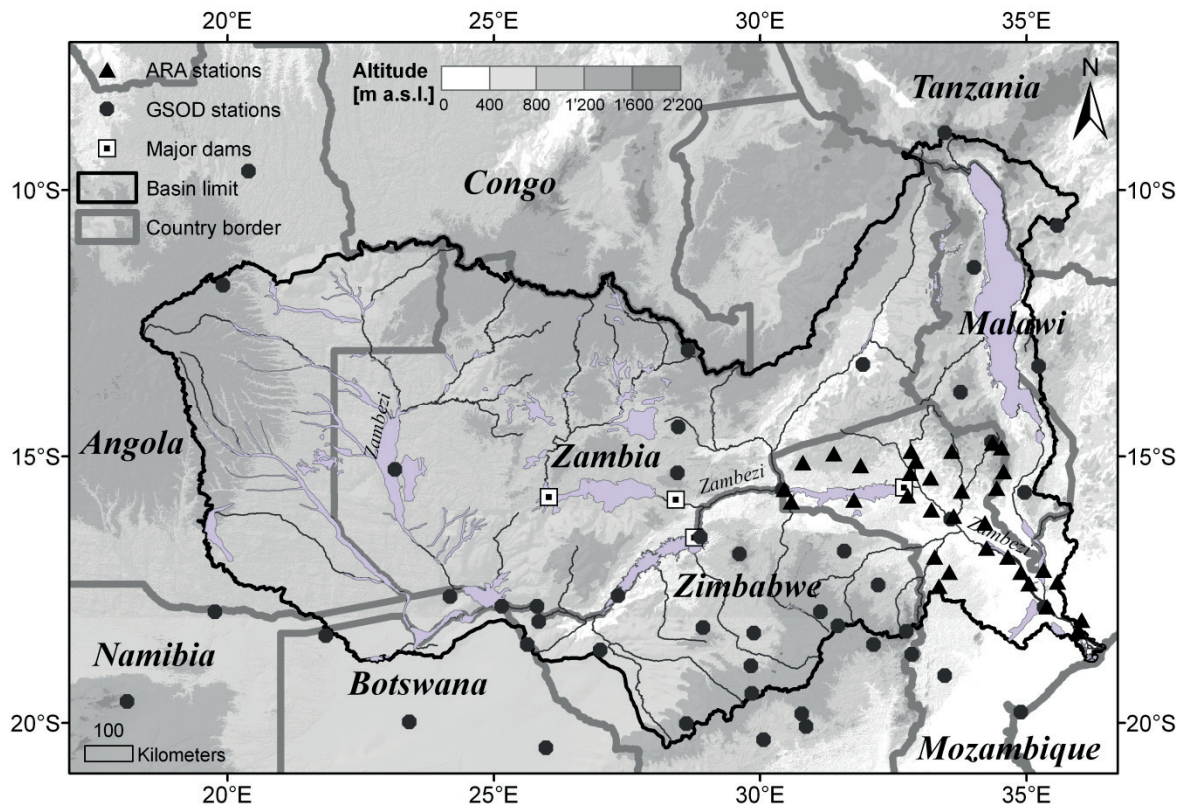
Figure 4-1. Map of the Zambezi River Basin showing countries borders, main river network with lakes and flats, major dams and gauges with available rainfall observations for the period 1998 to 2009.

4.2.2   Rainfall estimates

TRMM 3B42 version 6, NASA's standard precipitation product, is produced since 1998 in four steps [*Huffman et al.*, 2007]: (1) PM estimates are calibrated and combined, (2) IR estimates are computed using PM estimates for calibration, (3) PM and IR estimates area combined, (4) data are rescaled to monthly total using Global Precipitation Climatology Centre (GPCC) data. The estimates are released on a 0.25° by 0.25° grid at 3-hourly temporal resolution (00:00, 03:00,… , 21:00 UTC) in a global belt extending from 50°N to 50°S.

CMORPH is constructed from similar inputs as those used in TRMM 3B42 with the difference that it does not merge PM and IR rain estimates. At times and locations when PM data are unavailable, it uses the motion vector derived from half-hourly geostationary satellite IR data to interpolate precipitation [*Joyce et al.*, 2004]. Therefore, the analysis does not rely on IR data for direct rainfall estimation. The original product, starting in December 2002, has a very high spatial resolution: 8 km grid and half-hourly time step. However, historical data are available only at a spatial resolution of 0.25° and at 3-hourly temporal resolution (00:00, 03:00,… , 21:00 UTC) in a global belt extending from 60°N to 60°S.

FEWS RFE is computed by the NOAA/CPC [*Herman et al.*, 1997]. Since January 2001, the version 2.0 of the algorithm is used, integrating PM estimates. The data consist of a combination of PM and IR precipitation estimates merged with daily rainfall data from Global Telecommunication System (GTS) records. The spatial resolution corresponds to a 0.1° grid which extends from 40°N to 40°S and 20°W to 55°E. The time scale is daily (06:00 – 05:59 UTC). As precipitation mainly occurs in the afternoon, the time scale can be considered as 00:00 to 23:59 UTC. The algorithm contains rare high spikes in the precipitation estimates. Thus, the data have to be screened for intensities higher than a certain threshold.

The Global Precipitation Climatology Centre (GPCC) full data reanalysis product version 4 is based on synoptic weather observation data (SYNOP) and monthly CLIMAT report received near real-time via the World Meteorological Organization (WMO) Global Telecommunication System (GTS) (7'000-8'000 stations). Additional data from dense national observation networks and global and regional collections complete the database which is the most comprehensive global compilation of monthly precipitation data from in situ observation [*Schneider et al.*, 2008]. The processing steps include quality-control, inter-comparison of the data from different sources and interpolation to a regular mesh (0.5° grid). The Version 4 of the product covers the period 1901 to 2007 at a monthly time step with varying data coverage.

The daily ground rainfall observations are extracted from the Global Surface Summary of the Day (GSOD) product archived by the National Climatic Data Centre (NCDC) of the NOAA. Historical data are generally available from 1929 to the present. In deriving the Summary of the Day data, a minimum of 4 observations per day must be present. The data are reported and summarized based on coordinated universal time (00:00 – 23:59 UTC). An extensive automated quality control is applied to correctly 'decode' as much of the synoptic data as possible, and to eliminate the random errors.

The ground rainfall data registered at a daily basis on the Mozambican part of the Zambezi basin are collected by the Regional Administration of Zambezi Water (ARA-Zambeze). Table 4-1 summarizes the different characteristics of the rainfall estimates used.

Table 4-1. Summary of the precipitation products used in this study with input data type, combination method and spatial and temporal resolution.

Product name	Source data	Combination method	Temporal and spatial resolution
TRMM 3B42 version 6	Geo-IR, PM from TMI, SSM/I, AMSU, AMSR	Combination of PM and calibrated IR estimates, monthly scaling on ground station.	3 hourly 0.25° grid (1998-present)
FEWS RFE2.0	Geo-IR, PM from SSM/I and AMSU	Combination of PM and IR estimates, merging with daily ground data.	Daily 0.1° grid (2002-present)
CMORPH	Geo-IR, PM from TMI, SSM/I, AMSU, AMSR	Advection and evolution of PM rain rates according to IR imagery.	3 hourly 0.25° grid (2003-present)
GPCC full data reanalysis product version 4	SYNOP, CLIMAT, GHCN, CRU, FAO, national meteorological services, ...	Quality-control, inter-comparison of the data from different sources and interpolation of the data to a regular mesh system.	Monthly 0.5° grid (1901-2007)
GSOD version 7	SYNOP	Quality control.	Daily (1929-present)
ARA-Zambeze data	National meteorological service	-	Daily on the Mozambican area of the basin (1945-present)

4.3 COMPARISON AND EVALUATION OF SATELLITE DERIVED PRECIPITATION

The first part of the analysis is the comparison of the different satellite estimates in order to bring out the similarities and discordances. The spatial distribution of rainfall for the dry season (from May to September) and the wet season (from October to April) is mapped on a grid of 0.25° (Figure 4-2). In addition, the zones of agreement and divergence between the different estimates are illustrated by correlation maps (Figure 4-3). The Pearson correlation coefficient (R) between two time series at the same pixel is used for computation.

$$R(x,y) = \frac{\sum_{i=1}^{N}(x_i - \overline{x})\cdot(y_i - \overline{y})}{\sqrt{\sum_{i=1}^{N}(x_i - \overline{x})^2} \cdot \sqrt{\sum_{i=1}^{N}(y_i - \overline{y})^2}} \qquad [4\text{-}1]$$

In view of an application for hydrological modeling, the average size of a rainfall event is assessed for each of the products by calculating mean temporal correlation (Pearson) on a squared ring 1 pixel wide at a distance of r pixels from each pixel. The analysis is done assuming isotropy of the rainfall and over the period 2003 to 2009.

More precisely, for each pixel *p(i, j)*, the Pearson correlation coefficients are calculated between itself and all the other pixels:

$$COR_{p(i,j)}(k,l) = corr(p(i,j), p(k,l)) \qquad [4\text{-}2]$$

where *k* and l are the indexes of the pixel matrix, varying respectively between 18° and 26° longitude and -8° and -20° latitude.

The mean temporal correlation for each pixel at a distance r is calculated by subtracting the mean correlation at a distance of r-1 pixels to the mean correlation at a distance of r pixels.

$$\overline{COR}_{p(i,j)r} = \overline{\sum_{m=i-r}^{i+r}\sum_{n=j-r}^{j+r} COR_{p(i,j)}(m,n)} - \overline{\sum_{s=i-(r-1)}^{i+(r-1)}\sum_{t=j-(r-1)}^{j+(r-1)} COR_{p(i,j)}(s,t)} \qquad [4\text{-}3]$$

where *i* and *j* define the position of the pixel inside the matrix and *r* is the number of pixels corresponding to the ring of correlation varying from 0.01° (FEWS FE2.0) or 0.25° (TRMM and CMORPH) up to 6° latitude/longitude.

The global mean correlation at each radius ($\overline{\overline{COR}}_r$) is then computed as an average over the whole basin to underline the differences between the estimates and maps are produced for some of the key radius (Figure 4-4). The analysis is done at daily, 10-daily and monthly time steps.

During the second part of the analysis, the error property of the satellite derived data with reference to point ground gauge measurements is investigated for the wet seasons of the year 2003 to 2009 (Table 4-2). As the ground data contain large gaps, only time series with at

least 20 continuous daily values have been integrated in the analysis at daily time step. For the 10-daily rainfall accumulation, one day of missing data is accepted in the calculation and for the monthly accumulation, up to 5 days of missing data are accepted. Since there is nearly no rain during the dry season, this period was not taken into account for the performance assessment. The goal of this analysis is to evaluate the quality of the satellite products and to select the most reliable for the hydrological modeling. As the products will be used for the hydrological modeling at their optimal spatial resolution, the original grid size is used for each product. The smaller grid size of FEWS could lead to better results, a fact taken into account in the analysis.

Table 4-2. Characteristics of the gauges data used for the pixel to point analysis.

Time step	Number of gauges (ARA/GSOD)	Mean rainfall [mm] (ARA/GSOD)	Threshold [mm] (for POD and FAR calculation)
Daily	28/45	3.8/3.2	1
10 daily	28/30	38.0/29.6	10
Monthly	28/30	114.8/89.2	30

The two ground data set, GSOD and ARA are separated for the analysis as they come from different sources and do not cover the same area of the basin. Both sets of data (satellite product versus gauge data) are plotted at daily, 10-daily and monthly time steps for the pixels on which at least one gauge is available (Figure 4-5). The associated global characteristics: correlation (R), bias (eq. 4) and sample size are listed in the Table 4-3.

$$Bias = \frac{\sum (Sat - Obs)}{N} \qquad [4\text{-}4]$$

where *Sat* is the satellite data, *Obs* the ground observed data and *N* the sample size.

Statistics are calculated for each of the gauges, weighted by the number of available data per season, and a global value of the coefficients is determined by the weighted mean of all gauges based on the total number of records per gauge.

The ability for each of the products to detect rainfall is evaluated by the Probability Of Detection (*POD*) and the False Alarm Ratio (*FAR*) indices [*Ebert et al.*, 2007; *Layberry et al.*, 2006; *Stanski et al.*, 1989]. For each rainfall threshold (in mm) associated with a time step and at each point, it is estimated to have rained or not. This leads to three outcomes: estimated rain/observed rain (hit, *h*), estimated rain/observed no rain (false alarm, *f*) and estimated no rain/observed rain (miss, *m*). The indicators are derived from these outcomes:

$$POD = \frac{h}{h + m} \qquad [4\text{-}5]$$

$$FAR = \frac{f}{h + f} \qquad [4\text{-}6]$$

The precision of the satellite products is evaluated by the Relative Root Mean Square Error (*RRMSE*), the Pearson coefficient of correlation (R), the Volume Ratio (*RVol*) and the Index of agreement (*IA*) [*Daren Harmel and Smith*, 2007] (Figure 4-6 and Figure 4-7).

$$RRMSE = \frac{\sqrt{\frac{1}{N}\sum(Sat-Obs)^2}}{\overline{Obs}} \qquad [4\text{-}7]$$

$$RVol = \frac{\sum Sat}{\sum Obs} \qquad [4\text{-}8]$$

$$IA = \frac{\sum(Sat-Obs)^2}{\sum\left(\left|Sat-\overline{Obs}\right|+\left|Obs-\overline{Obs}\right|\right)^2} \qquad [4\text{-}9]$$

where *Sat* is the satellite data, *Obs* the ground observed data and $\overline{Obs}$ the mean of the ground observed data.

Finally, the pixel to pixel approach is applied to the satellite products in comparison with the GPCC ground data grid, taking into account only the pixels with at least one gauge. The data are compared by means of scatter plots (Figure 4-8) and maps of volume ratio (Figure 4-9) in order to evaluate the spatial distribution of the satellite precision. The global correlation, bias and sample size of the scatter plots are listed in the Table 4-3.

4.4   RESULTS AND DISCUSSION

4.4.1   Temporal and spatial distribution of the precipitation

The spatial variation analysis shows a general North-South gradient in the intensity of precipitation (Figure 4-2). The TRMM data set registers slightly lower rainfall intensities than the FEWS data set. The region of Lake Malawi, located in North-East side, is characterized by lower rainfall in comparison with the North-West area. The grid pixels above the ocean (South-East corner) reveal lower rainfall than those of the coastal areas. CMORPH displays the highest spatial variability of the rainfall, varying from 300 to 2'000 mm/year, and seems to overestimate the precipitated amount in the North-West region. During the dry season, it displays quite high rainfall intensities over the Kariba Lake area, probably due to some shortcomings in the computation procedure. FEWS reports both the lowest volume and the lowest variability of the three rainfall estimates. TRMM's spatial variability is moderate. Although the main characteristics of the rainfall are preserved in all estimates, its spatial patterns produced by the three algorithms show considerable differences.
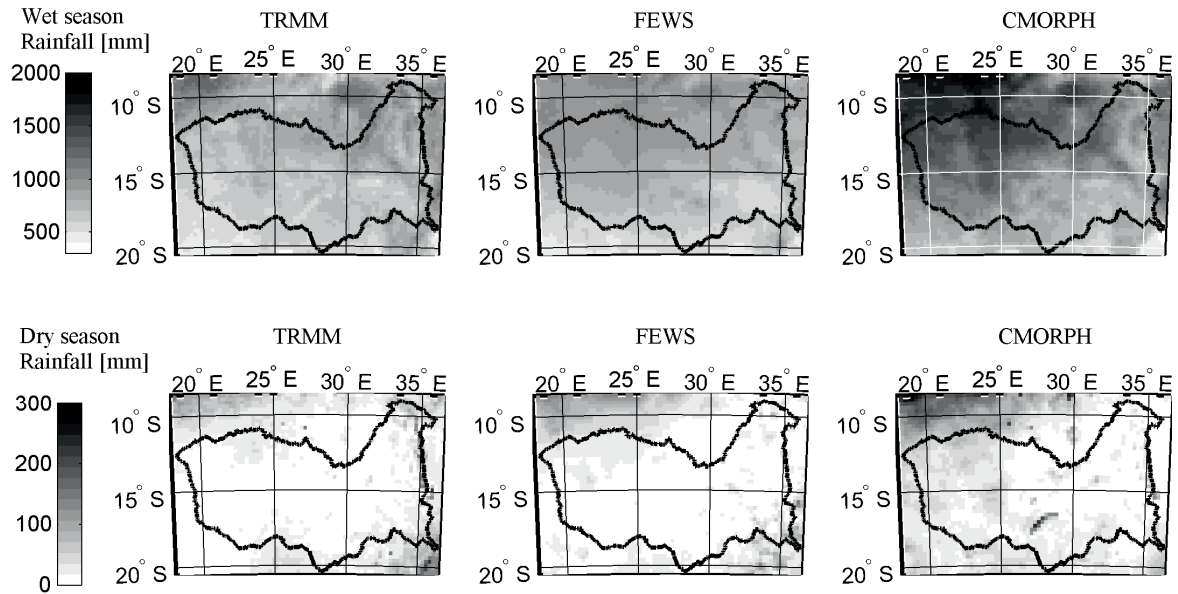
Figure 4-2. Mean seasonal rainfall map for wet (top) and dry (bottom) periods for the three satellites estimates. Data analyzed from January 2003 to December 2009.

The global correlation coefficients are 0.54 between TRMM and FEWS data sets, 0.76 between TRMM and CMORPH and 0.60 between FEWS and CMORPH. In terms of spatial distribution (Figure 4-3), the area at the North-West corner, the region over Lake Malawi (North-East limit of the basin) and the coast line (South-East corner) show the lowest agreement between data sets. The overall low correlation (*R*) between TRMM and FEWS as well as between FEWS and CMORPH is probably due to the difference in the IR-based estimates used in the algorithm. TRMM and CMORPH have the highest global correlation, reflecting that their algorithms are based on the same PM data and can indicate that the IR influence is not very big.
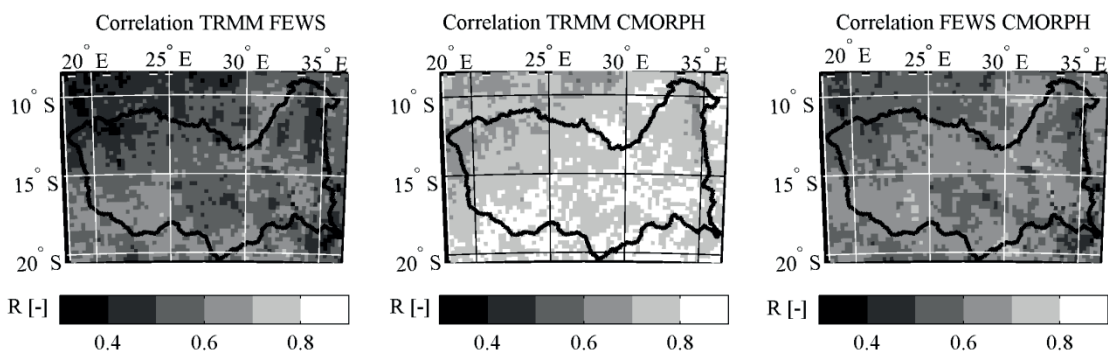
Figure 4-3. Correlation maps (*R*) of the three satellite estimates. Data analyzed from January 2003 to December 2009.

The homogeneity of the rainfall was evaluated through the correlation of the time series in each pixel with those of the surrounding pixels. FEWS exhibits the highest internal correlation ($\overline{\overline{COR_r}}$), different from TRMM and CMORPH, which show similar patterns

(Figure 4-4). At daily time step, FEWS has a mean correlation of 0.5 computed on a radius of 2.25° and the mean correlation of TRMM and CMORPH decreases rapidly with a correlation of 0.5 on a radius of only 0.75°. The spatial distribution of the correlation coefficient $\overline{COR}_{p(i,j)r}$ is different from one estimate to the other, however, regardless of the product, the central part of the basin seems to be homogeneous and the region over Malawi Lake rather heterogeneous.

At 10-daily time step, the 0.7 correlation pattern is similar for all the products: the area over the ocean has the highest heterogeneity along with the regions over Lake Malawi and the upper West corner of the basin. The zones of homogeneity over the delta present at daily time step for TRMM and CMORPH do not appear at 10-daily time step.

At monthly time step, the difference between the products for the global correlation is close to zero. In terms of spatial pattern, the area over the ocean is still a heterogeneous zone for all the products. TRMM exhibits a high correlation over the Western part of the basin whereas Kariba Lake is an area of high heterogeneity for CMORPH.
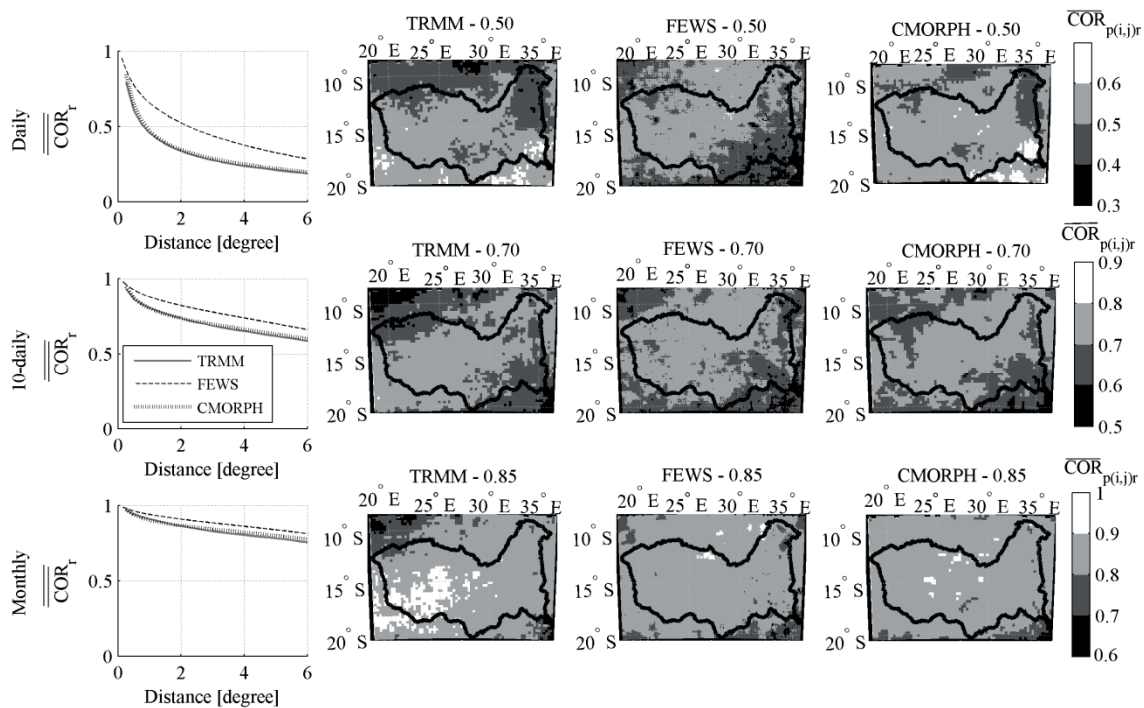
Figure 4-4. Global correlation ($\overline{\overline{COR}}_r$) for the three estimates and map of correlation ($\overline{COR}_{p(i,j)r}$) at different squared ring for daily, 10-daily and monthly time steps. Data analyzed from January 2003 to December 2009.

4.4.2   Validation of the satellite estimates on ground data

4.4.2.1   Point to pixel

Based on the scatter plots presented in Figure 4-5, it is clear that the time step has a large influence on the quality of the satellite estimates. At daily time step, no direct correlation exists between the satellite estimates and the ground data whereas monthly accumulation comparisons display already a marked trend.
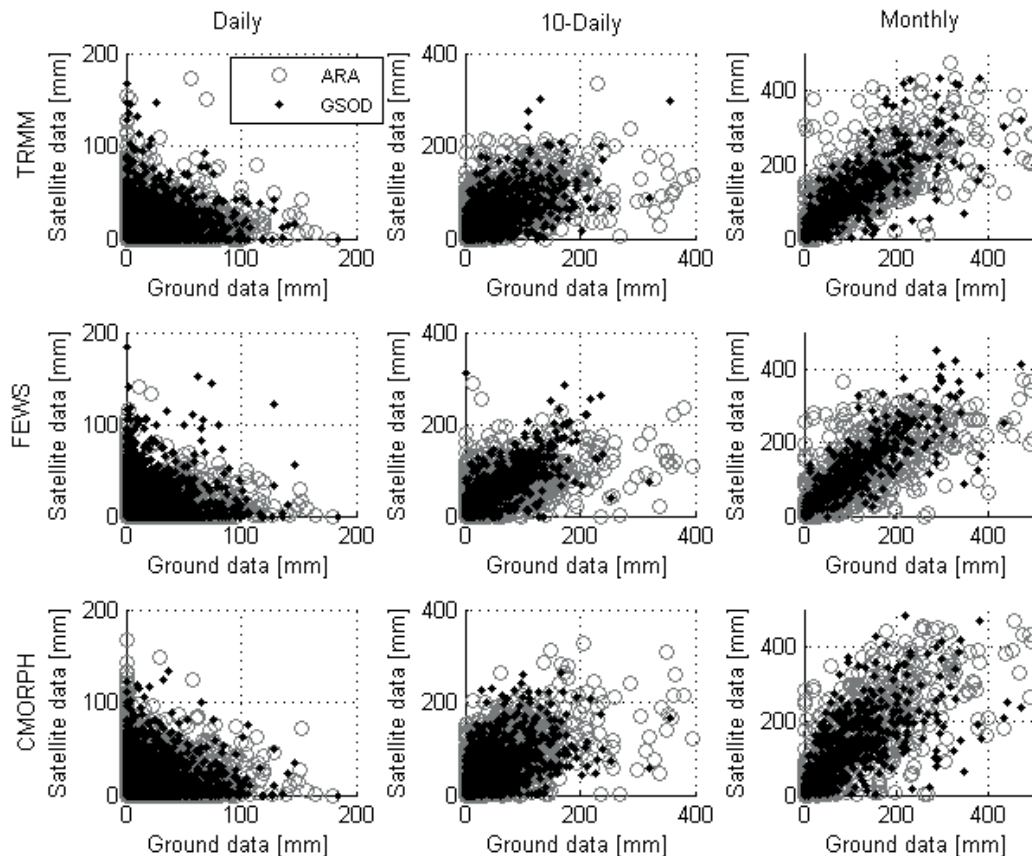
Figure 4-5. Scatter plot of satellite based estimates versus ground data for daily, 10-daily and monthly time steps for the period 2003 to 2009.

Especially at 10-daily and monthly time steps, TRMM and FEWS estimates are less correlated with the ARA-Zambeze data than with the GSOD data (Table 4-3). The global correlation is about 0.6 at 10-daily time step for both estimates compared to ARA-Zambeze data and reaches respectively 0.7 and 0.8 for TRMM and FEWS compared to GSOD data. FEWS has the lower dispersion as the algorithm uses GSOD data to rescale the satellite estimates. The TRMM product has the lowest bias but a big dispersion of the cloud. A strong overestimation is visible on the CMORPH cloud, confirmed by a global bias of about 24 mm at monthly time step (Table 4-3).

Table 4-3. Characteristics of the global satellite versus gauges data series.

Indicator (ARA/GSOD)	Satellite based estimates	Daily	10-Daily	Monthly
Bias [mm]	TRMM	0.09/-0.11	1.16/1.20	2.94/9.04
	FEWS	-0.32/-0.06	-2.98/2.17	-9.28/10.01
	CMORPH	0.67/00.41	7.25/5.97	22.31/25.22
Correlation [-]	TRMM	0.23/0.28	0.6/0.71	0.69/0.83
	FEWS	0.21/0.21	0.62/0.83	0.67/0.89
	CMORPH	0.22/0.25	0.62/0.64	0.69/0.67
Sample size	TRMM	21'333/27'600	2'083/1'905	683/625
	FEWS	21'333/27'600	2'083/1'905	683/625
	CMORPH	21'265/27'514	2'044/1'859	646/584

The statistics for the ARA-Zambeze data are presented on Figure 4-6. All the satellite products reach similar values, except for the volume ratio, for which CMORPH is overestimating the rainfall by about 40%, TRMM is overestimating the rainfall by about 20% and FEWS is close to 1. CMORPH's strong positive bias has already been documented for West Africa [*Jobard et al.*, 2011]. However, it seems to be more reliable over Ethiopia where it performs better than TRMM 3B42 and FEWS RFE2.0 at 10-daily time step [*Dinku et al.*, 2007] and underestimates the rainfall by 11% at daily time step [*Romilly and Gebremichael*, 2010]. As the time step increases, the performance of the estimates also increases (higher POD, IA and R and lower FAR and RRMSE). This is consistent with the results already published in terms of time step effect. The highest performance of FEWS may be due to its smaller grid size as it reduces the effect of pixel to point comparison.
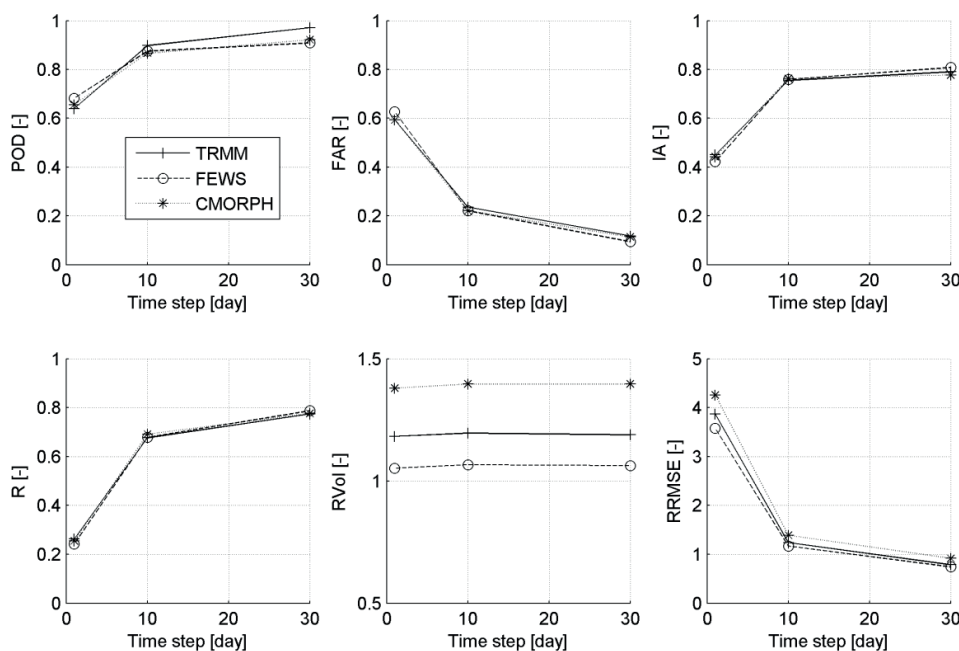
Figure 4-6. Statistics for the ARA-Zambeze gauges. Data analyzed from January 2003 to December 2009. *POD*: probability of detection, *FAR*: false alarm ratio, *R*: correlation coefficient, *RVol*: volume ratio, *RRMSE*: relative root mean square error.

For the GSOD data (Figure 7), the differences between the satellite estimates are more marked. At 10-daily and monthly time steps, the POD, FAR, R and IA of FEWS are the best, followed by the statistics of TRMM data. In terms of volume ratio, CMORPH is still showing an overestimation of about 40% but FEWS and TRMM have similar values, both close to 1.
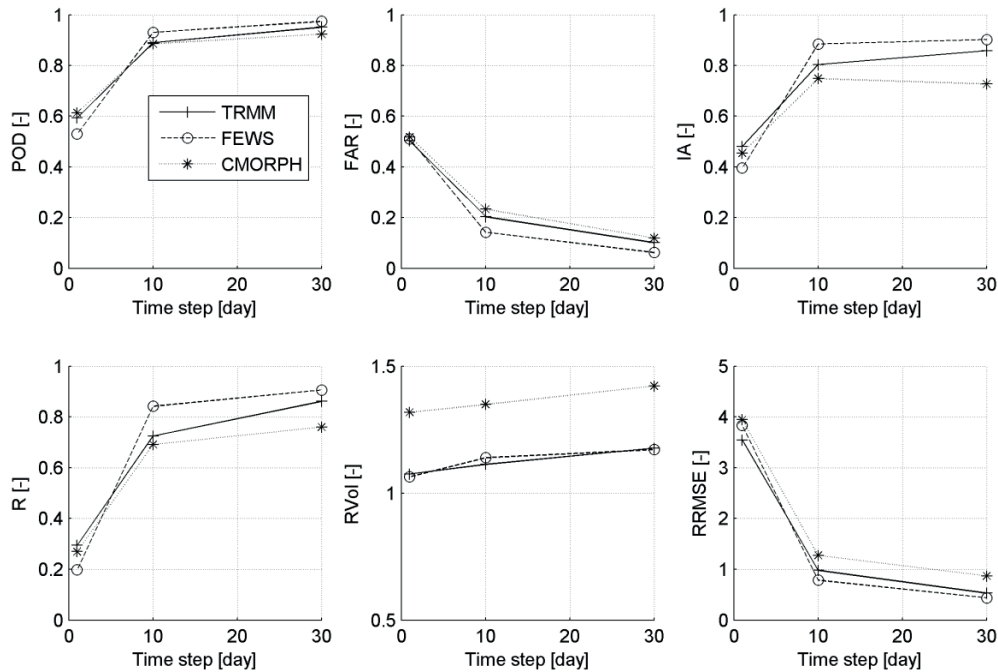
Figure 4-7. Statistics for the GSOD gauges. Data analyzed from January 2003 to December 2009. *POD*: probability of detection, *FAR*: false alarm ratio, *R*: correlation coefficient, *RVol*: volume ratio, *RRMSE*: relative root mean square error.

4.4.2.2 Pixel to pixel

The pixel to pixel comparison, carried out for a monthly time step on GPCC's 0.5° grid (Figure 4-8 and Table 4-4), shows the same trend as the point to pixel analysis. CMORPH is clearly overestimating the rainfall as the cloud of scatter plot points falls to the left side of the plot and the global bias reaches 25 mm. FEWS has the lowest dispersion of the cloud, the lowest bias (-6 mm) and the highest correlation (0.84).
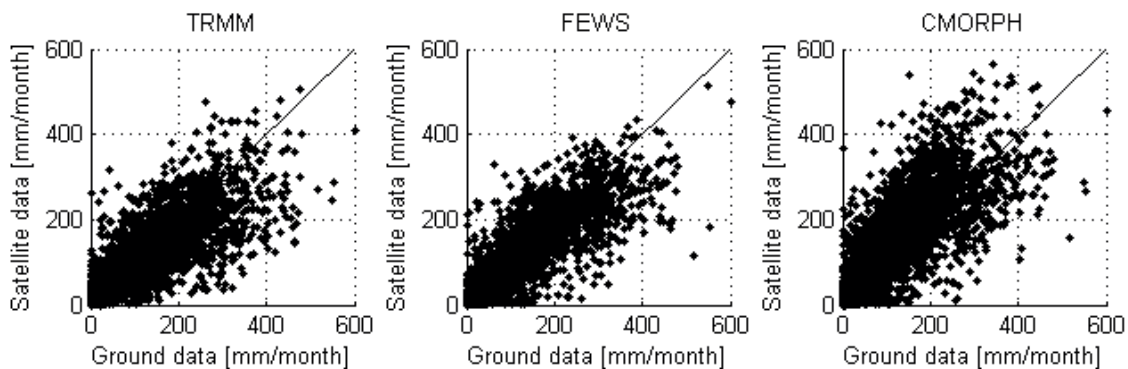
Figure 4-8. Scatter plot of satellite estimates versus GPCC data at monthly time step for the period 2003 to 2007.

Table 4-4. Characteristics of the global satellite versus GPCC series.

Indicator	TRMM	FEWS	CMORPH
Bias [mm]	-11.25	-5.96	25.28
Correlation	0.80	0.84	0.76
Sample size	3'225	3'225	3'017

Regarding the spatial distribution of the satellite performance (Figure 4-9), the precipitation are overestimated in the South-West corner, especially with CMORPH (volume ratio of about 2). On the contrary, an underestimation (below 0.75) occurs on some pixels over the Malawi Lake for all the estimates. For FEWS and TRMM, the major part of the basin has a volume ratio between 0.75 and 1.25.
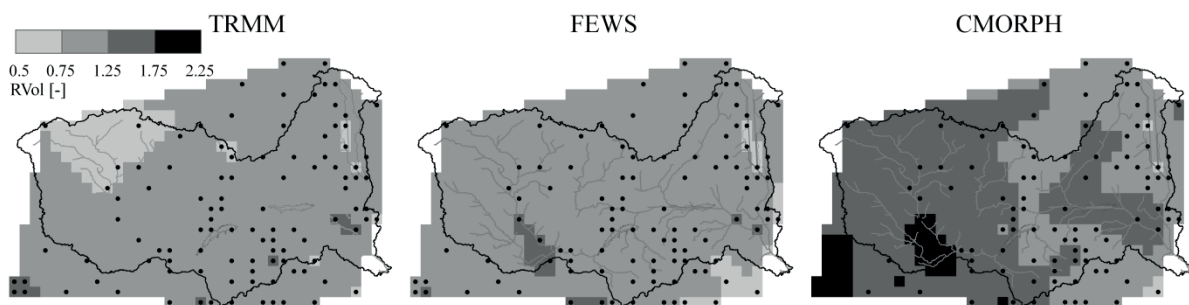
Figure 4-9. Spatial distribution of the volume ratio (*RVol*) for TRMM, FEWS and CMORPH estimates versus GCPP data at monthly time step for the period 2003 to 2007.

4.5 CONCLUSIONS

First, the three satellite estimates were compared. In terms of yearly rainfall, although main characteristics are preserved, the rainfall spatial patterns produced by the three algorithms show considerable differences. CMORPH seems to be highly influenced by Kariba Lake. Regarding the spatial heterogeneity, FEWS pixels are much more inter-correlated than TRMM pixels. For a rainfall homogeneity threshold criterion of 0.5 global mean correlation coefficient, the area of each subbasin should not exceed a circle of 2.5° latitude/longitude radius for FEWS and a circle of 0.75° latitude/longitude radius for TRMM and CMORPH considering rectangular mesh.

Secondly, the performance of the satellite estimates was assessed by comparisons with ground gauges. However, the satellite estimates cannot be expected to provide results identical to the gauge measurements as both the temporal and the spatial samplings are different. The gauging stations provide point measurements observed over continuous periods of time, while satellites deliver spatial averages based on intermittent rain rate estimates, having a tendency to smooth localized phenomena which can substantially affect gauging stations. Because of their lack of areal representativeness, the gauge measurements cannot be treated as the ground truth reference for the area-averaged rainfall. Therefore, as suggested in the literature [*Wang and Wolff*, 2010], the difference between satellite estimates and gauge

measures should be separated into the gauge area–point error variance and satellite-rain estimation error variance. In another perspective, the reliability of gauge data is also controversial because the series are often not continuous and subject to many possible error sources such as mechanical problems, interferences in the sampling mechanism or inadequate calibration [*Sieck et al.*, 2007]. Since the gauge data used in this study are not exempt of inherent errors and the area-point estimation error is not taken into account, the ground data are not considered as a prefect measure but rather as a comparator for the satellite estimates. At a daily time scale, the probability of rainfall being detected by the satellite appears nearly equivalent to a random simulation (POD of about 0.6 and FAR of about 0.5). At monthly time scale, all estimates have a good correspondence, CMORPH being less precise in terms of volume ratio as it overestimates the rainfall by about 40%. TRMM 3B42 and FEWS RFE2.0 show a very similar performance compared to ground data even if they are very different in the spatial distribution of the rainfall.

The objective of the research is to assess different scenarios of water use over the Zambezi River Basin using a calibrated hydrological model. The datasets are thus candidates for post-real-time research. Therefore, as TRMM produces data since 1998, which will increase the number of years available for calibration and validation of the model, it is chosen as the input data for hydrological modeling.

The results presented in this paper underline the fact that rainfall input data have to be studied before modeling the hydrological behavior of a basin in order to know the size of rainfall events and their distribution through space and time. Moreover, they illustrate the very strong dependency of the satellite product quality with the region of interest. An interesting addition to the study would be to calibrate the model with the different possible input data and evaluate the performance in terms of runoff simulation. However, in a basin like the Zambezi, one where only about 7% of the rainfall is contributing to runoff, the influence of other parameters like the wetland capacity, the evaporation and soil equations will be more significant.

5 HYDROLOGICAL MODELING SET-UP AND CALIBRATION

This chapter focuses on the development of the hydraulic-hydrological model which will be used to simulate water resources management scenarios. The main challenges on the implementation of the model are the scarcity of continuous reliable discharge data along the river and its tributaries and the significant influence of large floodplains. The Soil and Water Assessment Tool (SWAT), a semi-distributed physically based continuous time model, was chosen as simulation tool. Given the complexity and the size of the basin under study, an automated calibration procedure based on A Multi-ALgorithm Genetically Adaptive Multi-objective method (AMALGAM) is applied to optimize the relative error and the volume ratio at multiple discharge stations. The volume at the artificial reservoirs is derived from the measured water level and included in the calibration. Using data derived from satellite remote sensing techniques, the model is first stabilized during two years, then calibrated between 1998 and 2003 and finally validated over the 2004 to 2006 period. The study evidences the importance of evaluating the model at different points of the basin and the complementarities between performance measures, the graphical analysis of hydrographs and the reservoir volume variations in the assessment of model quality.

5.1 INTRODUCTION

The development of water resources models in Southern Africa is greatly challenging. Several factors contributing to the specific situation can be highlighted. Firstly, the order of relevance of hydrological processes in catchments below the Sahara Desert does not necessarily match what could be extensively observed in temperate catchments (i. e. evaporation is the dominant hydrological process) [*Pilgrim et al.*, 1988]. Secondly, there is a constraining and prevalent lack of hydrological data within most countries in this area. Although data scarcity usually appears as a usual problem to water resources modelers, in Southern African catchments it assumes large proportions having to be explicitly taken into account for the hydrological model choice and during the calibration and validation phases.

Within this framework, the African DAms ProjecT (ADAPT), from which this research stems, is focusing on the planning and operation of large dams in a complex river basin in order to meet social needs and environmental constraints. The present chapter discusses the development of a semi-distributed hydraulic-hydrological model, which will be used to simulate future mid-term hydropower development scenarios for a large catchment in Southern Africa, focusing on calibration issues. With a constraining lack of hydrological data and particular hydrological behavior, but also holding multiple hydropower schemes, lakes and large floodplains, the Zambezi River Basin was chosen as a case study.

Modeling the hydrology of the Zambezi River Basin has been attempted in global studies with poor results, namely on the timing and amplitude of peak flows [*Yates*, 1997]. For example, Schuol et al. [2008b] calibrated the Soil and Water Assessment Tool (SWAT) model over the whole African continent with monthly river discharges from 1971 to 1995 on a minimum of 3 years of data available splitting data in two, the more recent half used for calibration and the prior half for validation. Over the Zambezi catchment, the Nash-Sutcliffe coefficient was below zero for both periods.

Specific studies over the entire Zambezi catchment showed better results but illustrated also the difficulties related to model calibration. A water balance coupled with a water transport model was implemented operating at 0.5° spatial scale and at a monthly time step [*Vorosmarty et al.*, 1991; *Vörösmarty and Moore III*, 1991]. The result of the global calibration was a systematic and substantial overestimation of the mean annual runoff. By adjusting the precipitation, the evaporation and the available soil water capacity at each sub-basin, the final index of agreement reached 0.8 over 1 with a mean error of nearly 50% [*Vorosmarty et al.*, 1991]. More recently, Michailovsky [2008] and Landert [2008] implemented Soil and Water Assessment Tool (SWAT) at monthly time steps, calibrating it respectively manually and automatically using the SWAT-CUP2 software [*Abbaspour et al.*, 2007]. Both calibrations led to poor results in terms of hydrograph comparison. No validations were undertaken in any of the models.

A lumped rainfall-runoff model including surface and base flow, regulated dams for hydropower production and water storage dams for consumptive water use was calibrated on

long-term mean annual water flow for the period 1900 to 2002 using re-aggregated monthly precipitation data [*Beck and Bernauer*, 2011]. The results of the calibration were characterized by Pearson correlation coefficients varying from 0.6 to 0.98. Nevertheless, a validation on an independent period was not carried out.

In order to study the hydrology of a sub-basin un-influenced by large artificial reservoirs, the Upper Zambezi Basin (up to Victoria Falls) was modeled at a monthly time step for the period 1961 to 1990 as a single storage bucket with three parameters [*G P Harrison and Whittington*, 2002] and calibrated and validated using 15 years for each phase with a resulting Pearson correlation coefficient of 0.8. However, due to the poor high flow performance, a manual adjustment of the parameters was necessary leading to correlation coefficients of 0.6 and 0.5 respectively for calibration and validation periods. The Spatial Tools for River basin Environmental Analysis and Management (STREAM) [*Aerts et al.*, 1999] and a Lumped Elementary Watershed (LEW) model were calibrated on the same sub-basin over the period 1960 to 1972 at a monthly time step [*Winsemius et al.*, 2006a]. The Nash-Sutcliffe coefficient was about 0.8; similar to the results obtained by Gerrits [2005] for the period 1978 to 2004. Again, no validation was undertaken.

More recently, a forecasting framework for the discharge prediction on three different sub-basins of the Zambezi (Upper Zambezi, Luangwa and Kafue) for the period from July 1995 to January 2002 at 10-daily time step was developed by Meier et al. [2011]. A soil moisture runoff model was compared to a regression model in terms of performance simulating the observed discharge. The Nash-Sutcliffe coefficients were around 0.8 but no validation was implemented as the 6 years of data were used for calibration.

In all cases, calibration was difficult and a major concern remains regarding future model use. Reasons pointed out were not only the scarce data but mostly the uneven distribution of the existing gauging stations and hydrological particularities of the wetlands. Several studies addressed the problem of lack of data by using novel satellite derived data sources in addition to rainfall, such as terrestrial water storage change [*Winsemius et al.*, 2006b] and soil moisture [*Meier et al.*, 2011]. Others conditioned the model parameters based on alternative hydrological information such as remotely sensed evaporation [*Winsemius et al.*, 2008], soil moisture, water levels [*Michailovsky et al.*, 2012] or old discharge time series [*Winsemius et al.*, 2009].

Regarding the globally poor results obtained from the past studies, the necessity to develop a model able to represent the floodplain processes as well as taking into account the artificial reservoirs is evident. Moreover, no modeling effort has been undertaken below monthly time step, which is important for hydropower production. As extensions of the existing hydropower plants, new hydroelectric schemes and irrigation projects are planned on the Zambezi basin, an assessment of the development impact, accounting for the environmental flow would be of great help for local water resources management. Up to now, water resources management studies have been conducted without the use of validated global rainfall-runoff models [*Beilfuss and Brown*, 2010; The World Bank, 2010]. Instead, the observed data were completed by partial rainfall-runoff models [*Gandolfi and Salewicz*, 1991;

Gandolfi et al., 1997] or with simple water balance models [*Matondo and Mortensen*, 1998b]. Alternatively, hydrological sequences were generated from time series of historical natural discharges available at key locations throughout the basin [*Tilmant et al.*, 2010a; *Tilmant et al.*, 2012]. A finer evaluation of the economic implication of environmental flow as well as an optimization of the reservoirs operating rules would be an added value to the existing studies.

This chapter focuses on the development of a daily hydrological model for the entire Zambezi catchment including the hydraulic structures, based on the SWAT model and aimed at water resources management practices. Since the traditional calibration techniques are not adequate for model with insufficient calibration points, short data records, or overdetermined models due to the non-uniqueness of the solution [*Beven*, 1993; *Beven and Freer*, 2001], A Multi ALgorithm Genetically Adaptative Multiobjective (AMALAGM) approach [*Vrugt and Robinson*, 2007] is applied to the calibration process.

Below, Chapter 5.2 describes the study area, the model set-up and the data used. The methodology is presented in Chapter 5.3 and the results obtained in Chapter 5.4. Finally, conclusions are summarized in Chapter 5.5.

5.2 STUDY AREA AND DATA

5.2.1 The Zambezi River Basin

A detailed description of Zambezi river basin has been given already in Chapter 3.1. The basin lies fully within the tropics between 10°S and 20°S encompassing humid, semi-arid and arid regions dominated by seasonal rainfall patterns associated with the Inter-Tropical Convergence Zone (ITCZ). Rainfall varies considerably from year to year and occurs almost entirely between October and March. The resulting mean annual discharge at the delta is of 3800 m^3/s [*Tilmant et al.*, 2010a]. The river is characterized by large natural floodplains attenuating the runoff and big artificial impoundments regulating the flow. The long-term flow series as well as the climate observations reveals inter-annual cycles of high, medium, and low runoff with a duration varying from 10 to 80 years [*Jury*, 2003; *Mazvimavi and Wolski*, 2006; *Tyson et al.*, 2002]. It is therefore very difficult to get a time series of observed data which covers the whole runoff cycle. Since the runoff cycles have been reported to be primarily explained by rainfall cycles [*Beilfuss and Dos Santos*, 2001; *Farquharson and Sutcliffe*, 1998], the hypothesis adopted in this study is that a calibrated rainfall-runoff model is able to reproduce the observed cycles even if not tested over the entire climate cycle.

5.2.2 The hydrological model: SWAT 2009

Two criteria were defined to select the hydrological modeling tool: the application of a source code available in the public domain in order to be able to transfer the model to the stakeholders and the choice of a model already applied in Southern Africa with promising results which would contribute to an appropriate definition of the hydrological processes. Therefore, the Soil and Water Assessment Tool (SWAT), a river basin scale model available

in the public domain and actively supported by the USDA Agricultural Research Service at the Grassland, Soil and Water Research was chosen.

SWAT 2009 is a semi-distributed physically based continuous time model constituted in multiple components, including a hydrological module. The broad principle of the model is to simulate the water balance in each of the geographical sub-units for four storage volumes: snow, soil profile, shallow aquifer and deep aquifer by considering precipitation, interception, evapotranspiration, surface runoff, infiltration, percolation and subsurface runoff [*J G Arnold et al.*, 1998; *Neitsch et al.*, 2005]. Two methods for estimating surface runoff are available: the Green & Ampt infiltration method, which requires precipitation input in sub-daily scale [*Green and Ampt*, 1911] and the Soil Conservation Service (SCS) curve number procedure [*USDA Soil Conservation Service*, 1972] which relies on daily precipitation. A retention parameter is very significant in SCS method and it is defined by Curve Number (CN) which is a function sensitive to the soil's permeability, land use and antecedent soil water conditions. Finally, three options for estimating potential evapotranspiration (PET) are proposed: Hargreaves [*Hargreaves and Samani*, 1985], Priestley-Taylor [*Priestley and Taylor*, 1972] and Penman-Monteith [*Monteith*, 1965]. The inputs required for the Priestley-Taylor and Penman-Monteith methods are quite substantial: solar radiation, surface air temperature, relative humidity and wind (only for Penman-Monteith method) whereas the Hargreaves method estimates PET based only on maximum and minimum surface air temperature.

In order to adapt the model to the large floodplains and wetlands commonly found on African basins, the source code of the reservoir object was completed based on existing models [*McCartney et al.*, 2008; *Wolski et al.*, 2006]. The floodplains attenuate runoff, reducing and delaying flood peaks downstream [*Beilfuss and Dos Santos*, 2001]. They are characterized by significant evaporation losses and seasonal fluctuations. During high flow periods, water spreads over bank and inundates the floodplain whereas, during low flows, the water runs only along the main channel. Modeling some wetlands as natural reservoirs with specific storage and outlet characteristics proved successful for hydrological simulation in the Zambezi River basin [*The World Bank*, 2010]. The SWAT reservoir object receives water from all upstream sub-basins and computes the evaporation and rainfall based on surface area [*Neitsch et al.*, 2009]. To simulate the base flow constantly flowing out of the floodplain/wetland through the main channel and the upper flow, occurring when the floodplains are inundated, a double equation has been introduced for outflow computation. The base flow (Q_{base}) is made dependent of the water depth in the reservoir and of a release coefficient k [5-2]. The upper flow (Q_{up}) is computed through a free crest weir formula conditioned by an overflow constant (a) and an overflow exponent (b) when the water level inside the reservoir is above H_{min} [5-3].

$$Q_{outflow} = Q_{base} + Q_{up} \qquad\qquad\qquad [5\text{-}1]$$

$$Q_{base} = k \cdot H \qquad\qquad\qquad [5\text{-}2]$$

$$Q_{up} = \begin{cases} 0 & \text{if } H \leq H_{min} \\ a \cdot \left(H - H_{min} \right)^b & \text{if } H > H_{min} \end{cases}$$

[5-3]

where *k*, *a* and *b* are model parameters.

Due to the unusually large size of the main reservoirs, lakes and wetlands relatively to the sub-basins where they lay, the sub-basin surfaces were made dependent on reservoir surfaces, in order to take into account the expansion and reduction of the flooded surfaces in the water budget calculation. More details of these adaptations are given in Chapter 6.

5.2.3 Input data collection

5.2.3.1 *Topographic and land cover information*

Based on prior experiences of modeling in the Zambezi and usage of the SWAT model, to derive the river network and sub-catchments, as well as to characterize soils and land uses, the following data sets, available for Africa and a large part of the World, were chosen:

- the Digital Elevation Model (DEM) from the US Geological Survey's (USGC) public domain geographic database HYDRO1k which is derived from the 30° digital elevation model of the world GTOPO30 at a resolution of 1 km (http://eros.usgs.gov/#/Find_Data/Products_and_Data_Available/gtopo30_info);

- the soil map produced by the Food and Agriculture Organization of the United Nations at a resolution of 10 km [*FAO*, 1995]. A new version of the soil map is now available from the Harmonized World Soil Database of the FAO [*FAO/IIASA/ISRIC/ISSCAS/JRC*, 2012]. After a first comparison the differences on the Zambezi basin are not very big. However, it would be useful to include the refined data in a further version of the model, given that the new soil types can be documented in the SWAT database;

- the land-use grid from the Global Land Cover Characterization at a 1 km resolution (GLCC, Version 2, http://edcsns17.cr.usgs.gov/glcc/).

The soil and land-use associated characteristics were obtained from literature [*Schuol et al.*, 2008a; *Schuol et al.*, 2008b].

5.2.3.2 *Precipitation*

TRMM 3B42 version 6, NASA's standard precipitation product, was chosen as precipitation source based on a detailed study of the different satellite products [*Cohen Liechti et al.*, 2012]. It is produced since 1998 in four steps [*Huffman et al.*, 2007]: (1) passive microwave (PM) estimates are calibrated and combined, (2) infrared (IR) estimates are computed using PM estimates for calibration, (3) PM and IR estimates area combined, (4) data are rescaled to monthly total using Global Precipitation Climatology Centre (GPCC) data. The estimates are released on a 0.25° by 0.25° grid at 3-hourly temporal resolution

(00:00, 03:00,…, 21:00 UTC) in a global belt extending from 50°N to 50°S. The data have been changed during the calibration process to version 7 of the same product as it became available and constitutes an improvement in the rainfall estimation.

5.2.3.3 *Temperature*

The temperature grids (daily minimum and maximum) are compiled from the NCEP/DOE 2 Reanalysis data [*Kanamitsu et al.*, 2002] provided by the NOAA/OAR/ESRL PSD, Boulder, Colorado, USA, from their Website at http://www.esrl.noaa.gov/psd/. The spatial coverage varies from 88.542°N to 88.542°S and from 0°E to 358.125°E, stored on a Gaussian grid of 192 longitude bands of 1.875°.

5.2.3.4 *Discharge and water level*

The critical data set for reliable hydraulic-hydrological modeling is the time series of measured discharge which allows the calibration and validation of the model. The most extensive available database containing historical discharge records in the Zambezi Basin is managed by the Global Runoff Data Centre D - 56002 Koblenz, Germany (GRDC), which operates under the World Meteorological Organization (WMO) [*Fekete et al.*, 1999]. In the global database, 67 daily and 30 monthly stations located within the Zambezi basin have been identified. In addition, the Department of Water Affairs of Zambia (DWA, personal communication) provided a list of 34 stations with the associated discharge data over the Zambian part of the basin. The Zambezi River Authority (ZRA), managing the Kariba dam, Zambia Electricity Supply Corporation Limited (ZESCO), managing Itezhi Tezhi and Kafue Gorge dams and Hidroeléctrica de Cahora Bassa (HCB), managing the Cahora Bassa dam, shared some of the information recorded at the dams.

Despite these valuable contributions, most of the data series are not continuous and a few stations have not been considered as reliable. As can be seen in Figure 5-1, most of the available discharge data for the period of interest are distributed in the upper and middle parts of the basin and none downstream of Cahora Bassa.
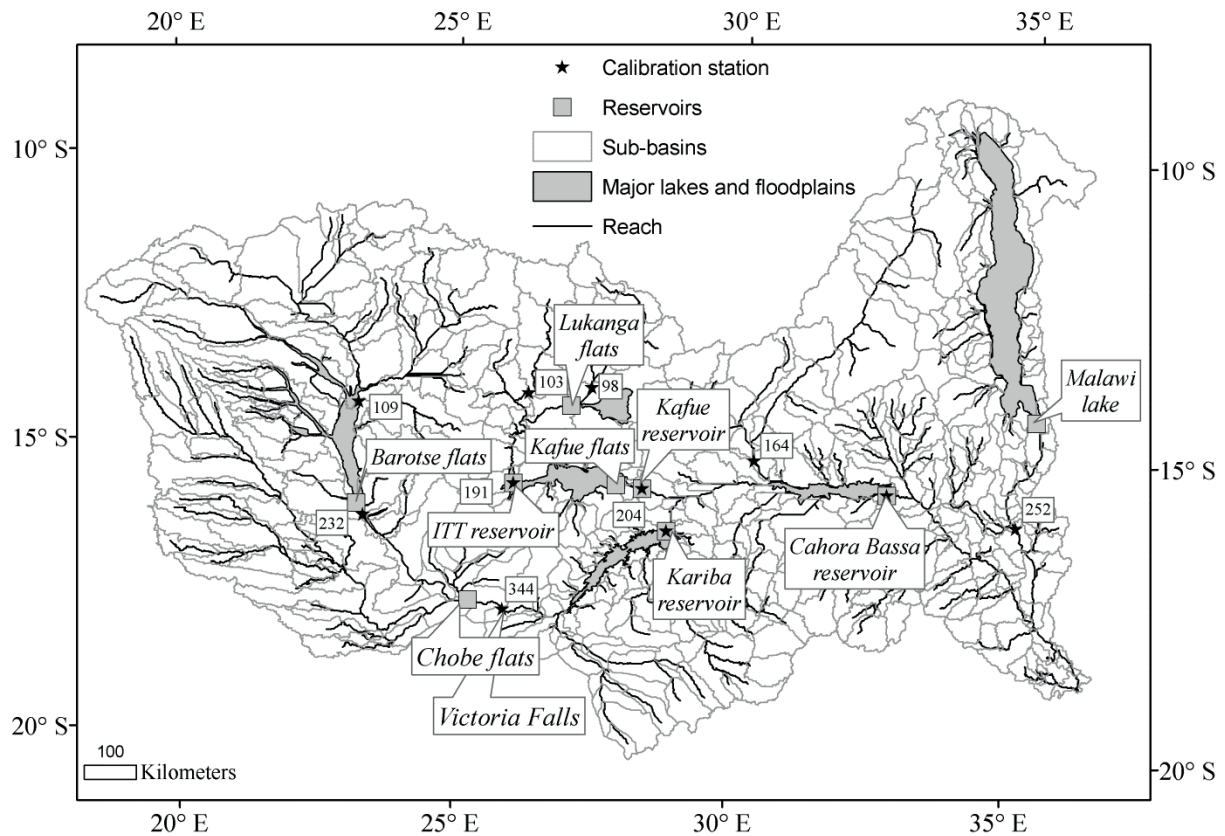
Figure 5-1. Sub-basin delineation with the corresponding reaches, the reservoirs and the calibration/validation stations.

The Zambezi River Authority (ZRA), Zambia Electricity Supply Corporation Limited (ZESCO) and Hidroeléctrica de Cahora Bassa (HCB) transmitted the water levels measured at Itezhi Tezhi, Kafue Gorge, Kariba and Cahora Bassa reservoirs. The water levels were converted to water volume using a linear relation as the level varies only by small amplitude compared to the reservoir height.

The years 1998 to 2006 were chosen as the period to be modeled. To assess the variability of the modeled years, the variability of the observed discharge at Victoria Falls from 1958 to 2007 has been compared to the variability of the observed discharge at the same place from 2000 to 2006 (Figure 5-2). From this analysis, the modeled period was considered representative of the multi-years cycles.
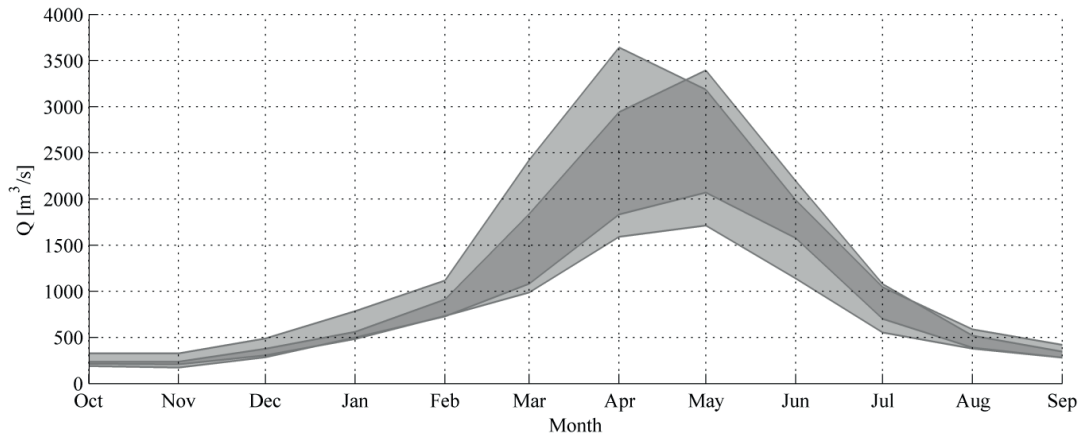
Figure 5-2. 25th and 75th quartile of the mean monthly discharge at Victoria Falls for the period 1958 to 2007 (light gray) and for the period 2000 to 2006 (dark gray).

After a compilation of the observed data from upstream to downstream and an assessment of the percentage of missing data for each station, only nine stations were kept as calibration/validation points (Figure 5-1). The three major reservoirs (Itezhi Tezhi, Kariba and Cahora Bassa) were selected as calibration/validation points for reservoir volume variation.

5.2.4 Model set-up

The SCS method for surface runoff was selected for model simulations. For evapotranspiration, as the inputs required by Priestley-Taylor and Penman-Monteith methods are demanding and the meteorological data available are limited, the Hargreaves method [*Hargreaves and Samani*, 1985], based solely on maximum and minimum surface air temperature, was chosen.

The preprocessing of model inputs was performed within the ESRI ArcGIS 9.3.1 software using the ArcSWAT interface version 2009.93.7a [*Winchell et al.*, 2007]. Based on the topography, a minimum drainage area of 5000 km^2 was defined to discretize the watershed in about 200 sub-basins. This threshold was chosen as a balance between the precision of the input data (soil and land use) and the complexity of the model, given the limited number of calibration points available. The sub-basins directly draining to reservoirs, lakes and wetlands were then refined by superposing to the previous discretization a GIS layer of lakes and flats of Africa, resulting in a total of 405 sub-basins (Figure 3-1).

The geomorphology, stream parameterization and overlay of soil and land cover were automatically accomplished within the interface. SWAT calculates the hydrological cycle over Hydrological Response Units (HRU) which consists in 'lumped land areas within the sub-basin that are comprised of unique land cover, soil and management combinations' [*Neitsch et al.*, 2009]. In the present case, the HRUs were delimitated using a threshold of 35% for the land use, the soil and the slope resulting in a total of 778 units. The threshold was chosen in order to take into account a large part of the information available on the soil and

land use map while keeping the complexity of the model low to reduce both the calculation time and the number of parameters to calibrate.

The artificial and natural lakes, as well as the major wetlands on the main channel, were modeled as unregulated reservoirs. Their volume and surface are listed in the Table 5-1 for typical flood and low flow periods. For the regulated reservoirs, the simulated outflow was constrained to the observed one in order to reproduce exactly the operations. The initial volumes were set according to the observations at the start of the calibration period.

Table 5-1. Reservoirs characteristics.

	Barotse flats [1,2]	Chobe flats [1]	Kariba Dam [3,4]	Lukanga flats [2,5]	ITT Dam [3,6]	Kafue flats [2,3,6]	Kafue Gorge Dam [3,6]	Cahora Bassa Dam [3]
Year of operation			1963		1977		1972	1977
Surface during flood / during low flows [10^6 m^3]	11,960 / 1.000	2,800 / 1,000	5,627 / 5,300	2,600 / 2,100	380 / 90	7,000 / 1,850	750 / 180	2,502 / 838
Volume during floods / during low flows [10^9m^3]	17 / 2	8.4 / 2.5	191 / 116	3.9 / 2.8	6.0 / 0.8	9.5 / 2.2	0.9 / 0.1	57 / 12.2
H_{min} [m]	1.00	2.50	-	1.30	-	1.17	-	-

[1] [**The World Bank**, 2010]
[2] **FAO http://www.fao.org/docrep/005/F9051F/F9051F02.htm#ch2.2**
[3] [**Beilfuss**, 2001; **Beilfuss and Dos Santos**, 2001]
[4] [**Mhlanga and Goguel**, 2007]
[5] **http://en.wikipedia.org/wiki/Lukanga_Swamp**
[6] [*Kunz et al., 2011a; McCartney and Houghton-Carr, 1998; Obrdlik et al., 1989*]

SWAT developers recommend at least one year of stabilization period to allow the model to properly reproduce the water cycling processes and diminish the influence of the inaccurate initial conditions (e.g. initial soil water content, initial depth of water in the shallow aquifer, and initial depth of water in the deep aquifer). Due to the size of the basin, two years of stabilization were adopted (1998-1999). In order not to "lose" scarce discharge data, in the final phase of the calibration the same years were reused for calibration (1998-2003) starting from the initial conditions reached at the end of the two years stabilization period and setting the initial volume in the artificial reservoirs to the observed value. The remaining years (2004 to 2006) were kept for validation.

5.3 CALIBRATION METHODOLOGY

5.3.1 Introduction

The calibration procedure was defined in three steps. At first, the model parameters which will be optimized were chosen. Secondly, the objective functions were defined based

on the future model use and thirdly an algorithm was implemented to find the "bests" parameter sets. Depending on the calibration results, the parameters as well as their bounds were refined and the objective function changed to improve the result in an iterative progression.

5.3.2   Choice of the parameters

The first step of the calibration procedure consists in parameters specification. As SWAT partitions the watershed into sub-basins and smaller Hydrologic Response Units (HRU), some parameters have a uniform value over the entire watershed and others depend on soil type, land use and/or topographic features. To select the most sensitive parameters and define their reasonable bounds, literature related to SWAT [*Bekele and Nicklow*, 2007; *Muleta and Nicklow*, 2005] and recent studies where it was applied to Africa [e.g. *Schuol and Abbaspour*, 2006; *Schuol et al.*, 2008a] were consulted. As a complement to this, the sensitivity analysis procedure of Van Griensven [2006] included in the ArcSWAT interface [*Winchell et al.*, 2010] was used to assess the importance of different parameters on runoff generation process. The method combines the Latin Hypercube (LH) and One-factor-At-a-Time (OAT) sampling, assuring that the changes in the outputs after each model run can be unambiguously attributed to the parameter that was changed [*van Griensven et al.*, 2006]. The parameters were defined according to the acceptance of a catchment-wide parameterization, being that the HRU parameters related to the soil or land cover were changed relatively to the global set, still translating the physical diversity defined by the GIS data and reducing the number of parameters to be calibrated.

The parameters calibrated during the last iteration of the calibration procedure are listed in the Table 5-2 and described below.

- The plant canopy can significantly affect infiltration, runoff and evapotranspiration by intercepting the rain. The maximum amount of water that can be trapped in the canopy is used for the calibration, defined as CANMX.

- Regarding the infiltration process, five parameters are integrated:

  o The curve numbers (CN_F) depend on the soil permeability, the land use and the antecedent moisture conditions and vary depending on the soil type. Its value is therefore change relatively during the calibration procedure keeping the spatial heterogeneity defined by the soil map.

  o The soil available water capacity (SOL_AWC) also referred as the plant available water is also depending on the soil type and therefore varied in relative terms during the calibration procedure.

  o The soil depth (SOL_Z) characterizes the thickness of the soil layer. It is defined for each soil type in the database and therefore changed relatively during the calibration procedure to keep the heterogeneity of the soil.

- o The soil evaporation compensation factor (ESCO) allows the user to account for the effect of capillary action during the evaporation from the soil. A low value signifies that the evaporative demand will be supply from the low levels of soil. It varies between 0 and 1.

- o The plant uptake compensation factor (EPCO) defines the capacity of the low soil layers to provide water to the plants. A high value allows more of the water uptake demand to be met by low layers in the soil. It varies between 0 and 1.

- The surface runoff lag coefficient (SURLAG) defines the portion of the surface runoff that will reach the main channel on the day it is generated. A low value signifies that a large quantity of water will be held in storage.

- The baseflow is adjusted based on five parameters;

  - o The groundwater coefficient (GW_REVA) characterizes the movement of water from the shallow aquifer to the overlying unsaturated zone. A high value results in a high transfer rate. It varies between 0.02 and 1.

  - o The threshold depth of water in the shallow aquifer for revap to occur (REVAPMN) fixes the limit of the water level for return flow to the unsaturated zone to occur.

  - o The threshold depth of water in the shallow aquifer for base flow to occur (GWQMN) fixes the limit of the water level for return flow to the reach to occur.

  - o The groundwater delay time (GW_DELA) defines the lag between the times that water exits the soil profile and enters the shallow aquifer.

  - o The baseflow recession constant (AlPHA_B) is a direct index of groundwater flow response to change in recharge. A high value characterizes the land with rapid response. It varies from 0 to 1.

- The effective hydraulic conductivity in the main channel alluvium /CH_KII) characterize the relation between the main channel and the groundwater. A low value signifies that there is a low loss from the channel to the groundwater.

- The outflow from the natural reservoirs, namely the floodplains, is calibrated on three parameters. The values are set independently for each floodplain.

  - o The reservoir overflow constant (a) defines the rate and the amount of water flowing as upper flow from the reservoir. A high value increases the upper flow.

  - o The reservoir overflow exponent (b) characterizes the relation between the depth of water inside the reservoir and the upper flow.

  - o The reservoir release coefficient (k) defines the rate at which the base flow exits the reservoir. A low value decreases the base flow.

Table 5-2. SWAT model parameters included in the final iteration of the calibration procedure with their upper and lower bounds.

Parameter	Description	Unit	Lower bounds	Upper bounds
CANMX	Maximum canopy storage	mm	0	30
Infiltration				
CN_F	SCS curve number for moisture condition	%	-0.25	0.15
SOL_AWC	Available water capacity of the soil layer	%	-0.5	1
SOL_Z	Depth from soil surface to bottom of the layer	%	-0.5	1
ESCO	Soil evaporation compensation factor	-	0.001	1
EPCO	Plant uptake compensation factor	-	0	1
SURLAG	Surface runoff lag time	day	0.5	1.5
Groundwater flow				
GW_REVA	Ground water coefficient for flow to move into the overlying unsaturated zone	-	0.1	0.4
REVAPMN	Threshold depth of water in the shallow aquifer for ground water to move into the overlying unsaturated layers	mm	1	400
GWQMN	Threshold depth of water in shallow aquifer for return flow (to the reach) to occur	mm	5	100
GW_DELA	Groundwater delay	day	20	300
ALPHA_B	Baseflow recession constant	day	0	0.5
CH_KII	Effective hydraulic conductivity in main channel alluvium	mm/hr	0.1	50
Floodplain				
a	Reservoir overflow constant	$m^{3/2}$/s	900	55,000
b	Exponent of overflow equation for reservoir	-	1	3.5
k	Reservoir release coefficient	m^2/s	35	350

5.3.3   Definition of the objective function

Since the success of an automatic calibration process is highly dependent on the objective function chosen [*Gupta et al.*, 1998], in the second step of the procedure, the objective function was defined. Before selecting the indicators the calibration objectives were defined as follows. (1) As the model is to be used to simulate different scenarios of water resource exploitation mainly focused on dam operations, the error in runoff volumes should be minimized (2) The global shape of the simulated hydrograph should be similar to that of the observed hydrograph.

The general form of a multi-objective calibration problem can be stated as follows:

$$\hat{\mathbf{x}}_{opt} = \arg\min_{\mathbf{x}} \mathbf{F}(\mathbf{x}) = \arg\min_{\mathbf{x}} \left[F_1(\mathbf{x}), F_2(\mathbf{x}),..., F_p(\mathbf{x}) \right], \quad \mathbf{x} = (x_1,...,x_i), \mathbf{x} \in X \qquad [5\text{-}4]$$

where X is the parameters space, $\mathbf{x}$ the parameter vector and $\mathbf{F}(\mathbf{x})$ the set of associated objective functions.

As the set of functions $\mathbf{F(x)}$ will be minimized by the algorithm in respect to the whole catchment, the performance measures have to be reformulated to be applicable to several discharge stations / reservoir storage areas.

In the present study, the following performance indicators along with the associated objective function to be minimized were used in the calibration procedure: the relative error (RE) [5-5], the Nash Sutcliffe coefficient (NS) [5-6] and the volume ratio (VR) [5-7].

$$\text{RE} = \frac{1}{n}\sum_{i=1}^{n}\frac{\left|Q_{s,i}-Q_{o,i}\right|}{Q_{o,i}}, \; OF = \frac{\sum_{j=1}^{N}\left(RE_j\right)}{N} \tag{5-5}$$

$$\text{NS} = 1 - \frac{\sum_{i=1}^{n}(Q_{s,i}-Q_{o,i})^2}{\sum_{i=1}^{n}(Q_{o,i}-\overline{Q_o})^2}, \; OF = \frac{\sum_{j=1}^{N}(1-NS_j)}{N} \tag{5-6}$$

$$\text{VR} = \frac{\sum_{i=1}^{n}Q_{s,i}}{\sum_{i=1}^{n}Q_{o,i}}, \; OF = \frac{\sum_{j=1}^{N}\left|1-VR_j\right|}{N} \tag{5-7}$$

where Q_s and Q_o are the simulated and observed discharge, n the number of discharge records available at each station and N the number of discharge stations.

In order to converge faster, the optimization algorithm was never set to optimize the three performance indicators but their values were calculated during the result analysis and used to select to most appropriate parameter sets among the "best" solutions generated by the algorithm.

5.3.4   Automatic calibration algorithm

As several (potentially conflicting) objectives are being optimized, the solution of Eq. [5-4] is not likely to be a unique set of parameters but rather a Pareto front of optimal non-dominated solutions. As the ensemble of possible solutions is quite large and the solution space is non-convex, the application of heuristic search algorithms is a sound option. To explicitly address the problematic of finding the front of non-dominated solutions the multi-algorithm genetically adaptive multi-objective method (AMALGAM), which has already been documented as a high performance solution compared to other evolutionary multi-objective algorithms for SWAT calibration [*Zhang et al.*, 2010; *Zhang et al.*, 2011], was implemented [*Vrugt and Robinson*, 2007; *Vrugt et al.*, 2009].

AMALGAM can be classified as a meta-algorithm for multi-objective optimization as it uses several particular algorithms incorporating different concepts and combines their results. By doing so, it draws from the particular strengths of the best performing algorithms for each given problem, possibly reaching better and faster results. Particularly, solutions are

adaptively changed based on the shape of the fitness landscape using four optimization methods: (i) non-dominated sorted genetic algorithm-II (NSGA-II) [*Deb et al.*, 2002], (ii) particle swarm optimization (PSO) [*Kennedy and Eberhart*, 1995], (iii) adaptive Metropolis search (AMS) [*Haario et al.*, 2001], and (iv) differential evolution (DE) [*Storn and Price*, 1997]. The population of parameter sets evolved based on the results of the previous population. The user defines the population size as well as the maximum number of iterations. Typically, the algorithm is stopped when it has reached a satisfying value of the objective function or when the convergence rate falls consistently below a certain threshold.

5.3.5   Result analysis

Two concepts illustrate the importance of non uniqueness of an optimal solution to the model calibration; the principle of equifinality [*Beven and Freer*, 2001] and the concept of Pareto front [*Gupta et al.*, 1998]. In light of these concepts, no unique optimal solution is likely to be found mathematically without an appreciable degree of subjectivity. As such, human capacity to appreciate errors induced by data and model structure, as well as expert knowledge of the catchment's hydrology, recommend user judgment as a complement to the automatic algorithms. Using AMALGAM as the optimization tool with multiple objectives allow defining a set of non-dominated solutions according to various trade-offs between objectives.

The following methodology is proposed to select the adequate parameter set(s):

1. Multiple parameter sets are selected from the automatic calibration algorithm results according to the objective function's values.

2. The objective function values, as well as complementary indicators are computed at each station for the calibration and the validation periods.

3. The best(s) solution(s) is(are) subjectively chosen based on the results obtained and the hydrographs and eventually manually adjusted to fit the specific needs of the user.

As the calibration method is developed for a basin equipped with hydraulic schemes, the measured water level is available at the main reservoirs and can be converted to reservoir volume. Therefore, performance measures are also computed for the reservoir volume variation.

5.4   RESULTS AND DISCUSSION

For the record, location of the discharge and controlled reservoir stations used during the calibration process is shown in Figure 5-1 along with the floodplains included in the model.

5.4.1   First iteration

The aim of the first iteration was to test the model over a short time period without validation and in an area without the influence of major dams or wetlands. Therefore, the area under calibration was restricted to the upper part of the Zambezi and the Kafue Basins. Also, only the calibration period was analysed. The calibration parameters are presented in the Table 5-3.

Table 5-3. SWAT model parameters calibrated in first iteration of the calibration procedure with their upper and lower bounds.

Parameter	Description	Unit	Lower bounds	Upper bounds	Calibrated value
SURLAG	Surface runoff lag time	day	0.5	4	0.50-0.56
ALPHA_B	Baseflow recession constant	day	0	1	0.1-0.16
GW_DELA	Groundwater delay	day	100	600	488-520
GW_REVA	Ground water 'revap' coefficient for flow to move into the overlying unsaturated zone	-	0.1	0.4	0.197-0.198
GWQMN	Threshold depth of water in shallow aquifer for return flow (to the reach) to occur	mm	5	100	5.00-6.89
ESCO	Soil evaporation compensation factor	-	0.001	1	0.60-0.65
CN_F	SCS curve number for moisture condition	%	-0.25	0.15	–0.070-–0.075
CH_KII	Effective hydraulic conductivity in main channel alluvium	mm/hr	0.1	30	10-17
SOL_AWC	Available water capacity of the soil layer	%	-0.3	1	0.98-0.99
SOL_Z	Depth from soil surface to bottom of the layer	%	-0.5	0.5	0.35-0.46
CANMX	Maximum canopy storage	mm	0	30	43-46

The objective function used was the relative error (RE) summed over all the selected calibration stations. The population was set to 100 and the model was run up to reaching a stable set of solutions.

From the last population, the best parameter sets were chosen according to the Nash-Sutcliffe coefficient value (NS) (higher than 0.35 at each of the station) (Table 5-4). They show the ability of the model to reproduce the flow pattern of the upper Zambezi and Kafue Basin (Figure 5-3). Due to the limited availability of registered data, the station # 103 has not been used for the continuation of the calibration.
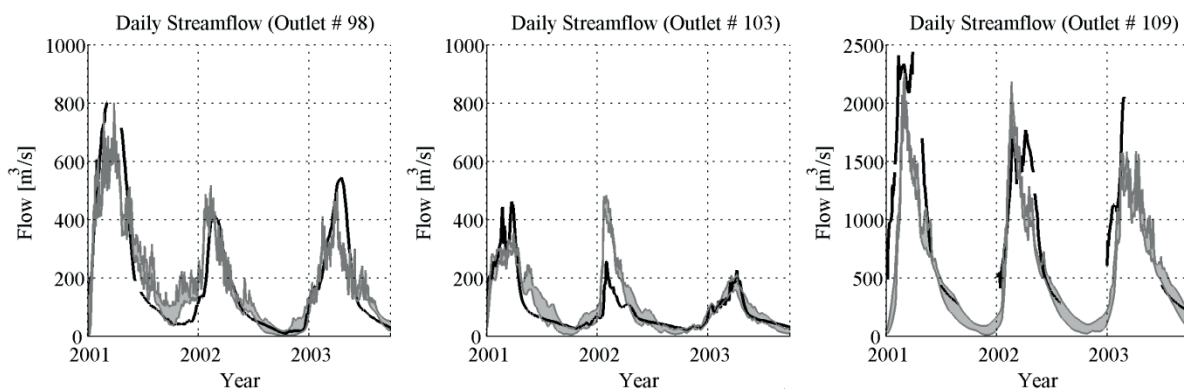
Figure 5-3. Hydrographs of observed (black line) and simulated data (grey line) for the first iteration of the calibration procedure, at stations #98 (Chilenga), #103 (Chifumpa) and #109 (Lukulu).

Table 5-4. Indicators values at the discharge stations after the first iteration of the calibration procedure (NS Nash-Sutcliffe coefficient, VR volume ratio, RE relative error).

	Global value	station # 98	station # 103	station # 109
RE	0.37-0.51	0.41-0.76	0.35-0.5	0.3-0.34
NS	0.55-0.61	0.72-0.79	0.38-0.55	0.46-0.55
VR	0.84-1.04	0.95-1.11	1.02-1.33	0.7-0.82

The results of the first iteration showed that the model is able to reproduce the flow of the Zambezi and the Kafue and can therefore be calibrated over the whole basin for a longer time period.

5.4.2 Second iteration

The second iteration aimed to calibrate the model down to Cahora Bassa dam separating the time period when observed data are available between a calibration period (from 2000 to 2003 leaving the years 1998 and 1999 for stabilization) and a validation period (from 2004 to 2006). In order to refine the evaporation estimation and therefore to improve the water balance, two original SWAT model parameters were added to the previous list (REVAPMN and EPCO). Moreover, the parameters related to the floodplains were also included in the calibration process (Table 5-5). The upper and lower bounds of the parameter values were adjusted based on the results of the previous iteration and on parallel simulations.

Discharge stations located on the Kafue sub-basin were added: station # 191 corresponding to the measured inflow of Itezhi Tezhi reservoir and station # 204 corresponding to a reconstructed series of inflow based on the water balance at the Kafue Gorge reservoir. On the Zambezi River, station # 344 is located at Victoria Falls and station # 208 consists of a reconstructed series of inflow at the Cahora Bassa reservoir. Figure 5-1 presents the stations on the basin map.

Table 5-5. SWAT model parameters included in second iteration of the calibration procedure with their upper and lower bounds.

Parameter	Description	Unit	Lower bounds	Upper bounds
SURLAG	Surface runoff lag time	day	0.5	1.5
ALPHA_B	Baseflow recession constant	day	0	0.5
GW_DELA	Groundwater delay	day	20	300
GW_REVA	Ground water 'revap' coefficient for flow to move into the overlying unsaturated zone	-	0.1	0.4
REVAPMN	Threshold depth of water in the shallow aquifer for ground water to move into the overlying unsaturated layers	mm	1	400
GWQMN	Threshold depth of water in shallow aquifer for return flow (to the reach) to occur	mm	5	100
ESCO	Soil evaporation compensation factor	-	0.001	1
CN_F	SCS curve number for moisture condition	%	-0.25	0.15
CH_KII	Effective hydraulic conductivity in main channel alluvium	mm/hr	0.1	50
SOL_AWC	Available water capacity of the soil layer	%	-0.5	1
SOL_Z	Depth from soil surface to bottom of the layer	%	-0.5	1
EPCO	Plant uptake compensation factor	-	0	1
CANMX	Maximum canopy storage	mm	0	30
Floodplain parameters				
a	Reservoir overflow constant	$m^{3/2}/s$	1,100	55,000
b	Exponent of overflow equation for reservoir	-	1.5	3.5
k	Reservoir release coefficient	m^2/s	35	70

To achieve a better correspondence between the observed and simulated data, two objective functions were optimized: the sum of the Nash-Sutcliffe coefficient (NS) and the sum of volume ratio (VR) at each station.

The population size was set to 100 and the optimization was stopped when reaching a global NS coefficient of 0.75 and a volume ratio between 0.99 and 1.01 (Table 5-6). However, the values dropped during the validation period to 0.22 for the global NS and 0.96 for the global VR (Table 5-6). The stations # 204 and 208, both corresponding to reconstructed discharge series at the inlet of reservoirs, displayed a negative NS value for the validation period.

Table 5-6. Indicators values at the discharge stations for the second iteration of the calibration procedure (NS Nash-Sutcliffe coefficient, VR volume ratio).

	Global value	station # 98	station # 109	station # 344	station # 191	station # 204	station # 208
NS calibration	0.75-0.76	0.62- 0.83	0.71-0.76	0.77-0.85	0.70-0.73	0.71-0.77	0.69-0.80
VR calibration	0.99-1.01	0.79-1.04	0.84-0.92	1.07-1.17	0.95-1.01	0.83-0.95	1.11-1.15
NS validation	0.17-0.28	0.78-0.86	0.07-0.25	0.77-0.81	0.22-0.42	–0.79--0.32	–0.58--0.06
VR validation	0.94-1.01	0.74-0.83	0.68-0.78	1.13-1.30	0.83-0.89	0.96-1.03	1.22-1.29

The optimal values were clearly defined for all the SWAT parameters (Figure 5-4), except for the plant compensation factor (EPCO) which appeared to have less influence on the result. For the floodplain parameters (Figure 5-5), the release coefficient (*k*) of the Lukanga and the Chobe floodplains was not determined as precisely as the other parameters, probably due to its lower influence on the simulated discharge. The parameter sets selected as optimal results for the second iteration are presented in the Appendix.

By looking at the hydrographs (Figure 5-6), it is clear that the time series reconstructed at station # 204 has a shape which is difficult to reproduce and probably influenced by imprecision in the water balance at the reservoir. The same remark can be applied to station # 208. In terms of discharge volume, the year 2005 is undervalued on the upper basin (stations # 109 and 344), probably due to an underestimation of the rainfall. The base flow is also undervalued every year at stations # 98 and 109.

Regarding the volume of water stored in the reservoirs, the following remarks can be done:

- A global overestimation of the volume was observed for all the reservoirs.

- At the Itezhi Tezhi reservoir (Figure 5-7, a), the surplus came mainly from the low flow overestimation and is relatively constant during calibration and validation periods.

- At the Kafue Gorge reservoir (Figure 5-7, b), due to its small size, the model is unable to reproduce the observed variations. For the following iterations of the calibration process, it has been considered as a run-of-river reservoir and only the observed discharge has been used for calibration.

- At Kariba reservoir (Figure 5-7, c), the discharge overestimation occurs mainly during the first year and is then limited except for the last year of the validation period.

- At Cahora Bassa reservoir (Figure 5-7, d), a constant increase of volume compared to the observed data can be observed. This is likely due to the overestimation of inflow (station # 208, Figure 5-6) particularly during validation period.

In order to improve the base flow simulation and to take into account the reservoir data during calibration, the objective function has been modified for the third iteration of the calibration procedure, focusing on the relative error (RE) and not on the NS coefficient.
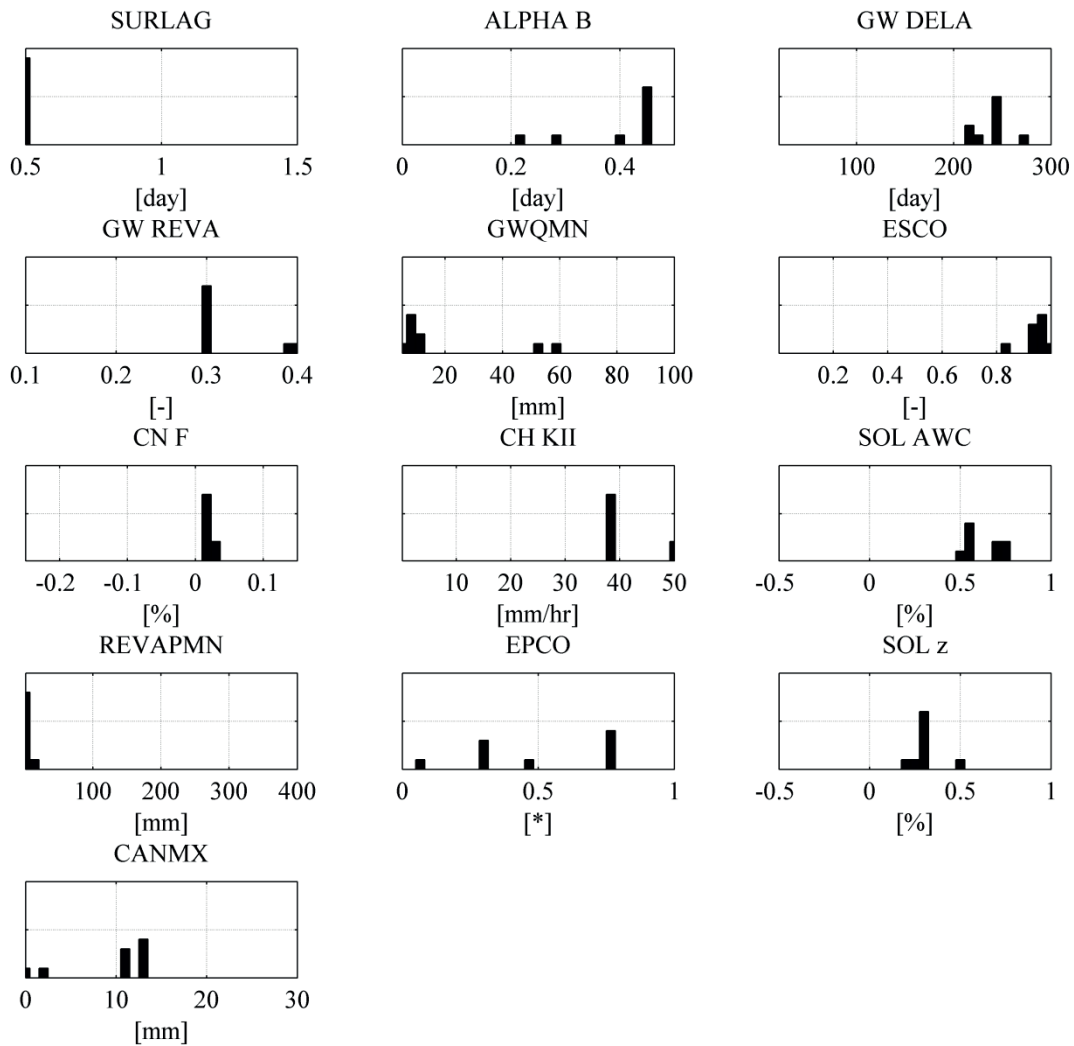
Figure 5-4. Histograms of the selected original SWAT parameters after the second iteration procedure. (SURLAG: surface runoff lag time, ALPHA_B: baseflow recession constant, GW_DELA: groundwater delay, GW_REVA: groundwater revap coefficient, GWQMN: threshold depth of water in the aquifer for return flow to occur, ESCO: soil evaporation compensation factor, CN_F: SCS curve number, CH_KII: effective hydraulic conductivity in main channel, SOL_AWC: available soil water capacity, REVAPMN: threshold depth of water in the shallow aquifer for 'revap' to occur, EPCO: plant uptake compensation factor, SOL_Z: depth of soil layer, CANMX: maximum canopy storage).
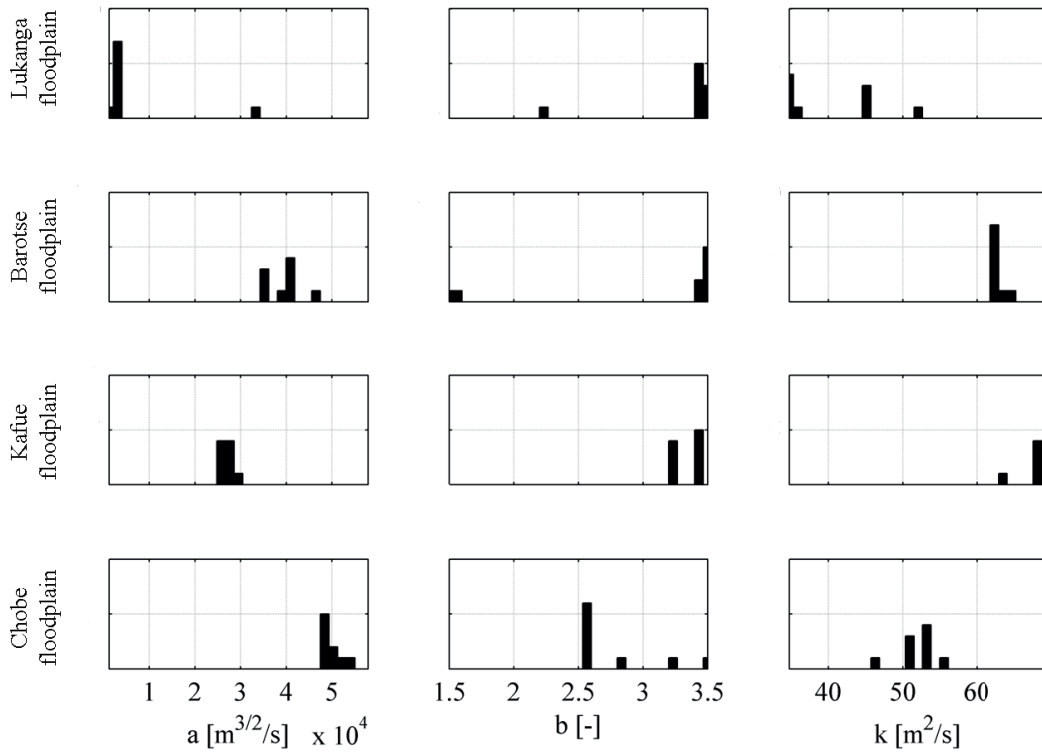
Figure 5-5. Histograms of the selected floodplain parameters after the second iteration of the calibration procedure. (a: reservoir overflow exponent, b: exponent of overflow equation for reservoir, k: reservoir release coefficient).
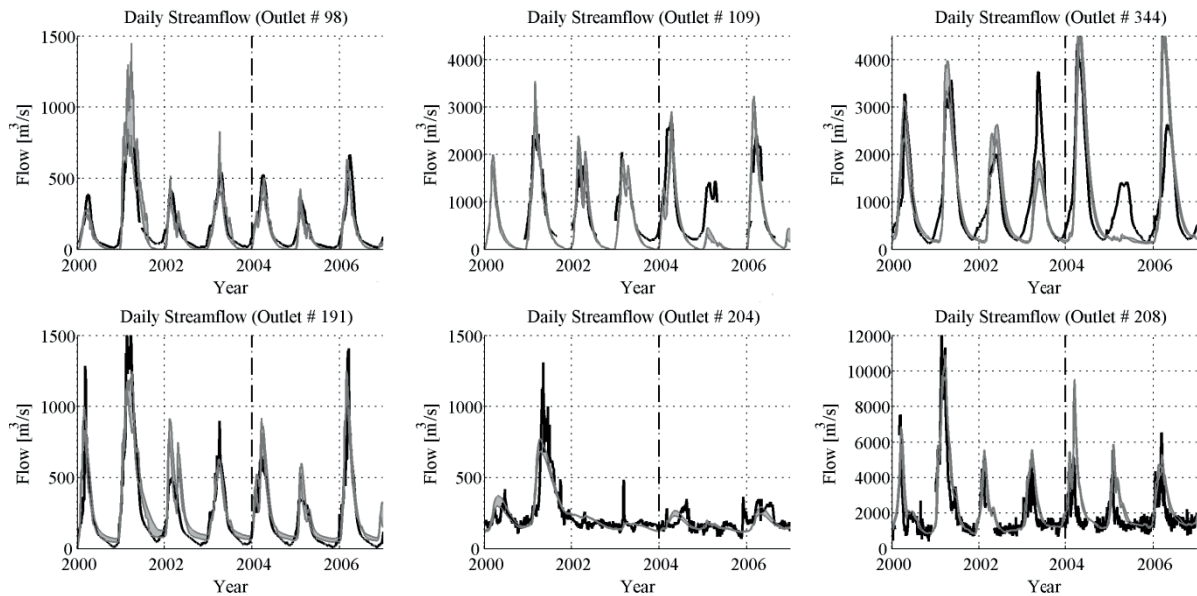
Figure 5-6. Hydrographs of observed (black line) and simulated data (grey line) after the second iteration of the calibration procedure at stations #98 (Chilenga), #109 (Lukulu), #344 (Victoria Falls), #191 (inflow of Itezhi Tezhi reservoir), #204 (inflow of Kafue reservoir) and #208 (inflow of Cahora Bassa reservoir).
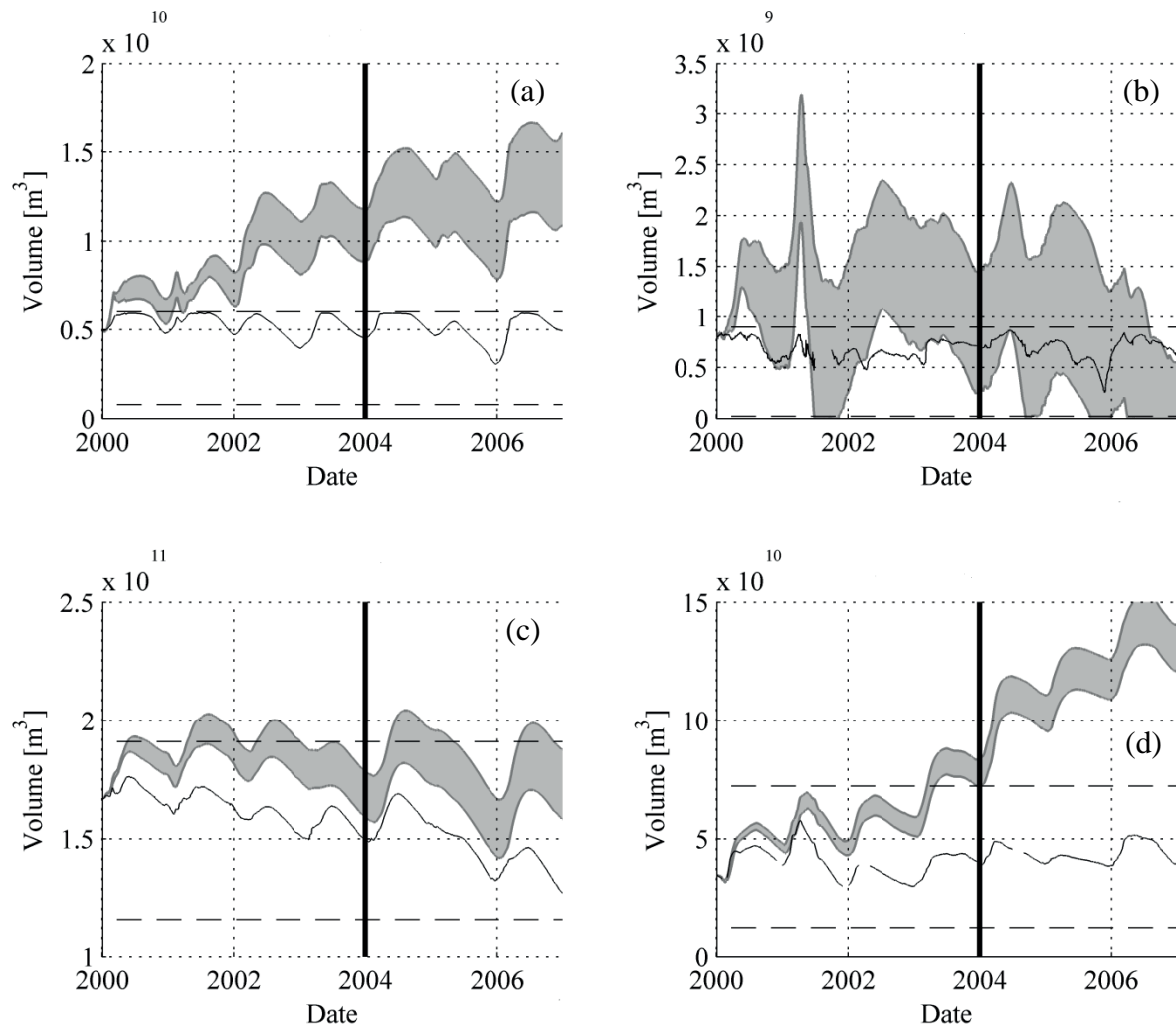
Figure 5-7. Simulated (grey line) and observed (black line) volume variation after the second iteration of the calibration procedure at Itezhi Tezhi (a), Kafue Gorge (b), Kariba (c) and Cahora Bassa (d) dams with the full reservoir and the minimum operating volumes (dashed lines) for the calibration and validation periods (separated by a black vertical line).

5.4.3 Third iteration

The third iteration goal was to improve the base flow simulation and to take into account the reservoir data during calibration. Therefore, the objective function has been modified to focus more on the low flow, replacing the NS by the relative error (RE) and keeping the volume ratio as the second objective function. The same calibration and validation periods that were used for the second iteration, respectively 2000 to 2003 and 2004 to 2006, were considered again. The volume variations observed at the reservoirs were added as calibration points, replacing the discharge in the equations. The population size was set to 100 and the algorithm was stopped when the objective functions reached 35% for RE and 20% for VR since there was no further improvement for few generations of parameter sets. The calibration was done on three discharge stations (# 98, # 109 and # 344) located upstream of the dams and on the three major reservoirs (Itezhi-Tezhi, Kariba and Cahora Bassa). The best parameter sets, below the objective function limits, were tested for the validation period. Values of RE, VR as well as NS coefficients at each station were computed for both calibration and validation periods (Table 5-7).

Even with the change of objective function and the addition of the volume variation, similar problems to those identified in the earlier iteration were detected:

- Negative NS value during the validation period for station # 109 and 344 (Table 5-7).

- Flood period of the year 2005 missing (Figure 5-10), probably due to an error in the rainfall data.

- Base flow undervalued at stations # 98 and # 109 (Figure 5-10).

Table 5-7. Indicators values at the discharge and reservoir stations after the third iteration of the calibration procedure (NS Nash-Sutcliffe coefficient, VR volume ratio, RE relative error).

	Global value	station # 98	station # 109	station # 344	Itezhi Tezhi	Kariba	Cahora Bassa
NS calibration	0.56-0.58	0.50-0.52	0.70-0.71	0.46-0.53	-	-	-
VR calibration	0.80-0.82	0.89-0.94	0.82-0.83	0.74-0.75	0.95-0.97	0.99-1.00	0.94-0.96
RE calibration	0.33-0.34	0.65-0.67	0.37-0.38	0.36-0.40	0.11-0.12	0.02-0.03	0.07-0.08
NS validation	−0.14--0.01	0.42-0.43	−0.05--0.04	−0.79--0.42	-	-	-
VR validation	0.73-0.75	0.46-0.47	0.63-0.64	0.83-0.85	0.79-0.90	0.84-0.86	1.53-1.57
RE validation	0.50-0.53	0.58-0.61	0.52-0.53	0.57-0.68	0.10-0.21	0.14-0.16	0.54-0.58

SWAT parameter values were all well-defined (Figure 5-8). By comparing the best parameter values obtained to the ones from the previous iteration, it can be seen that the surface runoff lag time (SURLAG), the groundwater delay coefficient (GW_DELA), the soil evaporation compensation factor (ESCO), the curve number coefficient (CN_F), as well as the threshold depth of water in the shallow aquifer for return flow to occur (REVAPMN) converge to identical values. The remaining parameters diverge. The parameter sets selected as optimal results for the third iteration are presented in the Appendix.
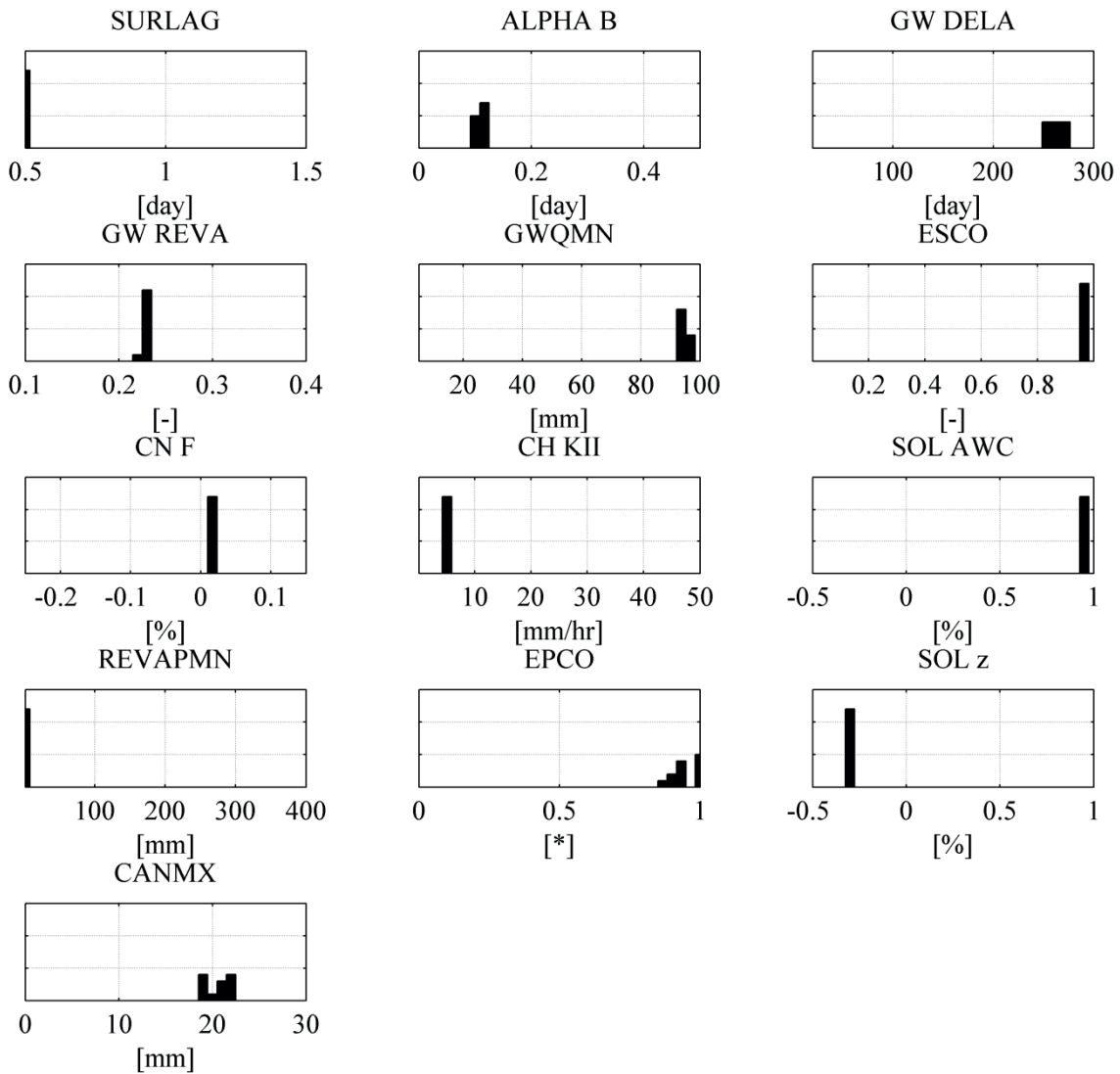
Figure 5-8. Histograms of the selected original SWAT parameters for the third iteration procedure. (SURLAG: surface runoff lag time, ALPHA_B: baseflow recession constant, GW_DELA: groundwater delay, GW_REVA: groundwater revap coefficient, GWQMN: threshold depth of water in the aquifer for return flow to occur, ESCO: soil evaporation compensation factor, CN_F: SCS curve number, CH_KII: effective hydraulic conductivity in main channel, SOL_AWC: available soil water capacity, REVAPMN: threshold depth of water in the shallow aquifer for 'revap' to occur, EPCO: plant uptake compensation factor, SOL_Z: depth of soil layer, CANMX: maximum canopy storage).

For the floodplain parameters (Figure 5-9), the best values are quite different from the ones attained in the previous iteration with the exception of Lukanga floodplain. The Chobe floodplain parameters are the most largely distributed, which is probably due to the small size of this floodplain compared to the others and, consequently, to its reduced influence on the overall discharge performance metrics.
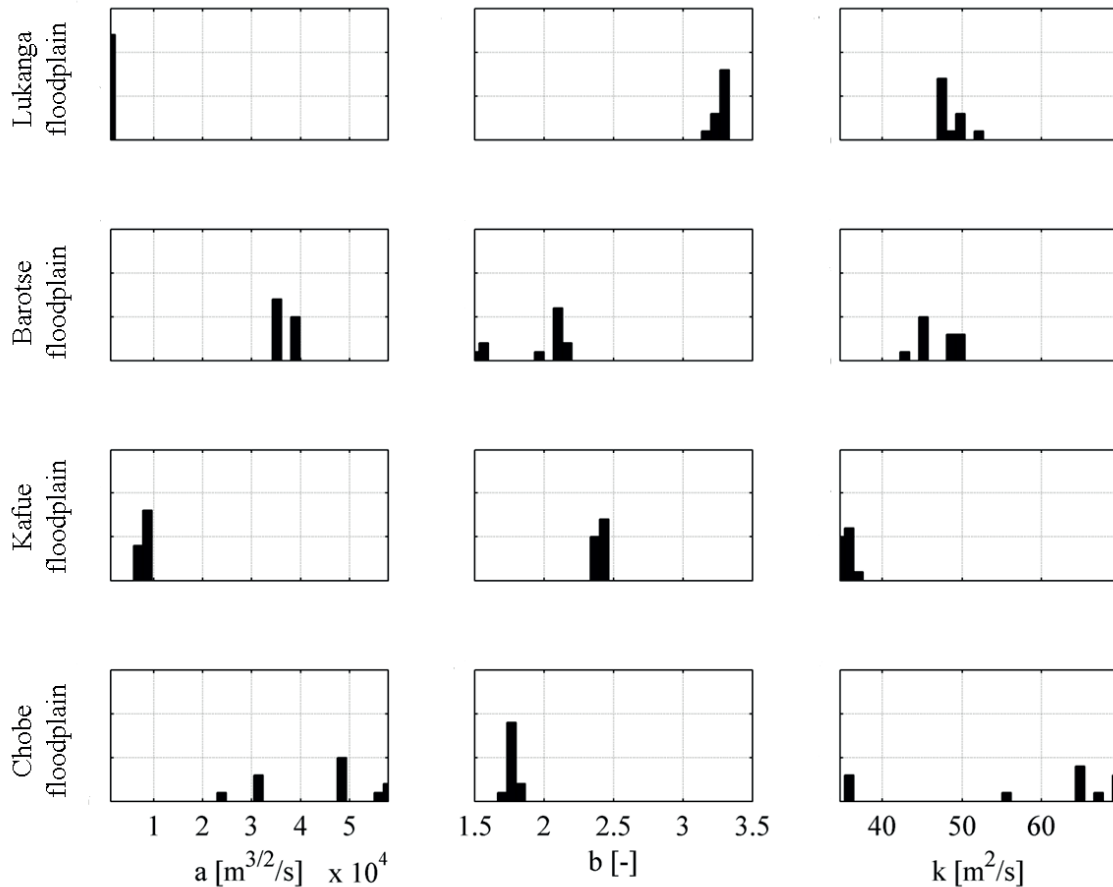
Figure 5-9. Histograms of the selected floodplain parameters after the third iteration of the calibration procedure. (a: reservoir overflow exponent, b: exponent of overflow equation for reservoir, k: reservoir release coefficient).

In terms of volume variation at the reservoirs, the results are more accurate (Figure 5-11) than in the previous iteration. At Itezhi-Tezhi (Figure 5-11, a), the variation is well reproduced, except during the year 2001. Including the reservoir data has considerably improved the calibration at this point. At Kariba (Figure 5-11, c), a slight underestimation occurs during the validation period (−15%). Finally, the volume at Cahora Bassa (Figure 5-11, d) is very close to the observed data during the calibration period but largely overestimated during validation period (+50%).

For the next iteration, the main goal is to improve the volume ratio at the hydropower plants and therefore to adapt the objective function. In parallel, the simulation of the hydrological processes in the floodplains will be refined based on the hydrographs obtained at station #344 and the discharge data at Kafue dam (station #204).
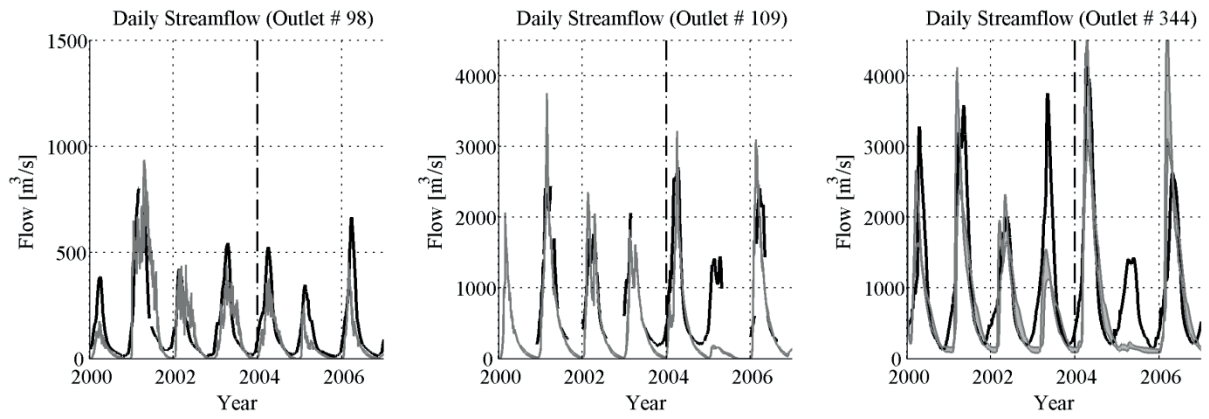
Figure 5-10. Hydrographs of observed (black line) and simulated data (grey line) after the third iteration of the calibration procedure at stations #98 (Chilenga), #109 (Lukulu) and #344 (Victoria Falls).
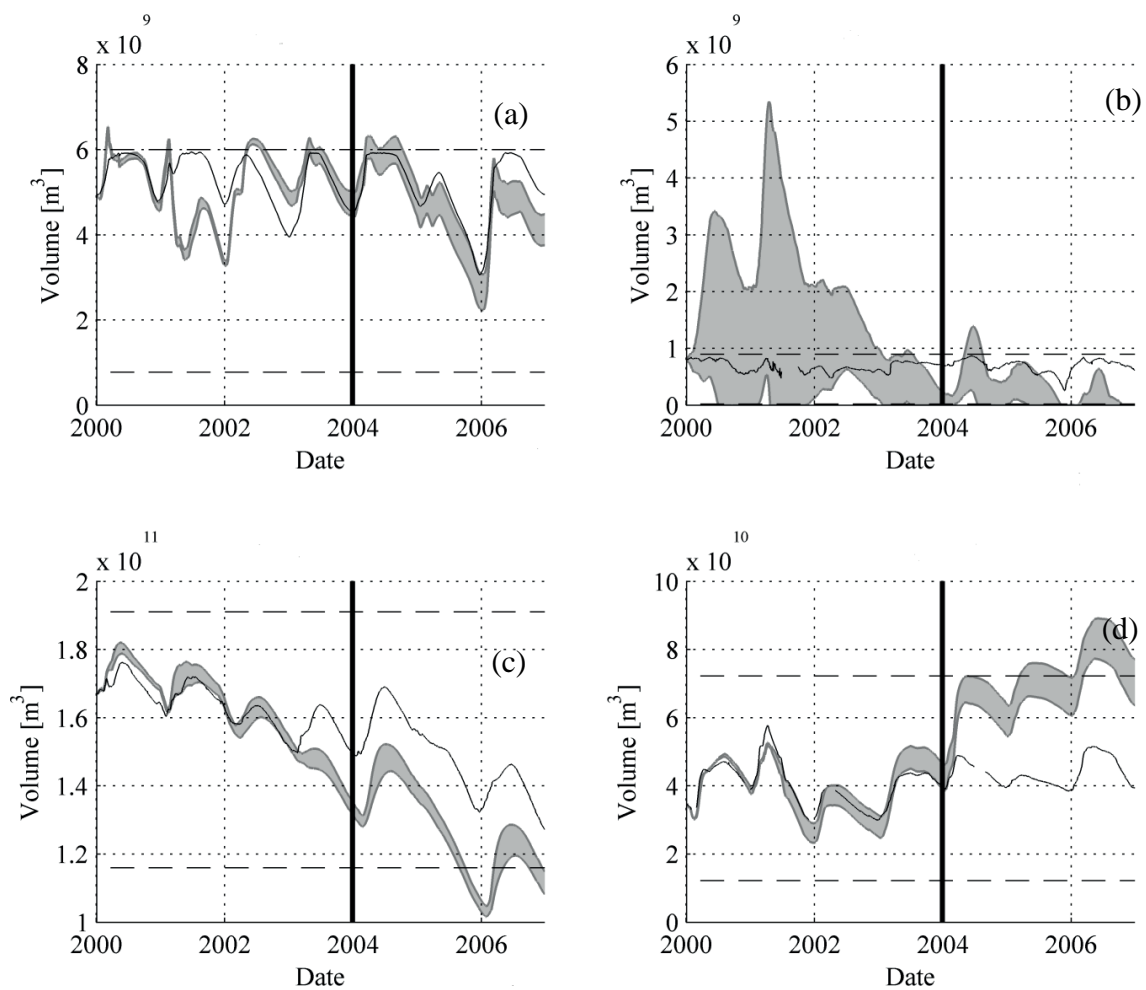
Figure 5-11. Simulated (grey line) and observed (black line) volume variation after the third iteration of the calibration procedure at Itezhi Tezhi (a), Kafue Gorge (b), Kariba (c) and Cahora Bassa (d) dams with the full reservoir and the minimum operating volumes (dashed lines) for the calibration and validation periods (separated by a black vertical line).

5.4.4 Fourth iteration

The fourth iteration aimed to improve the volume ratio at the hydropower plants. The optimization was therefore done on one objective which combines the two indicators used in the previous iteration – the global RE and the global VR – with a weight of one on the global RE and a weight of three on the global VR. An initial set of parameters corresponding to the best results of the previous iteration has been given as an input of the optimization algorithm in order to accelerate the optimization of the parameter's values and the population size has been reduced to 40. The algorithm was stopped after reaching a stable result, corresponding to a global RE of 0.3 and a global VR of 0.85.

The floodplain model was refined for the calculation of the water level in the reservoir to reproduce more precisely the processes observed in reality, according to the hydrograph obtained below the major wetlands. The parameter limits were slightly changed: the bounds of the reservoir overflow exponent (*b*) were extended to a lower value due to the results of the parameter distribution for the Barotse floodplain (Figure 5-9); the bounds of the reservoir overflow constant (*a*) were extended to encompass lower values due the parameter value distribution at the Lukanga floodplain (Figure 5-9); and the baseflow coefficient range has been extended to cover higher values in order to improve the low flow simulation.

To ameliorate the flow simulation in the Kafue floodplain, the station # 204, corresponding now to the observed outflow a Kafue Gorge dam has been reintroduce in the calibration process. New discharge data have become available and have been included in the optimization: station # 232, located just downstream of the Barotse floodplain, and station # 164, located on the Luangwa River, which has a limited amount of data but is the only one available in the region.

The indicators presented in Table 5-9 show that the global NS value for the discharge stations is higher than 0.5, the global error in terms of volume is less than 15% and the global relative error is about 30%. During the validation period, negative NS values are reported on the stations located in the upper Zambezi Basin (# 109, 232 and 344), which is related to a large error on the volume ratio. The station # 164 exhibits very low NS value and high VR and RE during the validation period. However, these results are only of limited significance due to the relatively small amount of data available.

Table 5-8. SWAT model parameters included in fourth iteration of the calibration procedure with their upper and lower bounds.

Parameter	Description	Unit	Lower bounds	Upper bounds
SURLAG	Surface runoff lag time	day	0.5	1.5
ALPHA_B	Baseflow recession constant	day	0	0.5
GW_DELA	Groundwater delay	day	20	300
GW_REVA	Ground water 'revap' coefficient for flow to move into the overlying unsaturated zone	-	0.1	0.4
REVAPMN	Threshold depth of water in the shallow aquifer for ground water to move into the overlying unsaturated layers	mm	1	400
GWQMN	Threshold depth of water in shallow aquifer for return flow (to the reach) to occur	mm	5	100
ESCO	Soil evaporation compensation factor	-	0.001	1
CN_F	SCS curve number for moisture condition	%	-0.25	0.15
CH_KII	Effective hydraulic conductivity in main channel alluvium	mm/hr	0.1	50
SOL_AWC	Available water capacity of the soil layer	%	-0.5	1
SOL_Z	Depth from soil surface to bottom of the layer	%	-0.5	1
EPCO	Plant uptake compensation factor	-	0	1
CANMX	Maximum canopy storage	mm	0	30
Floodplain parameters				
a	Reservoir overflow constant	$m^{3/2}/s$	900	55,000
b	Exponent of overflow equation for reservoir	-	1	3.5
k	Reservoir release coefficient	m^2/s	35	350

In terms of calibrated parameters, the selected parameter sets have very narrow limits around their values (Figure 5-12 and Figure 5-13) which proves the convergence of the calibration. Moreover, they reach a global best value similar to that of the previous iteration. For the floodplain parameters, the Chobe reservoir has still the highest variability probably due to its limited influence on the hydrograph. The other floodplains' parameters converge to specific values which are different from the previous iteration as the model was refined. The parameter sets selected as optimal results for the fourth iteration are presented in the Appendix.

Regarding discharge (Figure 5-14) and volume variations (Figure 5-15), the following remarks can be stated:

- The base flow in the upper Zambezi basin (stations # 109, 232 and 344) is still not well reproduced.

- The year 2005 is clearly problematic in terms of simulated water volume.

- The influence of the Kafue floodplain (upstream station # 204) is difficult to model even with an adapted reservoir approach.

- The limited amount of data available at station # 164 transforms it more into a comparison point than a real calibration station.

- The volume variations at the Itezhi-Tezhi reservoir are well reproduced. (Figure 5-15, a) During the calibration period, the volume is slightly overestimated (+10%) and during the validation period, underestimated (-20%) (Table 5-9).

- At Kariba (Figure 5-15, c), the underestimation of discharge during the years 2003 and 2005 results in an underestimation of the volume of nearly 20%. The other variations are well simulated by the model.

- The volume variations during the calibration period at Cahora Bassa are nearly perfectly reproduced by the model (Figure 5-15, d). However, during the validation period, the volume is overestimated by nearly 60%.

Table 5-9. Indicators values at the discharge and reservoir stations after the fourth iteration of the calibration procedure (NS Nash-Sutcliffe coefficient, VR volume ratio, RE relative error).

	Global value	station # 109	station # 232	station # 344	station # 98	station # 204	station # 164
NS calibration	0.53-0.57	0.69-0.70	0.59-0.68	0.43-0.54	0.55-0.56	0.34-0.43	0.54-0.55
VR calibration	0.87-0.89	0.82-0.84	0.74-0.76	0.72-0.74	0.58-0.59	0.94-0.99	0.90-0.93
RE calibration	0.30-0.31	0.39-0.41	0.27-0.34	0.35-0.39	0.49-0.52	0.26-0.29	0.57-0.60
NS validation	−35.23-−12.06	−0.15-−0.13	−0.13-0.21	−0.43-−0.06	0.46-0.47	0.2-0.24	−211-−72
VR validation	1.00-1.11	0.61-0.63	0.76-0.78	0.77-0.79	0.51-0.52	0.93-0.97	2.27-3.15
RE validation	0.53-0.62	0.53-0.54	0.61-0.70	0.53-0.57	0.45-0.51	0.16-0.19	1.29-2.2

Table 5-9 (continuation). Indicators values at the discharge and reservoir station after the fourth iteration of the calibration procedure (NS Nash-Sutcliffe coefficient, VR volume ratio, RE relative error).

	Itezhi-Tezhi	Kariba	Cahora Bassa
VR calibration	1.12-1.17	1.00-1.01	0.97-0.99
RE calibration	0.15-0.19	0.04-0.05	0.05-0.06
VR validation	0.73-0.86	0.80-0.84	1.56-1.62
RE validation	0.14-0.27	0.16-0.20	0.56-0.62
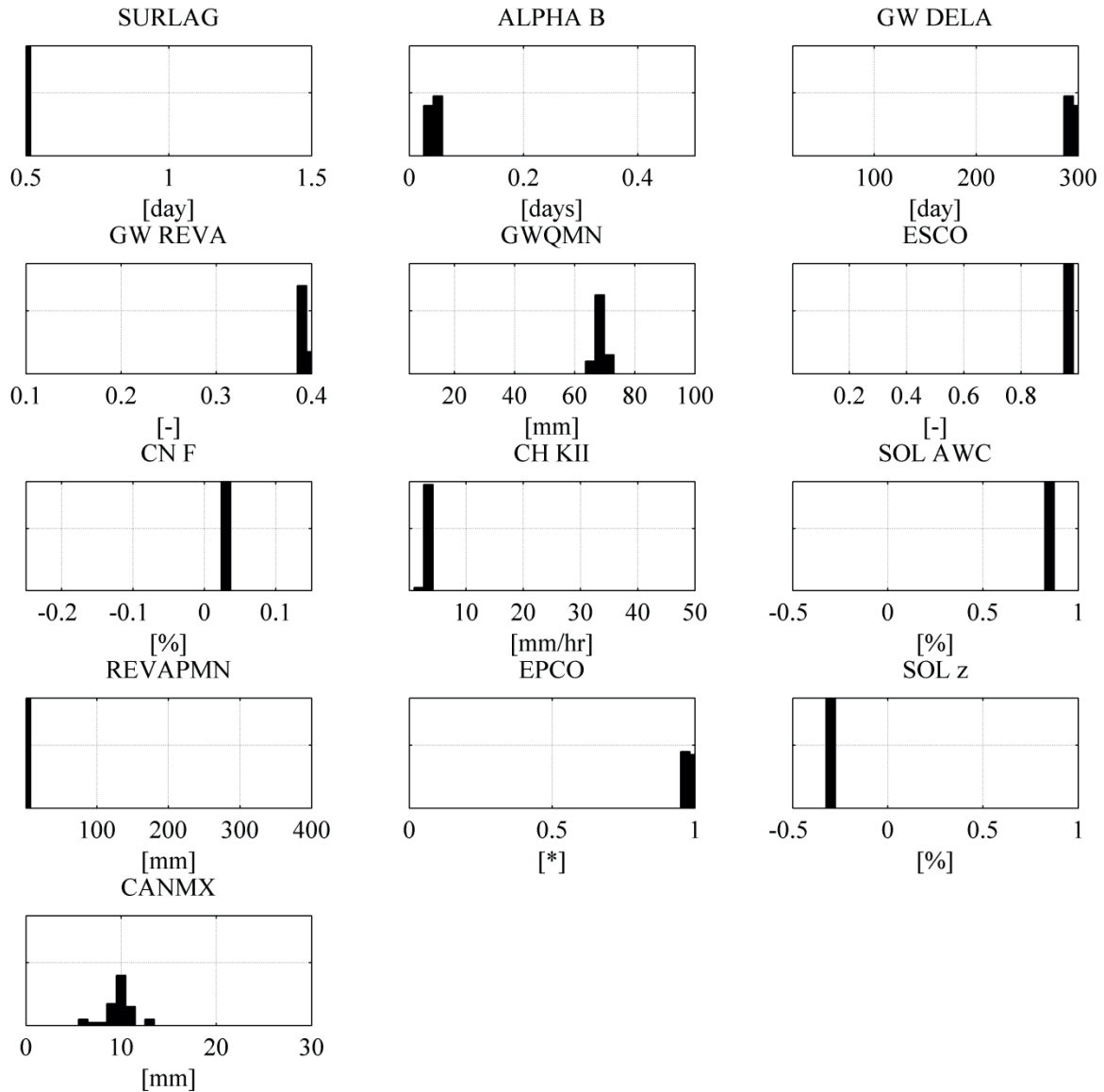
Figure 5-12. Histograms of the selected original SWAT parameters after the fourth iteration procedure. (SURLAG: surface runoff lag time, ALPHA_B: baseflow recession constant, GW_DELA: groundwater delay, GW_REVA: groundwater revap coefficient, GWQMN: threshold depth of water in the aquifer for return flow to occur, ESCO: soil evaporation compensation factor, CN_F: SCS curve number, CH_KII: effective hydraulic conductivity in main channel, SOL_AWC: available soil water capacity, REVAPMN: threshold depth of water in the shallow aquifer for 'revap' to occur, EPCO: plant uptake compensation factor, SOL_Z: depth of soil layer, CANMX: maximum canopy storage).
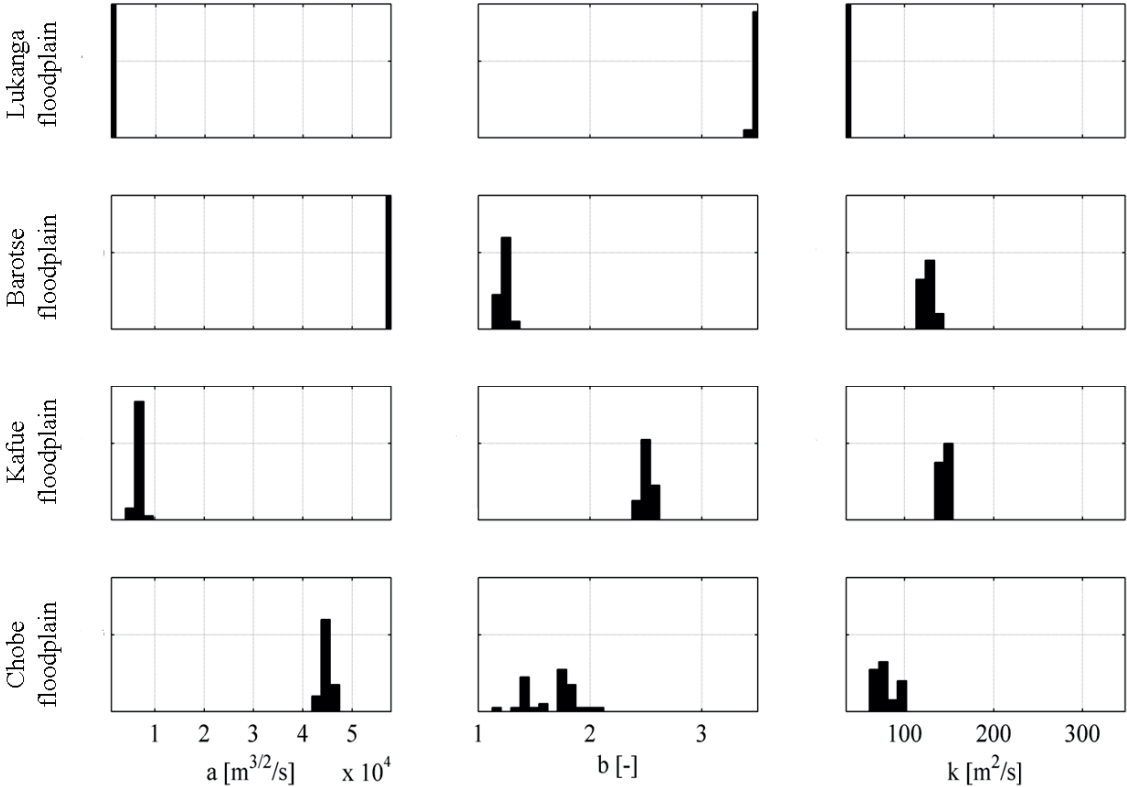
Figure 5-13. Histograms of the selected floodplain parameters after the fourth iteration of the calibration procedure. (a: reservoir overflow exponent, b: exponent of overflow equation for reservoir, k: reservoir release coefficient).
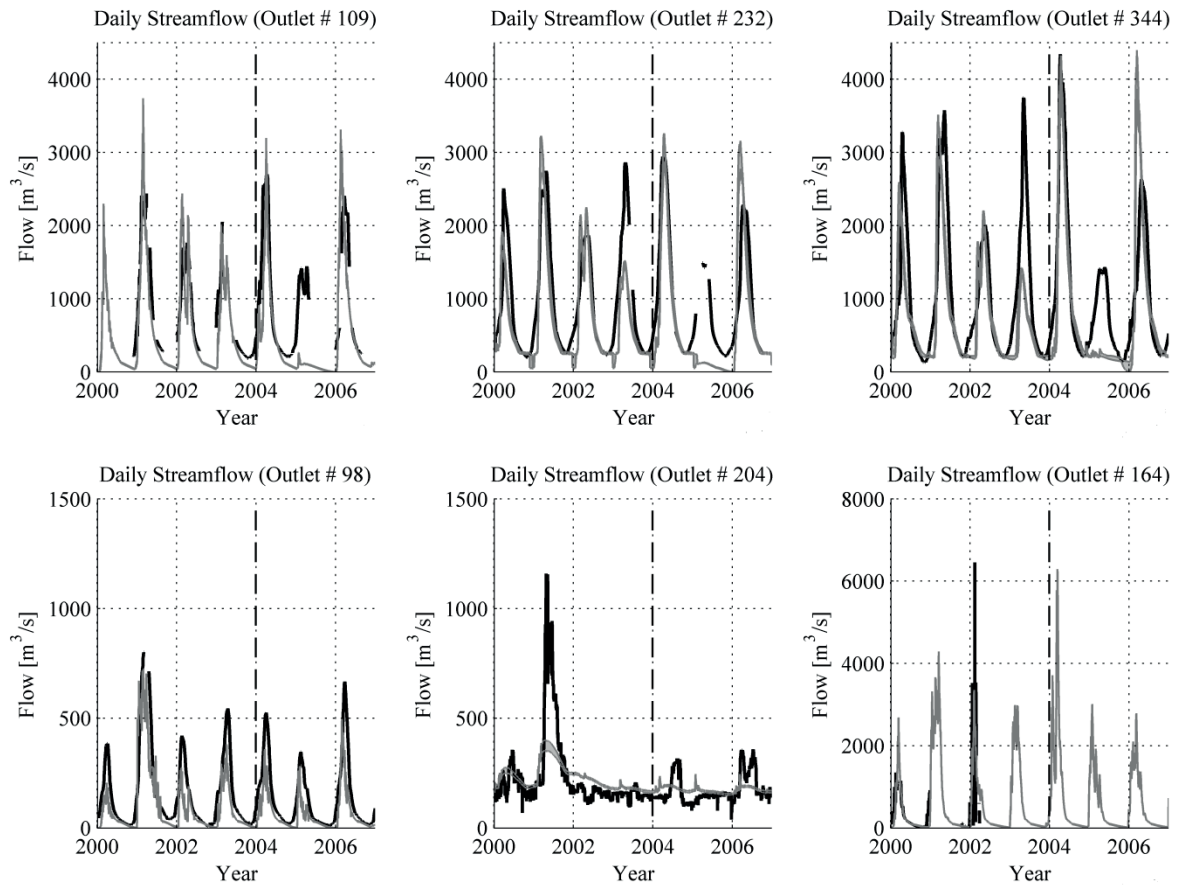
Figure 5-14. Hydrographs of observed (black line) and simulated data (grey line) after the fourth iteration of the calibration procedure at stations #109 (Lukulu), #232 (Senanga), #344 (Victoria Falls), #98 (Chilenga), #204 (outflow of Kafue reservoir) and #164 (Luangwa).
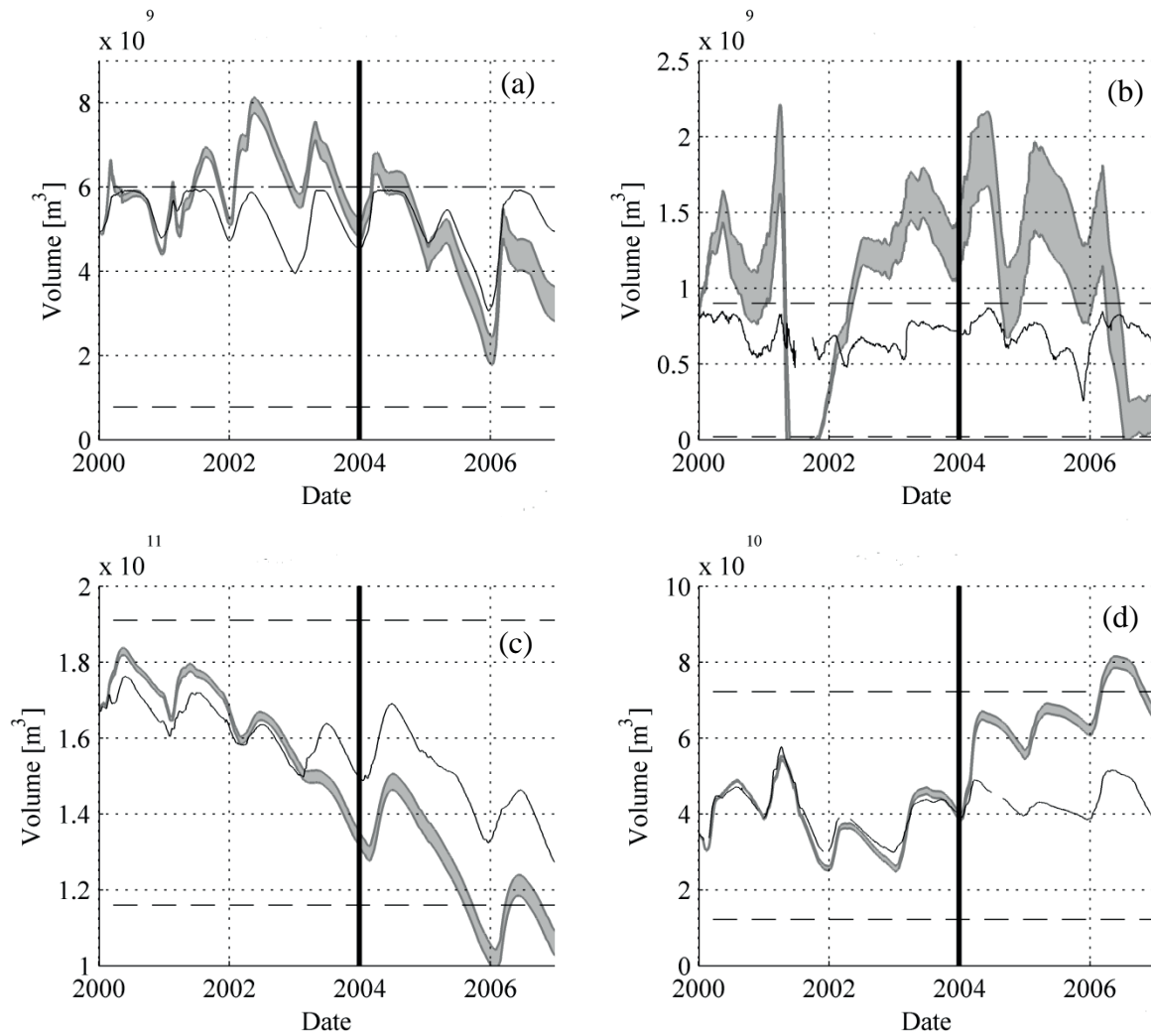
Figure 5-15. Simulated (grey line) and observed (black line) volume variation after the fourth iteration of the calibration procedure at Itezhi Tezhi (a), Kafue Gorge (b), Kariba (c) and Cahora Bassa (d) dams with the full reservoir and the minimum operating volumes (dashed lines) for the calibration and validation periods (separated by a black vertical line).

The results of the fourth iteration are considered as sufficient for the model calibration. However, the main problem remaining is missing flood during the year 2005. In the final iteration, the rainfall data have therefore been changed to the last version of TRMM 3B42 estimates.

5.4.5 Fifth and last iteration

To improve the results of the model and seeking to remove the problem of discharge undervaluation during the year 2005, the rainfall data were changed from the version 6 to the version 7a of the TRMM 3B42 algorithm. Due to this adjustment, the two years 1998 and 1999 could also be considered for the calibration period as their rainfall estimates were considerably improved compared to those of version 6. The data were used twice, at first for stabilizing the model and then for its evaluation.

Regarding the objective function, two objectives were optimized: the global RE and the global VR with a slight change in the RE calculation at the reservoirs where the error was calculated relatively to the difference between the minimum and maximum exploitation volumes and not relatively to the observed value [5-8].

$$RE_{res} = \frac{1}{n} \sum_{i=1}^{n} \frac{\left| Vol_{s,i} - Vol_{o,i} \right|}{Vol_{max} - Vol_{min}} \qquad [5\text{-}8]$$

where Vol_s and Vol_o are the simulated and observed volume, n the number of volume records available at each station ad V_{max} and V_{min} the minimum and maximum exploitation volumes.

The population size has been kept at 40. The algorithm was stopped when reaching a stable result, corresponding to a global RE of 0.31 and a global VR of 0.87.

One new station has been added to the calibration points, the # 252 located on the Shire River. The addition of this new station allows the model to be calibrated almost down to the delta. On the other hand, station # 164 located on the Luangwa River was removed from the calibration process. The same calibration parameters and the same bounds as for the fourth iteration were used.

The global indicators values for the calibration period (Table 5-10) are very similar to the one obtained after the previous iteration (Table 5-9). For the validation period, changing the rainfall input data to the version 7a of the satellite derived precipitation estimations considerably improved the results in the upper Zambezi Basin (stations # 109, 232 and 344). Not taking into account station # 164 contributed as well to improve the results.

On the Kafue River (Table 5-10), the indicator value for both calibration and validation periods at station # 204 are improved when compared to those of the previous iteration (Table 5-9). However, they have degraded at station # 98.

Comparing to the previous iteration (Table 5-9), the indicators at the reservoirs are worse at Itezhi-Tezhi and Kariba, but better at Cahora Bassa.

- At Itezhi-Tezhi, the volume was underestimated by 90% during the validation period due to low inflows over two of the three years.

- At Kariba, the volume was overestimated by 30% during the calibration period and about 30% in the course of the validation period. The error is concentrated on a small portion of the years under study.

- At Cahora Bassa, the overestimation during validation period is reduced by 35% relatively to the previous iteration.

In terms of calibrated parameters and for the original SWAT model parameters (Figure 5-16), the histograms are still centered on a narrow range of values compared to the calibration range. The values on which they converge are globally similar to the ones obtained after the previous iteration, except for the curve number (CH_F), the threshold depth of water in the aquifer for return flow to occur (GWQMN), the plant uptake compensation factor (EPCO) and the depth of the soil layer (SOL_Z). These modifications are likely due to the improvement of the input rainfall data which slightly changes the hydrological processes involved.

As for the floodplain parameters (Figure 5-17), the results for Kafue and Lukanga floodplains are again similar to those of the previous iteration, maintaining narrow bounds. Nonetheless, they are different for the Chobe and Barotse floodplains, with a larger distribution of parameter values in the case of the Barotse floodplain. The parameter sets selected as optimal results for the second iteration are presented in the Appendix.

In terms of hydrographs (Figure 5-18), as mentioned above, a net improvement is visible for the Upper Zambezi basin (stations # 109, 232 and 344) as the base flow at stations # 232 and # 344 is well reproduced and the year 2005 has ceased to be problematic in terms of simulated water volumes. On the Kafue Basin (stations # 98, 191 and 204), the hydrological processes are not as well represented as on the Upper Zambezi Basin. At station # 98, the model was not able to reproduce the flood peaks and the simulations appear to fluctuate much more than the observed discharge. The reason may be that the hydrological processes in this region are different from the one observed on the Upper Zambezi basin and that the global parameterization of the model does not allow the desirable differentiation of the two regions. At station # 191 (inflow to the Itezhi-Tezhi reservoir), the base flow and the flood peaks were close to the observed data during the calibration period except for the year 2001 which was also problematic at station # 204. The high flows during validation period have been underestimated over the whole Kafue subbasin, leading to a reservoir volume underestimation (Figure 5-19, a).

Regarding reservoir volume variations (Figure 5-19), the following remarks can be made:

- The volume variations at the Itezhi-Tezhi reservoir are well reproduced during the calibration period except for the year 2001. (Figure 5-19, a). However, the discharge underestimation of years 2004 and 2006 lead to a critical underestimation of the reservoir water volume during the validation period.

- At Kariba (Figure 5-19, c), the overestimation of discharge during years 1999 and 2001 leads to an overestimation of the volume of about 25% during the calibration period, which propagates into the validation period. The other variations have been well simulated by the model.

- The volume variations during the calibration period at Cahora Bassa are nearly perfectly reproduced by the model (Figure 5-19, d). During the validation period, the volume is overestimated by 35%.

Table 5-10. Indicators values at the discharge station located on the Zambezi River after the final iteration of the calibration procedure (NS Nash-Sutcliffe coefficient, VR volume ratio, RE relative error)

	Mean value	**station # 109**	**station # 232**	**station # 344**
NS calibration	0.54-0.56	0.72-0.74	0.77-0.78	0.61-0.65
VR calibration	0.92-0.93	0.74-0.77	0.82-0.84	0. 98-1.01
RE calibration	0.28-0.29	0.37-0.38	0.25-0.28	0.34-0.35
NS validation	0.46-0.50	0.81-0.84	0.85-0.89	0.81-0.83
VR validation	0.80-0.82	0.86-0.90	0.80-0.83	0.81-0.84
RE validation	0.35-0.36	0.25-0.25	0.20-0.23	0.24-0.25

Table 5-10 (continuation). Indicators values at the discharge station located on the Kafue and Shire Rivers after the final iteration of the calibration procedure (NS Nash-Sutcliffe coefficient, VR volume ratio, RE relative error).

	station # 98	**station # 191**	**station # 204**	**station # 252**
NS calibration	0.28-0.34	0.60-0.64	0.42-0.45	0.34-0.37
VR calibration	0.63-0.64	0.87-0.88	0.98-0.99	1.01-1.02
RE calibration	0.61-0.63	0.43-0.47	0.24-0.25	0.13-0.14
NS validation	0.33-0.37	0.54-0.58	$-0.43-{-}0.25$	0.22-0.28
VR validation	0.44-0.45	0.64-0.66	0.76-0.80	0.92-0.93
RE validation	0.58-0-62	0.30-0.31	0.22-0.25	0.11-0.12

Table 5-10 (continuation). Indicators values at the discharge and reservoir stations after the final iteration of the calibration procedure (NS Nash-Sutcliffe coefficient, VR volume ratio, RE relative error).

	Itezhi Tezhi	**Kariba**	**Cahora Bassa**
VR calibration	0.95-1.03	1.19-1.21	0.94-0.95
RE calibration	0.13-0.15	0.20-0.22	0.08-0.09
VR validation	0.07-0.10	1.29-1.35	1.34-1.36
RE validation	0.90-0.94	0.30-0.35	0.34-0.36
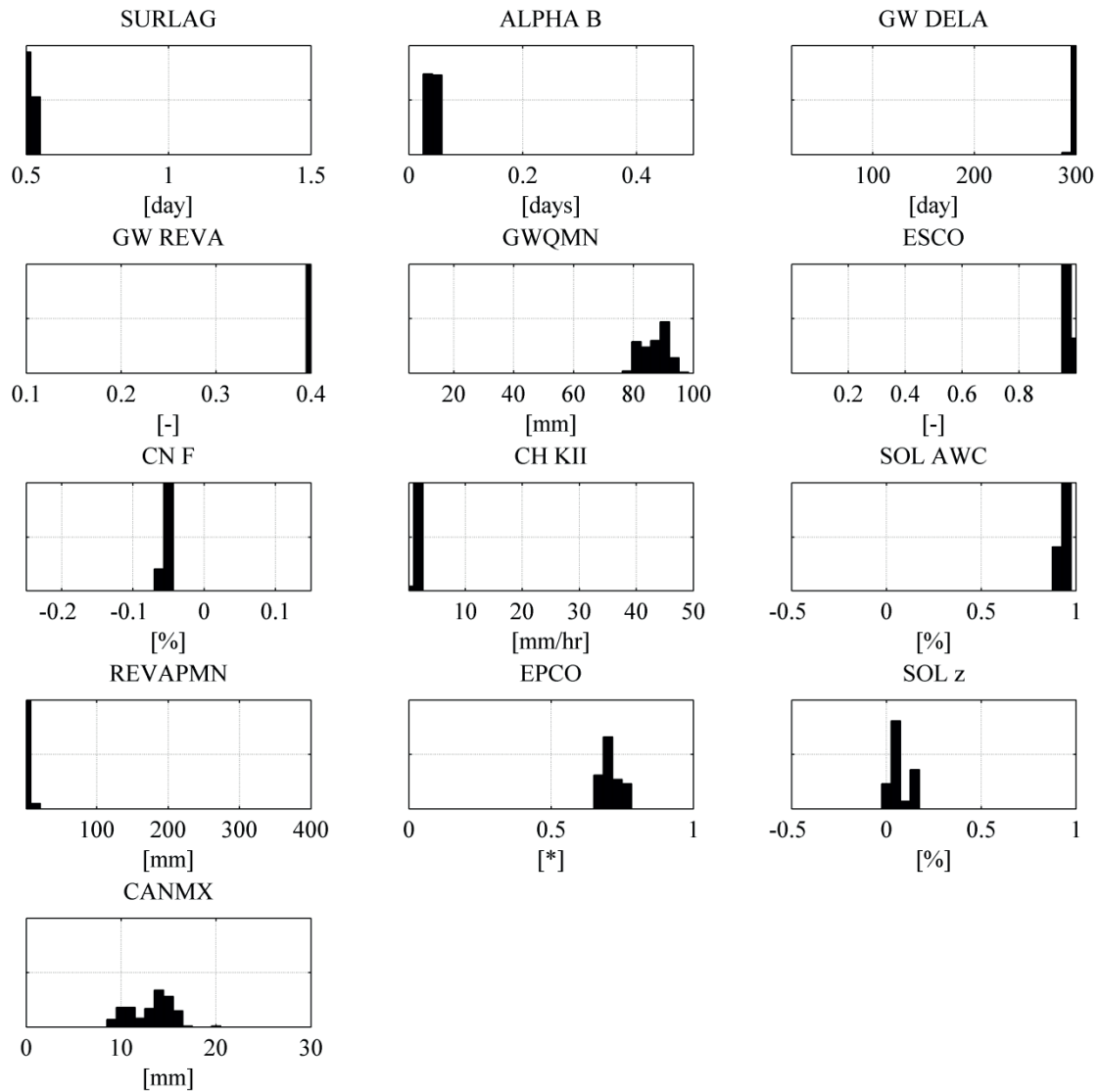
Figure 5-16. Histograms of the selected original SWAT parameters after the final iteration procedure. (SURLAG: surface runoff lag time, ALPHA_B: baseflow recession constant, GW_DELA: groundwater delay, GW_REVA: groundwater revap coefficient, GWQMN: threshold depth of water in the aquifer for return flow to occur, ESCO: soil evaporation compensation factor, CN_F: SCS curve number, CH_KII: effective hydraulic conductivity in main channel, SOL_AWC: available soil water capacity, REVAPMN: threshold depth of water in the shallow aquifer for 'revap' to occur, EPCO: plant uptake compensation factor, SOL_Z: depth of soil layer, CANMX: maximum canopy storage).
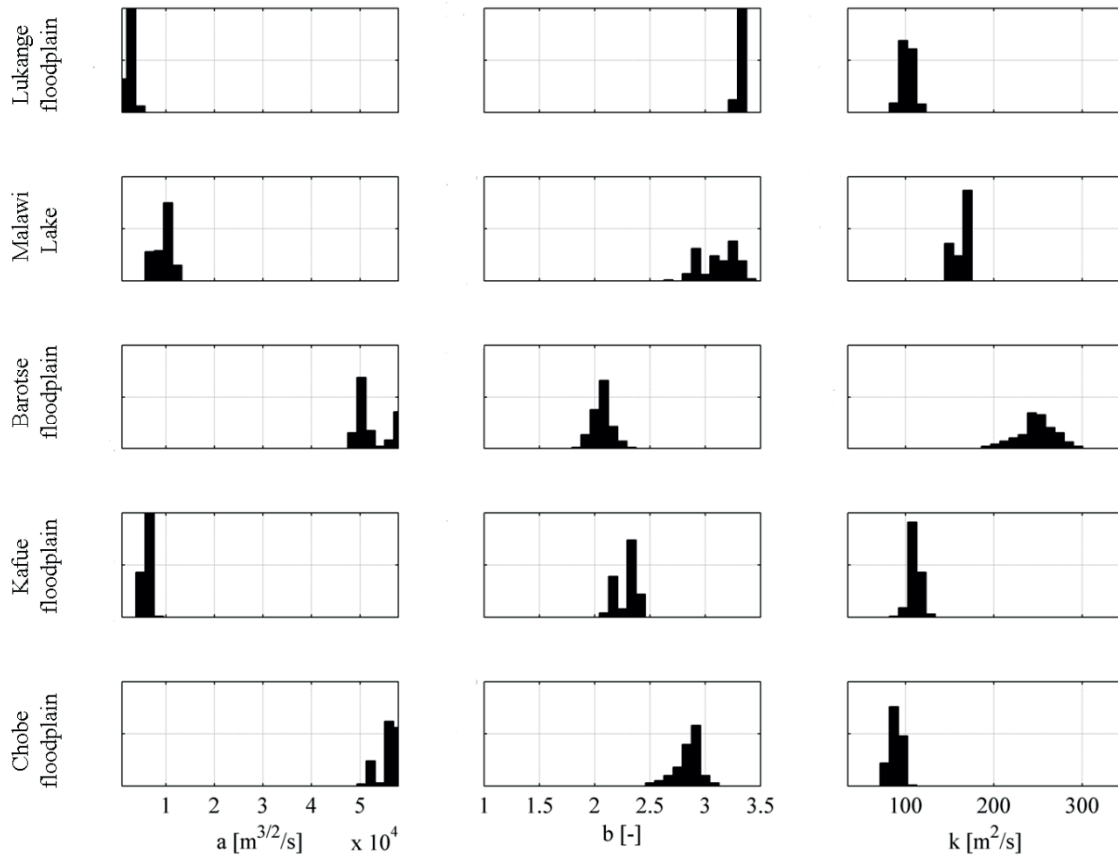
Figure 5-17. Histograms of the selected floodplain parameters after the final iteration of the calibration procedure. (a: reservoir overflow exponent, b: exponent of overflow equation for reservoir, k: reservoir release coefficient).
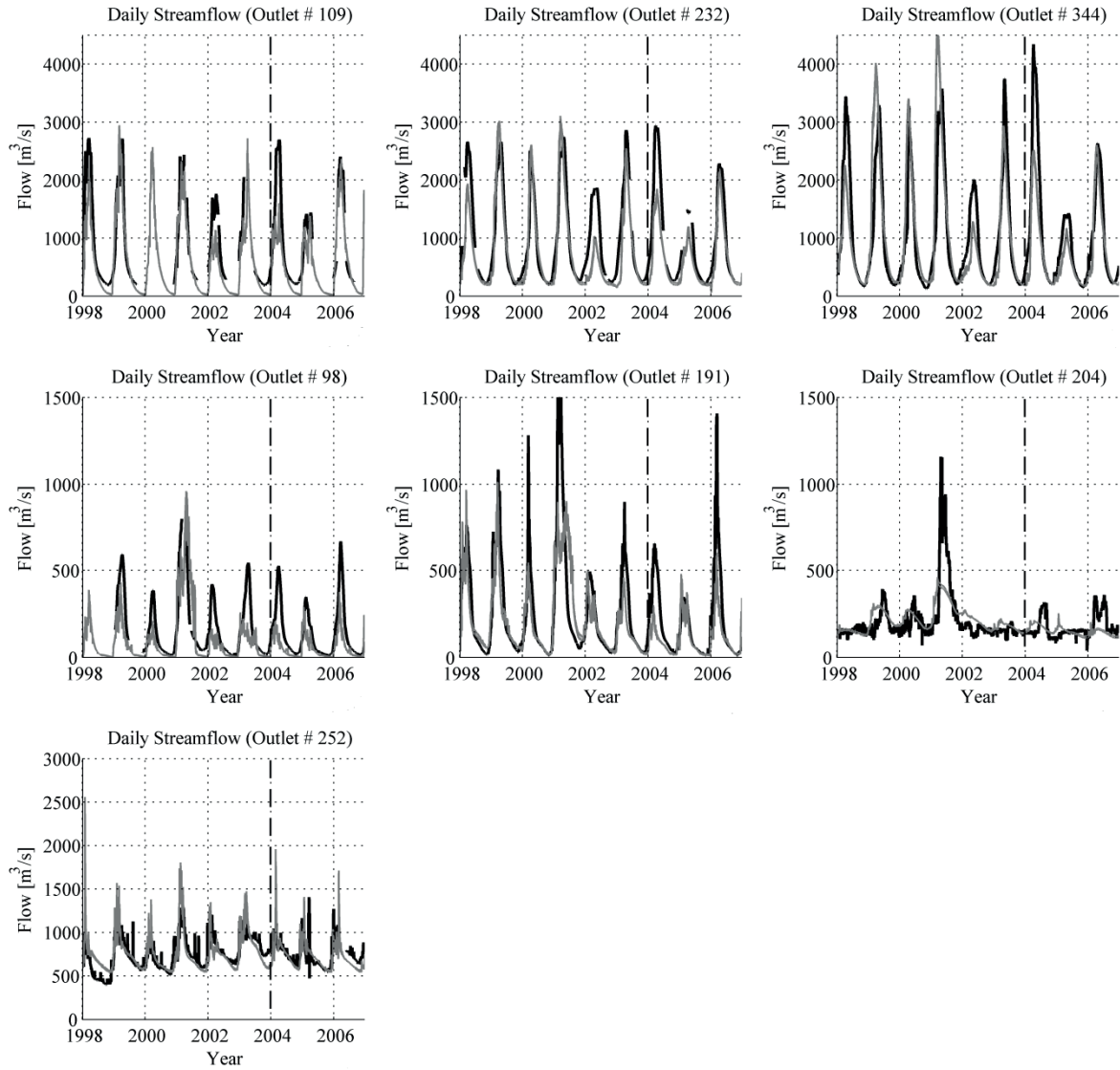
Figure 5-18. Hydrographs of observed (black line) and simulated data (grey line) after the final iteration of the calibration procedure at stations #109 (Lukulu), #232 (Senanga), #344 (Victoria Falls), #98 (Chilenga), #191 (inflow of Itezhi Tezhi reservoir), #204 (outflow of Kafue reservoir) and #252 (Shire).
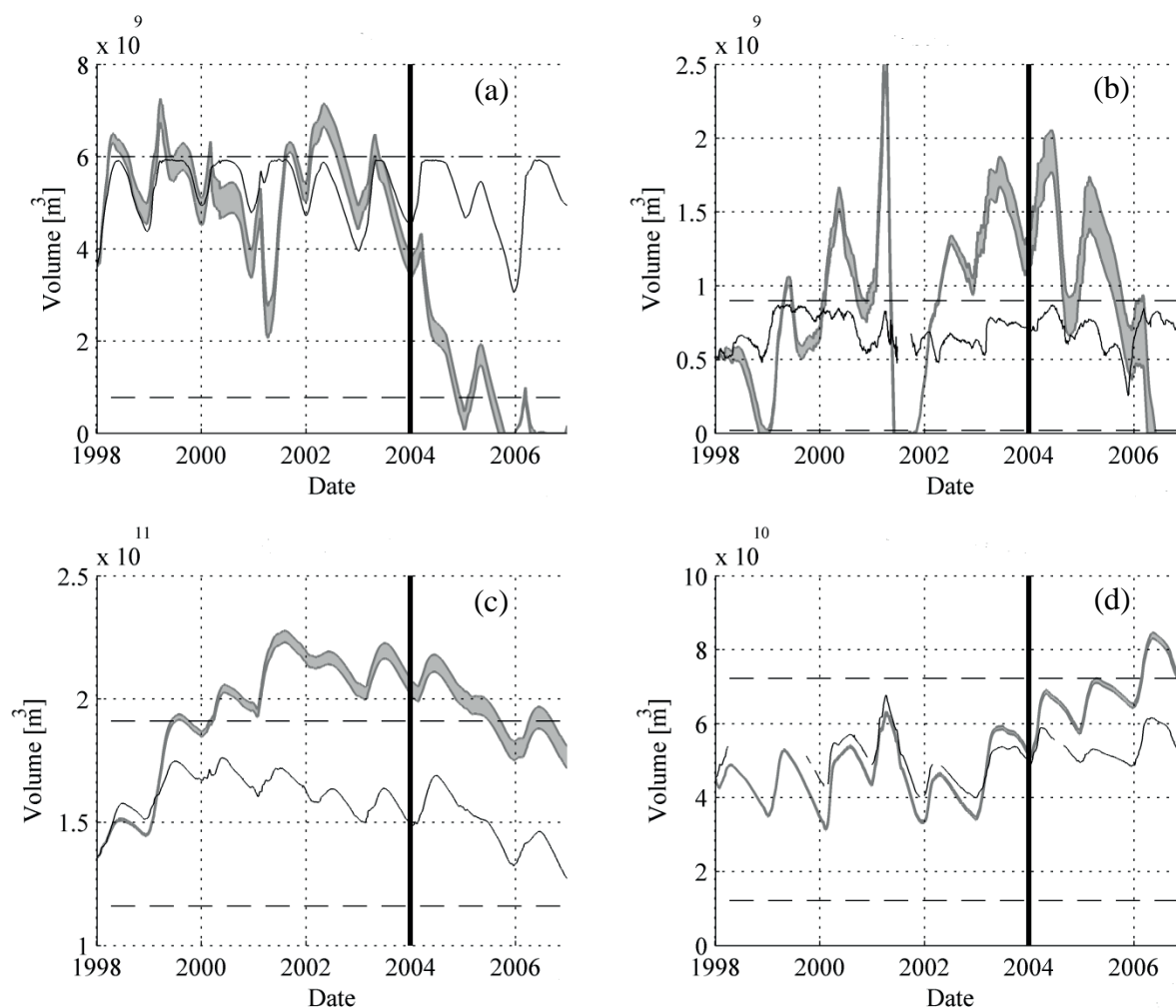
Figure 5-19. Simulated (grey line) and observed (black line) volume variation after the final iteration of the calibration procedure at Itezhi Tezhi (a), Kafue Gorge (b), Kariba (c) and Cahora Bassa (d) dams with the full reservoir and the minimum operating volumes (dashed lines) for the calibration and validation periods (separated by a black vertical line).

The fifth iteration was considered as the final iteration since it reached the calibration objectives. It minimizes the error in runoff volumes with a volume ratio higher than 0.9 during calibration and around 0.8 during the validation period. Moreover, the global shape of the observed hydrograph is reproduced with a mean relative error of 30% for the calibration period and 35% for the validation period. At the artificial reservoirs, the results for Kariba and Cahora Bassa showed that the model is able to reproduce the volume variations even if the volume is overestimated on particular years. At Itezhi Tezhi, the shape of the variations is followed by the model during calibration but not during validation. The other advantages of this iteration are that the model is calibrated nearly up to the Zambezi delta since discharge data on the Shire River were introduced in the calibration process and that the latest version of the rainfall estimates were used as input data, leading to an improvement of the flow simulation in the Upper Zambezi.

5.5 CONCLUSIONS

In this chapter, a hydrological modeling framework for water resources management in a complex African river basin with large hydraulic structures is presented. An enhanced version of SWAT 2009 is proposed to include the floodplains and the artificial reservoirs. The calibration and validation process was separated in four steps: (1) choice of calibration parameters, (2) definition of objective functions, (3) application of a Multi-ALgorithm Genetically Adaptive Multi-objective method (AMALGAM), and (4) analysis of the results in terms of statistics and hydrographs for the calibration and the validation periods. The methodology is applied on the Zambezi River basin. The discussion showed the importance of considering the hydrographs and volume variation plots for analyzing results as this allows the quality assessment of the model's estimates better than focusing on discharge's statistics and indicators alone. The methodology also emphasizes the need to define the future use of the model before calibration as this influences substantially the objective functions and, thus, the final solutions.

Globally, the mean relative error was equal to 30% for the calibration period and 35% for the validation period. Concerning the mean volume ratio, it was higher than 0.9 during calibration and around 0.8 during the validation period. At the discharge stations, the mean Nash-Sutcliffe coefficient was above 0.45 for the calibration and validation periods. The results at the major artificial reservoirs (Kariba and Cahora Bassa) show a volume overestimation of 20 to 35% mainly distributed on certain years.

The differences between observed and simulated data come from four error sources [*Madsen*, 2000; *Refsgaard and Storm*, 1996]: (1) the meteorological input data, (2) recorded observations, (3) model structure and (4) parameters values. Although the calibration attempts to optimize performance indicators, it may also compensate for errors on input data and inadequacies in model structure.

Input data uncertainty is relevant over the Zambezi basin as precipitation is estimated based on satellite observations and other variables are based on broad global datasets (temperature, land use, soil map, etc.). When compared to gauge data, the satellite rainfall estimates' volume ratio is close to 1 but the correlation at daily time step is quite low, near 0.25 [*Cohen Liechti et al.*, 2012]. Therefore, the model should be able to reproduce the runoff volume, but discrepancies in the runoff shape could be explained by errors in rainfall data.

The second source of error concerns recorded discharge and reservoir level observations. Uncertainty of river discharge simulations comes from errors in the rating curve estimations [*Di Baldassarre and Montanari*, 2009], individual measurements of discharge, which have uncertainties in the range of 2 to 19% using velocity-area methods [*McMillan et al.*, 2012] and data reporting and handling. When the flow is low or high, the uncertainty increases as the rating curves are interpolated in these domains. In the case of the Zambezi River, the large flow variation and the variable channel geometry in the floodplains results in low reliability of the discharge observations. Errors in observed outflows at the dams also

come from various sources. First, the turbine flow is not directly measured, being estimated from the electricity production. Secondly, during high flows, the outlet outflow is estimated based on the reservoir level and the spillway's capacity, but not directly measured neither. Moreover, a small error in the water level can cause a big divergence in the corresponding volume as the reservoirs are very large and without knowing precisely their geometry, the water level-volume relation is only estimated. For example, at Kariba reservoir the volume divergence between simulated and observed data corresponds to a constant overestimation of discharge of about 160 m^3/s, which is equivalent to 10% of the total turbine discharge.

Compared with past attempts to model discharges in key locations of the Zambezi basin [*G P Harrison and Whittington*, 2002; *Meier et al.*, 2011; *Vorosmarty et al.*, 1991; *Winsemius et al.*, 2006a], the results can be considered as acceptable for using the model to simulate development scenarios, taking into account the fact that the scenarios comparison will be based on relative values. The present work constitutes a real contribution in terms of reliability and error assessment as it implemented a thorough validation procedure and used a hydrological model tailored to meet some of the specificities of the Zambezi River basin.

Further improvement of the calibration could be reached by using a longer simulation period allowing more discharge data to be taken into account. However, it is actually limited by the availability of rainfall estimates. For real-time or even forecasting use, the model could be adapted including an update of the state variables like the reservoirs levels but it is beyond the scope of the present study.

6 MODELING FLOODPLAIN BEHAVIOR BY A MODIFIED RESERVOIR APPROACH

Floodplains are regions of great interest for environmental assessment as they constitute significant ecological reserves and contribute efficiently to natural flood attenuation. However, the implementation of a model describing the basic hydrological behavior of floodplains is not an easy task due to the complexity of the processes included. Although several attempts have been made to simulate floodplain effects in global rainfall-runoff models, no satisfactory routines have been developed yet. In this study, an adapted version of the Soil and Water Assessment Tool (SWAT 2009) reservoir model is proposed and applied to the Zambezi Basin at daily time step with the intention of adequately modeling floodplain behavior. The model separates the outflow of the reservoir simulating the floodplain into main channel flow and flow over the floodplain area. The improved solution was compared with the original model regarding its potential to simulate observed discharges in terms of volume ratio, Nash-Sutcliffe coefficient and hydrograph plots. These evaluation criteria attest, for both calibration and validation periods, that the modified model is superior to the original one for simulating the discharge downstream of large floodplains. A sensitivity analysis is carried out at two geographical levels: at the outlet of a floodplain and at the outlet of the entire basin. The results show that upper flow parameters are more sensitive than base flow parameters.

6.1 INTRODUCTION

The development of water resource models in southern Africa is a great challenge. Within the framework of the interdisciplinary research project ADAPT (African DAms ProjecT), the planning and operation of large dams in a complex river basin are investigated to meet social needs and environmental constraints. The hydrological processes in this region are significantly different from what has been extensively observed in temperate catchments [*Pilgrim et al.*, 1988]. A key component of the hydrological cycle in this region, namely the floodplains, has been identified as problematic areas for the hydrological modeling of watersheds in Africa [*Pedinotti et al.*, 2012; *Schuol et al.*, 2008b; *Tshimanga et al.*, 2011].

Floodplains are defined as 'areas of low lying land that are subject to inundation by lateral overflow water from rivers or lakes with which they are associated' [*Junk and Welcomme*, 1990]. These regions are of great interest for environmental assessment because they constitute an important ecological reserve and contribute to natural flood attenuation [*Mitsch and Gosselink*, 2007; *Tockner and Stanford*, 2002].

In previous studies, different models were developed to include floodplain hydrology. In the Niger basin [*Pedinotti et al.*, 2012], the ability of the ISBA-TRIP continental hydrologic system (Interactions between Soil, Biosphere, and Atmosphere–Total Runoff Integrating Pathways) [*Decharme et al.*, 2012] to represent key processes related to the hydrological cycle was assessed in four different configurations to evaluate the impact of the flooding scheme on discharge simulation. In this model, the floodplain reservoir fills when the river water depth exceeds the critical bank-full level and interacts with the other components through infiltration, precipitation and evaporation. Considering the inner delta of the Niger as a floodplain instead of a single river channel resulted in improved model performance, confirming the importance of the flooded area.

The eco-hydrological Soil and Water Integrated Model (SWIM) was extended to reproduce the relevant water and nutrient flows, including retention processes, in European riparian zones and floodplains [*Hattermann et al.*, 2006]. Daily groundwater table dynamics were implemented at the hydrotope level (a set of elementary units in the subbasin that have the same geographical features, such as land use and soil type). The results show that riparian zones and floodplains are important buffer systems influencing the water balance.

In the large scale hydrodynamic model developed by Paiva et al. [2011; 2013], the catchments are divided into floodplain units in which the inundation is simulated using a simple storage model. The floodplains are characterized by a function which relates flooded area to water level and by an equivalent width over which exchange with the main channel occurs, both defined based on the Digital Elevation Model.

Neal et al. [2012] presented a subgrid channel two-dimensional model which allows defining inside a grid cell a narrow channel and a floodplain area. The floodplain flow is

calculated based on water depth and floodplain geometry and evaporation is computed as from open water.

In southern Africa, multiple tools have been developed to simulate the hydrology of the Okavango delta, which is characterized by a large floodplain (mean inundated area of around 5,000 km^2 and intermittently inundated area exceeding 12,000 km^2) [*Milzow et al.*, 2009]. A successful model was established by Gieske [1997] based on the work of Dincer *et al.* [1987]. This model represents the floodplain as a set of inter-linked reservoirs (cells) and fixes the outflow from each cell as the overflow starting at a certain volume threshold mitigated by a time-specific constant for each reservoir. The same equations were used in a hybrid reservoir-GIS model implemented by Wolski *et al.* [2006].

In Tanzania, a simple model for the Usangu wetlands provided a useful basis for contemplating water management options [*McCartney et al.*, 2008]. Here floodplains are represented as a reservoir and the outflow computed by a rating equation that depends on the water level measured at the outlet.

Few large scale hydrological models have been applied in Africa. The Coupled Routing and Excess STorage (CREST) is a distributed hydrological model including a rainfall-runoff generation and cell-to-cell routing, feedback mechanisms and representation of sub-grid cell variability [*Wang et al.*, 2011]. It was successfully implemented for the Nzoia basin, a subbasin of Lake Victoria in Africa [*Khan et al.*, 2011]. The Variable Infiltration Capacity (VIC) model, a semi-distributed hydrology model calculating evapotranspiration, soil moisture storage, baseflow, and runoff for each simulation grid cell at each simulation time step, was applied over an ungauged African basin [*Minihane*, 2012].

The Soil and Water Assessment Tool (SWAT, version 2009) was introduced as a semi-distributed physically based continuous time model that is able to handle very large watersheds due to its high computational efficiency. SWAT simulates four types of water bodies: wetlands, ponds, depressions/potholes and reservoirs. However, only the reservoir module receives water from all upstream subbasins, whereas the other water bodies collect the water flowing from their subbasin only [*Neitsch et al.*, 2009]. Moreover, the variation in surface area of the water body is not taken into account in the subbasin water balance calculation. Therefore, modifications are needed to apply the model to regions with significantly large floodplains.

An integrated modeling system for riparian floodplains was developed in SWAT and successfully applied to a watershed in Canada [*Liu et al.*, 2008]. This system includes a function to delineate a sub-watershed into three types of drainage areas: (1) isolated floodplains, (2) riparian floodplains and (3) direct streams. The riparian floodplains receive water from upland fields, including surface runoff, interflow and groundwater flow, and possibly from the river reach if the river water level is higher than the floodplain's. The floodplain water is lost by evapotranspiration, seepage and outflow into the river reach. While this modeling approach is detailed, it also requires numerous parameters and intensive geographical knowledge of the catchment.

The purpose of this study is to develop a simplified model for floodplain hydrology being incorporated in SWAT and able to reproduce the observed discharge in African basins characterized by large seasonally flooded floodplains. The model will be evaluated over multiple yearly cycles focusing on its ability to simulate the measured flow in terms of annual volume and hydrograph shape, especially during the flood season. The original SWAT reservoir model was used to represent the floodplains and a new outflow computation method was implemented. The case study comprises large floodplains which perform in a similar way as reservoirs, buffering and attenuating the flood waves during rainy periods. In the Zambezi basin four floodplains have been taken into account with a total extension of about 25,000 km^2 when inundated, pointing out the importance but also the complexity of the processes to be modeled.

The numerical model and its new developments are described in Chapter 6.2. The study area and the methodology are presented in Chapter 6.3. Three model configurations are compared in Chapter 6.4: (1) the modified reservoir model, (2) the original reservoir model and (3) a model without reservoirs. A sensitivity analysis on the modified reservoir parameters is also discussed. Conclusions are summarized in the Chapter 6.5.

6.2 NUMERICAL MODEL (SWAT 2009)

6.2.1 General description

The Soil and Water Assessment Tool (SWAT), a river basin scale model available in the public domain and actively supported by the USDA Agricultural Research Service at the Grassland, Soil and Water Research is used in the present study. Two criteria led to the choice of this tool for hydrological modeling: (1) the choice of a model already applied in Africa with promising results which would contribute to an appropriate definition of the hydrological processes [*Dessu and Melesse*, 2012; *Mango et al.*, 2011; *Schuol et al.*, 2008b] and (2) the application of a source code available in the public domain in order to be able to transfer the model to the stakeholders.

SWAT 2009 is a semi-distributed physically based continuous time model. The model uses hydrologic response units (HRUs) to describe the spatial heterogeneity in land cover, soil types and terrain slopes within a watershed. The model estimates the water balance in each HRU for four storage volumes, snow, soil profile, shallow aquifer and deep aquifer by considering processes of precipitation, interception, evapotranspiration, surface runoff, infiltration, percolation and subsurface runoff [*J G Arnold et al.*, 1998; *Neitsch et al.*, 2009]. Two methods for estimating surface runoff are available: the Green & Ampt infiltration method, which requires precipitation input in sub-daily scale [*Green and Ampt*, 1911] and the Soil Conservation Service (SCS) curve number procedure [*USDA Soil Conservation Service*, 1972] which uses daily precipitation. The latter was selected for model simulations as the simulation time step is daily. A retention parameter is very significant in SCS method, being defined by the Curve Number (CN) which is a sensitive function of the soil's permeability,

land use and antecedent soil water conditions. The SWAT model offers three options for estimating potential evapotranspiration (PET): Hargreaves [*Hargreaves and Samani*, 1985], Priestley-Taylor [*Priestley and Taylor*, 1972] and Penman-Monteith [*Monteith*, 1965]. The inputs required for the Priestley-Taylor and Penman-Monteith methods are quite substantial: solar radiation, surface air temperature, relative humidity and wind (only for Penman-Monteith method) whereas the Hargreaves method estimates PET based only on maximum and minimum surface air temperature. Due to limitations in the available meteorological data, the Hargreaves method was applied in this study.

6.2.2 Original reservoir model

In the original SWAT 2009 code (revision number 477) [*Neitsch et al.*, 2009], two types of reservoir model exist: (1) a reservoir placed out of the main channel, receiving water only through runoff from the subbasin in which it is located and not from the upstream parts of the basin through main channel and (2) a reservoir located on the main channel, receiving water from the upstream parts of the basin as well as from its own subbasin. In the literature [*Ndomba and Van Griensven*, 2011; *Schuol et al.*, 2008a; *Schuol et al.*, 2008b; *Van Griensven et al.*, 2012], the floodplains located on the main channel were simulated using the latter alternative, which is described below.

The reservoir model includes in the daily water balance inflow (V_{flowin}), outflow ($V_{flowout}$), seepage from the reservoir bottom (V_{seep}), rainfall (V_{pcp}) and evaporation (V_{evap}) [6-1]

$$V = V_{stored} + V_{flowin} - V_{flowout} + V_{pcp} - V_{evap} - V_{seep} \qquad [6\text{-}1]$$

where V is the volume of water in the impoundment at the end of the day and V_{stored} is the volume of water stored in the water body at the beginning of the day.

The amount of precipitation and evaporation is calculated based on the area of the reservoir's surface. To relate this surface area (SA) to the volume stored in the reservoir [6-2], two surface-volume couples need to be defined: one corresponding to the volume of water permanently stored in the main channel during low flow (V_{min}) and one corresponding to the maximum capacity of the reservoir simulating the floodplain (V_{max}). Both values can be fixed based on a literature review or field survey.

$$SA = \beta \cdot V^{\alpha} \qquad [6\text{-}2]$$

where β and α are adjustment coefficients relating the volume and the surface of a reservoir by a power law.

The daily outflow volume may be determined using four different methods: (1) measured daily outflow, (2) measured monthly outflow, (3) average annual release rate (recommended for uncontrolled reservoirs) and (4) controlled outflow with targeted release (developed for artificial reservoirs). Among these, the average annual release rate is the best candidate to model floodplains.

The volume at the beginning of the time step is calculated by [6-3]:

$$V' = V_{stored} + V_{flowin} + V_{pcp} - V_{evap} - V_{seep} \qquad\qquad \text{[6-3]}$$

When the average annual release rate method is chosen to calculate the reservoir outflow, the reservoir releases water whenever its volume exceeds the minimum. While the volume is between the minimum (V_{min}) and the maximum (V_{max}), the outflow depends on the average daily release rate (q_{rel}):

$$V_{flowout} = V' - V_{min} \qquad \text{if } V' - V_{min} \leq q_{rel} \cdot \Delta t \qquad\qquad \text{[6-4]}$$

$$V_{flowout} = q_{rel} \cdot \Delta t \qquad \text{if } V' - V_{min} > q_{rel} \cdot \Delta t \qquad\qquad \text{[6-5]}$$

If the volume exceeds the maximum, the outflow increases in order to maintain it within bounds:

$$V_{flowout} = (V' - V_{max}) + (V_{max} - V_{min}) \qquad \text{if } V_{max} - V_{min} \leq q_{rel} \cdot \Delta t \qquad\qquad \text{[6-6]}$$

$$V_{flowout} = (V' - V_{max}) + q_{rel} \cdot \Delta t \qquad \text{if } V_{max} - V_{min} > q_{rel} \cdot \Delta t \qquad\qquad \text{[6-7]}$$

The average daily release rate (q_{rel}) has to be defined by the user based on his knowledge of the reservoir.

The volume at the end of the time step is finally defined as [6-8]:

$$V = V' - V_{flowout} \qquad\qquad \text{[6-8]}$$

The main disadvantages of this method when modeling floodplains are that the outflow does not always depend on the volume of stored water and that there will be no outflow if the volume decreases below the minimum.

Additionally, even if the surface area of the reservoir is computed at each time step, it has no influence on the subbasin surface area where it is located. Therefore, the water balance of the subbasin does not take into account the surface reduction/increase caused by the extension/reduction of the reservoir. In the case of floodplains, with highly variable surface and with large extents compared to the subbasins where they are located, this may cause substantial deviations in the subbasins' water balances.

6.2.3 Modified reservoir model

The original SWAT reservoir model has been used to simulate the African floodplains [*Schuol et al.*, 2008b]. However, the results on Zambezi Basin reached a Nash-Sutcliffe coefficient below zero, which was justified by the authors with the difficulty of simulating outflow from the wetlands. The authors believe that there was, indeed, an inadequacy with the original SWAT reservoir model. Despite this, and overlooking the secondary effect of

reservoir surface evaporation, a tendency to delay (or rush) flows in reservoirs will not contribute appreciably to a large bias (as over a sufficiently large number of years roughly what goes in the reservoir must come out). Large floodplains attenuate runoff, reducing and delaying flood peaks downstream [*Beilfuss and Dos Santos*, 2001; The World Bank, 2010], and are characterized by significant evaporation losses and seasonal fluctuations. During high flow periods, water spreads over bank and inundates the floodplains whereas during low flows, it runs only along the main channel. It has been observed that such floodplains have a great impact on the water storage capacity of the subbasins [*Meier et al.*, 2011].

Modeling floodplains as natural reservoirs with specific storage and outlet characteristics proved to be a successful approach for hydrological simulation [The World Bank, 2010]. As such, a set of two equations to reproduce the outflow from the floodplains [6-9] was developed and appended to the original SWAT reservoir model. The base flow (Q_{base}) is defined by a release coefficient and depends on the water depth (H) in the reservoir simulating the floodplain [6-10]. The additional inflow is stored in the reservoir and released as an upper flow (Q_{up}) if the water depth exceeds a fixed threshold (H_{min}), corresponding to the minimum water level in the main channel, as from a free crest weir [6-11].

$$Q_{outflow} = Q_{base} + Q_{up} \qquad [6\text{-}9]$$

$$Q_{base} = k \cdot H \qquad [6\text{-}10]$$

$$Q_{up} = \begin{cases} 0 & if\ H \leq H_{min} \\ a \cdot (H - H_{min})^b & if\ H > H_{min} \end{cases} \qquad [6\text{-}11]$$

where k (release coefficient), a (overflow coefficient) and b (overflow exponent) are the model parameters used in the calibration process.

The overflow coefficient is an aggregate of the constants for weir flow rate definition and the weir width [6-12]. The weir width corresponds to the mean width of the floodplain; it is assumed to be different for each floodplain but constant through time.

$$a = C_d \cdot \sqrt{2 \cdot g} \cdot w \qquad [6\text{-}12]$$

where C_d is the discharge constant for the weir, g is the gravitational constant and w is the weir width in meters. The bounds for the overflow coefficient depend on the geometrical characteristics of the floodplain. The calibration process could be done on the discharge constant (C_d) alternatively to the overflow coefficient (a) if enough data were available to define the weir width (w). However, in the present case study, in light of insufficient information on the geometry of the floodplains, the overflow coefficient (a) was used as a calibration parameter.

The standard value for the overflow exponent is 1.5, but in order to account for specificity of the floodplains, it was assumed that it can vary from 1 to 3.5. Accordingly, the units of the discharge constant (C_d) will vary to provide a discharge result in m^3/s.

The release coefficient controlling the base flow (*k*) varies on a wide range as it allows the simulation of the main channel flow and can be very different between floodplains.

The daily water depth in the reservoir is calculated based on its volume [6-13]. As for the surface-volume relation [6-2], two depth-volume couples need to be defined, one corresponding to the volume of water permanently stored into the main channel during low flow (V_{min}) and one corresponding to the maximum capacity of the reservoir simulating the floodplain (V_{max}). Such parameters can be derived from a Digital Elevation Model analysis if the data are available at a scale corresponding to the floodplain characteristics or defined based on literature review or field survey. The parameters can also be adapted by the user depending on the simulation results. For example, if V_{min} is too low, the downstream base flow will be too high and if V_{min} is too high the downstream baseflow will be too low. Vmax will not affect the simulation results.

$$H_t = \gamma \cdot V_t^{\delta} \qquad\qquad [6\text{-}13]$$

where δ and γ are adjustment coefficients linking the volume and the water depth of a reservoir assumedly by a power law.

Finally, an improvement has been made to the original model concerning the relation between subbasin and reservoir surface. Because the reservoir surface can be considerable relatively to the subbasin surface and can be subject to substantial fluctuations in time, it is subtracted at every time step from the subbasin surface to compute an accurate water balance.

The initial volume of water inside the floodplain should be defined by the user. If no data are available, it is recommended to run the model starting from a period with minimum flow so that the floodplain would be as empty as possible and that the initial conditions would have a limited influence on the simulation results.

6.3 MODEL IMPLEMENTATION AND APPLICATION TO THE ZAMBEZI BASIN

In order to evaluate the adequacy of the modified reservoir model, it was applied on the Zambezi River Basin considered as representative for large floodplains regions. The proposed methodological approach was conceived to be suitable for wider applications. Its particularities are to rely on global data sets for model set up, to proceed with automatic calibration process and to include a sensitivity analysis of the floodplain simulation parameters.

6.3.1 Study area

The Zambezi River Basin, located in the southern part of the African Continent, is the fourth largest drainage basin in Africa. From its headwaters in Angola to the delta in Mozambique, the Zambezi River runs over 2,600 km and connects eight nations that share

different portions of its 1.4 M km^2 drainage basin (Figure 6-1) [*Vörösmarty and Moore III*, 1991]. The climate is dominated by seasonal rainfall patterns associated with the Inter-Tropical Convergence Zone (ITCZ).

The river includes three distinct stretches: the Upper Zambezi, the Middle Zambezi and the Lower Zambezi [*Beilfuss and Dos Santos*, 2001; *Moore et al.*, 2007]. The Upper Zambezi is characterized by the Northern Highlands and the Central Plains, which are constituted by two major floodplains attenuating the runoff: the Barotse and the Chobe flats. Between Victoria Falls and the Cahora Bassa reservoir (Middle Zambezi), the river connects with the Kafue River, a major tributary characterized by two large floodplains (the Lukanga and the Kafue flats) and two large dams (Itezhi-Tezhi and Kafue Gorge). In total, four major floodplains are located in the basin (Barotse, Chobe, Lukanga and Kafue) from which the two majors are the Barotse flats (permanently inundated area of around 1,000 km^2 and intermittently inundated area of about 11,000 km^2) and the Kafue flats (permanently inundated area of around 2,000 km^2 and intermittently inundated area of about 7,000 km^2).

To illustrate the influence of the floodplains, two gauging stations were chosen as reference for the analysis: the first one located at the outlet of the Kafue flats and the second one located at the outlet of the Barotse flats (Figure 6-1). The discharge data at the station downstream of the Kafue flats consists of a reconstructed inflow hydrograph of the Kafue Gorge reservoir based on the observed outflow and water level.

Figure 6-1. Basin map with countries, gauging stations, major reservoirs and floodplains.

6.3.2   Model set up

The Digital Elevation Model (DEM) from the United States Geological Survey's (USGC) public domain geographical database HYDRO1k, at a spatial resolution of 1 km (http://eros.usgs.gov/#/Find_Data/Products_and_Data_Available/gtopo30_info), was used to delineate the subbasins. A minimum drainage area unit of 5,000 km^2 was first set to delineate these. Subsequently, subbasins around the lakes and floodplains were refined by overlapping a GIS layer of lakes and flats of Africa, increasing the number of subbasins to a total of 405.

To define the Hydrological Response Units (HRUs), the soil map produced by the Food and Agriculture Organization of the United Nations [*FAO*, 1995] and the land-use grid from the Global Land Cover Characterization (GLCC, Version 2, http://edcsns17.cr.usgs.gov/glcc/) were included. The minimum percentage a land use, slope or soil class must cover within a subbasin in order to generate a particular HRU was set to 35%, resulting in a total of 778 HRUs. This criterion results from a compromise aiming to limit the number of HRUs while keeping a substantial level of information.

The artificial and natural lakes, as well as the largest floodplains located on the main channel, were modeled as reservoirs. For the artificial reservoirs, namely the hydropower plant reservoirs, the simulated outflow was constrained to the observed outflow records to reproduce the operations in conformity. For the floodplains, the initial volume was adjusted to match observed initial conditions at the downstream gauging station when available or adjusted depending of the season at the start of the calibration period.

According to a previous reliability analysis [*Cohen Liechti et al.*, 2012], TRMM 3B42 version 7, NASA's standard precipitation product was selected as the precipitation source. The estimates for this product are published on a 0.25° by 0.25° grid with a 3-hourly temporal resolution (00:00, 03:00,…, 21:00 UTC). The temperature grids (daily minimum and maximum) are compiled from the NCEP/DOE 2 Reanalysis data [*Kanamitsu et al.*, 2002] provided by the NOAA/OAR/ESRL PSD, Boulder, Colorado, USA, from their Website at http://www.esrl.noaa.gov/psd/. All input data were aggregated to daily in order to match with the simulation time step. Discharge data were provided by the Global Runoff Data Centre (GRDC) [*Fekete et al.*, 1999] and the Department of Water Affairs of Zambia (DWA, personal communication).

6.3.3   Model calibration and validation

The years 1998 and 1999 were used as a stabilization period to allow the model to converge towards the "true" water cycle and, thus, rule out influence of imperfect initial conditions. In order to increase the number of available calibration data the final conditions of the stabilization period were used as initial values to calibrate the model on the period 1998 to 2003. The years 2004 to 2006 were kept for validation.

At first, the original SWAT calibration parameters were chosen based on the sensitivity analysis tool included in the ArcSWAT interface [*Winchell et al.*, 2010]. The incorporated

method combines the Latin Hypercube (LH) and One-factor-At-a-Time (OAT) sampling, assuring that the changes in the output of each model run can be unambiguously attributed to the parameter that was changed [*van Griensven et al.*, 2006]. More precisely, during the analysis, SWAT runs *(p+1)*m* times, where *p* is the number of parameters being evaluated and *m* is the number of LH loops. Then, the list of selected parameters was compared to the one used in previous studies [*Schuol et al.*, 2008b; *Zhang et al.*, 2009] and the associated boundaries for calibration were defined (Table 6-1). Finally, the new reservoir model parameters (*a*, *b* and *k*) were added to the list. On the Zambezi basin, given that floodplains can cover vast areas, over thousands of kilometers and that the water head over the "weir" at the outlet will typically not be superior to 1 m, the overflow coefficient (*a*) will have large values varying from 1,100 to 55,000 $m^{3/2}$/s for an overflow exponent (*b*) equal to 1.5. Concerning the release coefficient (*k*), its bounds were set from 35 to 350 m^2/s to account for the large base flow produced by the floodplain located in the downstream part of the basin.

Table 6-1. SWAT model parameters included in the final calibration procedure with their upper and lower bounds.

Parameter	Description	Unit	Lower bound	Upper bound
SURLAG	Surface runoff lag time	day	0.5	1.5
ALPHA_B	Baseflow recession constant	day	0	0.5
GW_DELA	Groundwater delay	day	20	300
GW_REVA	Ground water 'revap' coefficient for flow to move into the overlying unsaturated zone	-	0.1	0.4
REVAPMN	Threshold depth of water in the shallow aquifer for ground water to move into the overlying unsaturated layers	mm	1	400
GWQMN	Threshold depth of water in shallow aquifer for return flow (to the reach) to occur	mm	5	100
ESCO	Soil evaporation compensation factor	-	0.001	1
CN_F	SCS curve number for moisture condition	%	-0.25	0.15
CH_KII	Effective hydraulic conductivity in main channel alluvium	mm/hr	0.1	50
SOL_AWC	Available water capacity of the soil layer	%	-0.3	1
SOL_Z	Depth from soil surface to bottom of the layer	%	-0.5	1
EPCO	Plant uptake compensation factor	-	0	1
CANMX	Maximum canopy storage	mm	0	30
Floodplain parameters				
a	Reservoir overflow parameter	$m^{3/2}$/s	1,100	55,000
b	Exponent of overflow equation for reservoir	-	1	3
k	Reservoir release coefficient	m^2/s	35	350

The multi-algorithm genetically adaptive multi-objective method (AMALGAM) was chosen as the heuristic search algorithm for generating optimized parameter sets [*Vrugt and Robinson*, 2007; *Vrugt et al.*, 2009] based on two evaluation criteria, the Nash-Sutcliffe coefficient and [6-14] the volume ratio [6-15]. The averaged value for both criteria over all the discharge stations available was optimized.

$$NS = 1 - \frac{\sum (Q_{obs} - Q_{sim})^2}{\sum (Q_{obs} - \overline{Q_{obs}})^2} \qquad [6\text{-}14]$$

$$VR = \frac{\sum Q_{sim}}{\sum Q_{obs}} \qquad [6\text{-}15]$$

Three different configurations for floodplain modeling were calibrated and tested: (1) simple channel routing (no reservoir for the floodplains), (2) the original SWAT reservoir model defined by an average release rate and (3) the modified SWAT reservoir model. Each configuration was calibrated separately, and the set of parameters having the best indicators value was selected for plotting the simulated hydrographs.

6.3.4   Sensitivity analysis

A sensitivity analysis was carried out with the goals of determining the importance of the new reservoir parameters over the whole hydrological model outcome and qualitatively assessing its implications on the model's uncertainty.

The results of the sensitivity analysis are given in terms of sensitivity index: the fraction of the variance in the model due to a certain parameter in respect to the total variance of the model due to the whole parameter space. Resulting from this definition, the sensitivity indices vary in the range between 0 and 1. A sensitivity index equal to 0 indicates that the system is insensitive to the corresponding parameter. Vice versa, values close to 1 mean a high sensitivity to the parameter being assessed.

The analyzed hydrological model is a spatially and temporally extended nonlinear dynamic system. Due to the nature of such a system, the global sensitivity analysis method selected is the Fourier Amplitude Sensitivity Test (FAST). The FAST method is used to estimate the expected value and the contribution of individual inputs to the variance of the output [*Cukier et al.*, 1973]. The main advantage of a global method is that multiple locations in the physically plausible parameter space are evaluated.

The FAST method was first applied based on temporal dynamics of parameter sensitivity (TEDPAS) which allows the quantification of the model components that dominate the simulation response [*Reusser and Zehe*, 2011]. In a second step, a non-time dependent FAST was carried out for a year of simulation (2000 for the Barotse plains and 2001 for the whole Zambezi) based on the Nash–Sutcliffe coefficient (NS) [6-14] and the volume ratio (VR) [6-15]. These indicators express how good the model fits the observed data.

The implementation has been done using the FAST R package which is reported by Reusser *et al*. [2011]. The methodology can be summarized in the following steps:

1. Select the parameters to be assessed.
2. Generate sets of parameter values and launch SWAT simulations for each set.

3. Carry out a FAST applied to direct model outputs (discharge, water level and volumes in the reservoirs) at each time step (TEPDAS).
4. Carry out a FAST applied to performance criteria for a selected simulation period.

The effect of the new floodplain parameters was determined at two geographical levels: (1) at the outlet of the Barotse floodplains for the parameters of this floodplain and (2) at the outlet of the entire basin for the parameters of the two major floodplains (the Barotse and the Kafue).

The local assessment at the outlet of the floodplain gives qualitative understanding of the order of importance of each parameter according to the floodplain characteristics and discharge; it allows the identification of the principal components of the system. This sensitivity analysis was conducted dynamically (TEDPAS) and averaged over time using NS and VR as objective functions. The assessment of the two sets of floodplain parameters on the discharge at the outlet of the basin allows evaluating the importance of the floodplain effect on the global hydrograph.

6.4   RESULTS AND DISCUSSION

6.4.1   Comparison of the reservoir models

The NS and VR indicators have been calculated based on daily, monthly and yearly mean discharge to validate the modified model. At monthly and yearly time step, the indicators are given for the whole period whereas at daily time step, the calibration and validation periods are separated. Due to the discontinuity of the observed data series downstream of the Barotse floodplain no pertinent indicators could be computed at yearly time step.

Downstream of the Barotse floodplain, the modified reservoir model, the original reservoir model and the model with no reservoir are nearly equivalent in terms of VR (Table 6-2). The NS during calibration period is improved by more than 15% by the modified model compared to the original model which corresponds to a better reproduction of the hydrograph shape as shown in Figure 6-2. At monthly time step, the difference between the models is lower, the modified model still reaching the highest NS. By looking at the hydrograph (Figure 6-2, a), the modified reservoir model perform better in two aspects. The smoothing effect of the floodplain is reproduced both during low and high flows and the decrease in discharge follows the observed pattern whereas it drops too much in the case of the original reservoir model (Figure 6-2, b).

Table 6-2. NS and VR values of the three configurations tested for daily, monthly and yearly time steps.

Configuration (calibration/validation)	NS Barotse	NS Kafue	VR Barotse	VR Kafue
Upstream floodplain	0.80 / 0.86	0.50 / 0.45	0.87 / 0.88	0.94 / 0.70
With modified reservoir				
• Daily	0.77 / 0.81	0.51 / 0.05	0.86 / 0.78	1.08 / 0.81
• Monthly	0.77	0.53	0.82	1.03
• Yearly	-	0.79	-	1.03
With original reservoir				
• Daily	0.65 / 0.78	0.44 /–0.10	0.90 / 0.84	1.09 / 0.94
• Monthly	0.72	0.46	0.87	1.07
• Yearly	-	0.67	-	1.07
Without reservoir				
• Daily	0.66 / 0.76	–4.04 /–2.27	0.93 / 0.87	1.34 / 0.99
• Monthly	0.71	-3.79	0.90	1.29
• Yearly	-	0.09	-	1.27

Downstream of the Kafue floodplain, the NS is improved with the modified reservoir model compared to the original reservoir model, especially during the validation period, as it passes from -0.10 to 0.05 (Table 6-2). In terms of VR, the two reservoir models are equivalent, again pointing towards the adequacy of the annual water balance reproduction. The superiority of the modified representation is also shown at monthly and yearly time step as the NS is higher than with the original model. The model without reservoir clearly overestimates the flow volume and is qualified by negative NS values.

The hydrograph observed below the Kafue floodplain is not very smooth as it is calculated based on the water balance equation at the Kafue Gorge reservoir. None of the models were able to fully reproduce the observed peaks. Nonetheless, the reconstructed series is uncertain as it relies on water level variation and on observed outflow both at the turbines and at the spillways, which may be subject to non-negligible deviations. With the modified reservoir model, the base flow of the hydrograph is reproduced and the peak flows are closer to what is observed than the original reservoir model's estimates, even if they are sometimes still too low or too early (Figure 6-2, c). The original reservoir model does not delay the peaks, but attenuates excessively the flood (Figure 6-2, d). Without reservoir, the model cannot reproduce the effect of the large floodplain (Figure 6-2, d).

Globally, the most inadequate model configuration is, as expected, the configuration without a reservoir (Figure 6-2, b and d), which emphasizes the necessity to include the floodplains in the hydrological model. The modified reservoir model allows for a more accurate simulation of the discharge pattern, especially for the very large floodplains. Moreover, the model can be calibrated for each floodplain with the parameters *a*, *b* and *k*, which ensures the best possible fit.
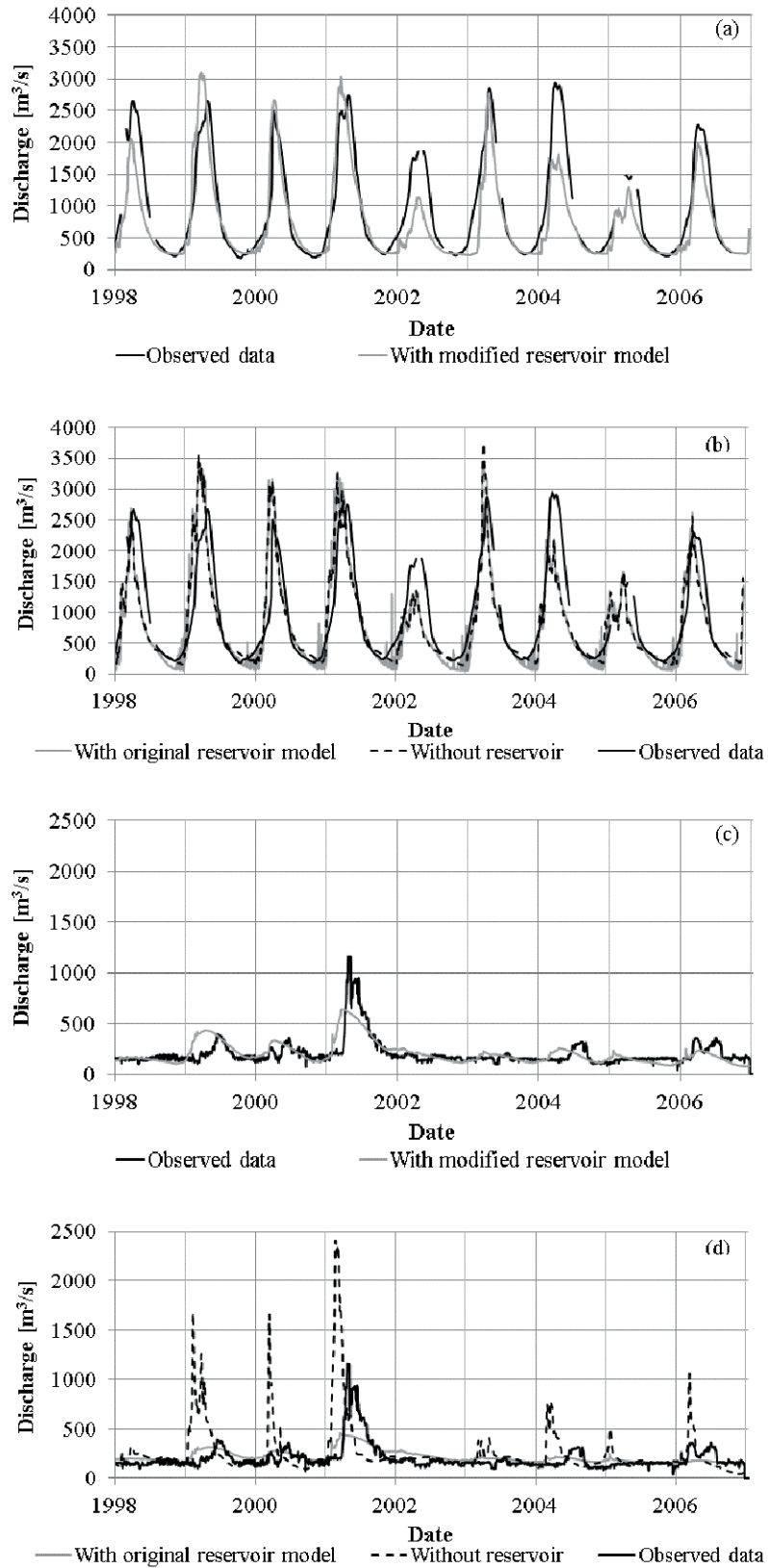
Figure 6-2. Discharge observed at the stations below Barotse flat (a and b) and below Kafue flats (c and d) compared with the discharge modelled with the new reservoir model (a and c), the original reservoir model and without a reservoir (b and d). Both calibration (1998-2003) and validation period (2004-2006) are presented.

147

6.4.2   Sensitivity analysis

6.4.2.1   Sensitivity analysis at the Barotse floodplain

Table 6-3 presents the information of the FAST sensitivity indices of the floodplain parameters in regard to NS and VR for the year 2000. For both indicators the SWAT model appears to be most sensitive to the overflow coefficient (*a*) followed by the overflow exponent (*b*) and the release coefficient (*k*).

Table 6-3. Sensitivity indices of the Barotse floodplain parameters regarding NS and VR (a: overflow parameter, b: overflow exponent, k: release coefficient).

Parameter	NS FAST index	VR FAST index
a	0.64	0.54
b	0.15	0.26
k	0.03	0.11

In the Barotse floodplain, according to the model set up and for the simulated year, the upper flow is predominant to base flow. In a calibration run the overflow parameters (*a* and *b*) would take a more significant role than the base flow parameter (*k*). One explanation is that the high flows have more influence on both VR and NS values than low flows. It is likely that, depending on the discharge and the floodplain features, the predominant processes can be governed mainly by either base or upper flows; if so, it would be expected that the relative importance of the three proposed parameters varies accordingly.

To evaluate how sensible is the model to each parameter depending on time, the TEDPAS was launched for the same location and period. Figure 6-3 represents the FAST sensitivity indices per each time step and parameter and in regard to volume in the reservoir and outflow from the reservoir. The fluctuation of the FAST index regarding volume (Figure 6-3, a) is smooth and shows the relatively constant value of the overflow parameter (*a*). On the other hand, the overflow exponent (*b*) index increases during the high flow period (April-May) corresponding to a decrease of influence of the release coefficient (*k*). This means that the reservoir level is higher than the minimum thorough the year as there is constantly an upper flow and that the overflow exponent is sensible mainly when the water level is high. In terms of sensitivity to the outflow (Figure 6-3, b) the fluctuations are more pronounced. The sensitivity of the overflow parameter (*a*) is high during the whole period except when the discharge is increasing (March) or decreasing (July). During these months, the overflow exponent (*b*) gains importance. The index of the release coefficient (*k*) is, as expected, higher during the dry period (September-February) than during the wet periods.
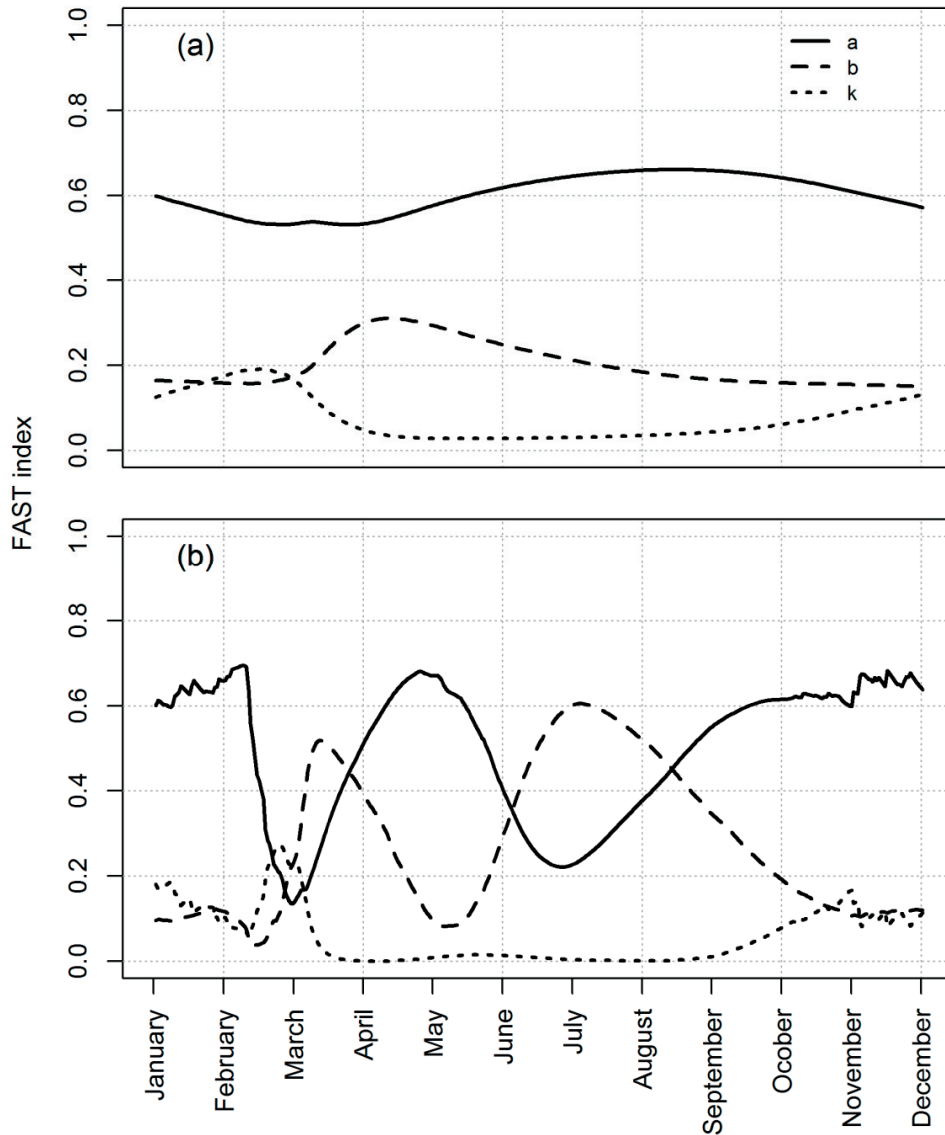
Figure 6-3. FAST index of the Barotse floodplain parameters (a: overflow parameter, b: overflow exponent, k: release coefficient) for the year 2000 over the volume of the reservoir (a) and the outflow from the reservoir (b).

The discharge output resulting from all the simulations in the parameter space is presented in Figure 6-4. As expected from the parameter index, a high variance on discharges can be observed during wet season.
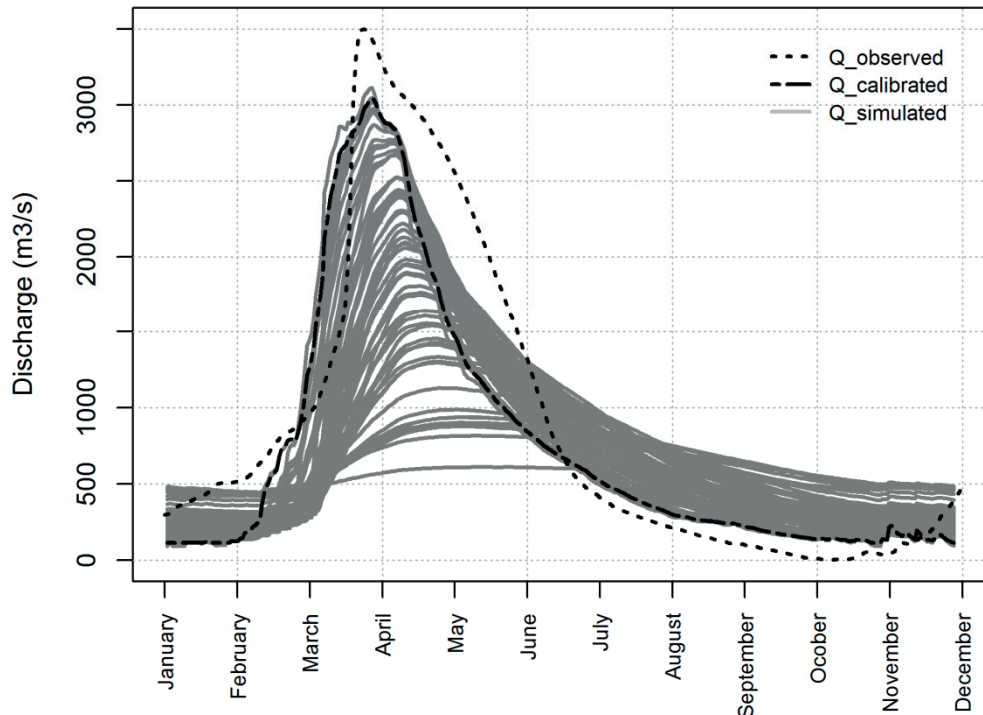
Figure 6-4. Discharge variation due to the floodplain parameters variation for the year 2000 at the outlet of the Barotse floodplain.

6.4.2.2 *Sensitivity analysis at the Zambezi basin outlet*

The aim of this approach was to assess the influence of the floodplain parameters over the whole Zambezi basin. For this purpose the two major floodplains in the basin (Barotse and Kafue), belonging to different subbasins, were selected.

In Figure 6-5, the discharges are displayed for the different set of parameters used in the FAST assessment (91 sets in total). A thicker line indicates higher discharge variance. It can be observed that for years with low peaks, e. g. 1998, the variation of the discharges is low, so in such years the model will be less sensitive to the floodplain parameters being assessed. During wet years the variation of discharges occurs mainly during the recession period due to a delay on the response of the floodplains. For this reason the year selected to evaluate FAST indices was 2001, when the peak is clearly higher and presents a stronger variation of the discharges.
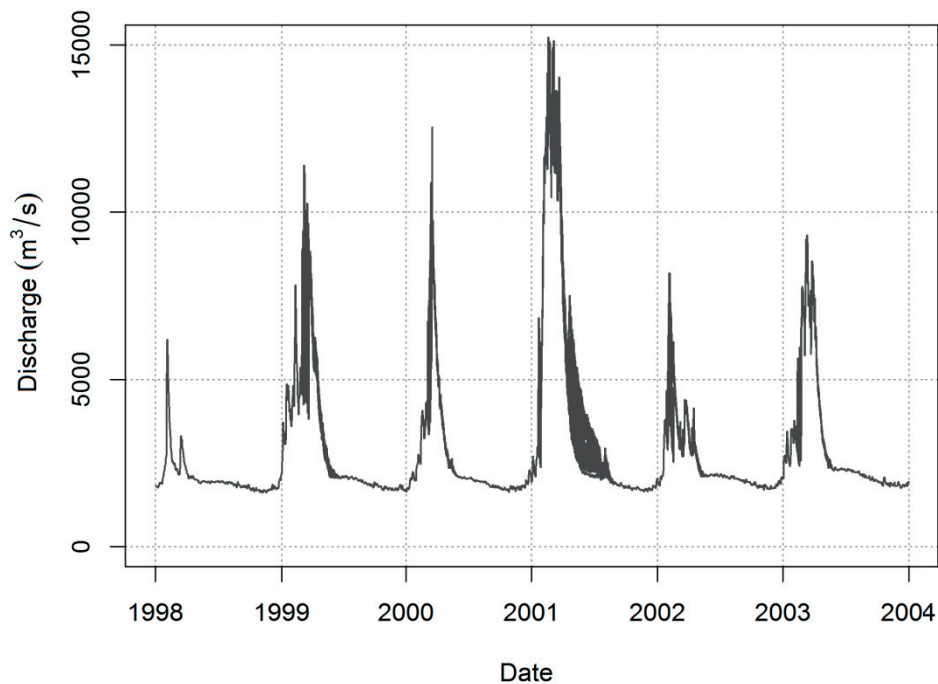
Figure 6-5. Discharge variation due to the floodplain parameters variation at the outlet of the basin.

The comparison of the sensitivity of both floodplains is presented in Figure 6-6 for the year 2001. For the overflow parameters (Figure 6-6, a and b) the sensitivities from both floodplains follow similar patterns with a clear delay for the Barotse floodplain, located more upstream than the Kafue floodplain. A different pattern is observed in the comparison between the base flow parameter (Figure 6-6, c), which appears to be more influent in the Kafue floodplain than in the Barotse floodplain. As its sensitivity depends on the floodplain geometry and on the flow regime and can therefore vary from one floodplain to the other, this fact indicates the importance on considering individual parameterizations for each floodplain. Despite the fact that the relative importance of each parameter depends on floodplain geometry, the sensitivity to overflow parameters has a natural tendency to be higher than to base flow parameters for indicators as NS and VR which are more influenced by high discharges than low discharges. Globally, it is during wet periods that the hydrological model is more sensitive to reservoir parameters.
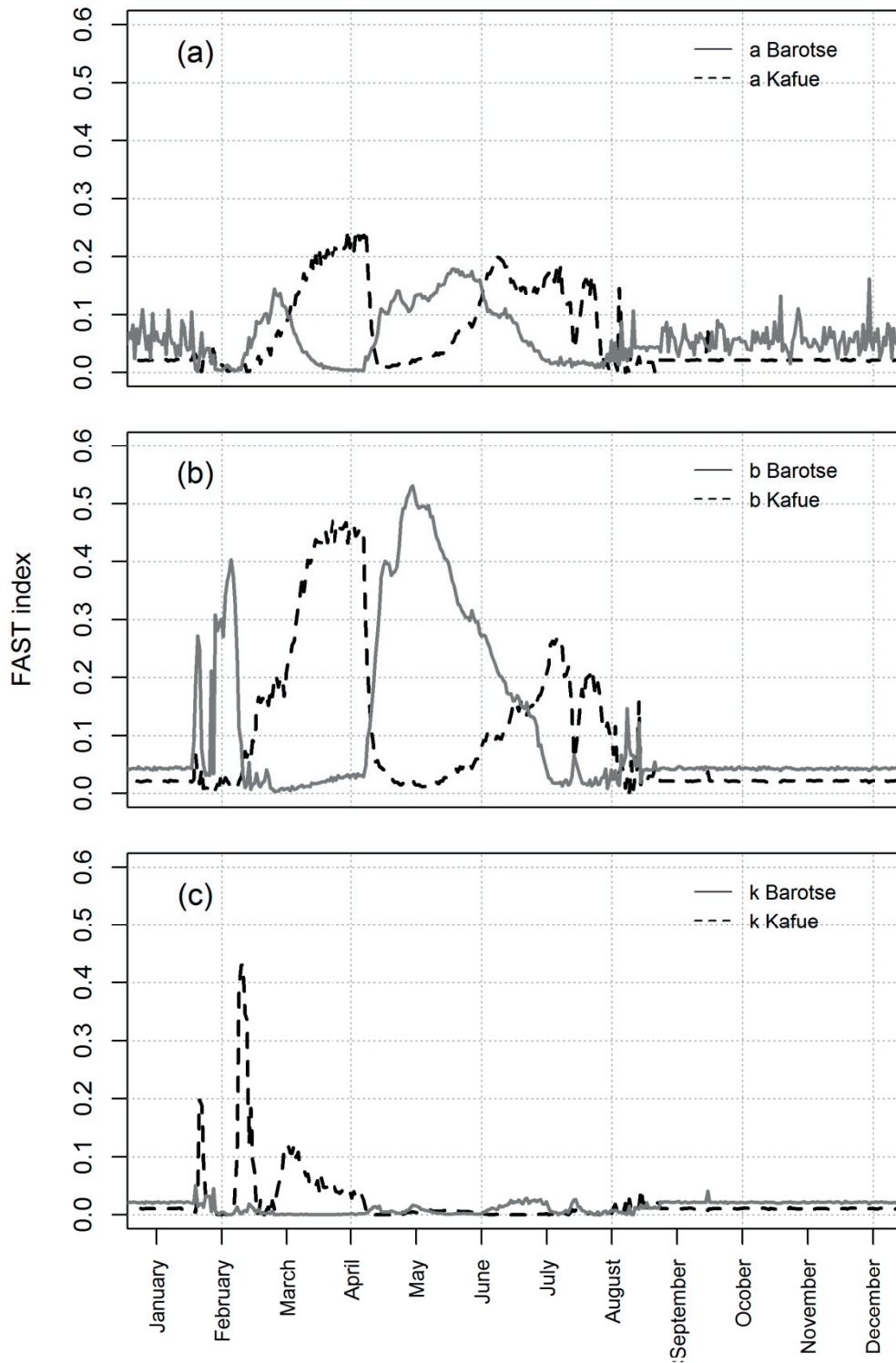
Figure 6-6. FAST index on discharge for the year 2001 at the outlet of the basin for the floodplain parameters of the Barotse and Kafue reservoirs (a: overflow parameter, b: overflow exponent, k: release coefficient).

6.5 CONCLUSIONS

Important ecological reserves are created by floodplains and they act as natural flood attenuators by delaying and smoothing flow peaks. In the African Continent, these geographical features are characterized by large evaporation losses and seasonal fluctuations: during high flow periods, water spreads over the bank and inundates the floodplain, whereas during low flows the stream propagates solely along the main channel. In this study, the reservoir model of SWAT 2009 was adapted to model large floodplains and applied to the Zambezi Basin. The outflow was computed using a double equation separating the overflow from the base flow. The modified and the original reservoir models were compared with the observed discharge in terms of volume ratio (VR), Nash-Sutcliffe coefficient (NS) and hydrographs. The results confirmed that the modified model improves the simulation of the discharge below large floodplains both during high flow and low flow periods. With the modified reservoir model, NS values are higher than 0.5 for the calibration period and do not drop below zero during validation, evidencing the ability of the model to reproduce floodplain effects. The model developed in the present study follows a conceptual approach and does not represent in detail the process operating on the floodplain as backward flows or multichannel flows.

The sensitivity analysis showed that the overflow parameters have more influence on the NS and VR criteria than the base flow parameters as they are effective during high flow periods. As a consequence, at least overflow parameters should be considered in a calibration stage. The differences between two floodplains' behavior was also highlighted, underlying the need of individual parameterization. Considering the particularities of floodplain regions, the modified model reveals its ability to simulate the behavior of large inundated area thanks to its spatial flexibility.

As further research, since the separation between base flow and upper flow can be a proxy allowing for different processes of degradation and/or transport of chemicals, sediments, etc. inside the floodplain, equations for water quality and sediment transport could be added to the outflow computation in the modified approach.

7 ANALYSIS OF HYDROPOWER DEVELOPMENT SCENARIOS IN VIEW OF SUSTAINABLE AND ECOLOGICAL CATCHMENT DEVELOPMENT

At the end of the 20th century, the number of large dams has climbed to more than 50,000 and the water demand is exponentially increasing, especially in developing countries. As the needs for further water services are increasing, the challenges for the future are to operate existing large hydraulic systems in more sustainable ways; to develop future water resource schemes that achieve a better balance between ecological and socioeconomic demands. In this chapter, scenarios combining different levels of environmental requirements as well as multiple hydropower development schemes were simulated at a daily time step with a hydraulic-hydrological model on the Zambezi River Basin. The hydropower operation rules were simulated in detail and the mean annual energy produced, the firm power as well as the spilled volume during flood season were computed for each scenario. The impact on flow regime was characterized as low when the mean hydrological alteration was between 0 and 0.33, medium when the global hydrological alteration was between 0.34 and 0.66 and high when the global hydrological alteration was between 0.67 and 1. Pardé coefficients as well as duration curves were plotted to achieve the analysis.

The results showed that in the present state the total mean annual energy production is about 30,000 GWh and that the firm power is about 2,200 MW. The effect of the dams on the flow regime are characterized as low on the Kafue flats, high on the Mana Pools and low on the Zambezi delta. This impact can be reduced to a lower level on the Kafue flats and a medium level on the Mana Pools by e-flows release. Implementing new turbines at the existing dams impacts negatively the flow regime while increasing by 19% the mean annual energy production. The new run-of-river hydropower plants planned in the near future increase the mean energy produced by more than 90% and the firm power by about 40%. Releasing e-flows reduces the impact on the Kafue flats to a low level and on the Zambezi delta to a medium level with a loss of less than 10% in terms of mean annual energy and about 15% in terms of firm power at Itezhi Tezhi and Cahora Bassa. Such analysis shows that a compromise between energy production and environmental sustainability can be reached.

Chapter 7 Analysis of hydropower development scenarios in view of sustainable and ecological catchment development

7.1 INTRODUCTION

Hydroelectric power dams currently provide 19% of the world's electricity supply; one in three nations depends on hydropower to meet at least half of its electricity demands [*World Commission on Dams*, 2000]. At the end of the 20th century, the number of large dams (higher than 15 m) has climbed to more than 50,000 and the water demand is exponentially increasing, especially in developing countries [*International Commission On Large Dams*, 2007]. However, the modification of water flow regimes caused by dams is one of the primary causes of the degradation of freshwater ecosystems worldwide [*D Harrison et al.*, 2007]. More precisely, dam induced changes affect water temperature and chemistry, sediment transport, floodplain vegetation communities and downstream deltas [*Richter and Thomas*, 2007]. As the needs for further water services are increasing, the challenges for the future are to avoid past mistakes; that is, to operate existing large hydraulic systems in more sustainable ways; to develop future water resource schemes that achieve a better balance between ecological and socioeconomic demands; and to improve the institutional settings for transboundary water management [*International Commission On Large Dams*, 2012; *United Nations Development Programme*, 2006].

'*The concept of environmental flows (e-flows) has been advanced to meet ecosystem demands for water. E-flows are defined as the volume of water that should flow in a river and its variation over time to maintain specific indicators of ecosystem health*' [*Yin et al.*, 2012]. Historically, the e-flows were defined as a single minimum 'compensation' or 'reserved' flow. Nowadays, experts has reached a consensus: e-flows should represent the full range of natural flow variations, taking into consideration the magnitude, frequency, timing, duration and rate of change of the flow event [*Arthington et al.*, 2006; *Yin et al.*, 2012]. However, it results a loss in terms of energy production.

Multiple methodologies for evaluating natural flows and quantifying the effect of dam on flow alteration are available. They are mainly based on aquatic ecology theory and require as starting point either measurements or synthesized daily streamflows from a period with no human perturbations on the hydrological regime. The Range of Variability Approach (RVA) [*Richter et al.*, 1997] characterizes the flows using 32 different parameters derived from long term (> 20 years) daily streamflow records defining the timing, magnitude, duration, frequency and rate of change of the regime. A multi-objective optimization algorithm was applied to a reservoir in Taiwan to determine the trade-offs between human and ecosystem needs [*Suen and Eheart*, 2006]. A set of six indicators characterizing the difference to the natural hydrographs was defined to determine the ecosystem needs objective (coefficient of efficiency of the yearly trend of the hydrograph, dry season 10-days minimum, wet season 3-days maximum, number of high flows events, mean duration of low flow events and rising rate during wet season).

Richter and Thomas [2007] described a framework for planning and implementing a dam re-operation project. They separated the approach in six steps: (1) assess dam-induced hydrological alteration based on the RVA approach [*Richter et al.*, 1997], (2) describe ecological and social consequences, (3) specify goals for dam re-operation, (4) design dam re-operation strategies, (5) implement the strategies and (6) assess the results against the goals. For the hydropower systems, they proposed the solution of building a re-regulation reservoir downstream of the dam or use one of the dam already constructed in a cascade as the re-regulation reservoir. In the case of a multi-dam hydropower system, they stated that a computer-based decision support system is one of the most cost-effective ways to optimize the performance by balancing the impact of environmental flow release among the dams.

A reservoir operating approach combining reservoir operating rule curves and e-flow strategy was developed to optimize e-flow provision under given water supply constraints [*Yin et al.*, 2011; 2012]. The flows were divided into four functional components (floods, high-flow pulses, base flows and extreme low flows) and the flow regime alteration was quantified by the range of variability approach (RVA) [*Richter et al.*, 1997], deriving the range of variation for each hydraulic indicator from the natural hydrograph. The case study chosen was the Tanghe reservoir in China's Tang River Basin. The developed methodology was compared to conventional methods achieving a significant lower degree of flow alteration.

Ecological and economical profits of dynamic release policies within a diverted river reach were evaluated by Perona *et al.* [2013]. The hydrological differences from the natural flow regime were used as a proxy to assess environmental benefits and the mean of the ratio of the allocated net flows between environment and hydropower was implemented as a suitable engineering parameter to represent their relative value.

A summary of the research done to support possible re-operation of dams in Southern Africa is presented by Brown and King [2012]. For the Zambezi Delta, they stated that there is no e-flow requirement at this stage and that recreating a flood would generate costs in terms of hydropower loss.

The Zambezi River Basin contains many of southern Africa's largest and most intact freshwater and estuarine wetlands, e. g. the Kafue flats, the Mana Pools and the Zambezi delta as well as several free-flowing yet unprotected river reaches. Three of Africa's largest dams (Kariba dam, Cahora Bassa dam and Kafue scheme) inundate hundreds of square kilometers of river habitat and modify the natural flow patterns that sustain floodplains. Increasing electricity demand by cities and industry is causing a regional energy shortage, and governments and investors are planning yet more dams in the Zambezi Basin. Therefore, the basin constitutes a particularly interesting and important system for further developing existing approaches of integrated water resources management. Several studies have already assessed the impact of new operation rules coupled with economic development on the environment. More precisely, optimal flow allocation was assessed by pricing the irrigated

land and the energy generated, considering the environmental flow as constraints [*Gandolfi et al.*, 1997] or setting a value for the flooded area [*Tilmant et al.*, 2010a; *Tilmant et al.*, 2012]. Different economic development scenarios including environmental flows and irrigated area as constraints were simulated and their impact on energy production was assessed [*Beilfuss*, 2010; *The World Bank*, 2010]. Discussions are ongoing on the future operating rules of Cahora Bassa, including the new dam projected downstream but they will have little effect as Kariba sited upstream Cahora Bassa is mainly controlling the flooding pattern of the Zambezi. However, none of the study has assessed the state of the basin at a daily time step which is of relatively high importance considering that the future hydropower production will be more fluctuating following the energy prices. Concerning the key locations taken into account, a wide range of environmental flows have been defined and tested for the Zambezi delta but the Kafue flat and the Mana Pool were not always included in the analysis.

In this chapter, a set of scenarios combining different levels of environmental requirements as well as multiple hydropower development schemes were evaluated at daily time step and the balance between energy generation and environmental satisfaction was evaluated through indicators. It completes the previous study in the sense that the hydropower operation rules are modelled in details and that different indicators are applied to evaluate the hydrological alteration based on the simulation of the natural state.

In Chapter 7.2, the case study is presented in detail. In Chapter 7.3, the hydrological model is introduced along with the modifications brought to the source code to simulate the floodplains and the hydropower plants. The scenarios are presented in Chapter 7.4 and the results discussed in Chapter 7.5. Finally conclusions are listed in Chapter 7.6.

7.2 THE ZAMBEZI WATER RESOURCES SYSTEM

7.2.1 General characteristics of the basin

A detailed description of the basin and the hydropower plants has been given already in Chapter 3.1 and Chapter 3.2. The Zambezi River Basin, located in the southern part of the African Continent, is the fourth largest drainage basin in Africa (1.4 M km^2). From its headwaters in Angola to the delta in Mozambique, the Zambezi River runs over 2,600 km and touches eight nations [*Vörösmarty and Moore III*, 1991]. Kariba dam reservoir, the largest artificial reservoir on the basin, is located downstream Victoria Falls in the middle part of the Zambezi Basin. A major tributary, the Kafue River, connects to the Zambezi downstream Kariba and is characterized by two large floodplains (the Lukanga and the Kafue flats) and two large dams (Itezhi-Tezhi and Kafue Gorge). The lower part of the Zambezi includes Cahora Bassa dam and the delta. Multiple small run-of-river reservoirs are constructed on the Shire river downstream the Malawi Lake. There is still a huge potential for hydropower development and multiple projects will be implemented in the next 20 years.

7.2.2 Actual water utilization and future demand

Four major sectors of water demand are identified on the basin [*Euroconsult Mott MacDonald*, 2007]: the domestic water use, the industrial water use, the agriculture needs and the hydropower production (Table 7-1). The hydropower has by far the highest water consumption created by the evaporation from the reservoirs. It is followed by agriculture with a large potential of increase in the near future. The irrigation developments have not been included in the scenarios but would be an interesting aspect to take into account in further studies. The domestic and industrial sectors have a lower impact on the water balance and will therefore not be included in the development scenarios.

Table 7-1. Actual and future annual water consumption for the main sectors [based on *Euroconsult Mott MacDonald*, 2007]

	Domestic	Industry	Agriculture	Hydropower
Actual consumption [Mm^3]	200	Insignificant	1,472	17,000
Future demand (2025) [Mm^3]	700	500	4,635	-

7.2.3 Key points

Three key points for discharge analysis were defined based on previous studies of the basin [*Beilfuss*, 2010; 2012; *Beilfuss and Brown*, 2010; *The World Bank*, 2010; *Tilmant et al.*, 2012]: the Kafue flats, the Mana Pools and the Zambezi delta; their characteristics are listed in the Table 7-2. All the selected points are influenced by at least one of the existing or future hydropower schemes.

Table 7-2. Hydraulic characteristics of the key points used for scenario analysis.

	Kafue flats	**Mana Pools**	**Zambezi delta**
Mean annual flow prior regulation	-	-	9,800 m^3/s [*Beilfuss and Brown*, 2010]
Bank full discharge	250 m^3/s [*Beilfuss*, 2012]	-	4,500 m^3/s [*Beilfuss and Brown*, 2010]
Mean monthly target flow defined in the literature	300 m^3/s in February and March [*Tilmant et al.*, 2012]	2'500 m^3/s in February and March [*Tilmant et al.*, 2012]	6,000 m^3/s in February and March [*Tilmant et al.*, 2012]
	400 m^3/s in February and 600 m^3/s in March and April [*Euroconsult Mott MacDonald*, 2007].		4,500, 7,000 and 10,000 m^3/s in February or December [*The World Bank*, 2010]
			5000 to 8000 m^3/s in February or December [*Beilfuss*, 2010]
			4 500 m^3/s during two weeks in February [*Euroconsult Mott MacDonald*, 2007].
Threshold flow to evaluate the hydrological alteration	300 m^3/s	2,500 m^3/s	4,500 m^3/s

7.3 THE HYDROLOGICAL MODEL

The concept of the hydrological model is described in detail in Chapter 3.5 along with the modified reservoir sub-model used to simulate floodplain hydrology (Chapter 3.5.2) and to simulate the hydropower operations (Chapter 3.5.3). The setup is presented in Chapter 3.5.4 and the calibration procedure in Chapter 5.

7.4 SCENARIOS

The objective of the scenarios analysis is mainly to determine the impacts of the new hydropower plants on the energy production as well as on the environment. Three principal scenarios have been defined (Table 7-3):

- The first one (A) is the reference case for environmental flows as it considers the basin without hydraulic structures.

- The second one (B) models the actual state of the basin. It includes sub-scenarios with different environmental flow constraints: low, moderate and high corresponding to different level of ecological satisfaction.

- The third one (C) includes the projected hydropower plants. It separates the effect of the extension of the existing structures from the new structures. Sub-scenarios of different environmental flows are also tested.

Table 7-3. List of scenarios tested.

Scenario	Description	Environmental flow	Hydropower plants	Question
A	Reference scenario for the natural state	No constraints	No hydropower plants	What is the impact of existing hydropower plants on the natural discharge?
B	Present state of the basin (2010)	Existing constraints Low constraints Medium constraints High constraints	Existing structures (ITT, Kafue Gorge Upper, Kariba, Cahora Bassa)	What would be the cost in terms of energy production of environmental floods?
C	Include the most advanced hydropower projects	Existing constraints Low constraints Medium constraints High constraints	Existing structures + extensions of existing hydropower plants Existing structures + extensions + new projected structures (Kafue Gorge Lower, Batoka Gorge, Mphanda Nkuwa)	What is the energy production gained from the new dam projects? What would be the cost in terms of energy production of environmental floods?

All the scenarios are simulated for a period of 13 years from 1998 to 2010 and are evaluated in relation to the generated energy as well as to their impact on the flow regime at key points.

7.4.1   Environmental flow

The environmental flow constraints found in the literature are defined in terms of mean monthly discharge [*Beilfuss and Brown*, 2010; *Gandolfi et al.*, 1997; *The World Bank*, 2010]. These values were used as a basis for reconstructing a daily flood hydrograph considered as a constraint on the outflow at the hydropower plants. The e-flows hydrograph generation is based on the flood duration, the starting date of the flood event and the mean e-discharge as defined in the literature. As the flooding pattern is seasonal, the flood will occur over a long time period. Therefore, the shape of the hydrograph is approximated as trapezoidal. Since the turbines are expected to operate at full capacity when the superior e-flow is released through the spillway in order to minimize the loss in energy production the flood hydrograph starts

from the maximum turbine discharge. The flow increases gradually during the first one-third of the flood duration up to the peak discharge being 1.5 times the mean monthly e-discharge. During the second one-third of the flood duration, the flow stays constant at the maximum discharge. Finally, the flow decreases gradually down to the mean turbine discharge. The e-flood is released only if the volume of water inside the reservoir exceeds 30% of the active storage or if it is higher than the target volume. If the calculated outflow based on the business as usual operation rules is superior to the desired e-flow, no additional constraints are given.

Four levels of environmental satisfaction were simulated for each scenario (Table 7-4). The minimum constrain corresponds to the status quo, the low constraint provides a yearly flood in the delta, the moderate constraint increases the flood in the Kafue flats and introduces a flood in the Mana Pools and the high constraint imposes a large flood in the Kafue flats, the Mana Pools as well as in the delta.

Table 7-4. Environmental flow scenarios.

Name	Description	Environmental flow at Itezhi Tezhi	Environmental flow at Kariba	Environmental flow at Cahora Bassa (and Mphanda Nkuwa)
E1	Existing constraint	300 m^3/s in March, 25 m^3/s min	-	-
E2	Low constraint	300 m^3/s from mid-February to mid-April, 25 m^3/s min	-	4,500 m^3/s in February
E2	Moderate constraint	400 m^3/ from mid-February to mid-April, 25 m^3/s min	2'500 m^3/s in February	7,000 m^3/s in February
E3	High constraint	500 m^3/s from mid-February to mid-April, 25 m^3/s min	2'500 m^3/s in February and March	10,000 m^3/s in February

7.4.2   Hydropower plants

The characteristics of the existing and projected hydropower plants included in the model are presented in Table 7-5. The new hydropower projects are the following: Batoka Gorge, Kafue Gorge Lower, Mphanda Nkuwa and Kholombidzo. Moreover, four extensions of existing hydropower plants are considered: Kariba North and South bank extensions, Itezhi Tezhi power extension, Cahora Bassa North Bank extension and Kapichira extension.

The **Batoka Gorge** hydropower project, located about 50 km downstream the Victoria Falls and about 400 km upstream from Kariba, bilateral between Zambia and Zimbabwe, is considered for development in the medium term. The relatively small storage capacity means that the plant is intended to operate as a run-of-river plant maximising firm power delivery on a system level [*G P Harrison and Whittington*, 2002].

Two **extensions** have been developed for **Kariba** in both banks. On the North bank (Zambian side), the new powerhouse of about 360 MW is actually under construction by Sinhydro. On the South bank (Zimbabwean side), the extension is planned for the medium term.

The **Itezhi Tezhi power extension** would not be operated to firm up energy but rather to generate available energy in accordance with reservoir variation as the reservoir is used for regulation of the Kafue Gorge Upper dam [*The World Bank*, 2010]. As Zambia has a large power deficit, the project is on fast-track for development. In the medium term, the construction of **Kafue Gorge Lower** downstream of Kafue Gorge Upper is also foreseen.

The **Cahora Bassa North Bank extension** consists in a new underground powerhouse. Combined with a new spillway, it would allow the operation of Cahora Bassa reservoir without lowering the lake level before the high flow period (flat rule curve) [*The World Bank*, 2010]. The impact of using a flat rule curve (at 326 m a.s.l.) for hydropower generation would result in an increase of nearly 6% of the firm power generated in the actual state [*Beilfuss*, 2010].

The **Mphanda Nkuwa** project is located 70 km downstream Cahora Bassa. Two options of operation have been proposed, a run-of-river plant or a peaking mode plant which would necessitate a reservoir downstream for reregulation [*The World Bank*, 2010].

Two alternatives have been analyzed for hydropower development at **Kholombidzo** located on the Shire River just downstream Lake Malawi [*The World Bank*, 2010]. The High Kholombidzo would have highest regulated water level to exploit a hydraulic head of about 75 meter and control the level of Lake Malawi. The Low Kholombidzo would have the same layout but with a lower head pond and would not be able to regulate the level of Lake Malawi. In the present study, the High Kholombidzo alternative has been included in the simulations.

Table 7-5. Characteristics of the existing and projected hydropower plants included in the model.

Reservoir name		Commi-ssioning year	Opera-tion level	Volume	Reser-voir area	Turbine capacity planned (observed)		Spillway capacity and associated water level		Tailwater level and associated discharge	
			[m a.s.l.]	[10^9m^3]	[10^6m^2]	[m^3/s]	[MW]	[m^3/s]	[m a.s.l.]	[m a.s.l.]	[m^3/s]
Itezhi Tezhi	Max	1977	1030.5	6.00	380	160	-	4425	1030.5	-	-
	Min		1006.0	0.78	90			402	1020.0	-	-
Itezhi Tezhi power extension		*2013*				*312*	*120*			*1003.3*	*-*
Kafue Gorge (upper)	Max	1972	976.6	0.90	750	252 (170)	900	3600	978.0	572,1	-
	Min		975.4	0.13	180			780	972.3		
Kafue Gorge (lower)	*Max*	*2017-2022*	*582.0*	*0.06*	*1.5*	*442*	*750*	*5200*	*582.0*	*389.6-*	*-*
	Min		*530.0*	*0.01*	*0.5*			*780*	*560.0*		
Batoka Gorge	*Max*	*2023-2024*	*762.0*	*1.68*	*26*	*1100*	*1600*	*20000*	*765.0*	*597.2*	*-*
	Min		*746.0*	*1.29*	*22*			*7200*	*762.0*		
Kariba	Max	1961	489.0	191.0	5627	1800 (1200)	1470	9402	488.6	403.0	10100
	Min		475.5	116.0	5300			8502	484.0	392.0	400
Kariba North bank extension		*2012-2014*				*+430*	*+360*				
Kariba South bank extension		*2014-2016*				*+370*	*+300*				
Cahora Bassa	Max	1974	329.0	63.0	2974	2250 (1600)	2075	15683	331.0	232.0	22000
	Min		295.0	12.2	838			6760	295.0	221.0	500
Cahora Bassa extension		*2013*				*3200*	*2925*	*18700*	*331*		
Mphanda Nkuwa	*Max*	*2024*	*210.0*	*2.5*	*100*	*2450*	*1500*	*33000*	*207.0*	*137.7*	*-*
	Min		*195.0*	*2.0*	*80*			*10000*	*195.0*		
Kholombidzo	*Max*	*2025*	*475.3*	*0.9*	*152*	*372*	*240*	*5000*	*475.3*	*402.2*	*-*
	Min		*471.0*	*0.4*	*92*			*1000*	*471.0*		
Nkula Falls	Max	1966	378.5	7.0	0.4	246	124	5000	378.0	319.9	-
	Min		377.0	4.0	0.3						
Tedzani	Max	1973	320.0	5.0	0.8	276	92	5000	320.0	282.4	-
	Min		315.0	3.0	0.6						
Kapichira	Max	2000	147.0	20.0	2.0	134	64	5000	146.5	92.3	-
	Min		144.6	9.0	1.5						
Kapichira extension		*2010*				*268*	*128*				

7.4.3 Indicators

7.4.3.1 *Flow alteration*

Based on the Range of Variability Approach (RVA) [*Richter et al.*, 1997] and on the indicators derived by Yin *et al.* [2011; 2012], the flows are evaluated in terms of magnitude, timing, duration and volume of annual high flow conditions (Table 7-6). Since the major flow alteration caused by the reservoir operation occurs during the flood period and considering that the e-flows aim to recreate floods, the incorporation of indicators related to low flow and monthly mean flows would mask the impacts of the e-flows. Therefore, the magnitude of high flow is evaluated only on 1, 3, 7 and 30 day maximum flow. To characterize the duration of flood, the mean duration of high pulse each year has been described by the fraction of the year during which the flow lies above a threshold defined by the user. In the present study, it corresponds to the flood discharge given in Table 7-2. Compared to the study of Yin *et al.* [2011; 2012], no indicator related to the frequency of flood or to the rate and frequency of flow condition changes has been incorporated in the analysis as the floods are occurring on an annual basis and the goal of the e-flow is to recreate one flood event per year. To characterize the volume of flood, the cumulated volume of flow above the annual 30-day maximum flow is added to the analysis.

Table 7-6. Indicators of hydrological alteration.

Group	Indicators
Group 1: Magnitudes of annual high flow conditions	Annual 1-day maximum flow (D_{Q1})
	Annual 3-day maximum flow (D_{Q3})
	Annual 7-day maximum flow (D_{Q7})
	Annual 30-day maximum flow (D_{Q30})
Group 2: Timing of annual high flow conditions	Date of annual 1-day maximum flow (D_{dateQ1})
Group 3: Duration of annual high flow conditions	Fraction of the year during which the flow is above the flow threshold (D_{Qthres})
Group 4: Volume of annual flood	Cumulated volume of flow above the annual 30-day maximum flow (D_{volQ30})

The range of variation of each hydrological indicator is derived from the natural hydrological time series and is set as the flow management target. The range of the 75th and 25th percentiles of the natural daily flows has been recommended [*Richter et al.*, 1998]. The deviation of the impacted flow regime from the natural one is measured for each indicator by the degree of alteration (*D*):

$$D = \frac{|N_o - N_e|}{N_e}$$

[7-1]

where N_o is the observed number of years in which the value of the hydrological indicator falls within the RVA target range (75th and 25th percentiles); and N_e is the expected number of years in which the indicator value falls within the RVA target range (75th and 25th percentiles).

The overall impact (D_{mean}) is expressed as follows:

$$D_{mean} = \frac{1}{M} \sum_{i=1}^{H} D_i \qquad \text{[7-2]}$$

where M is the number of hydrological indicators.

The degree of alteration to flow regime can be separated into three classes [*Richter et al.*, 1997; *Richter et al.*, 1998]: low (values of D between 0 and 33%), moderate (values of D between 33 and 67%), and high (values of D between 67 and 100%).

The flow alteration is also evaluated in terms of annual distribution of the discharge by the monthly Pardé coefficients defined as the mean monthly discharge over the mean annual discharge [*Matos et al.*, 2010; *Meile et al.*, 2011] [7-3].

$$PC_{m,a} = \frac{Q_{mean\ month\ m,a}}{Q_{mean\ annual\ a}} \qquad \text{[7-3]}$$

where $1 \leq m \leq 12$ indicates the month, and a indicates the year.

When the Pardé coefficient is close to one, it means that the flow during the month is close to the mean annual flow. When the coefficient is higher than one, it indicates that the month receives more flow than the mean annual flow and when the coefficient is lower than one the month receives less water than the mean annual flow.

7.4.3.2 *Energy production*

The energy generated by the hydropower plants is evaluated by two indicators: the firm power and the total annual energy. More precisely, the firm power is defined as the power exploited 90% of the year (346 day a year) in MW and the annual energy is the total energy generated during the year in GWh. The spilled volume is included in the analysis as a complementary index to evaluate the quantity of water "lost" by the reservoir.

To compare the different scenarios to the base scenario, the difference of annual energy, firm power and spilled volume are calculated as well as the ratio between the variation of the results (D_{var}) characterized by the gap between the 25th and 75th quartiles of these indicators [7-4].

$$D_{var,i} = \frac{(q_{75,i} - q_{25,i})}{(q_{75,bs} - q_{25,bs})} \qquad \text{[7-4]}$$

where *i* is the scenario under comparison, *bs* is the base scenario, q_{75} and q_{25} the 75th and 25th quartiles.

7.5   ANALYSIS OF SIMULATION RESULTS

At the end of the calibration procedure, five sets of parameters values have been considered as equally appropriate for the model simulation (see Chapter 5.4.5). The scenarios have therefore been simulated with the different parameter values and the influence on the total annual power as well as on the hydrological alteration was assessed. In terms of hydrological alteration, the variability associated with the different parameter sets is between 2 and 7% and in terms of energy production between 1 and 5%. Thus, the difference between the scenarios is considered as significant only if it exceeds 5%.

7.5.1   Present state

7.5.1.1   Hydropower production

Based on the study of the registered outflow at the dams, the following exploitation percentage could be determined: at Kariba dam the turbines are used at about 65% of their maximum capacity, at Cahora Bassa dam and at Kafue Gorge Upper dam the turbines are used at about 70% of their maximum capacity. Regarding operation rules, at Kariba and Cahora Bassa, the volume is lowered below the target volume to continue turbining (Figure 7-3, b; Figure 7-4, b). At Itezhi Tezhi and Kafue Gorge Upper, the rule curve is followed more strictly as the volume in the reservoir is kept higher (Figure 7-1, b; Figure 7-2, b).

Itezhi Tezhi dam was designed to route outflow for the Kafue Gorge dam located below. Consequently, it releases a constant flow of about 150 m³/s over the year and uses its storage capacity to transfer a part of the flood volume to the dry season. The actual environmental constraint at Itezhi Tezhi is a minimum flow of 25 m³/s and 300 m³/s in March which was implemented in the model. From the observed outflow, it is clear that the constraint is not fulfilled every year (Figure 7-1, a).
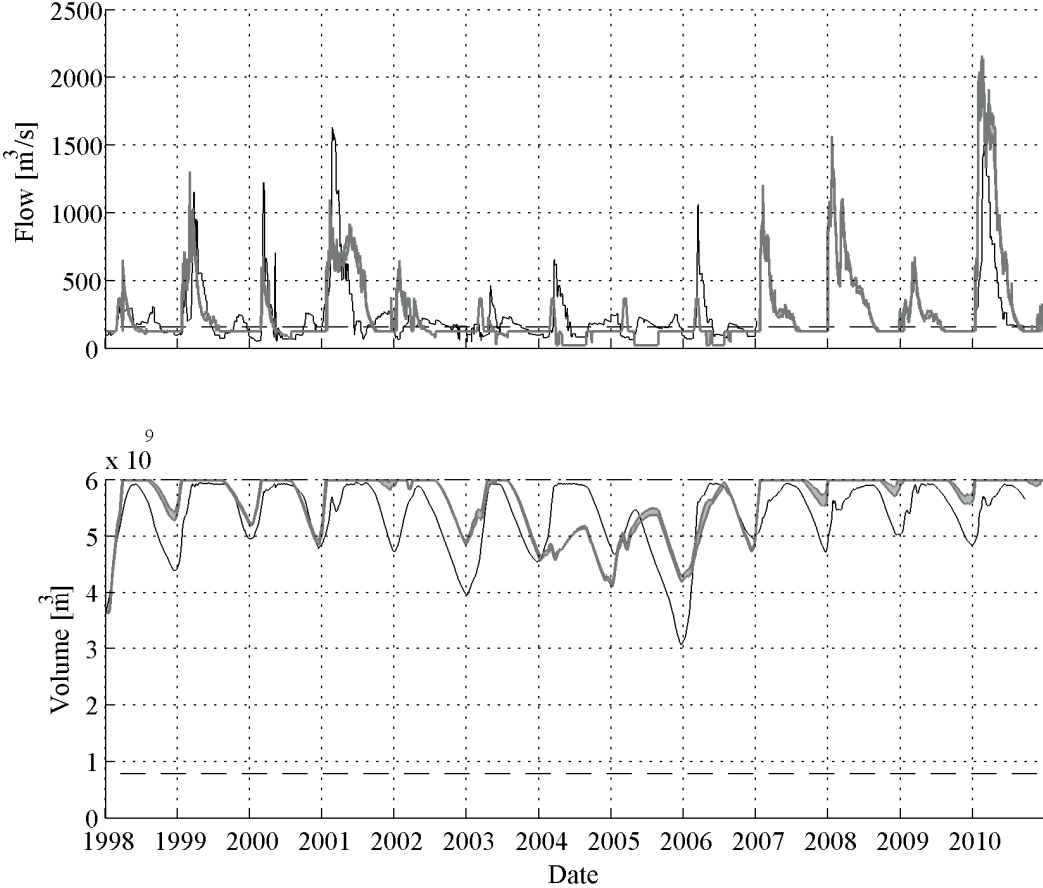
Figure 7-1. Observed (black line) and simulated (grey area) outflow (a) and volume (b) at Itezhi Tezhi reservoir for the present state scenario with the maximum turbine capacity and the minimum and maximum operation volumes (dashed lines).

Since Kafue Gorge has a small reservoir compared to the other hydropower schemes, the outflow and volume fluctuations are more intense (Figure 7-2). Compared to the observed data, the model is more reactive but still able to reproduce the main trend observed. A mean discharge of about 170 m³/s has been adopted for the simulation (turbine maximum capacity of 252 m³/s) (Figure 7-2, a).

168
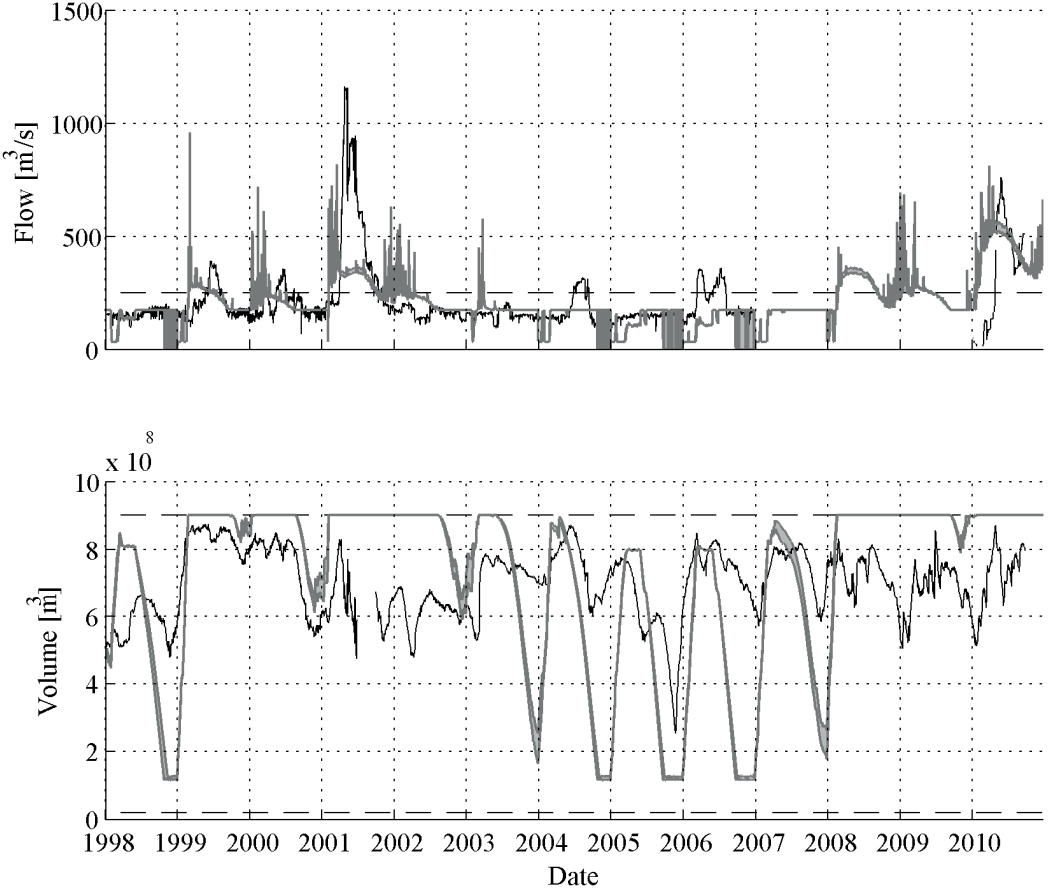
Figure 7-2. Observed (black line) and simulated (grey area) outflow (a) and volume (b) at Kafue Gorge (upper) reservoir for the present state scenario with the maximum turbine capacity and the minimum and maximum operation volumes (dashed lines).

Kariba turbines were upgraded from 1200 MW to 1470 MW recently. Therefore, the observed base discharge increases during the analyzed period (Figure 7-3, a). For the simulation, a mean outflow of 1200 m³/s was set according to the registered outflow during 2004 to 2007 which allows the model to follow the observed fluctuation in volume. It overestimates the outflow observed from 1998 to 2004 avoiding nearly entirely the spillway releases from 2000 to 2002. The maximum turbine capacity is actually 1800 m³/s. In terms of reservoir volume, the dam is operated below the flood rule curve and the volume is reduced before the flooding season (minimum in January) (Figure 7-3, b).
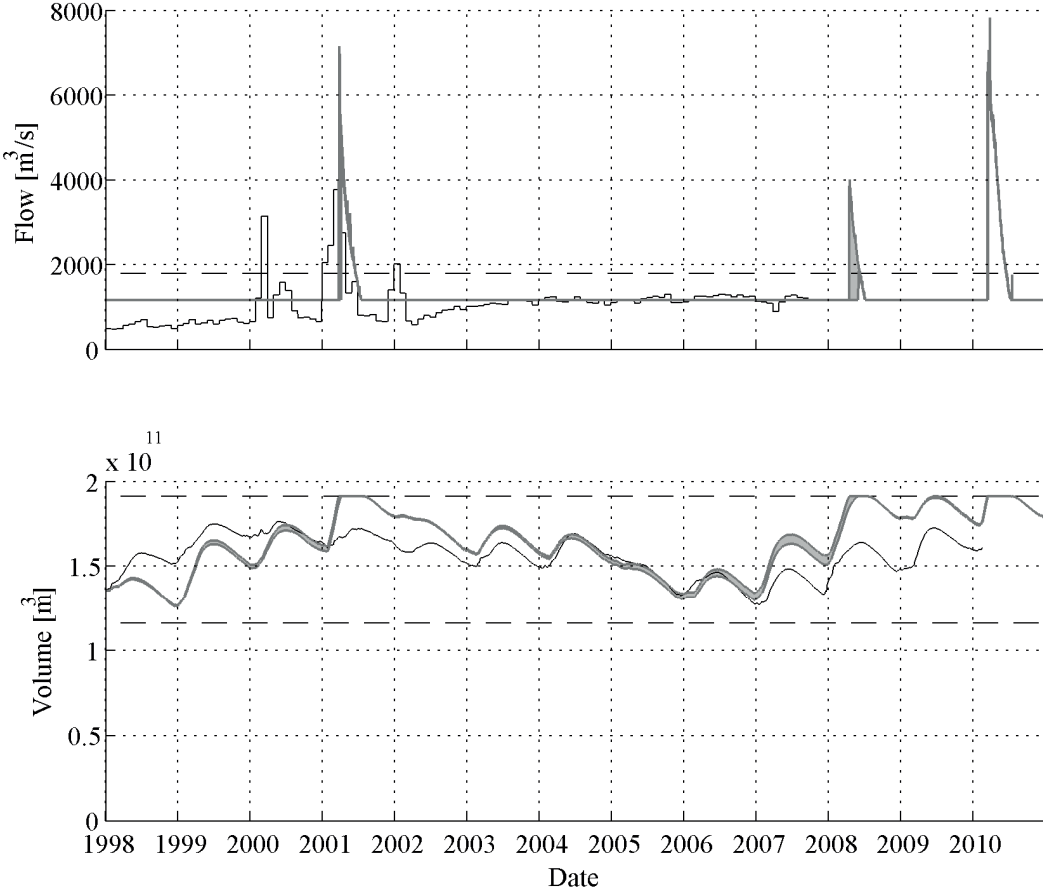
Figure 7-3. Observed (black line) and simulated (grey area) outflow (a) and volume (b) at Kariba reservoir for the present state scenario with the maximum turbine capacity and the minimum and maximum operation volumes (dashed lines).

At Cahora Bassa, the average discharge at the turbines is about 1,600 m^3/s whereas the full turbine capacity would reach 2,250 m^3/s (Figure 7-4, a). The year 2001 was characterized by an extreme high volume in the reservoir and the opening of all spillways in emergency (Figure 7-4, b). During the following years, the volume has been preventively reduced. Maximising the water level in the model leads to more spillage than observed but it is considered as a realistic operation of the hydropower plant.
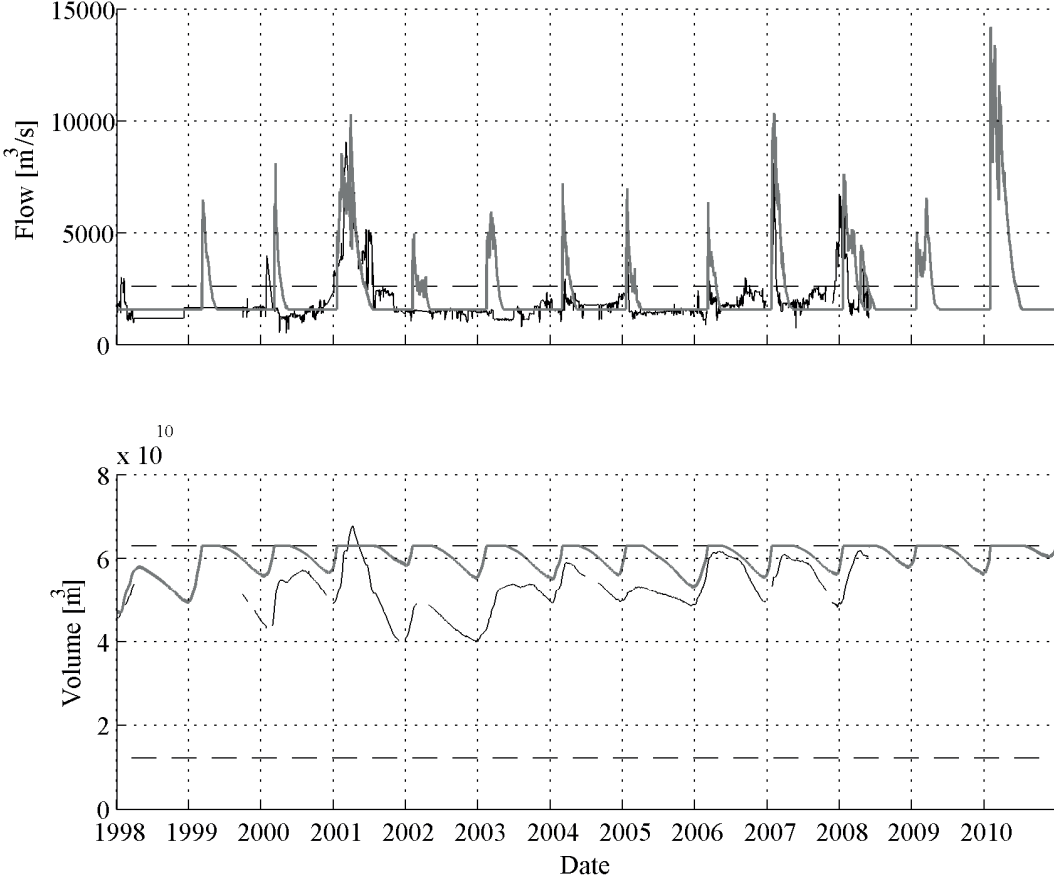
Figure 7-4. Observed (black line) and simulated (grey area) outflow (a) and volume (b) at Cahora Bassa reservoir for the present state scenario with the maximum turbine capacity and the minimum and maximum operation volumes (dashed lines).

In terms of energy production (Table 7-7), about 30,000 GWh/year are generated on the basin with a firm power of about 2,200 MW which is similar to the results obtained by previous studies [*The World Bank*, 2010; *Tilmant et al.*, 2010a]. The hydropower plant with the highest production is Cahora Bassa, followed by Kariba and Kafue Gorge Upper. The run-of-river plants located on the Shire River generate only a limited amount of energy compared to the others.

Chapter 7 Analysis of hydropower development scenarios in view of sustainable and ecological catchment development

Table 7-7. Energy production for the present state scenario.

Hydropower plant	Mean annual energy [GWh]	25th quartile [GWh]	75th quartile [GWh]	Mean firm power [MW]	25th quartile [MW]	75th quartile [MW]	Mean annual spilled volume [10^9m^3]	25th quartile [10^9m^3]	75th quartile [10^9m^3]
Kafue Upper	4'930	4'586	5'474	372	125	625	1.71	0.00	2.39
Kariba	8'309	8'128	8'546	923	894	943	3.93	0.00	1.97
Cahora Bassa	12'928	12'923	12'972	1'449	1'442	1'458	20.61	9.26	28.37
Nkula Falls	893	892	893	102	102	102	15.96	15.10	16.10
Tedzani	644	644	645	73	73	73	15.36	14.44	15.41
Kapichira	484	571	572	55	65	65	15.51	16.49	18.20
Total	**28'188**	27'744	29'101	**2'975**	2'701	3'265	**73.08**	55.29	82.45

The influence of the turbine capacity use is assessed by simulating the hydropower plants working at 60%, 70% and 80% of their maximum capacity (Table 7-8). Operating all dams at 60% reduces the hydropower production without reducing the hydrological alteration. Operating all dams at 70 % of their maximum capacity modifies only the Kariba outflows compared to the present state. The influence on the hydropower production is negligible and it lowers the hydrological alteration of flows in the delta as more flows are released from Cahora Bassa. The total energy generated over the basin is increased if the dams are operated at 80% but not the firm energy compared to the present state. In terms of hydrological alteration, the situation is kept similar.

Table 7-8. Influence of the percentage of maximum turbine capacity used by the hydropower plants.

% use of the maximum capacity	Total mean annual energy [GWh]	Total mean firm power [MW]	Total mean annual spilled volume [10^9m^3]	Mean hydrological alteration D_{tot} [-]
Present state	28'188	2'975	73.08	0.51
60%	(-11%) 24'949	(-10%) 2'674	(+18%) 86.52	(+5%) 0.54
70%	(+1%) 28'528	(+1%) 3'011	(-1%) 72.00	(-13%) 0.44
80%	(+10%) 31'132	(+1%) 3'010	(-14%) 63.15	(+4%) 0.53

To evaluate the influence of the rule curve on the energy production, Kariba and Cahora Bassa dams are simulated with the hydropower model following strictly the rule curve. The results (Table 7-9) show that the strict application of the rules would decrease the energy production and increase the spillage. This is the outcome of a target volume too high compared to the incoming flows which forces the operators to reduce the turbine flow in order to keep the volume in the reservoir high and to release the flood through the evacuators as not enough storage capacity is available at the beginning of the flooding season. In terms of hydrological alteration, the flow downstream Kariba (at Mana Pools) is closer to the natural discharge since the floods are released by the spillways.

Table 7-9. Energy production at Kariba and Cahora Bassa under the operation rules following the target volume for both high and low volumes.

	Mean annual energy [GWh]	Mean firm power [MW]	Mean annual spilled volume [10^9m^3]	Mean hydrological alteration D_{tot} [-]
Kariba	(-14%) 7'126	(-48%) 482	(+158%) 10.15	(-20%) 0.58
Cahora Bassa	(-8%) 11'883	(-22%) 1'123	(+20%) 24.74	(+5%) 0.46

For the scenario comparison, it is assumed, based on the previous analysis that the turbines are used on average at 70% of their maximum capacity at all existing and planned hydropower plants. The detailed results for the base scenario are presented in Table 7-10. The resulting outflows and volume variations at Kariba and Cahora Bassa are presented respectively in Figure 7-5 and in Figure 7-6.

Table 7-10. Energy production for the base scenario (all dams operated at 70% of their maximum capacity).

| Hydropower plant	Mean annual energy [GWh]	25th quartile [GWh]	75th quartile [GWh]	Mean firm power [MW]	25th quartile [MW]	75th quartile [MW]	Mean annual spilled volume [10^9m^3]	25th quartile [10^9m^3]	75th quartile [10^9m^3]
Kafue Upper	4'930	4'586	5'474	372	125	625	1.71	0.00	2.39
Kariba	8'806	8'530	9'043	974	937	1'004	1.19	0.00	1.19
Cahora Bassa	12'964	12'962	12'997	1'456	1'453	1'467	20.62	11.94	26.74
Nkula Falls	781	781	781	89	89	89	16.23	15.88	16.88
Tedzani	564	563	564	64	64	64	15.51	15.31	16.28
Kapichira	484	571	572	55	65	65	72.00	16.49	18.20
Total	28'528	27'994	29'432	3'011	2'733	3'313	72.00	59.61	81.68
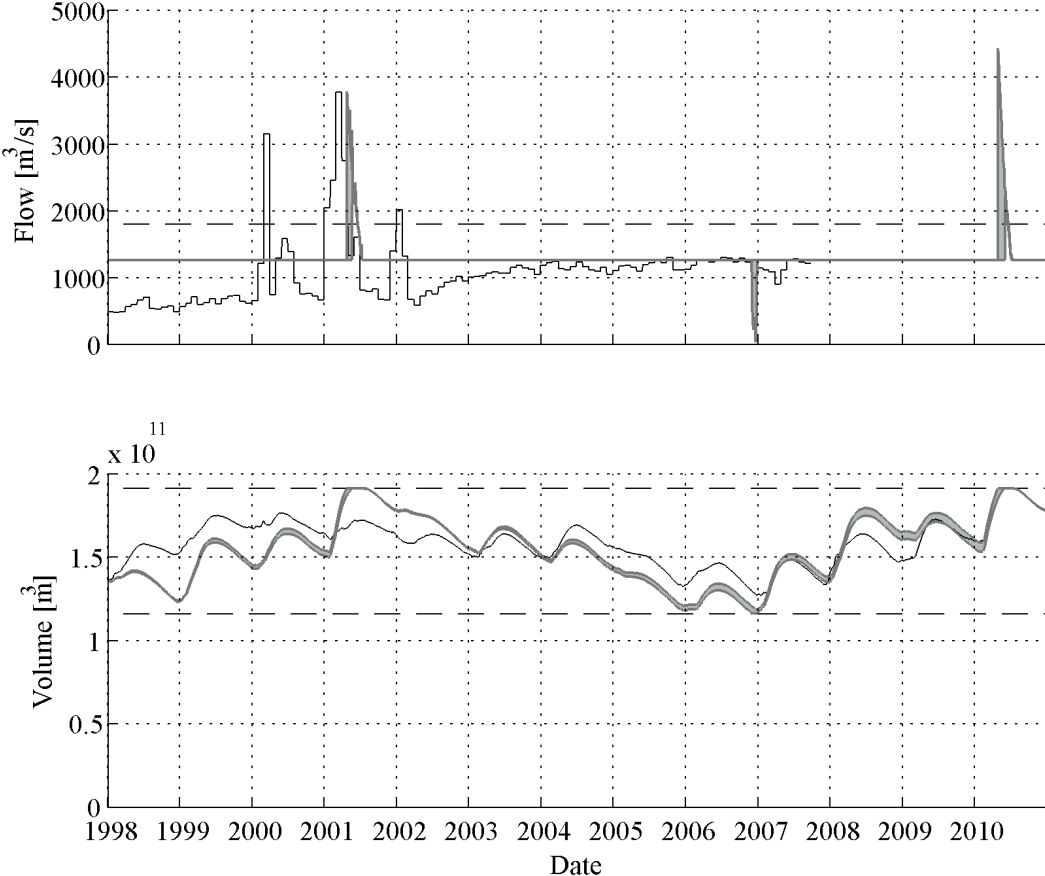
Figure 7-5. Observed (black line) and simulated (grey area) outflow (a) and volume (b) at Kariba reservoir for the base scenario (70% of maximum turbine capacity used) with the maximum turbine capacity and the minimum and maximum operation volumes (dashed lines).
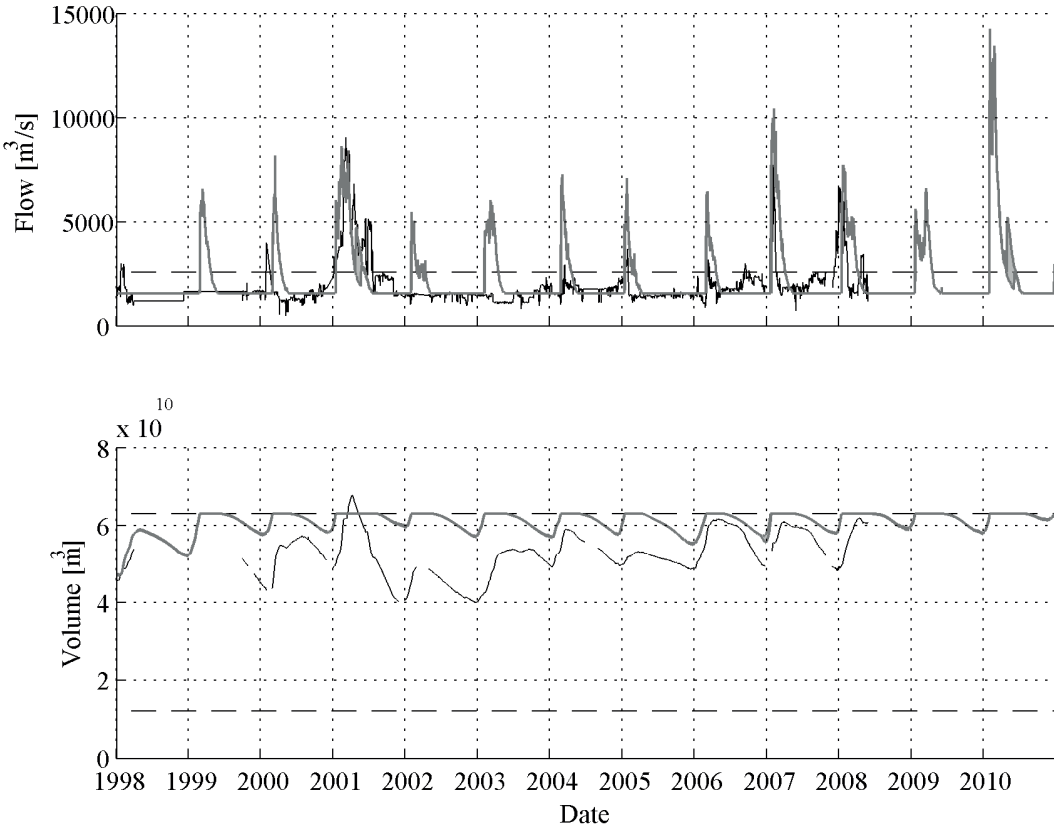
Figure 7-6. Observed (black line) and simulated (grey area) outflow (a) and volume (b) at Cahora Bassa reservoir for the base scenario (70% of the maximum turbine capacity used) with the maximum turbine capacity and the minimum and maximum operation volumes (dashed lines).

7.5.1.2 *Hydrological alteration*

Kariba is the hydropower plant affecting the most the discharge of the Zambezi since its reservoir has the highest storage capacity and transfers the flood volume to the dry season. The result in terms of Pardé coefficient shows a flattening of the curve with a nearly constant monthly discharge over the entire year (Figure 7-7). At Itezhi Tezhi dam, the influence of the flow change is especially noticeable during the dry months when the mean monthly discharge stays close to the mean annual discharge (Figure 7-7).. At Cahora Bassa, the flood volume is not entirely transferred to the dry season but the low discharges are much higher than the natural state (Figure 7-7). This includes also the influence of the upstream Kariba dam.

175
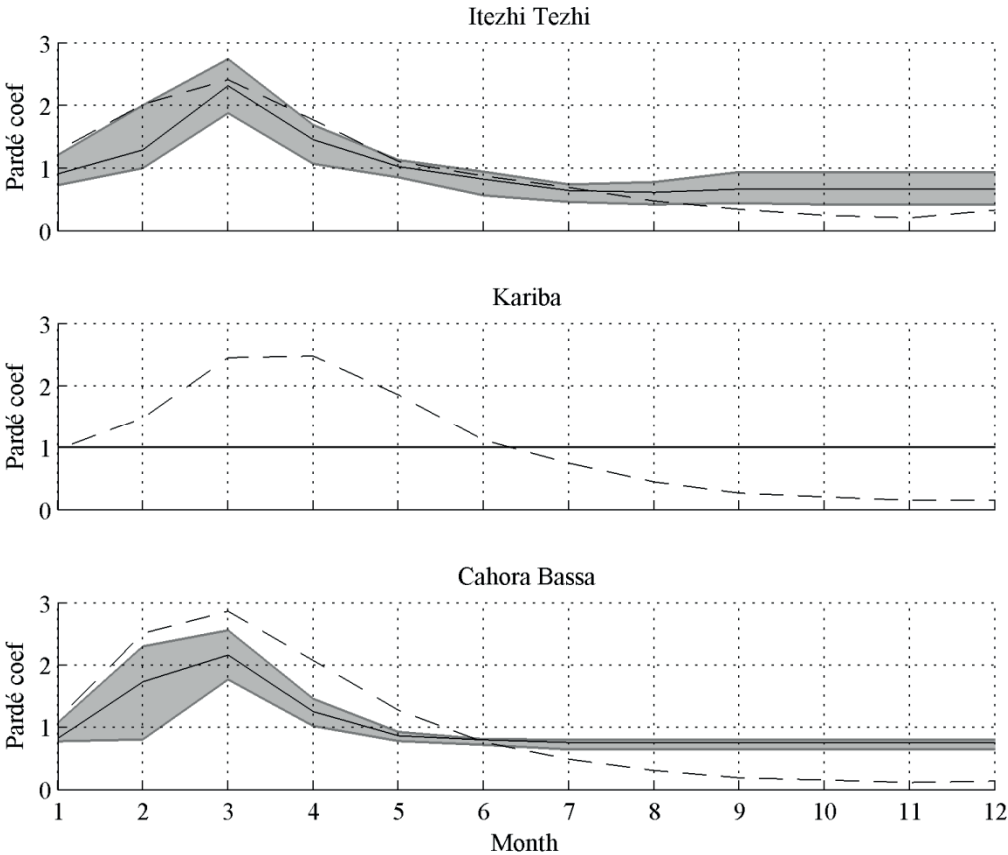
Figure 7-7. Pardé coefficients at Itezhi Tezhi, Kariba and Cahora Bassa dams for the base scenario (dashed line: natural state, grey area: 25th and 75th quartile of model simulations, black line: median of model simulations).

The duration curves at the key points (Figure 7-8) result in the same observations than for the Pardé coefficient. The flow alteration is significant at the Mana Pools (downstream Kariba dam) and less considerable in the Kafue flats (downstream Itezhi Tezhi). In the Zambezi delta, the high flows are reduced by the combined influence of Kariba and Cahora Bassa dams and the base flow is substantially increased.
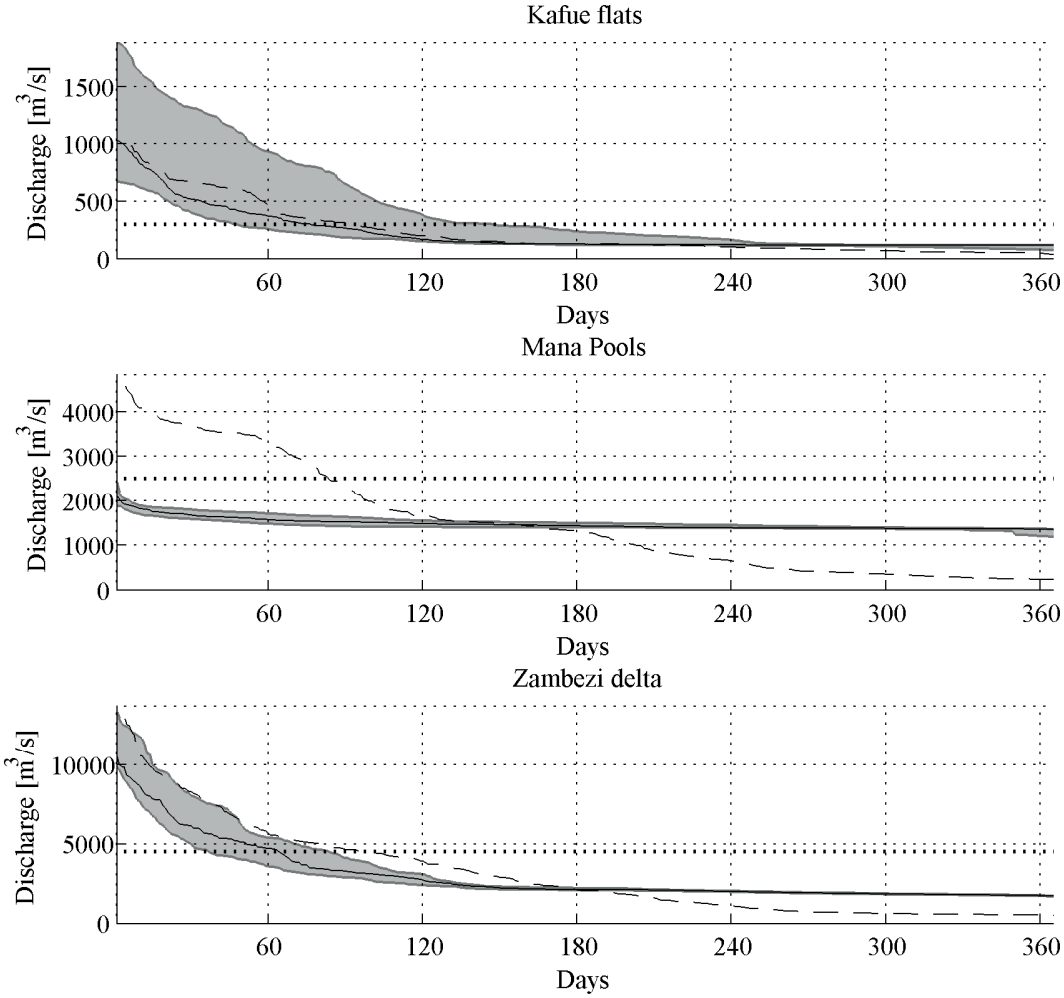
Figure 7-8. Duration curves at the key points for the base scenario (dashed line: natural state, grey area: 25th and 75th quartile of model simulations, black line: median of model simulations, tilled line: flow threshold).

The indicators derived from the Range of Variability (RVA) approach confirm the results characterizing the effect of the dams as low on the Kafue flats (between 0 and 0.33), high on the Mana Pools (between 0.67 and 1) and low on the Zambezi delta (between 0 and 0.33) (Table 7-11).

Table 7-11. Indicators of hydrological alteration for the base scenario (D_{Q1}: annual 1-day max flow, D_{Q3}: annual 3-days max flow, D_{Q7}: annual 7-days max flow, D_{Q30}: annual 30-days max flow, D_{Qthres}: fraction of year during which flow is above threshold, D_{date}: date of 1-day max flow, D_{vol}: volume of flow above 30-days max flow).

	D_{Q1}	D_{Q3}	D_{Q7}	D_{Q30}	D_{Qthres}	D_{dateQ1}	D_{volQ30}	D_{mean}
Kafue flats	0.29	0.29	0.43	0.43	0.29	0.00	0.43	0.31
Mana Pools	0.71	0.71	0.71	1.00	1.00	0.71	0.71	0.80
Zambezi delta	0.29	0.33	0.29	0.14	0.14	0.14	0.29	0.23

7.5.2   Present state with e-flows

7.5.2.1   *Hydropower*

The influence of e-flow release (see Chapter 7.4.1) on energy production is presented in Table 7-12 and in Figure 7-9. The introduction of an e-flood at Itezhi Tezhi does not influence significantly the energy production at Kafue Gorge Upper except in terms of firm power, which is reduced by 10% for all the simulated levels of e-flows. At Kariba, the medium and the high e-flows cause a reduction of 13% to 15% to the firm power and a large increase of spilled volume (70% to 180%). The variability of annual energy and firm power generated over the 13 years decreases while the variability of spilled volume increases 2 to 5 times. At Cahora Bassa, the loss in firm power is significant for the high e-flow scenario (12%) combined with a large increase of variability in energy production.

Globally, releasing low to medium e-floods would not significantly affect the energy production over the basin. Compared to the previous studies which quantify the decrease in energy production of about 6% if e-flows are released at Itezhi Tezhi and Kariba [*Gandolfi et al.*, 1997] and of 6 to 10% if e-flows are released at Cahora Bassa [*Beilfuss*, 2010; *Tilmant et al.*, 2010a], the values obtained in the present study are slightly lower. This is due to a finer implementation of the e-flows regarding the operation rules which allow the hydropower plants to keep a higher production, and to the daily time step of the simulations.

Table 7-12. Energy production for the base scenario with three e-flows levels.

Hydropower plant	Mean annual energy [GWh]		D_{var}	Mean firm power [MW]		D_{var}	Mean annual spilled volume [10^9m^3]		D_{var}
Low e-flows (see Chapter 7.4.1)									
Kafue Upper	4'927	0%	0.95	335	-10%	1.00	1.71	0%	0.98
Kariba	8'806	0%	1.00	974	0%	1.00	1.19	0%	1.00
Cahora Bassa	12'439	-4%	1.48	1'391	-4%	1.82	20.38	-1%	1.08
Total	28'002	-2%	-	2'909	-3%	-	71.75	0%	-
Medium e-flows (see Chapter 7.4.1)									
Kafue Upper	4'919	0%	1.01	333	-11%	1.00	1.70	0%	0.95
Kariba	8'615	-2%	0.90	849	-13%	0.74	2.02	70%	2.64
Cahora Bassa	12'265	-5%	15.08	1'353	-7%	6.84	20.68	0%	0.76
Total	27'628	-3%	-	2'745	-9%	-	72.88	1%	-
High e-flows (see Chapter 7.4.1)									
Kafue Upper	4'911	0%	1.01	333	-11%	1.00	1.70	-1%	0.93
Kariba	8'402	-5%	0.71	832	-15%	0.53	3.37	183%	5.33
Cahora Bassa	11'910	-8%	22.46	1'287	-12%	7.22	21.49	4%	0.02
Total	27'600	-5%	-	2'764	-12%	-	75.01	4%	-
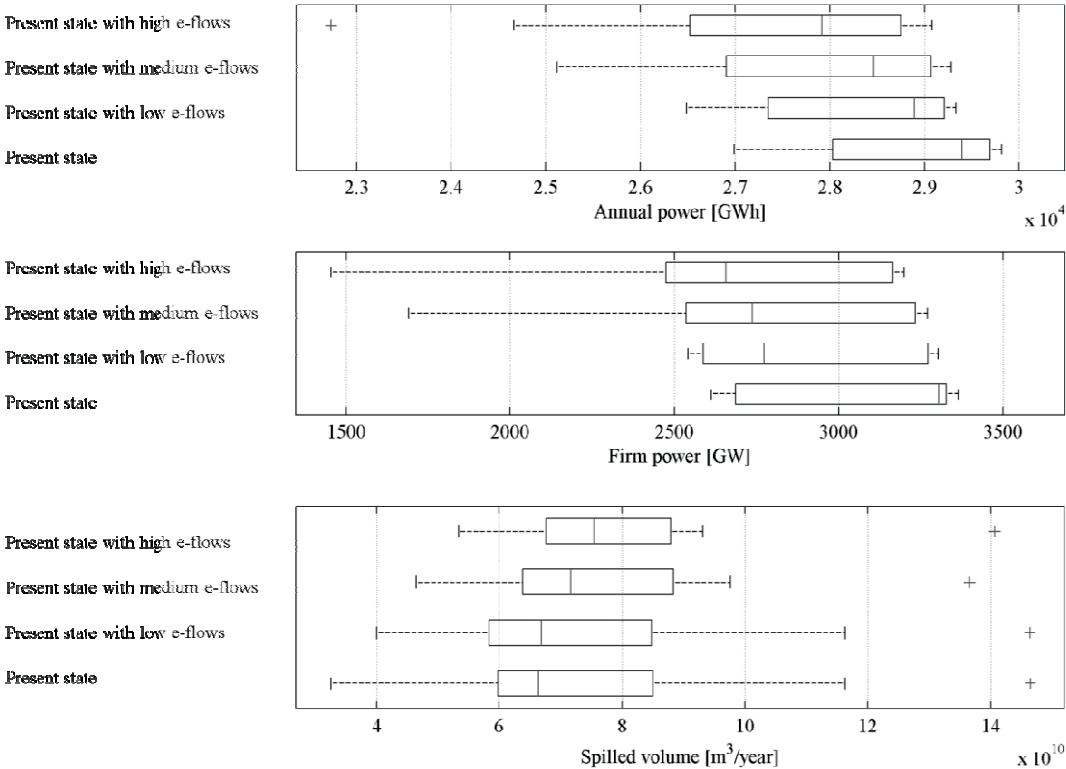
Figure 7-9. Total annual power, firm power and spilled volume distribution for the present state scenario with three e-flows levels.

7.5.2.2 *Hydrological alteration*

The effects of e-flows on the hydrological alteration are presented in the Table 7-13. The e-flows are defined as a trapezoidal shape flood which has to be released through the turbine and the spillways at a specified date as long as the volume in the reservoir remains higher than 30% of the active storage (see Chapter 7.4.1). In a global perspective, the influence is positive on the Kafue flats and the Mana Pools, especially in terms of flow magnitude. The dam impact decreases as the e-flow constraint increases. At Cahora Bassa more floods are released through the spillways in the base scenario compared to the observed data since the dam is operated at a higher level. The resulting effect on the Zambezi delta is quite low (hydrological alteration of 0.23). The defined e-flows have therefore a negative influence on the hydrological alteration since the dam is forced to release the same amount of water every year at the same date resulting in a decrease of flow variation compared to the base scenario.

Table 7-13. Indicators of hydrological alteration for the base scenario with e-flows release (D_{Q1}: annual 1-day max flow, D_{Q3}: annual 3-days max flow, D_{Q7}: annual 7-days max flow, D_{Q30}: annual 30-days max flow, D_{Qthres}: fraction of year during which flow is above threshold, D_{date}: date of 1-day max flow, D_{vol}: volume of flow above 30-days max flow). In yellow, no influence; in green, reduction of the alteration.

	D_{Q1}		D_{Q3}		D_{Q7}		D_{Q30}		D_{Qthres}		D_{date}	D_{vol}	D_{mean}	
Low e-flows (see Chapter 7.4.1)														
Kafue flats	0.29	0%	0.29	0%	0.43	0%	0.14	-67%	0.14	-50%	0.14	0.29	0.24	-20%
Mana Pools	0.71	0%	0.71	0%	0.71	0%	1.00	0%	1.00	0%	0.71	0.71	0.80	0%
Zambezi delta	0.43	50%	0.33	0%	0.43	50%	0.14	0%	0.43	200%	0.14	0.57	0.35	53%
Medium e-flows (see Chapter 7.4.1)														
Kafue flats	0.14	-50%	0.14	-50%	0.29	-33%	0.14	-67%	0.43	50%	0.14	0.29	0.22	-27%
Mana Pools	0.57	-20%	0.71	0%	0.71	0%	1.00	0%	1.00	0%	0.86	1.00	0.84	5%
Zambezi delta	0.14	-50%	0.00	-100%	0.57	100%	0.29	100%	0.57	300%	0.71	0.71	0.43	85%
High e-flows (see Chapter 7.4.1)														
Kafue flats	0.00	-100%	0.00	-100%	0.14	-67%	0.43	0%	0.29	0%	0.00	0.00	0.12	-60%
Mana Pools	0.71	0%	0.57	-20%	0.43	-40%	0.57	-43%	1.00	0%	0.43	0.43	0.59	-26%
Zambezi delta	0.43	50%	0.00	-100%	1.00	250%	0.57	300%	0.86	500%	0.86	0.43	0.59	156%

The Pardé coefficients at Itezhi Tezhi, Kariba and Cahora Bassa are presented in Figure 7-10, Figure 7-12 and Figure 7-14 for the low, medium and high e-flows (see chapter 7.4.1). At Itezhi Tezhi, releasing a flood of 300 m³/s over two month (low e-flow) reproduces nearly the same volume distribution over the year as the natural state. Increasing the artificial flood above 300 m³/s results in a higher seasonal transfer from the low flow season to the high flow season than in the natural state. At Kariba, e-flows reintroduce a variation in the Pardé coefficient proportional to the size of the flood but still much lower than in the natural state. The effect of the e-flows at Cahora Bassa is clearly visible as the Pardé coefficient is high in February only and the area between the 25th and the 75th percentile is quite narrow.

Regarding the duration curves (Figure 7-11, Figure 7-13 and Figure 7-15), at Itezhi Tezhi, the effect of the e-flows are not substantial. At Mana Pools, the artificial flood is visible on the curve resulting to an increase of the high discharges close to the natural state. The variation between the years is quite big. In the Zambezi delta, the implementation of a medium or high e-flood increases the high discharges higher than the natural state with a low variation, confirming the negative influence of a constant flood compared to operating the dam at a high level and releasing the extra volume when needed.
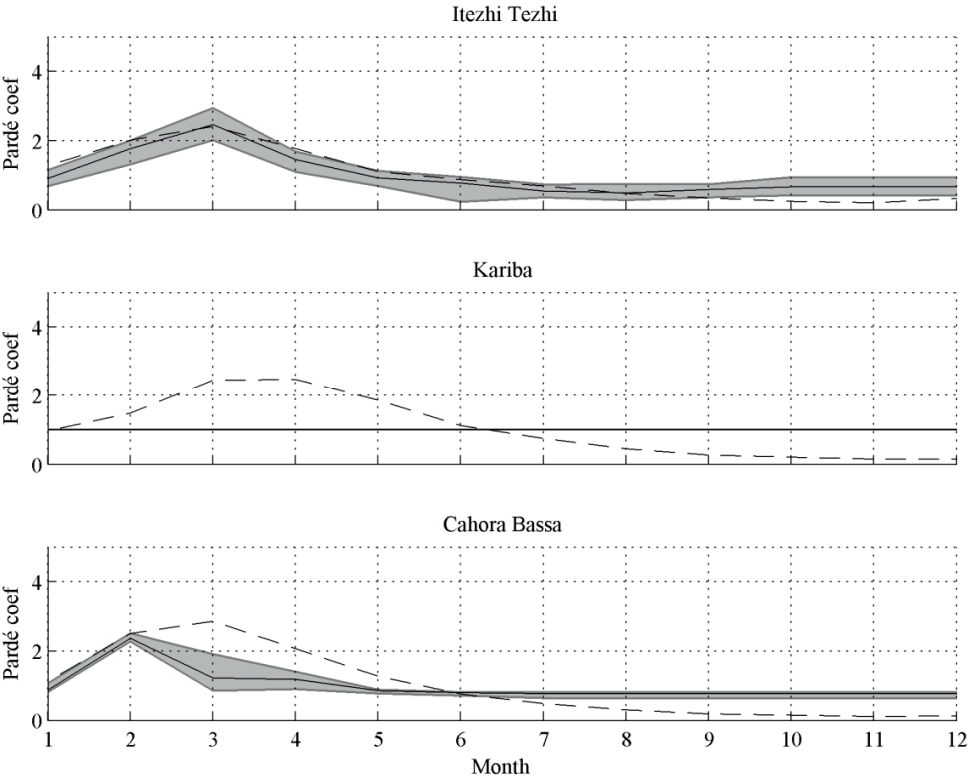
Figure 7-10. Pardé coefficients at Itezhi Tezhi, Kariba and Cahora Bassa dams for the low e-flow (300 m³/s from Itezhi Tezhi in February and March, 4'500 m³/s from Cahora Bassa in February) base scenario (dashed line: natural state, grey area: 25th and 75th quartile of model simulations, black line: median of model simulations).
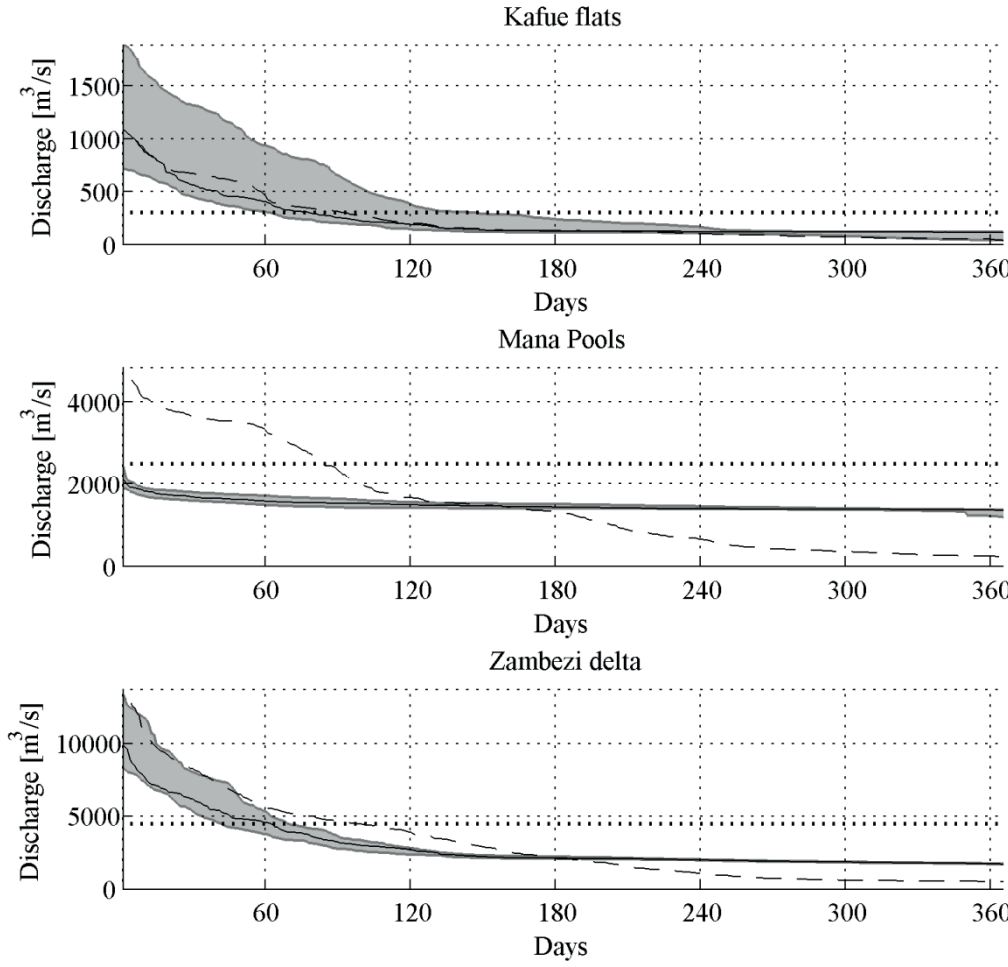
Figure 7-11. Duration curves at the key points for the low e-flow (300 m³/s from Itezhi Tezhi in February and March, 4'500 m³/s from Cahora Bassa in February) base scenario (dashed line: natural state, grey area: 25th and 75th quartile of model simulations, black line: median of model simulations, tilled line: flow threshold).
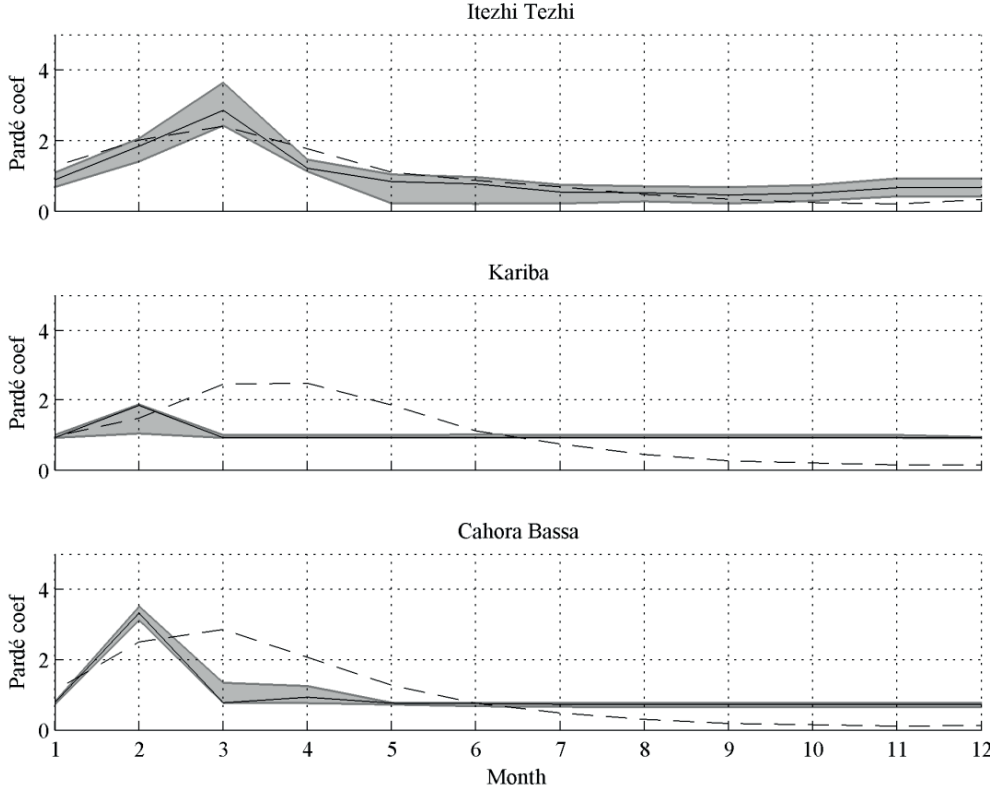
Figure 7-12. Pardé coefficients at Itezhi Tezhi, Kariba and Cahora Bassa dams for the medium e-flow (400 m^3/s from Itezhi Tezhi in February and March, 2'500 m^3/s from Kariba in February, 7'000 m^3/s from Cahora Bassa in February) base scenario (dashed line: natural state, grey area: 25th and 75th quartile of model simulations, black line: median of model simulations).
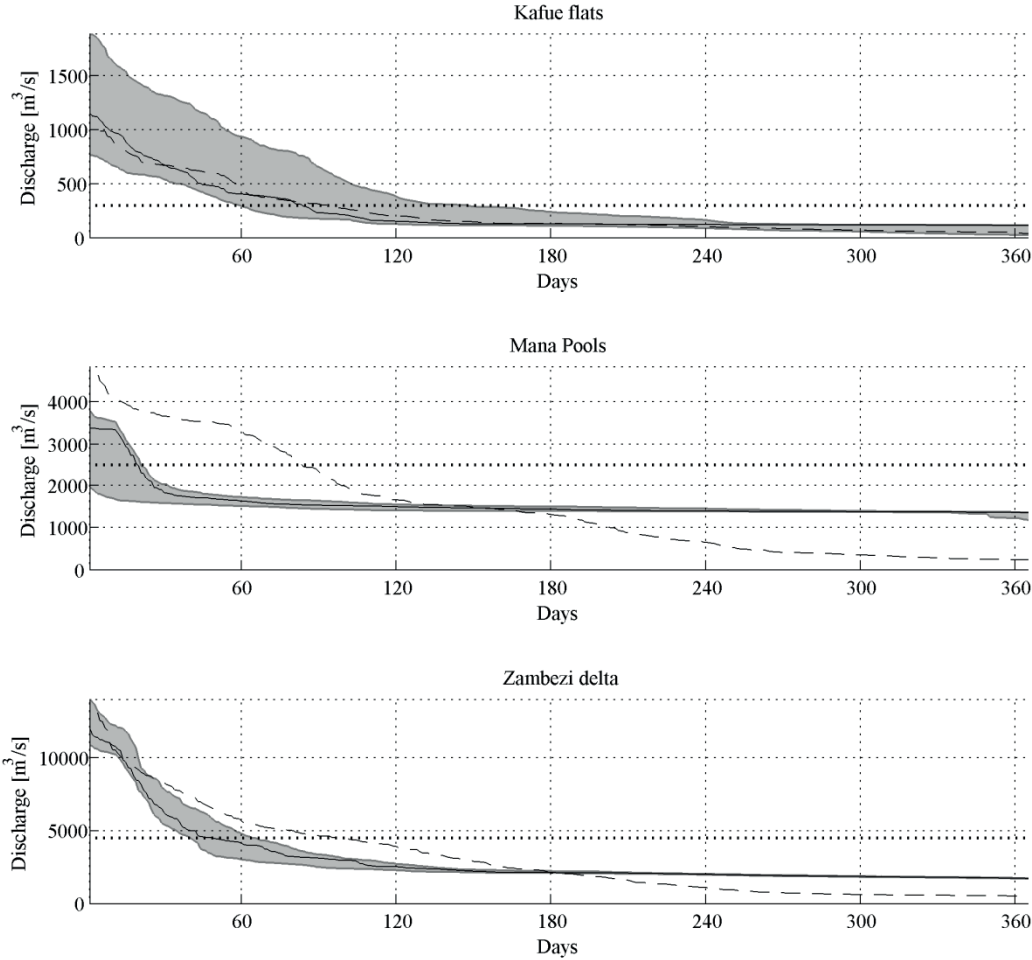
Figure 7-13. Duration curves at the key points for the medium e-flow (400 m^3/s from Itezhi Tezhi in February and March, 2'500 m^3/s from Kariba in February, 7'000 m^3/s from Cahora Bassa in February) base scenario (dashed line: natural state, grey area: 25th and 75th quartile of model simulations, black line: median of model simulations, tilled line: flow threshold).
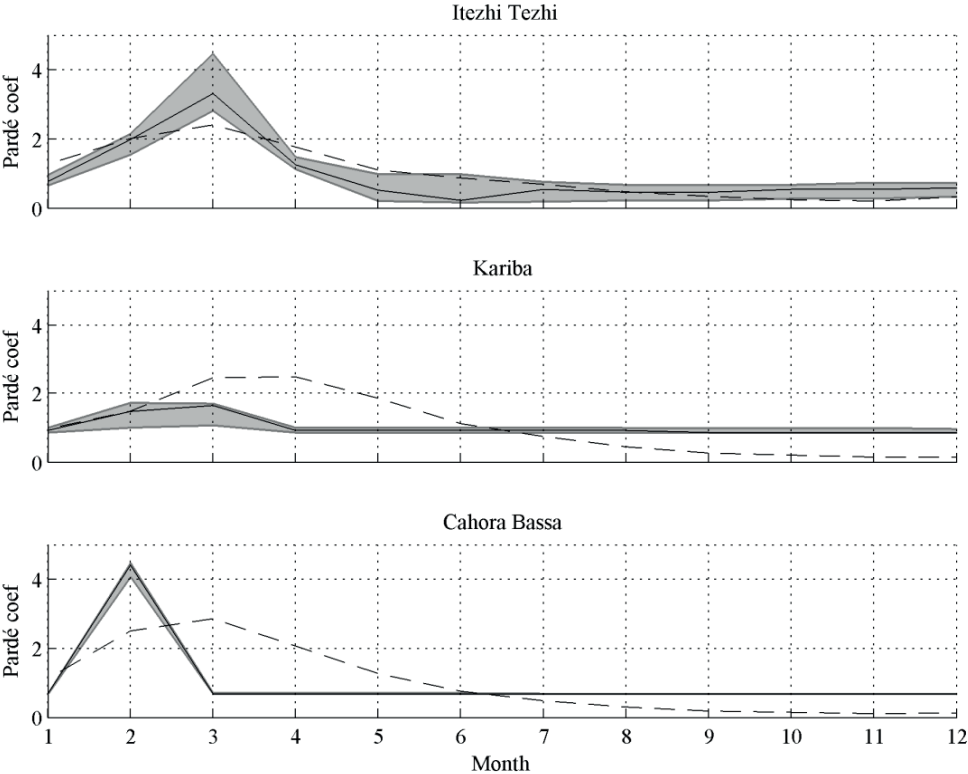
Figure 7-14. Pardé coefficients at Itezhi Tezhi, Kariba and Cahora Bassa dams for the high e-flow (500 m^3/s from Itezhi Tezhi in February and March, 2'500 m^3/s from Kariba in February and March, 10'000 m^3/s from Cahora Bassa in February) base scenario (dashed line: natural state, grey area: 25th and 75th quartile of model simulations, black line: median of model simulations).

Figure 7-15. Duration curves at the key points for the high e-flow (500 m³/s from Itezhi Tezhi in February and March, 2'500 m³/s from Kariba in February and March, 10'000 m³/s from Cahora Bassa in February) base scenario (dashed line: natural state, grey area: 25th and 75th quartile of model simulations, black line: median of model simulations, tilled line: flow threshold).

7.5.3 Influence of the extension of existing hydropower plants and new dams

7.5.3.1 *Hydropower production*

Regarding energy production, the extension of the existing hydropower plants by increasing installed capacity is above all highly profitable to Cahora Bassa (Table 7-14). It increases both the mean annual energy produced and the firm power, reducing the spilled volume by nearly 70%. At Kariba, the new turbines avoid completely the spillage but reduce the firm power by nearly 60% without increasing substantially the mean annual energy production. The capacity extension amplifies the variability in firm power and mean annual energy both at Kariba and Cahora Bassa. The introduction of a high turbine capacity and new operation rules at Itezhi Tezhi decreases slightly the firm power at Kafue Upper.

The increase of capacity is mainly foreseen for supplying peak energy. The full capacity would be used only few hours a day and should therefore not influence the mean annual energy. This would introduce the problematic of hydropeaking in the basin and cause more hydrological alteration than the present state.

Table 7-14. Energy production for the scenario considering the existing hydropower plants extensions (see Chapter 7.4.2) compared to the base scenario (all the dams operated at 70% of their maximum capacity).

Hydropower plant	Mean annual energy [GWh]	D_{var}	Mean firm power [MW]	D_{var}	Mean annual spilled volume [10^9m^3]	D_{var}
Itezhi Tezhi	572	-	46	-	2.41	-
Kafue Upper	4'950	1.00	339 (-9%)	1.01	1.67 (-3%)	0.95
Kariba	9'343 (+6%)	8.70	395 (-59%)	12.09	0.00 (-100%)	0.00
Cahora Bassa	16'841 (+30%)	54.97	1'635 (12%)	27.89	6.52 (-68%)	0.68
Total (including Shire hydropower plants)	34'010 (+19%)	-	2'678 (-11%)	-	56 (-23%)	-

The increase of the mean annual energy generated by the construction of new hydropower plants namely Batoka, Kafue Gorge Lower, Mphanda Nkuwa and Kholombidzo is of 93% compared to the base scenario (Table 7-15). This value is very close to what has been estimated by the previous studies [*The World Bank*, 2010; *Tilmant et al.*, 2012]. The firm power is amplified by about 40% showing that a huge development potential is remaining on the basin.

Table 7-15. Energy production for the scenario with extended capacity and new hydropower plants compared to the base scenario (all the dams operated at 70% of their maximum capacity).

Hydropower plant	Mean annual energy [GWh]	25th quartile [GWh]	75th quartile [GWh]	Mean firm power [MW]	25th quartile [MW]	75th quartile [MW]	Mean annual spilled volume [10^9m^3]	25th quartile [10^9m^3]	75th quartile [10^9m^3]
Itezhi Tezhi (new turbines)	572	425	713	46	15	77	2.41	0.21	3.00
Kafue Upper	4'950	4'630	5'519	339	126	630	1.67	0.00	2.28
Kafue Lower (new dam)	2'698	1'781	3'383	149	0	229	0.44	0.00	0.25
Batoka (new dam)	6'799	6'335	7'406	245	209	274	18.73	10.62	30.32
Kariba (extension)	9'338	7'348	11'815	395	0	809	0.00	0.00	0.00
Cahora Bassa (extension)	16'836	16'562	18'490	1'636	1'632	2'016	6.52	0.00	10.12
Mphanda Nkuwa (new dam)	9'981	10'273	10'412	992	1'172	1'172	24.66	17.96	27.97
Kholombidzo (new dam)	1'481	1'480	1'482	169	169	169	13.77	12.92	14.03
Nkula Falls	781	781	781	89	89	89	16.74	15.86	16.87
Tedzani	564	563	564	64	64	64	16.23	15.31	16.27
Kapichira (extension)	960	1'134	1'135	109	129	129	11.96	12.31	14.02
Total	54'960 (+93%)	51'313	61'700	4'233 (+41%)	3'605	5'658	113 (+57%)	85	135

7.5.3.2 *Hydrological alteration*

In terms of hydrological alteration, since the new hydropower plants in the basin have a limited reservoir capacity and will be operated as run-of-river dams, their influence on the hydrological alteration is negligible. The extension of the existing schemes causes more hydrological alteration than the actual state (Table 7-16). In the Zambezi delta, the reduction of high flows results in an increase of nearly 200% of the mean hydrological alteration compared to the base scenario. At the Mana Pools, the alteration is enlarged by about 20% compared to the base scenario.

The Pardé coefficients (Figure 7-16) show the increase of variability at Kariba as well as the flattened curve at Cahora Bassa. In Figure 7-17, the duration curves illustrate the influence of the capacity extension at Kariba on the low flows.

Table 7-16. Indicators of hydrological alteration for the scenario including extension of existing hydropower plants and new structures compared to the base scenario (D_{Q1}: annual 1-day max flow, D_{Q3}: annual 3-days max flow, D_{Q7}: annual 7-days max flow, D_{Q30}: annual 30-days max flow, D_{Qthres}: fraction of year during which flow is above threshold, D_{date}: date of 1-day max flow, D_{vol}: volume of flow above 30-days max flow).

	D_{Q1}	D_{Q3}	D_{Q7}	D_{Q30}	D_{Qthres}	D_{dateQ1}	D_{volQ30}	D_{mean}
Kafue flats	0.29	0.29	0.29	0.43	0.43	0.14	0.29	0.31
Mana Pools	1.00	1.00	1.00	1.00	1.00	0.57	1.00	0.94 (+18%)
Zambezi delta	0.86	0.83	0.86	0.71	0.43	0.14	0.71	0.65 (+181%)
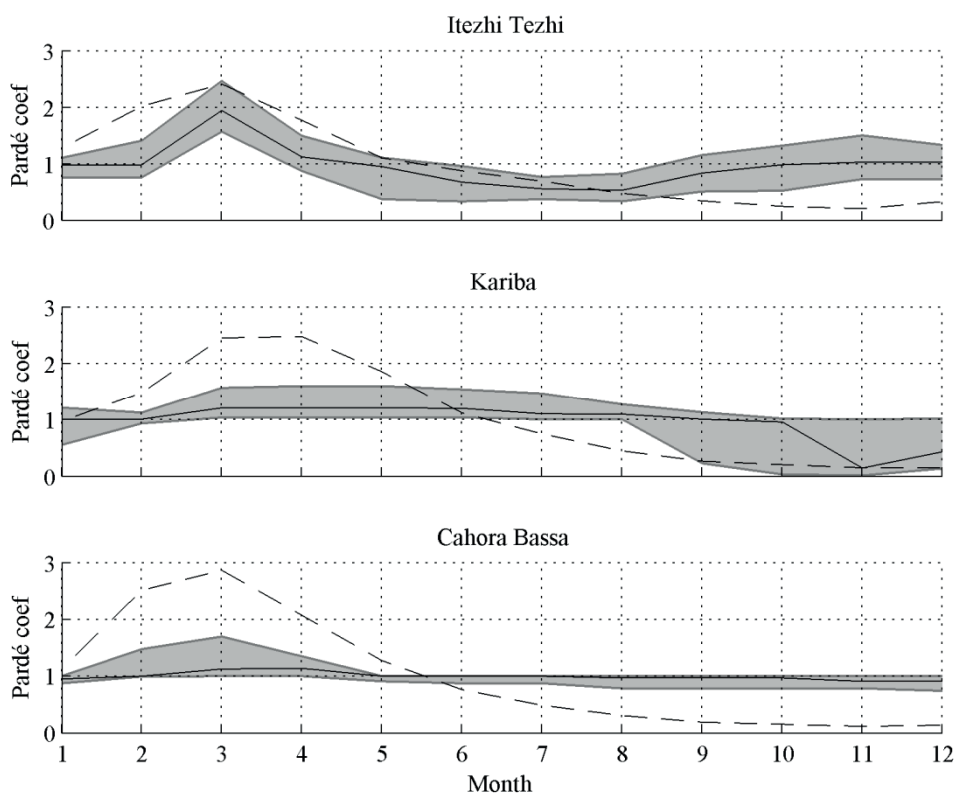
Figure 7-16. Pardé coefficients at Itezhi Tezhi, Kariba and Cahora Bassa dams for the scenario including extensions of existing hydropower plants and new schemes (dashed line: natural state, grey area: 25th and 75th quartile of model simulations, black line: median of model simulations).
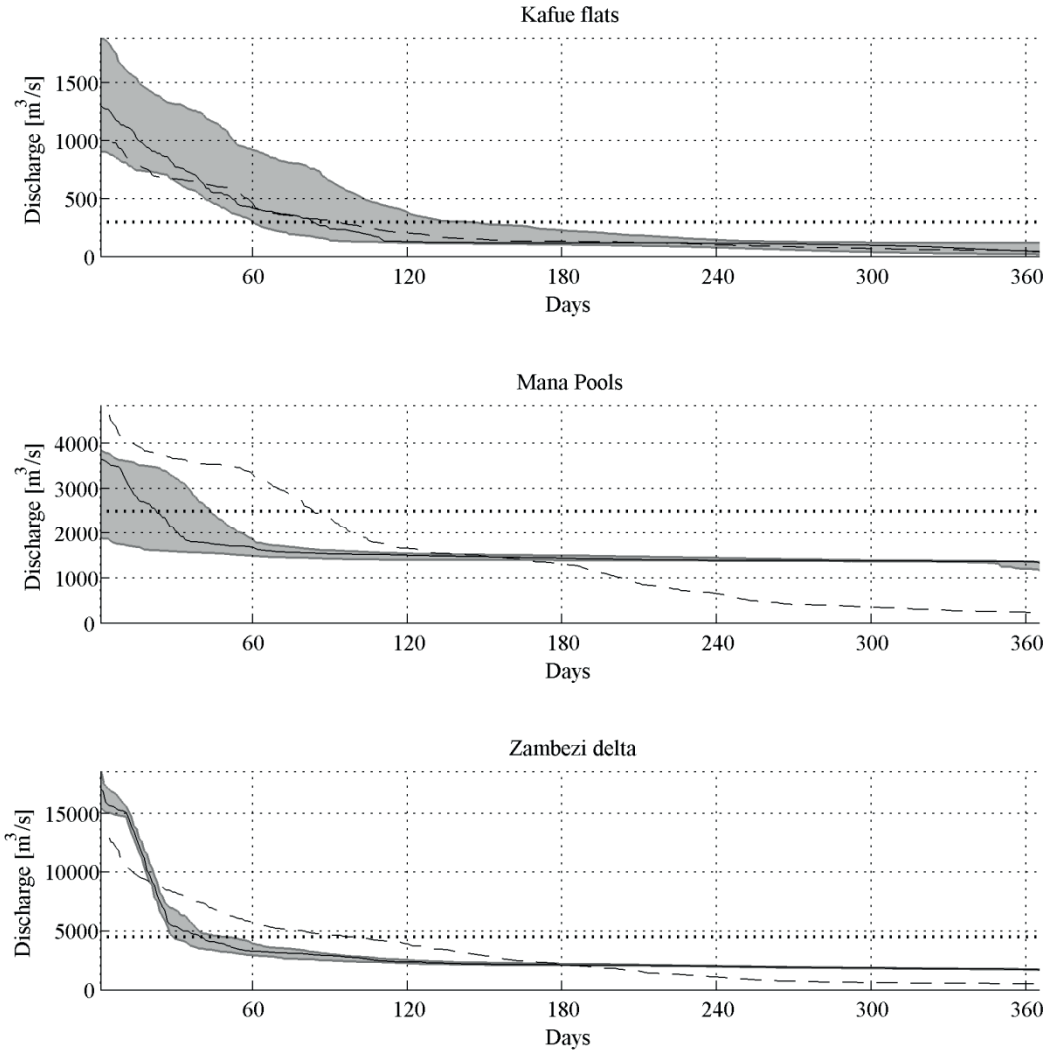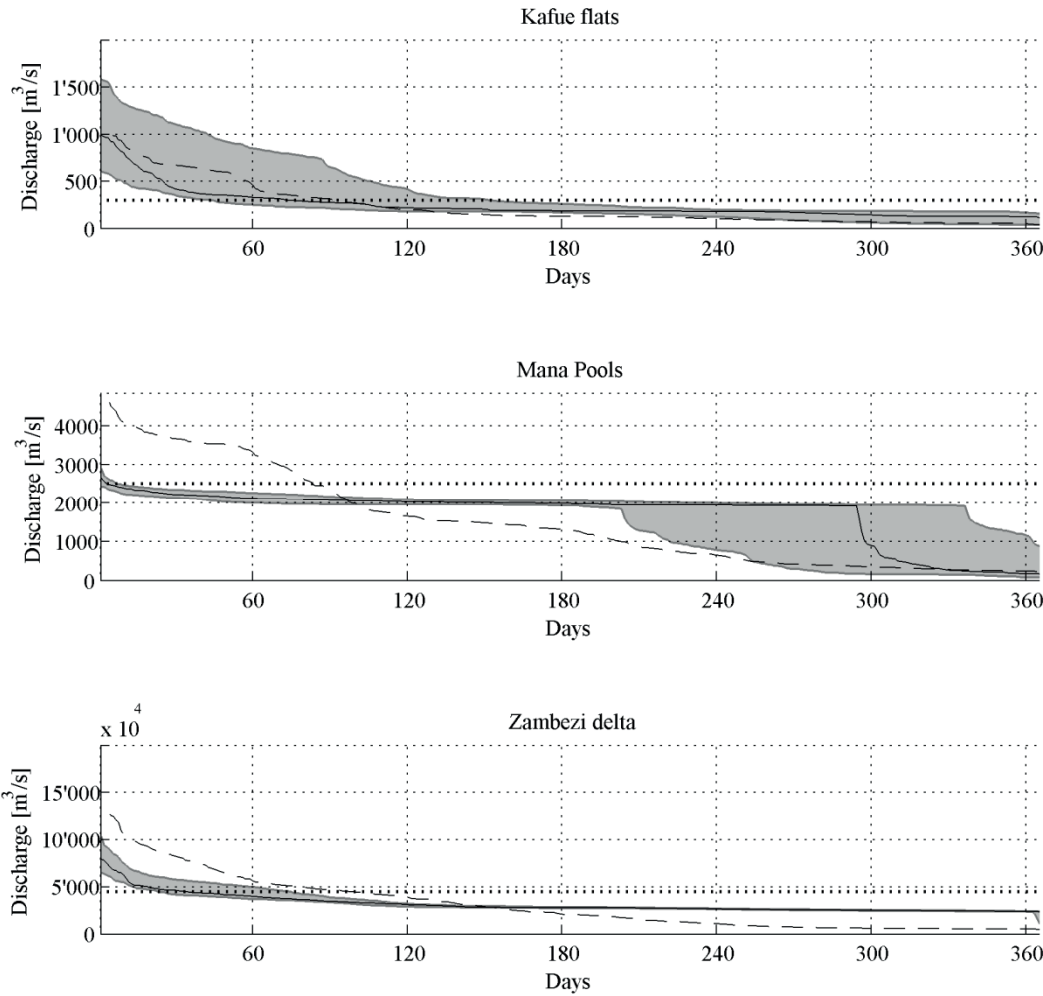
Figure 7-17. Duration curves at the key points for the scenario including extensions of existing hydropower plants and new schemes (dashed line: natural state, grey area: 25th and 75th quartile of model simulations, black line: median of model simulations, tilled line: flow threshold).

7.5.3.3 *Future state with e-flow release*

The influence of e-flows on the hydropower production for the scenario with the extensions of existing hydropower plants and new dams is quantified in Table 7-17. At Kariba, no e-flows are released since the reservoir level is kept below 30% of the active storage to use the turbine extension. As for the base scenario, the low e-flow constraint does not affect significantly the hydropower production. Medium to high e-flow constraints reduce the total firm power by 9 to 19% and the total mean energy by 5%, Itezhi Tezhi, Cahora Bassa and Mphanda Nkuwa being the most affected dams. The variability in energy production is increased by the e-flows constraints proportionally to the degree of e-flow defined.

Table 7-17. Energy production for the scenario including the extension of existing hydropower plants and the new schemes with three e-flows levels compared to the same scenario without e-flows. In orange, significant decrease.

Hydropower plant	Mean annual energy [GWh]		D_{var}	Mean firm power [MW]		D_{var}	Mean annual spilled volume [10^9m^3]		D_{var}
Low e-flows (see Chapter 7.4.1)									
Itezhi Tezhi (new turbine)	559	-2%	1.08	44	-4%	0.96	2.52	4%	0.91
Kafue Upper	4'944	0%	1.01	339	0%	1.00	1.67	0%	1.00
Kafue Lower (new dam)	2'701	0%	0.98	149	0%	1.00	0.43	-1%	0.96
Kariba (extension)	9'338	0%	1.00	395	0%	1.00	0.00	-	-
Cahora Bassa (extension)	16'412	-3%	1.08	1'594	-3%	1.09	6.96	7%	0.55
Mphanda Nkuwa (new dam)	9'820	-2%	2.17	969	-2%	550.00	25.28	3%	0.46
Total	54'359	-1%	1.03	4'166	-2%	1.08	114.28	1%	0.80
Medium e-flows (see Chapter 7.4.1)									
Itezhi Tezhi (new turbine)	526	-8%	1.26	38	-18%	0.96	2.82	17%	0.72
Kafue Upper	4'938	0%	1.02	339	0%	1.00	1.67	0%	0.99
Kafue Lower (new dam)	2'704	0%	0.98	148	-1%	1.00	0.42	-3%	0.85
Kariba (extension)	9'338	0%	1.00	395	0%	1.00	0.00	-	-
Cahora Bassa (extension)	15'593	-7%	1.17	1'396	-15%	1.65	7.71	18%	1.19
Mphanda Nkuwa (new dam)	9'655	-3%	5.67	874	-12%	1818.20	26.13	6%	0.88
Total	53'340	-3%	1.10	3'867	-9%	1.34	116.18	3%	1.00
High e-flows (see Chapter 7.4.1)									
Itezhi Tezhi (new turbine)	492	-14%	1.51	36	-21%	0.91	3.12	29%	0.53
Kafue Upper	4'940	0%	1.02	338	0%	1.00	1.66	0%	0.97
Kafue Lower (new dam)	2'706	0%	0.98	132	-11%	1.00	0.41	-7%	0.58
Kariba (extension)	9'307	0%	1.01	394	0%	1.00	0.13	-	-
Cahora Bassa (extension)	14'892	-12%	1.45	1'143	-30%	4.20	9.68	48%	1.94
Mphanda Nkuwa (new dam)	9'420	-6%	8.09	720	-27%	4684.00	28.17	14%	1.60
Total	52'341	-5%	1.20	3'441	-19%	2.17	120.60	7%	1.28

The effects of e-flows on the hydrological alteration at the key points are presented in Table 7-18. At the Kafue flats, the implementation of e-flows improves the hydrological regime but not proportionally to the magnitude of e-flows since the best effect occurs for medium e-flows. The reason is that for high e-flows, Itezhi Tezhi reservoir is emptied and therefore cannot release e-flows over a few years. At the Mana Pools, no improvement is produced because Kariba reservoir is maintained at a low level by the increase of turbine capacity and does not meet the request for e-flow release (30% of the active storage flows, see Chapter 7.4.1). In the Zambezi delta, e-flows improve the hydrological conditions. As for the base scenario simulations, the high e-flows are too high compared to the natural floods and therefore do not reduce the hydrological alteration as much as with the medium e-flows. To synthesize the results, a medium e-flow constraint is sufficient to improve the hydrological conditions in the Kafue flats and the Zambezi delta.

Table 7-18. Indicators of hydrological alteration for the scenario including new and extensions of existing hydropower plants with e-flows compared to the scenario without e-flow release (D_{Q1}: annual 1-day max flow, D_{Q3}: annual 3-days max flow, D_{Q7}: annual 7-days max flow, D_{Q30}: annual 30-days max flow, D_{Qthres}: fraction of year during which flow is above threshold, D_{date}: date of 1-day max flow, D_{vol}: volume of flow above 30-days max flow). In yellow, no influence; in green reduction of the alteration.

	D_{Q1}		D_{Q3}		D_{Q7}		D_{Q30}		D_{Qthres}		D_{date}	D_{vol}	D_{mean}	
Low e-flows (see Chapter 7.4.1)														
Kafue flats	0.29	0%	0.29	0%	0.29	0%	0.14	-67%	0.57	33%	0.14	0.14	0.27	-13%
Mana Pools	1.00	0%	1.00	0%	1.00	0%	1.00	0%	1.00	0%	0.57	1.00	0.94	0%
Zambezi delta	0.57	-33%	0.67	-20%	0.71	-17%	0.57	-20%	0.43	0%	0.14	0.71	0.54	-16%
Medium e-flows (see Chapter 7.4.1)														
Kafue flats	0.00	-100%	0.00	-100%	0.00	-100%	0.29	-33%	0.43	0%	0.00	0.00	0.10	-67%
Mana Pools	1.00	0%	1.00	0%	1.00	0%	1.00	0%	1.00	0%	0.57	1.00	0.94	0%
Zambezi delta	0.14	-83%	0.17	-80%	0.14	-83%	0.43	-40%	0.71	67%	0.86	0.00	0.35	-46%
High e-flows (see Chapter 7.4.1)														
Kafue flats	0.14	-50%	0.14	-50%	0.14	-50%	0.43	0%	0.29	-33%	0.00	0.29	0.20	-33%
Mana Pools	1.00	0%	1.00	0%	1.00	0%	1.00	0%	1.00	0%	0.71	1.00	0.96	2%
Zambezi delta	0.29	-67%	0.33	-60%	0.86	0%	0.71	0%	0.86	100%	0.86	0.00	0.56	-14%

Looking at the Pardé coefficients (Figure 7-18), the negative influence of the turbine extension is clearly visible at Cahora Bassa along with the improvement coming from e-flows. At Itezhi Tezhi, the situation is close to the natural state, even without e-flows constraint. At Kariba, the turbine extension changes the discharge distribution, introducing a variation compared to the present state.
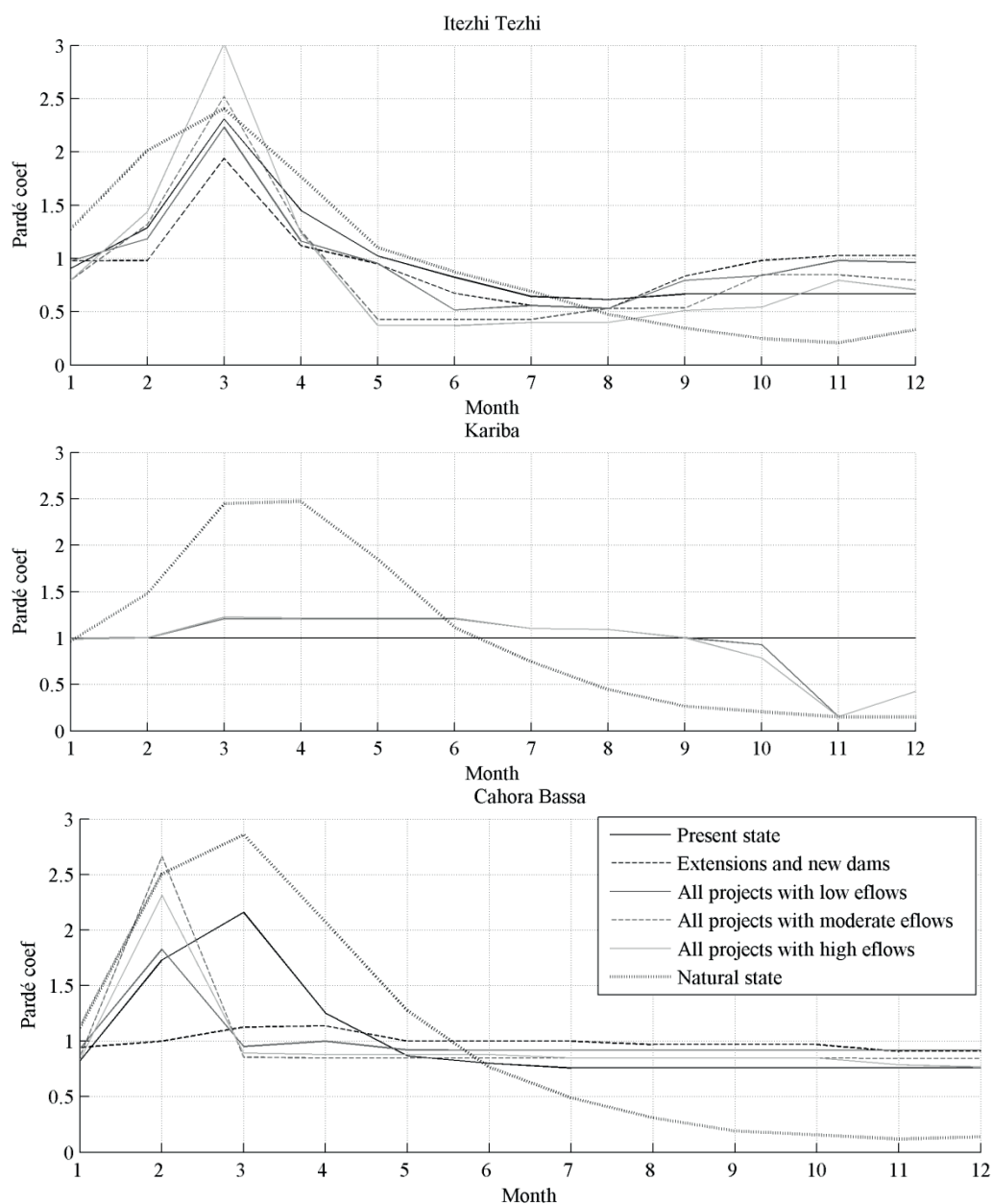
Figure 7-18. Pardé coefficients for the scenario with all projects with e-flows in comparison with the present state.

With the new scheme Mphanda Nkuwa constructed below Cahora Bassa, e-flows could be released from it instead of using Cahora Bassa. This hypothesis was simulated and the results are presented in the Table 7-19. Since Mphanda Nkuwa reservoir is much smaller than Cahora Bassa, it cannot release as much e-flow as planned and the reduction of hydrological alteration is lower (10% instead of 87% for the medium e-flow).

Table 7-19. Energy production for the scenario including the extension of existing hydropower plants and the new schemes with three e-flows levels releasing the e-flows from Mphanda Nkuwa.

Degree of e-flow	Total mean annual energy [GWh]	Total mean firm power [MW]	Mean hydrological alteration in the delta
Low	54'675 (-1%)	4'107 (-3%)	0.63 (-3%)
Medium	54'499 (-1%)	4'042 (-5%)	0.58 (-10%)
High	54'302 (-1%)	3'959 (-6%)	0.62 (-5%)

7.5.4 Synthesis

Figure 7-19 presents a synthesis of the results obtained by the scenarios simulation. It shows the combined effect of all the hydropower plants in the present and future state on the hydrological regime at the Kafue flats downstream Itezhi Tezhi, at the Mana Pools downstream Kariba and at the Zambezi delta downstream Cahora Bassa. The mean hydrological alteration is zero for the natural state.

The base scenario, corresponding to the present state, has a mean hydrological impact at the key points of 0.44. As the implementation of e-flows worsened the situation in the Zambezi delta, no global improvement can be achieved even if the flow regime is ameliorated in the Kafue flats and the Mana Pools.

Including the extensions of the existing hydropower plants and the new dams increases the mean annual energy production by more than 90% and the mean hydrological alteration by about 40% by compared to the present state. The impacts can be mitigated by the implementation of medium e-flow release with a loss of only 3% in energy production. Compared to the base scenario, the global hydrological alteration remains at the same level (+0%) while the energy production increases substantially (+90%), corresponding to an ecological sustainable development.
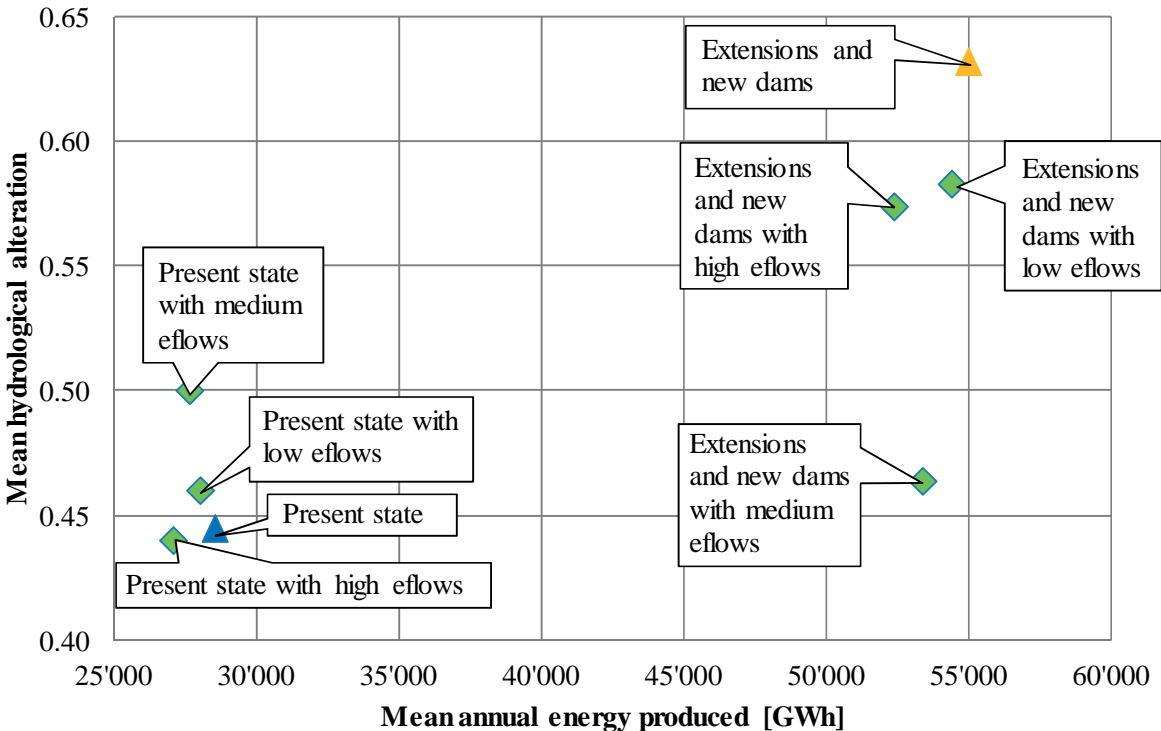
Figure 7-19. Total mean annual energy produced versus mean hydrological alteration for all the simulated scenarios.

7.6 CONCLUSIONS

In this chapter, scenarios combining different levels of environmental requirements as well as multiple hydropower development schemes were simulated at a daily time step by a hydraulic-hydrological model on the Zambezi River Basin. The hydropower operation rules were simulated in detail and the mean annual energy production, the firm power as well as the spilled volume was computed for each scenario. The hydrological alteration was evaluated by a set of indicators based on the Range of Variability Approach, by Pardé coefficients and duration curves.

The results of the present state scenario simulation show that the total mean annual energy production is about 30,000 GWh and that the firm power is about 2,200 MW. The effects of the dams on the flow regime are characterized as low on the Kafue flats, high on the Mana Pools and low on the Zambezi delta. It is important to note that the turbines are assumed to be used at 70% of their maximum capacity during the whole year to account for technical problems or revisions. This value corresponds to the observed operations at the existing schemes except for Kariba which is operated at about 65% of its maximum turbine capacity. The operation rules adopted at Cahora Bassa differ from the observed data. The volume in the reservoir is kept at a higher level than the observed data which results in more spillage during the flood season. The effect on the flow regime downstream is therefore lower

than observed actually. Recreating floods by e-flow release reduces the impact of the dam to a lower level on the Kafue flats and a medium level on the Mana Pools. The global loss in terms of mean annual energy production is almost negligible for the low and medium e-flows constraint and of 5% for the high e-flows.

Implementing new turbines at the existing hydropower plants increases the mean annual energy production by 19% but decreases the firm power. It is due to the fact that the high energy production is possible only during a small portion of the year and decreases the level in the reservoir, lowering the production for the rest of the year. The resulting impact on the flow regime is high at Mana Polls as well as at the Zambezi delta and still low at the Kafue flats. The new run-of-river hydropower plants (Batoka, Kafue Lower, Mphanda Nkuwa and Kholombidzo) planned in the near future allows increasing the mean energy produced by more than 90% and the firm power by about 40%. Releasing e-flows reduces the impact on the Kafue flats to a low level and on the Zambezi delta to a medium level resulting in a loss of less than 10% in terms of mean annual energy and about 15% in terms of firm power at Itezhi Tezhi and Cahora Bassa. In a global perspective, the implementation of e-flows along with the hydropower development of the basin could keep the impact on the flow regime at the same level than in the actual state while increasing substantially the energy production. The analysis showed that it is possible to reach a compromise between energy production and environmental sustainability.

Introducing the agriculture development in the model would allow quantifying the impact of irrigation and would complete the investigation but was beyond the scope of the present study. A first assessment was done by a Master Thesis on integrated water resources management in the Zambezi River Basin [*Perrin*, 2013]. The extension of the irrigated surfaces was derived from the World Bank report [2010] and three scenarios were implemented: (1) same crop type as the actual state, (2) production oriented toward crop for exportation, (3) production oriented toward crop for local consumption. The results showed that a development of the irrigated area targeted to exportation will consume more water than the other scenarios. The influence on the hydropower production was qualified as negligible for all the scenarios even considering that the water for irrigation was abstracted directly from the dam reservoirs.

Finally, some remarks should be useful for further studies. (1) The turbines are assumed to be used at 70% of their maximum capacity. However, exploiting the full capacity could be done especially during the period of e-flow release which would reduce the losses in energy production. (2) Since the inter-annual variability of flow is very high, the idea of defining the e-flow each year depending of the rainy season prevision should be examined. This would lead to a better reproduction of the natural discharge downstream of the dams. (3) As the increase of turbine capacity at the existing hydropower plants will conduct the operation to vary the energy production sub-daily and generate hydropeaking, the new hydropower plants could be used to attenuate the flow fluctuation, especially downstream Cahora Bassa in order to limit the impact on the delta.

8 IMPACT OF CLIMATE CHANGE ON FUTURE ENERGY PRODUCTION

Southern African climate will be subject to changes in the next century. The Intergovernmental Panel on Climate Change (IPCC) stated in its fourth report [*IPCC*, 2007] that in Africa, the regional models estimate a larger warming than the global annual mean throughout the continent and in all seasons. Regarding precipitation, the tendency is to an increase of heavy rainfall events on the humid regions and an increase of dryness in the arid regions. The effects over the Zambezi Basin are therefore highly uncertain being predicted by some General Circulation Models (GCMs) to increase and by others to decrease.

In this chapter, a comprehensive hydraulic-hydrological model of the Zambezi River Basin including the new planned hydropower schemes as well as the extension of the existing projects was used to evaluate the impacts of climate change on the energy production. The results of two GCMs (GFDL-CM2.0 and CCCma-CGCM3) have been used to simulate the hydrology during 2045-2065 and 2080-2100 periods. The consequences on the hydropower production are very different consisting respectively to an increase of 12 to 15% for GFDL-CM2.0 and a decrease of more than 40% for CCCma-CGCM3 in mean annual energy. It is therefore very difficult to conclude on the required adaptations of the design of the new projects. However, it is clear that the uncertainty in the future climate has to be taken into count during the development of the new hydropower schemes.

8.1 INTRODUCTION

Southern African climate will be subject to changes in the next century. An increase in the severity of dry extremes along with a significant decrease in mean precipitation during austral summer months was predicted by Shongwe *et al.* [2009]. The observed and projected changes in the climate of southern Africa in the period 1900–2100 were analyzed by Jury [2013]. Surface air temperature trends were positive leading to a +2 °C anomaly by the end of the 21st century. Rainfall trends were mixed and generally negative across marine latitudes (35–40°S) decreasing from South to North with a deficit of -0.3 mm/day by the end of the 21st century. Giannini *et al.* [2008] confirms the increase of air temperature and describes a tendency of rainfall to increase in the wet region and decrease in the dry region. The Intergovernmental Panel on Climate Change (IPCC) stated in its fourth report [*IPCC*, 2007] that in Africa, the regional models estimate a larger warming than the global annual mean throughout the continent and in all seasons. The uncertainty in precipitation prediction depending of the General Circulation Model (GCM) used to simulate the climate is transposed in uncertainty in runoff prediction [*Gosling et al.*, 2011].

The Zambezi River Basin is an interesting and challenging area to develop Integrated Water Resources Management (IWRM). The rising demand for electricity, corresponding to the development of the countries and the need for clean emission-free generation sources appears to be in favour of new hydropower projects. The new plants design should take into account the impacts of climate changes on river discharge as it influences the economic viability of the scheme.

In the third assessment report of the IPCC [*IPCC*, 2001], the results from Arnell [1999] were cited for the Zambezi Basin consisting in a significant warming trend of 10-25% associated with a decrease of rainfall by 10-20% which results in a decrease of the runoff by 26-40%.

Beilfuss [2012] summarized the results of peer-reviewed studies of climate in Southern Africa by an increase of temperature between 0.3 and 0.6°C per decade and a slight decrease of annual precipitation associated with an increase of inter-annual variability and heavy rainfall events. The conclusions were that climate change scenarios should be incorporated into hydropower design and operation to ensure the project sustainability.

The World Bank [2010] assessed the changes in runoff for the major Zambezi sub-basins by 2030, relative to the 1961-1990 baseline. A reduction of 16% in the Upper Zambezi, 24-34% in the Middle Zambezi, and 13-14% in the Lower Zambezi was estimated based on the midrange of 23 GCMs with the emission scenario SRES-A1B.

The changes in water supply across Africa was examined by De Wit and Stankiewicz [2006]. For the Zambezi Basin, they showed that it is located on a zone where both decrease (Southern part of the basin) and increase (Northern part of the basin) of precipitation is predicted by the GCMs. They modelled the change in drainage density resulting from the

climate change and concluded that a 10% drop in rainfall would result in a 17% reduction in surface drainage for regions receiving ~1000 mm rainfall.

Specific studies have already showed the importance of climate change impact on the new hydropower plants. The impact of climate change was evaluated on the planned Batoka Gorge hydroelectric scheme [*G P Harrison and Whittington*, 2002]. A hydrological model, a reservoir operation model and an electricity market model were coupled to explore the relationship between climate, hydropower production and financial performance. The hydrological model was calibrated and validated on two series of 15 years of data at a monthly time step. Three climate change projections based on General Circulation Models (GCM) simulations for the 2080s were implemented: two from the HadCM2 GCM developed by the Hadley Centre at the UK Meteorological Office and one from the ECHAMC4 GCM developed by the Max Planck Institute for Meteorology. The range of change predicted by the models varies from −1 to −18% for precipitation and from +4.4 to +5.3°C for temperatures. The operation of Batoka Gorge was examined over the 30 years between 1961 and 1990 for climate changes predicted by the three scenarios. In all cases, annual flow levels at Victoria Falls decrease between 10 and 35.5% resulting in a reduction of annual electricity production by 6.1 to 21.4% particularly during the dry season. The conclusion was that it is no longer prudent to rely on historic river flow data to assess potential hydroelectric schemes.

Two scenarios of reduced mean monthly inflow by 10 and 20% were tested on a multi-reservoir multi-purpose model of the Zambezi River Basin to assess the effect of climate change [*Beilfuss*, 2010]. The average annual power generated was respectively reduced by 4% and 14%.

The multi-sector investment opportunity analysis of the World Bank [2010] simulated moderate climate change scenario with a resulting decrease of 32% in firm energy and 21% in average energy compared to the baseline.

The Zambezi region is subject to long term hydrological cycles which contribute to complicate the climate predictions. Based on recreated rainfall records extending back to 1800, Mason [2013] identified four separate cycles of 70, 130, 35 and 44 years. Between 1924 and 2004, the duration of the main runoff cycle was estimated at about 40 years with secondary cycles of 10 to 20 years [*Mazvimavi and Wolski*, 2006]. The same analysis conducted between 1950 and 1995 results in a dominant runoff cycle of 5.6 years [*Jury*, 2003]. Finally, an extensive analysis of southern African climate reveals variability patterns with main components of 80 and 18 years [*Tyson et al.*, 2002].

Monthly mean precipitation in 2050 were simulated for the Zambezi Basin based on the IPCC SRES A2 scenario using two GCM results (UKMO-HADCM3 and GFDL-CM2.0) combined with water demand scenarios [*Beck and Bernauer*, 2011]. The changes in precipitation modeled vary between +11 to +28% and the changes in temperature between +2.5 and +2.9 °C. The temperature effects were included in the model by scaling the potential evaporation proportionally. The simulations showed that the effect of increasing water demand is clearly higher than the effects of projected climate change.

The implications of climate change on hydroelectricity generation at the existing and proposed future hydropower plants in the Zambezi Basin were assessed by Yamba *et al.* [2011]. The climate scenario was defined as a combination of the results of three GCMs (CCCMA version 2, CSIRO-Mk2 and HADCM3) under the emission scenario SRES A2. Monthly precipitation was derived for the period 2010-2070 based on the control period 1970-2000. Augmentation of water demand was simulated along with climate change in a simple water balance model. The results showed that the hydroelectric potential has a tendency towards a gradual reduction for all the hydroelectric power schemes included in the model (Itezhi-Tezhi, Kariba, Cahora Bassa and Mphanda Nkuwa).

The changes in precipitation and temperature have always been assessed at monthly time step and by alteration of historical data. No detailed hydraulic-hydrological modeling has been done at daily time step. The innovative contribution of the present study is to use the results of two opposite climate change predictions (GFDL-CM2.0 and CCCma-CGCM3) to simulate the hydrology at daily time step during 2045-2065 and 2080-2100 periods. For this purpose, a comprehensive model of the Zambezi River Basin including the new planned hydropower schemes as well as the extension of the existing projects was developed.

In Chapter 8.2, the case study and the data are presented. The model and the indicators implemented are listed in Chapter 8.3. Chapter 8.4 consists in the presentation of the results and some conclusions are summarized in Chapter 8.5.

8.2 CASE STUDY AND DATA

8.2.1 The Zambezi River basin

A detailed description of the basin and the hydropower plants has been given already in Chapter 3.1 and Chapter 3.2. From its headwaters in Angola to the delta in Mozambique, the Zambezi River runs over 2600 km and connects eight African nations that share different portions of its 1.4 M km^2 large drainage basin [*Vörösmarty and Moore III*, 1991]. Rainfall varies considerably from year to year and occurs almost entirely between October and March. The mean annual discharge at the delta is of 3800 m^3/s [*Tilmant et al.*, 2010a]. Three major hydropower schemes are actually operated on the basin (Kariba dam, Kafue dam and Itezhi Tezhi reservoir and Cahora Bassa dam). A huge potential for further development exists with multiple hydropower projects that will be implemented in the next 20 years.

8.2.2 Climate change scenarios

The climate scenarios are based on the SRES-A2 scenario of the IPCC report which expects economic development regionally oriented in which technological change is more fragmented and slower than in the other SRES story-lines [*IPCC*, 2007].

In the present study, we used the results of the version 2.0 of the US Geophysical Fluid Dynamic Laboratory Climate Model (GFDL-CM2.0) [*Delworth et al.*, 2006] and of the third

version of the Canadian Centre for Climate Modeling and Analysis Coupled Global Climate Model (CCCma-CGCM3) [*Scinocca et al.*, 2008]. The data are available at daily time step for the period 2046 to 2085 and 2081 to 2100. The CCCma-CGCM3 version T47 has a surface grid whose spatial resolution is roughly 3.75 degrees lat/lon and the GFDL-CM2.0 has a surface grid whose spatial resolution is about 2 degrees latitude and 2.5 degrees longitude. Minimum and maximum surface air temperature as well as ground precipitation were selected from the data sets and time series for each sub-basin was generated to be used as input data for the hydraulic-hydrological model. The two GCMs predictions are quite different (Table 8-1) both in amplitude and in tendency. For the precipitation, an increase is simulated by the GFDL-CM2.0 model and a decrease by the CCCma-CGCM3 model. For the temperature, the two models predict an increase which will intensify at the end of the century.

Table 8-1. Synthesis of the climate change predicted by the GCMs CCCma-CGCM3 and GFDL-CM2.0 under the emission scenario SRES A2.

	Actual state	Projections 2045-2065		Projections 2081-2100	
	(mean over the period 1998-2010)	CCCma-CGCM3	GFDL-CM2.0	CCCma-CGCM3	GFDL-CM2.0
Precipitation	2.8 mm/day	-5%	+9%	-2%	+2%
Temperature	23.4 °C	+1.1 °C	+0 °C	+2.8 °C	+1.9 °C

8.3 METHODOLOGY

8.3.1 Hydraulic-hydrological model

The concept of the hydraulic-hydrologic model is described in detail in Chapter 3.5 along with the modified reservoir sub-model used to simulate floodplain hydrology (Chapter 3.5.2) and to simulate the hydropower operations (Chapter 3.5.3). The setup is presented in Chapter 3.5.4 and the calibration procedure in Chapter 5.

8.3.2 Indicators

The energy generated by the hydropower plants is evaluated by two indicators: the firm power and the total annual energy. More precisely, the firm power is defined as the power available 90% of the year (346 days a year) in MW and the annual energy is the total energy generated over the year in GWh. The spilled volume is included in the analysis as a complementary index to evaluate the quantity of water "lost" by the dam.

To compare the different scenarios to the base scenario, the difference of annual energy, firm power and volume spilled are calculated as well as the ratio between the variation of the results (D_{var}) characterized by the distance between the 25th and 75th quartiles of these indicators [7-4].

$$D_{var,i} = \frac{(q_{75,i} - q_{25,i})}{(q_{75,bs} - q_{25,bs})}$$ [8-1]

where i is the scenario compared, bs is the base scenario, q_{75} and q_{25} the 75th and 25th quartiles.

The duration curves at the key points (Victoria Falls, Kafue flats and the Zambezi Delta) are plotted to show the influence of the climate change on the flow regime.

8.4   RESULTS AND DISCUSSION

8.4.1   Actual state

The energy production for the period 1998-2010 is presented in Table 8-2. The power is mainly generated on the Kafue and the Zambezi Rivers while the dams located on the Shire have only a limited production. The inter-annual variability is quite high characterized by the 25th and 75th quartiles of the indicators (-6% to +12% for the mean annual energy and -14% to +33% for the firm power).

Table 8-2. Energy production for the actual state scenario (1998-2010).

Hydropower plant	Mean annual energy	25th quartile	75th quartile	Mean firm power	25th quartile	75th quartile	Mean annual spilled volume	25th quartile	75th quartile
	[GWh]	[GWh]	[GWh]	[MW]	[MW]	[MW]	$[10^9 m^3]$	$[10^9 m^3]$	$[10^9 m^3]$
Itezhi Tezhi	572	425	713	46	15	77	2.41	0.21	3.00
Kafue Upper	4'950	4'630	5'519	339	126	630	1.67	0.00	2.28
Kafue Lower	2'698	1'781	3'383	149	0	229	0.44	0.00	0.25
Batoka	6'799	6'335	7'406	245	209	274	18.73	10.62	30.32
Kariba	9'338	7'348	11'815	395	0	809	0.00	0.00	0.00
Cahora Bassa	16'836	16'562	18'490	1'636	1'632	2'016	6.52	0.00	10.12
Mphanda Nkuwa	9'981	10'273	10'412	992	1'172	1'172	24.66	17.96	27.97
Kholombidzo	1'481	1'480	1'482	169	169	169	13.77	12.92	14.03
Nkula Falls	781	781	781	89	89	89	16.74	15.86	16.87
Tedzani	564	563	564	64	64	64	16.23	15.31	16.27
Kapichira	960	1'134	1'135	109	129	129	11.96	12.31	14.02
Total	54'960	51'313	61'700	4'233	3'605	5'658	113	85	135

8.4.2 Effects of an decrease of precipitation and an increase of temperature (CCCma-CGCM3 model)

The losses in energy production resulting from a decrease of precipitation combined with an increase of temperature (CCCma-CGCM3) are dramatic for the basin (Table 8-3). Globally, the total mean annual energy would be reduced by more than 40% and the firm energy by about 80% compared to the actual state. There is not a significant difference between the two simulated periods (2046-2065 and 2081-2100).

Regarding the spatial distribution, the Kafue sub-basin, characterized by Itezhi Tezhi and Kafue Gorge, is more affected than the Upper Zambezi, characterized by Batoka and Kariba. The impacts at Cahora Bassa are quite substantial.

The duration curves at the key points (Kafue flats, Victoria Falls and the Zambezi delta) show that the high discharges are considerably reduced in the upper basins (from about 1'000 to about 500 m³/s for Kafue flats, from about 3'000 to less than 1'000 m³/s for Victoria Falls) (Figure 8-1). Victoria Falls is the only key point not influenced by the hydropower plants and therefore represents the effect of climate changes on the natural flow.

Figure 8-1. Duration curves at the key points for the climate change scenario CCCma-CGCM3 for the period 2046-2065 (dashed line: actual state, grey area: 25th and 75th quartile of model simulations, black line: median of model simulations, tilled line: flow threshold).

203

Table 8-3. Energy production for the climate change scenario CCCma-CGCM3 (in red, -100 to -51%; in orange, -50 to -21%; in yellow, -20 to -1%).

Hydropower plant	Mean annual energy [GWh]	Diff	D_{var}	Mean firm power [MW]	Diff	D_{var}	Mean annual spilled volume [$10^9 m^3$]	Diff	D_{var}
2046-2065 period									
Itezhi Tezhi (existing)	196	-66%	0.50	10	-78%	0.08	0.14	-94%	0.07
Kafue Upper (existing)	3'246	-34%	2.07	14	-96%	0.00	0.01	-100%	0.00
Kafue Lower (future project)	1'263	-53%	0.43	0	-100%	0.00	0.00	-100%	0.00
Batoka (future project)	4'116	-39%	1.92	160	-35%	0.04	2.39	-87%	0.14
Kariba (extension)	5'609	-40%	0.75	39	-90%	0.00	0.00	-	-
Cahora Bassa (extension)	8'023	-52%	3.02	288	-82%	0.19	0.00	-100%	0.00
Mphanda Nkuwa (future project)	5'821	-42%	30.17	175	-82%	0.00	8.18	-67%	0.68
Kholombidzo (future project)	1'352	-9%	107.17	148	-12%	-	3.10	-77%	5.19
Nkula Falls (existing)	781	0%	2.60	89	0%	1.00	5.28	-68%	7.00
Tedzani (extension)	555	-2%	2.75	62	-3%	11.00	4.89	-70%	7.21
Kapichira (existing)	785	-18%	0.04	88	-20%	-	5.20	-57%	4.00
Total	31'747	-42%	1.76	1'072	-75%	0.06	29.19	-74%	0.73
2081-2100 period									
Itezhi Tezhi (existing)	239	-58%	0.63	11	-77%	0.06	0.21	-91%	0.00
Kafue Upper (existing)	3'147	-36%	1.48	7	-98%	0.00	0.01	-99%	0.00
Kafue Lower (future project)	1'216	-55%	0.32	0	-100%	0.00	0.00	-100%	0.00
Batoka (future project)	4'479	-34%	1.82	170	-31%	0.02	2.13	-89%	0.16
Kariba (extension)	5'493	-41%	0.65	0	-100%	0.00	0.00	-	-
Cahora Bassa (extension)	7'676	-54%	2.85	151	-91%	0.08	0.00	-100%	0.00
Mphanda Nkuwa (future project)	5'577	-44%	27.03	88	-91%	0.00	7.65	-69%	0.71
Kholombidzo (future project)	1'340	-9%	105.19	145	-14%	-	2.97	-78%	4.90
Nkula Falls (existing)	781	0%	0.39	89	0%	1.00	5.03	-70%	6.41
Tedzani (extension)	552	-2%	8.89	62	-4%	528.0	4.61	-72%	6.65
Kapichira (existing)	781	-19%	4.87	88	-20%	-	4.84	-60%	3.72
Total	31'281	-43%	1.57	810	-81%	0.04	27.44	-76%	0.70

8.4.3 Effects of an increase of precipitation and of temperature (GFDL-CM2.0 model)

The changes predicted by the GFDL-CM2.0 model (an increase of precipitation associated with an increase of temperature) have a lower impact than the CCCma-CGCM3 model results on the energy production (Table 8-4). During the first period (2046-2065), the total mean annual energy will increase by 12% and the firm energy by 36% compared to the actual state. During the second period (2081-2100), the effects are not significant for the mean annual energy and an increase of 15% for the firm power is predicted. The spilled volumes increase varies from more than 250% during the first period to more than 130% during the second period.

Regarding the spatial variability, the Kafue sub-basin is still the most affected by the changes. In the Upper Zambezi, Batoka is characterized by a diminution in firm power which increases from the first to the second period. The mean annual energy increases at Kariba during the first period and decreases during the second period. In terms of inter-annual variability, the spilled volumes will vary much more than experienced actually but the total mean annual energy as well as the total firm power will stay more constant.

The duration curves for the period 2046-2065 (Figure 8-2) show that the effect of the climate change is especially big on the high discharges with a large inter-annual variability.
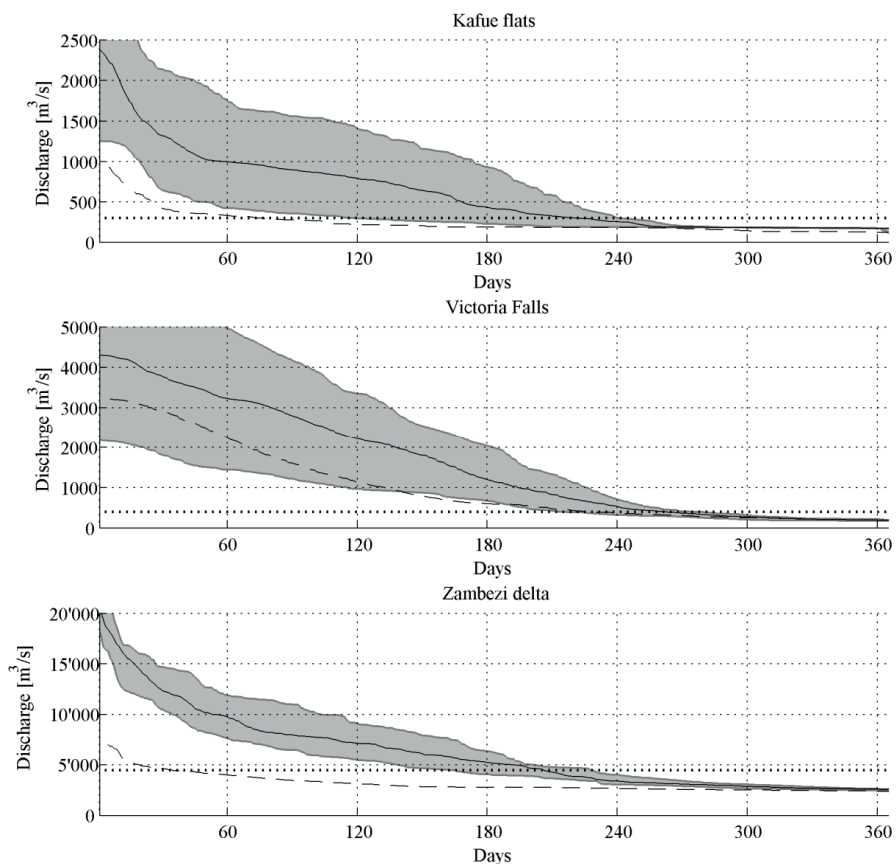
Figure 8-2. Duration curves at the key points for the climate change scenario GFDL-CM2.0 for the period 2046-2065 (dashed line: actual state, grey area: 25th and 75th quartile of model simulations, black line: median of model simulations, tilled line: flow threshold).

During the period 2081 to 2100, the simulated duration curves are much closer to the actual state than over the previous period (Figure 8-3). The effects are still more significant on the high discharges and the variability is quite large.
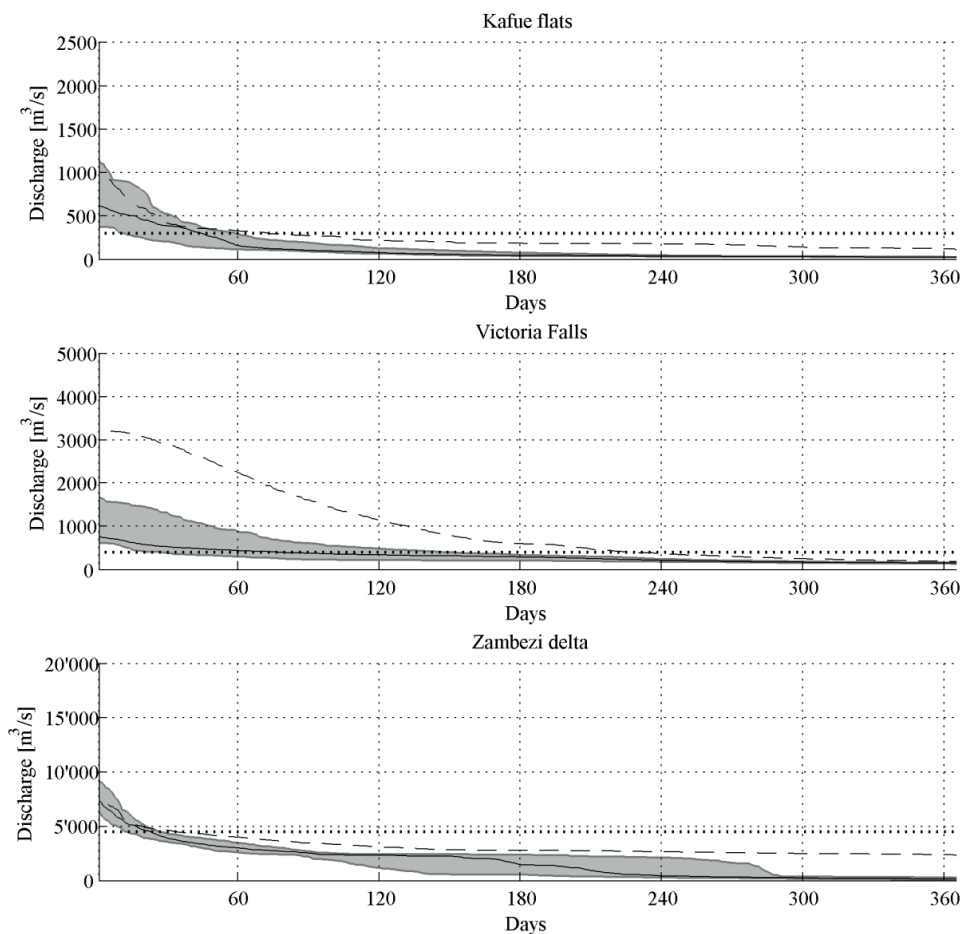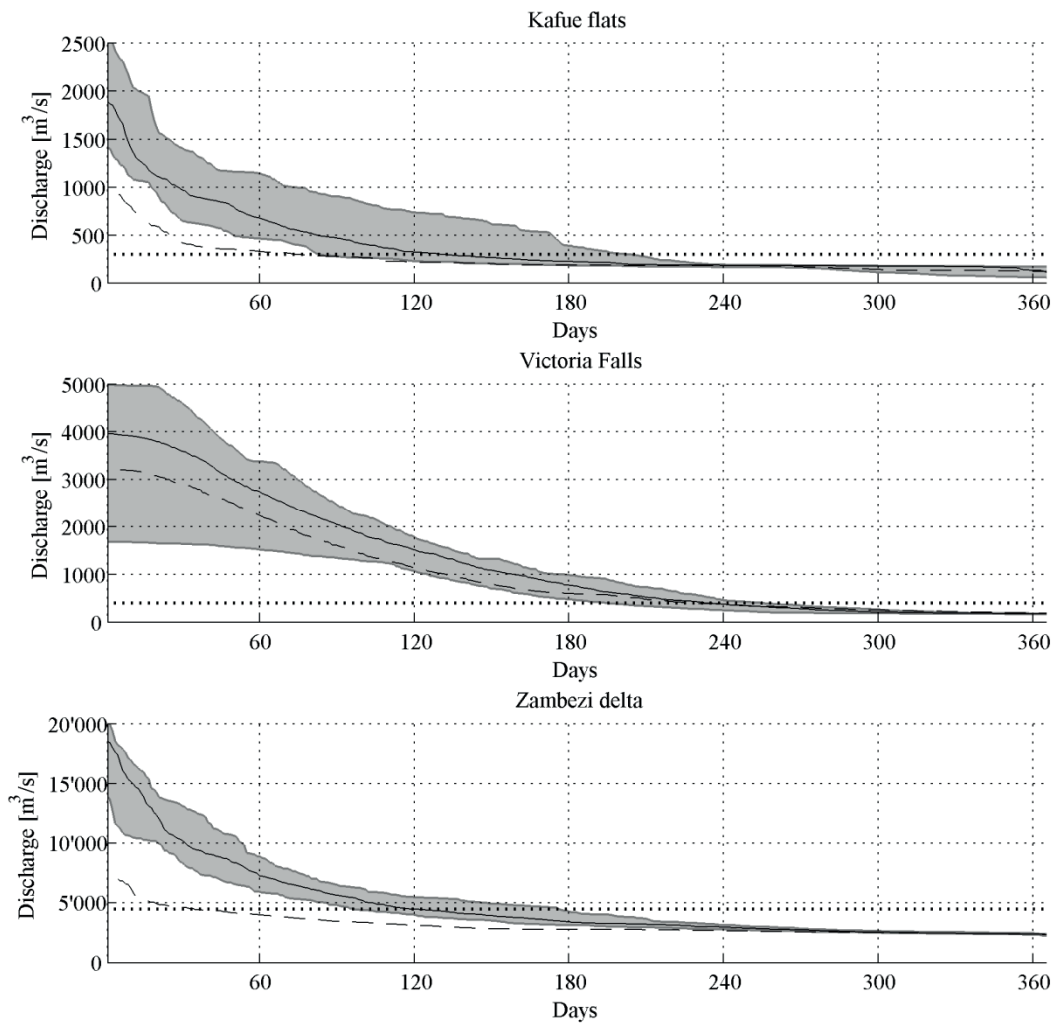

Figure 8-3. Duration curves at the key points for the climate change scenario GFDL-CM2.0 for the period 2081-2100 (dashed line: actual state, grey area: 25th and 75th quartile of model simulations, black line: median of model simulations, tilled line: flow threshold).

Table 8-4. Energy production for the climate change scenario GFDL-CM2.0 (in orange, -50 to -1%; in yellow, +0 to +50%; in green, +51 to +100%; in blue, more than +100%).

Hydropower plant	Mean annual energy [GWh]	Diff	D_{var}	Mean firm power [MW]	Diff	D_{var}	Mean annual spilled volume [10^9m^3]	Diff	D_{var}
2046-2065 period									
Itezhi Tezhi (existing)	697	22%	0.10	69	48%	0.14	10.31	327%	5.24
Kafue Upper (existing)	5'524	12%	0.01	630	86%	0.00	10.29	518%	5.92
Kafue Lower (future project)	4'498	67%	0.73	386	158%	1.50	6.94	1482%	50.43
Batoka (future project)	7'375	8%	1.39	242	-1%	0.76	35.89	92%	2.31
Kariba (extension)	10'569	13%	1.18	843	113%	1.69	11.41	-	-
Cahora Bassa (extension)	18'390	9%	0.12	2'006	23%	0.20	69.58	967%	7.52
Mphanda Nkuwa (future project)	10'944	10%	4.95	1'171	18%	0.00	89.02	261%	7.66
Kholombidzo (future project)	1'491	1%	3.66	169	0%	-	42.68	210%	24.21
Nkula Falls (existing)	782	0%	3.48	89	0%	1.00	45.86	174%	26.39
Tedzani (extension)	566	0%	3.02	64	0%	5.00	45.54	181%	27.30
Kapichira (existing)	795	-17%	2.15	91	-17%	-	46.01	285%	15.17
Total	61'629	12%	0.86	5'758	36%	0.90	413.51	266%	7.15
2081-2100 period									
Itezhi Tezhi (existing)	632	11%	0.34	52	12%	0.98	4.72	96%	2.78
Kafue Upper (existing)	5'346	8%	0.14	536	58%	0.00	5.40	224%	3.68
Kafue Lower (future project)	3'744	39%	1.32	313	110%	1.15	2.96	575%	21.90
Batoka (future project)	6'161	-9%	1.24	189	-23%	0.09	20.56	10%	1.16
Kariba (extension)	8'667	-7%	1.13	438	11%	1.43	0.00	-	-
Cahora Bassa (extension)	17'399	3%	0.18	1'826	12%	0.70	38.11	484%	2.16
Mphanda Nkuwa (future project)	10'256	3%	1.52	1'106	12%	0.00	56.90	131%	2.55
Kholombidzo (future project)	1'487	0%	2.42	169	0%	-	30.78	123%	7.58
Nkula Falls (existing)	782	0%	0.99	89	0%	0.00	33.89	102%	9.56
Tedzani (extension)	565	0%	2.59	64	0%	3.00	33.54	107%	10.81
Kapichira (existing)	794	-17%	0.20	91	-17%	-	33.96	184%	6.55
Total	55'833	2%	0.89	4'873	15%	0.85	260.81	131%	2.63

8.5   CONCLUSION

The data of two Global Circulation Models (GFDL-CM2.0 and CCCma-CGCM3) have been used to simulate the hydrology in the Zambezi Basin over 2045-2065 and 2080-2100 periods. The prediction of the climate models diverge in terms of precipitation as GFDL-CM2.0 forecasts an increase while CCCma-CGCM3 a diminution but agree on the increase of temperatures. As a consequence the mean yearly hydropower production increases by 12 to 15% with the GFDL-CM2.0 data and decreases by more than 40% with the CCCma-CGCM3 data. If a global averaged effect is calculated, it would be of about -13%. Therefore, the design of new hydropower schemes should take into account the uncertainty in the future climate.

To define more accurately what would be the climate in the next 100 years, existing regional models should be implemented for the Zambezi Basin. By modeling in details the climate process specific to the region, the prediction should converge regarding precipitation and result in clear recommendations for the hydropower development.

9 CONCLUSIONS

This chapter summarizes the achievements of the research project and presents the outlook for future studies.

9.1 ACHIEVEMENTS

The major contribution of the present research project was to set-up a detailed hydrologic-hydraulic model of a large African catchment including the hydraulic schemes and the floodplains under scarce data constraints. The innovative multi-objective modelling method provides a powerful instrument to assess how power schemes operation can be adapted to get the highest environmental results under the highest energy production. The use of open source data and tools leads to the implementation of an "open" strategy easily transferable to the stakeholders. For the first time, a detailed evaluation of the satellite derived precipitation on the Zambezi Basin has been conducted before implementing the hydrological model. Moreover, a new reservoir model has been developed to simulate the floodplain hydrology. Finally, the compromise between hydropower development and minimization of the hydrological alteration has been characterized by original daily time step simulations through an innovative combination of indicators.

Worldwide, almost 50,000 dams over 15 m height have been built during the last six decades with an aggregated storage capacity of 6,000 km^3 [*International Commission On Large Dams*, 2007]. The fact that large dams by supplying irrigation and hydroelectricity production can sustain development and reduce poverty has led developing countries to undertake major investments in dam construction. Africa is the continent with the lowest degree of electrification and water storage capacity per capita worldwide. In exploiting the potential of African rivers, major challenges will be to improve the operation of existing dams and to avoid past mistakes when designing new ones.

The Zambezi River basin contains many of southern Africa's largest and most intact freshwater and estuarine wetlands, e. g. the Kafue flats, the Mana Pools and the Zambezi delta as well as several free-flowing yet unprotected river reaches. The basin supports some of the world's largest remaining elephant herds and serves as a refuge for many other large animals, including African buffalo, hippopotamus and crocodile. Three of Africa's largest dams (Kariba, Cahora Bassa and Kafue) inundate hundreds of square kilometers of river habitat and modify the natural flow patterns that sustain floodplains. Increasing electricity demand from cities and industry is causing a regional energy shortage, leading governments and investors to plan yet more dams in the Zambezi Basin. This constitutes therefore a particularly interesting and considerable challenge for further developing approaches of integrated water resources management.

Evaluation of the quality of available input data

The quality of available input data for hydrological modeling has been evaluated thoroughly, focusing on the rainfall estimates (see Chapter 4). The results underline the fact that input data have to be analyzed before modeling the hydrological behavior of a basin in order to know the extent of rainfall events and their distribution through space and time. Moreover, these data illustrate the very strong dependency of the satellite product quality with the region of interest.

Three operational and acknowledged satellite derived precipitation products (the Tropical Rainfall Measuring Mission product 3B42 -TRMM 3B42-, the Famine Early Warning System product 2.0 -FEWS RFE2.0- and the National Oceanic and Atmospheric Administration/Climate Prediction Centre (NOAA/CPC) morphing technique -CMORPH-) were analyzed in terms of spatial and temporal distribution of the precipitation.

At a daily time scale, the probability of rainfall being detected by the satellite appears nearly equivalent to a random simulation. At monthly time scale, all estimates have a good correspondence, CMORPH being less precise in terms of volume ratio as it overestimates the rainfall by about 40%. TRMM 3B42 and FEWS RFE2.0 show a very similar performance compared to ground data even if they are very different in the spatial distribution of the rainfall. The datasets were candidates for post-real-time use. Therefore, as TRMM produces data since 1998, it was chosen as the input data for hydrological modeling.

Definition of the specific hydrological processes required for hydraulic-hydrological modeling

The Soil and Water Assessment Tool (SWAT) a semi-distributed physically based continuous time model (see Chapter 3) was chosen to simulate the hydrological behavior of the basin. Due to the specificities of the Zambezi River basin, two main additional functions had to be developed.

First, a floodplain sub-model based on a reservoir approach was defined (see Chapter 6). The model separates the outflow of the reservoir simulating the floodplain into main channel flow and flow over the floodplain area. The results confirm that the model is able to simulate the discharge during both high flow and low flow periods. Moreover, considering the particularities of floodplain regions, the developed model reveals its ability to simulate the behavior of large inundated area thanks to its spatial flexibility.

Secondly, the hydropower plant operations were simulated based on the rule curve and the technical characteristics of the dams (see Chapter 7). The pertinence of the implemented approach was verified by modeling the existing hydropower plants on the basin.

Establishment of a calibration procedure

Given the complexity and the size of the basin under study, a calibration procedure taking into account the data scarcity was developed in four steps: (1) choice of the calibration parameters, (2) definition of objective functions, (3) application of a an automated calibration procedure based on the Multi-ALgorithm Genetically Adaptive Multi-objective method (AMALGAM) and (4) analysis of the results in terms of statistics and hydrographs for the calibration and the validation periods. It constitutes a real contribution in terms of reliability. The discussion showed the importance of considering the hydrographs and volume variation plots for analyzing results as this allows the quality assessment of the model's estimates better than focusing on discharge's statistics and indicators only.

Globally, the mean relative error was equal to 30% for the calibration period and 35% for the validation period. Concerning the mean volume ratio, it was higher than 0.9 over calibration and around 0.8 over the validation period. At the discharge stations, the mean Nash-Sutcliffe coefficient was above 0.45 for the calibration and validation periods. The results at the major artificial reservoirs (Kariba and Cahora Bassa) show a volume overestimation of 20 to 35% mainly distributed on certain years. This outcome was considered as acceptable in view of the scarce observed data to simulate development scenarios, taking into account the fact that the scenarios comparison would be based on relative values.

Assessment of the impact of hydropower development on the flow regime at critical points

In a global perspective, the analysis showed that it is possible to reach a compromise between energy production and environmental sustainability. Developing hydropower with an implementation of e-flows allows keeping the impact on the flow regime at the same global level than in the present state while increasing substantially the energy production.

More precisely, the results for the present state scenarios showed that the total mean annual energy production is about 30,000 GWh and the firm power about 2,200 MW. The effects of the dams on the flow regime are characterized as low on the Kafue flats, high on the Mana Pools and low on the Zambezi delta. Recreating floods by e-flow release reduces the impact of the dam to a lower level on the Kafue flats and to a medium level on the Mana Pools with a global loss of 5% in the mean annual energy production. The refurbishment of the existing hydropower plants increases the mean annual energy production by 19% but decreases the firm power. The resulting impact on the flow regime is higher at Mana Pools and at the Zambezi delta than in the present state. The construction of new hydropower plants operated as run-of-river dams increases the mean yearly energy produced by more than 90% and the firm power by about 40%. Releasing e-flows reduces the impact on the Kafue flats to a low level and on the Zambezi delta to a medium level with a loss of less than 10% in terms of mean annual energy and about 15% in terms of firm power at Itezhi Tezhi and Cahora Bassa.

Evaluation of climate change effects

As the prediction of the different climate models diverge in terms of precipitation tendency, it is difficult to conclude on a relevant adaptation. However, it is clear that the design of new hydropower schemes has to take into account the uncertainty in the future climate.

The data of two Global Circulation Models (GFDL-CM2.0 and CCCma-CGCM3) for the emission scenario SRES A2 of the IPCC report were used to simulate the hydrology during 2045-2065 and 2080-2100 periods. The consequences on the mean annual energy produced are quite different as GFDL-CM2.0 predicts an increase of 12 to 15% and CCCma-CGCM3 a decrease of more than 40% resulting respectively from an increase and a diminution of the precipitation. The averaged impact would be a diminution of about 14% due to the global increase of temperature.

9.2   CONCLUDING DISCUSSION AND OUTLOOK

A multi-objective modelling methodology was developed to define how dam operation can be adapted to get a compromise between the best environmental quality under the highest energy production. As a consequence of the wide range of modeled and analyzed fields, a certain loss of detail has resulted. Nevertheless, the presentation of coherent methodological steps contributes to a transparent analysis approach.

Hydrological modeling as well as scenarios simulation is subject to several uncertainties. The main sources for the present research project are discussed hereafter:

- **Input data** uncertainty is relevant over the Zambezi basin as precipitation is estimated based on satellite observations and other variables are based on broad global datasets (temperature, land use, soil map, etc.).

- The **model structure** represents a considerable vector of uncertainty as the sub-basins could be delineated differently or other hydrological equations implemented to describe the processes.

- **Parameter estimation** is dependent on the selected calibration methodology and multiple solutions exist depending on the defined objective function.

- A significant source of error concerns **recorded discharge and reservoir level observations**. Uncertainty of river discharge estimations issues from errors in the rating curve definition, individual measurements of discharge or water levels and data reporting and handling. At the hydropower schemes, the turbine flow is not directly measured but estimated from the electricity production and the outlet outflow is estimated based on the reservoir level and the spillway's capacity.

- The **lack of knowledge** of the physical processes, particularly in the floodplains, is a major source of uncertainty.

- The **climate change** scenarios exhibits a high variability which results in a high uncertainty for the future hydrological behavior in the basin and accordingly for hydropower production.

Several extensions could add value to the presented approach by increasing knowledge or by integrating new aspects of the problematic:

- The model could be calibrated with different possible input data and the performance in terms of runoff simulation could be evaluated by comparison. However, in a basin like the Zambezi, where only about 7% of the rainfall is contributing to runoff, the influence of other parameters like the wetlands capacity, the evaporation and soil equations are certainly of higher importance.

- Water quality and sediment transport modeling could be added to the floodplain model using the novel separation between base flow and upper flow.

- A longer time period for calibration could be defined based on extended input data series. This would allow taking more observed discharge data into account and improve the calibration reliability.

- For real-time or even forecasting use, the model could be adapted including an update of the state variables like reservoirs levels.

- Concerning scenarios definition, the turbines are assumed to be exploited at 70% of their maximum capacity. However, employing the full capacity could be done especially during the periods of e-flow release which would limit the losses in energy production. This could be done only if there is enough water in the reservoirs and if the demand in energy is sufficient.

- Regarding e-flows, since the inter annual variability of flow is very high, they could be defined yearly based on the rainy season prevision, particularly in case of real-time modelling. This would lead to a better reproduction of the natural discharge downstream of the dams.

- Simulation of flow at sub-daily time step could be done to assess the impact of sub-daily variation in energy production as the increase of turbine capacity aims to produce peak energy.

- Introducing the agriculture development in the model would allow quantifying the impact of irrigation and would complete the investigation on water demand.

- Last but not least, existing regional climate models should be implemented on the Zambezi Basin to define more accurately the climate change for the next 100 years.

The multi-objective modeling approach presented in this research project is of crucial importance for water resources planning and management. Efforts should be undertaken to proceed in the analysis by developing an operational real-time model benefiting from the institutional framework available.

Appendix:
Values of the calibrated parameters

A1 SECOND ITERATION

Table A-1. Values of the parameters related to surface flow for the second iteration.

	SURLAG	ESCO	CN_F	EPCO	SOL_AWC	SOL_z	CH_KII	CANMX
	[day]	[-]	[%]	[-]	[%]	[%]	[mm/hr]	[mm]
Set 1	0.51	0.96	0.02	0.75	0.53	0.28	38.10	12.73
Set 2	0.50	0.83	0.03	0.75	0.49	0.22	49.72	2.15
Set 3	0.50	1.00	0.03	0.75	0.76	0.49	49.98	0.06
Set 4	0.50	0.96	0.02	0.75	0.53	0.28	38.10	12.73
Set 5	0.51	0.96	0.02	0.75	0.53	0.28	38.10	12.73
Set 6	0.51	0.96	0.02	0.75	0.53	0.24	38.10	12.75
Set 7	0.50	0.94	0.02	0.75	0.72	0.28	38.93	10.75
Set 8	0.50	0.94	0.02	0.76	0.72	0.28	38.93	10.75
Set 9	0.50	0.94	0.02	0.75	0.74	0.28	38.93	10.77

Table A-2. Values of the parameters related to groundwater flow for the second iteration.

	GW_DELA	GW_REVA	GWQMN	REVAPMN	ALPHA_B
	[day]	[-]	[mm]	[mm]	[day]
Set 1	248.00	0.30	8.52	2.25	0.46
Set 2	274.23	0.39	59.54	17.31	0.22
Set 3	227.46	0.40	52.15	1.01	0.29
Set 4	248.00	0.30	8.52	1.04	0.46
Set 5	248.00	0.30	9.92	2.25	0.46
Set 6	248.00	0.30	9.92	2.52	0.45
Set 7	217.50	0.30	8.58	1.01	0.45
Set 8	246.10	0.30	5.94	1.01	0.41
Set 9	217.41	0.30	7.47	1.00	0.45

Appendix: Value of the calibrated parameters

Table A-3. Values of the floodplain parameters for the second iteration.

	Lukanga			Barotse		
	a	b	k	a	b	k
	[m$^{3/2}$/s]	[-]	[m^2/s]	[m$^{3/2}$/s]	[-]	[m^2/s]
Set 1	202'387'529.77	3.45	3'868'784.01	3'582'184'833.00	3.50	5'406'329.41
Set 2	2'835'142'823.21	3.50	3'117'264.63	3'374'921'184.47	1.59	5'451'249.40
Set 3	162'439'887.31	2.25	4'465'302.14	4'031'590'610.01	1.51	5'644'870.34
Set 4	202'387'529.77	3.45	3'046'814.77	3'582'184'833.00	3.50	5'406'329.41
Set 5	202'387'529.77	3.49	3'868'784.01	3'575'305'929.94	3.50	5'405'737.99
Set 6	208'307'236.62	3.49	3'868'784.01	3'575'305'929.94	3.48	5'400'231.10
Set 7	202'384'716.18	3.45	3'015'968.51	2'972'508'451.92	3.46	5'406'335.56
Set 8	202'384'716.18	3.45	3'015'968.51	2'972'508'451.92	3.50	5'406'326.15
Set 9	192'816'887.60	3.44	3'044'669.20	2'972'508'451.92	3.42	5'395'044.78

Table A-4. Values of the floodplain parameters for the second iteration.

	Kafue			Chobe		
	a	b	k	a	b	k
	[m$^{3/2}$/s]	[-]	[m^2/s]	[m$^{3/2}$/s]	[-]	[m^2/s]
Set 1	2279057180.31	3.24	5998772.66	4183951126.11	2.58	4573038.22
Set 2	2591932300.95	3.46	5540127.15	4582607577.60	2.84	3997652.54
Set 3	2376616266.74	3.46	5945861.95	4657459654.15	3.49	4842142.58
Set 4	2279057180.31	3.24	5998772.66	4193926706.99	2.58	4573038.22
Set 5	2279057180.31	3.24	5998772.66	4183951126.11	2.58	4574433.37
Set 6	2279057180.31	3.24	5998772.66	4183951126.11	3.26	4574433.37
Set 7	2375194284.57	3.46	5905678.50	4360617495.28	2.58	4431156.73
Set 8	2375194284.57	3.46	5905678.50	4357092501.98	2.58	4431156.73
Set 9	2385259165.01	3.45	5905678.50	4193926706.99	2.58	4422799.50

A2 THIRD ITERATION

Table A-5. Values of the parameters related to surface flow for the third iteration.

	SURLAG	ESCO	CN_F	EPCO	SOL_AWC	SOL_z	CH_KII	CANMX
	[day]	[-]	[%]	[-]	[%]	[%]	[mm/hr]	[mm]
Set 1	0.51	0.97	0.02	0.94	0.97	-0.30	4.73	20.75
Set 2	0.50	0.97	0.02	0.94	0.97	-0.30	4.52	18.60
Set 3	0.51	0.97	0.02	0.99	0.97	-0.30	4.92	21.51
Set 4	0.51	0.97	0.02	0.94	0.97	-0.30	4.73	20.75
Set 5	0.50	0.97	0.02	0.99	0.97	-0.30	4.26	19.04
Set 6	0.51	0.97	0.02	0.99	0.97	-0.30	4.92	21.51
Set 7	0.58	0.97	0.02	1.00	0.97	-0.30	9.83	29.09

Appendix: Value of the calibrated parameters

Table A-6. Values of the parameters related to groundwater flow for the third iteration.

	GW_DELA [day]	GW_REVA [-]	GWQMN [mm]	REVAPMN [mm]	ALPHA_B [day]
Set 1	258.20	0.23	96.78	1.91	0.10
Set 2	274.58	0.23	93.89	2.48	0.12
Set 3	257.72	0.23	94.16	2.52	0.11
Set 4	258.20	0.23	96.78	1.91	0.10
Set 5	261.56	0.22	96.71	1.20	0.10
Set 6	257.72	0.23	94.16	2.52	0.11
Set 7	279.26	0.22	96.59	1.08	0.16

Table A-7. Values of the floodplain parameters for the third iteration.

	Lukanga			Barotse		
	a $[m^{3/2}/s]$	b [-]	k $[m^2/s]$	a $[m^{3/2}/s]$	b [-]	k $[m^2/s]$
Set 1	116'656'615.90	3.30	4'109'256.22	3'048'292'311.00	1.51	4'242'466.37
Set 2	112'199'413.30	3.27	4'538'395.83	3'327'728'917.00	2.09	4'305'208.98
Set 3	117'903'924.00	3.31	4'132'234.76	3'054'542'868.00	2.10	3'721'825.22
Set 4	116'656'615.90	3.30	4'109'256.22	3'048'292'311.00	1.54	4'242'466.37
Set 5	104'460'117.40	3.23	4'195'805.40	3'375'294'932.00	1.96	3'918'083.74
Set 6	100'000'000.00	3.31	4'132'234.76	3'054'312'094.00	2.07	3'940'267.73
Set 7	337'236'521.50	3.44	4'233'607.16	656'319'365.20	2.07	3'651'757.92

Table A-8. Values of the floodplain parameters for the third iteration.

	Kafue			Chobe		
	a $[m^{3/2}/s]$	b [-]	k $[m^2/s]$	a $[m^{3/2}/s]$	b [-]	k $[m^2/s]$
Set 1	706'611'444.90	2.40	3'000'000.00	2'722'432'260.00	1.79	3'144'687.73
Set 2	626'786'449.40	2.35	3'020'119.93	4'885'078'762.00	1.75	6'000'000.00
Set 3	726'853'741.10	2.40	3'001'268.96	4'138'778'589.00	1.79	5'583'380.96
Set 4	706'611'444.90	2.40	3'000'000.00	2'722'432'260.00	1.79	3'144'687.73
Set 5	694'916'444.50	2.40	3'123'116.52	1'988'356'750.00	1.67	4'819'362.16
Set 6	726'853'741.10	2.42	3'122'993.34	4'138'778'589.00	1.79	5'583'380.96
Set 7	3'700'000'000.00	2.50	6'000'000.00	5'000'000'000.00	1.56	5'829'558.28

Appendix: Value of the calibrated parameters

A3 FOURH ITERATION

Table A-9. Values of the parameters related to surface flow for the fourth iteration.

	SURLAG [day]	ESCO [-]	CN_F [%]	EPCO [-]	SOL_AWC [%]	SOL_z [%]	CH_KII [mm/hr]	CANMX [mm]
Set 1	0.50	0.96	0.03	0.99	0.87	-0.29	2.79	7.67
Set 2	0.50	0.96	0.03	0.98	0.87	-0.30	2.68	10.45
Set 3	0.50	0.96	0.03	0.98	0.87	-0.29	2.96	6.20
Set 4	0.50	0.96	0.03	0.98	0.87	-0.29	2.63	10.48
Set 5	0.50	0.96	0.03	0.98	0.87	-0.29	2.62	6.54
Set 6	0.50	0.96	0.03	0.98	0.87	-0.29	2.90	9.65
Set 7	0.50	0.96	0.03	0.98	0.87	-0.30	2.84	10.71
Set 8	0.50	0.96	0.03	0.99	0.87	-0.30	2.67	10.45
Set 9	0.50	0.96	0.03	0.98	0.87	-0.29	2.61	9.57
Set 10	0.50	0.96	0.03	0.98	0.87	-0.30	2.92	12.90

Table A-10. Values of the parameters related to groundwater flow for the fourth iteration.

	GW_DELA [day]	GW_REVA [-]	GWQMN [mm]	REVAPMN [mm]	ALPHA_B [day]
Set 1	298.83	0.40	65.08	2.28	0.04
Set 2	295.85	0.40	67.78	1.92	0.05
Set 3	290.37	0.40	70.26	3.94	0.04
Set 4	294.63	0.40	66.25	1.00	0.04
Set 5	292.43	0.39	69.84	1.54	0.04
Set 6	294.51	0.39	68.17	3.12	0.04
Set 7	293.17	0.40	71.24	1.06	0.04
Set 8	295.85	0.40	67.78	1.42	0.05
Set 9	294.48	0.40	68.10	2.96	0.04
Set 10	293.46	0.39	70.41	2.64	0.04

Appendix: Value of the calibrated parameters

Table A-11. Values of the floodplain parameters for the fourth iteration.

	Lukanga			Barotse		
	a	b	k	a	b	k
	[m$^{3/2}$/s]	[-]	[m^2/s]	[m$^{3/2}$/s]	[-]	[m^2/s]
Set 1	83'508'183.07	3.50	3'058'695.18	4'992'876'599.00	1.22	11'236'443.22
Set 2	87'981'615.79	3.50	3'084'143.46	4'992'791'526.00	1.17	10'332'003.92
Set 3	80'084'835.16	3.50	3'103'762.02	4'986'509'481.00	1.32	11'059'832.88
Set 4	88'946'679.67	3.50	3'000'000.00	5'000'000'000.00	1.23	11'130'353.08
Set 5	87'930'891.52	3.50	3'073'084.87	4'991'002'070.00	1.27	10'794'734.76
Set 6	84'655'037.97	3.50	3'094'749.43	4'992'195'847.00	1.26	10'632'055.61
Set 7	93'805'075.21	3.42	3'098'375.54	4'999'132'651.00	1.15	10'241'332.01
Set 8	87'815'567.24	3.50	3'084'143.46	4'989'040'197.00	1.17	10'325'545.56
Set 9	84'798'546.04	3.50	3'082'796.29	4'999'587'187.00	1.27	10'795'298.38
Set 10	88'372'088.02	3.49	3'142'350.08	4'991'019'867.00	1.20	10'612'812.52

Table A-12. Values of the floodplain parameters for the fourth iteration.

	Kafue			Chobe		
	a	b	k	a	b	k
	[m$^{3/2}$/s]	[-]	[m^2/s]	[m$^{3/2}$/s]	[-]	[m^2/s]
Set 1	605'622'165.00	2.55	13'079'287.58	3'952'941'518.00	1.75	8'189'554.29
Set 2	567'667'157.10	2.52	12'537'182.18	3'938'289'846.00	1.39	6'845'515.83
Set 3	577'588'034.20	2.58	12'020'630.69	3'796'407'558.00	1.15	6'090'548.29
Set 4	597'211'386.70	2.50	12'462'851.02	3'974'969'489.00	2.01	6'970'022.52
Set 5	630'585'464.30	2.60	12'427'174.43	3'828'409'729.00	1.71	6'797'106.44
Set 6	644'215'567.60	2.54	12'267'971.00	3'832'208'352.00	1.41	6'057'165.37
Set 7	649'577'385.80	2.54	12'414'916.75	3'714'281'563.00	1.40	6'053'119.29
Set 8	594'753'589.30	2.52	12'537'182.18	3'938'289'846.00	1.39	8'232'847.18
Set 9	496'576'849.70	2.54	12'674'167.22	3'829'871'783.00	1.81	8'372'643.36
Set 10	630'479'099.80	2.46	12'442'510.92	3'775'524'036.00	1.40	5'603'210.62

A4 FINAL ITERATION

Table A-13. Values of the parameters related to surface flow for the final iteration.

	SURLAG	ESCO	CN_F	EPCO	SOL_AWC	SOL_z	CH_KII	CANMX
	[day]	[-]	[%]	[-]	[%]	[%]	[mm/hr]	[mm]
Set 1	0.50	0.99	-0.06	0.68	0.92	0.04	1.41	15.46
Set 2	0.50	0.98	-0.05	0.67	0.92	0.03	1.19	14.74
Set 3	0.50	0.97	-0.05	0.71	0.93	0.06	1.15	15.31
Set 4	0.51	0.97	-0.05	0.68	0.93	0.05	1.26	14.46
Set 5	0.50	0.97	-0.05	0.69	0.93	0.05	1.29	15.06

Table A-14. Values of the parameters related to groundwater flow for the final iteration.

	GW_DELA [day]	GW_REVA [-]	GWQMN [mm]	REVAPMN [mm]	ALPHA_B [day]
Set 1	296.73	0.40	89.81	4.41	0.04
Set 2	297.12	0.40	92.40	4.92	0.04
Set 3	297.86	0.40	89.29	2.66	0.05
Set 4	297.50	0.40	86.43	1.77	0.05
Set 5	297.26	0.40	92.64	2.12	0.05

Table A-15. Values of the floodplain parameters for the final iteration.

	Lukanga			Barotse		
	a $[m^{3/2}/s]$	b [-]	k $[m^2/s]$	a $[m^{3/2}/s]$	b [-]	k $[m^2/s]$
Set 1	323'326'764.20	3.32	9'813'326.93	4'362'440'984.00	1.99	21'888'247.50
Set 2	276'751'833.00	3.32	9'130'490.43	4'243'450'006.00	2.19	21'968'867.32
Set 3	235'923'279.60	3.32	8'924'413.80	4'364'163'700.00	2.08	21'895'624.16
Set 4	239'729'865.60	3.33	7'864'234.91	4'338'905'496.00	2.15	17'834'558.54
Set 5	272'316'315.10	3.33	8'953'896.32	4'222'905'520.00	2.09	20'383'337.89

Table A-16. Values of the floodplain parameters for the final iteration.

	Kafue			Chobe		
	a $[m^{3/2}/s]$	b [-]	k $[m^2/s]$	a $[m^{3/2}/s]$	b [-]	k $[m^2/s]$
Set 1	602'462'184.30	2.37	9'277'327.62	4'526'918'632.00	2.79	6'593'364.36
Set 2	609'445'185.00	2.39	8'978'376.71	4'776'522'817.00	2.87	7'155'833.67
Set 3	517'783'341.60	2.34	9'647'829.36	4'923'630'867.00	2.91	7'119'755.24
Set 4	550'650'169.20	2.29	8'837'166.74	4'958'760'178.00	3.03	7'606'150.45
Set 5	574'861'175.90	2.35	8'942'041.91	4'865'835'412.00	3.01	6'972'441.73

REFERENCES

Abbaspour, K. C., M. Vejdani, and S. Haghighat (2007), SWAT-CUP calibration and uncertainty programs for SWAT, Proc. of International Congress on Modelling and Simulation - Land, Water and Environmental Management: Integrated Systems for Sustainability, Christchurch, New Zealand, 10-13 December 2007, 1596-1602.

Abbott, M. B., J. C. Bathurst, J. A. Cunge, P. E. O'Connell, and J. Rasmussen (1986), An introduction to the European Hydrological System - Systeme Hydrologique Europeen, "SHE", 2: Structure of a physically-based, distributed modelling system, *Journal of Hydrology*, *87*(1-2), 61-77.

ADAPT (2008), Project summary, Unpublished report.

Adeyewa, Z. D., and K. Nakamura (2003), Validation of TRMM radar rainfall data over major climatic regions in Africa, *Journal of Applied Meteorology*, *42*(2), 331-347.

Aerts, J. C. J. H., M. Kriek, and M. Schepel (1999), STREAM (Spatial Tools for River basins and Environment and Analysis of Management options): 'Set up and requirements', *Physics and Chemistry of the Earth, Part B: Hydrology, Oceans and Atmosphere*, *24*(6), 591-595.

Allen, R., L. Pereira, D. Raes, and M. Smith (1998), Guidelines for computing crop water requirements, *FAO Irrigation and drainage paper 56*, FAO - Food and Agriculture Organization of the United Nations, Rome, Italy.

Anagnostou, E. N. (2004), Overview of overland satellite rainfall estimation for hydro-meteorological applications, *Surveys in Geophysics*, *25*(5-6), 511-537.

Arnell, N. W. (1999), Climate change and global water resources, *Global Environmental Change*, *9*(SUPPL.), S31-S49.

Arnold, J., J. R. Kiniry, R. Srinivasan, J. R. Williams, E. B. Haney, and S. L. Neitsch (2011), Soil and Water Assessment Tool - Input/Output file documentation (Version 2009), Temple, Texas, USA.

Arnold, J. G., R. Srinivasan, R. S. Muttiah, and J. R. Williams (1998), Large area hydrologic modeling and assessment part I: Model development, *Journal of the American Water Resources Association*, *34*(1), 73-89.

Arthington, A. H., S. E. Bunn, N. L. Poff, and R. J. Naiman (2006), The challenge of providing environmental flow rules to sustain river ecosystems, *Ecological Applications*, *16*(4), 1311-1318.

Beck, L., and T. Bernauer (2011), How will combined changes in water demand and climate affect water availability in the Zambezi river basin?, *Global Environmental Change*, *21*(3), 1061-1072.

Beilfuss, R. (2001), Prescribed flooding and restoration potential in the Zambezi Delta, Mozambique, Unpublished report.

Beilfuss, R. (2010), Modelling trade-offs between hydropower generation and environmental flow scenarios: A case study of the Lower Zambezi River Basin, Mozambique, *International Journal of River Basin Management*, *8*(3-4), 331-347.

Beilfuss, R. (2012), A Risky Climate for Southern African Hydro - Assessing hydrological risks and consequences for Zambezi River Basin dams, International Rivers, Berkeley, USA.

Beilfuss, R., and D. Dos Santos (2001), Patterns of hydrological change in the Zambezi Delta, Mozambique, Unpublished report.

Beilfuss, R., and C. Brown (2010), Assessing environmental flow requirements and trade-offs for the Lower Zambezi River and Delta, Mozambique, *International Journal of River Basin Management*, *8*(2), 127 - 138.

Bekele, E. G., and J. W. Nicklow (2007), Multi-objective automatic calibration of SWAT using NSGA-II, *Journal of Hydrology*, *341*(3-4), 165-176.

Beven, K. (1993), Prophecy, reality and uncertainty in distributed hydrological modelling, *Advances in Water Resources*, *16*(1), 41-51.

Beven, K., and A. Binley (1992), The future of distributed models: model calibration and uncertainty prediction, *Hydrological Processes*, *6*(3), 279-298.

Beven, K., and J. Freer (2001), Equifinality, data assimilation, and uncertainty estimation in mechanistic modelling of complex environmental systems using the GLUE methodology, *Journal of Hydrology*, *249*(1-4), 11-29.

Bitew, M. M., and M. Gebremichael (2011), Assessment of satellite rainfall products for streamflow simulation in medium watersheds of the Ethiopian highlands, *Hydrology and Earth System Sciences*, *15*(4), 1147-1155.

Bollaert, E. F. R., M. C. Munodawafa, and D. Z. Mazvidza (2013), Kariba dam plunge pool scour: Quasi-3D numerical predictions, *Houille Blanche*(1), 42-49.

Brown, C., and J. King (2012), Modifying dam operating rules to deliver environmental flows: Experiences from southern Africa, *International Journal of River Basin Management*, *10*(1), 13-28.

Butts, M. B., J. T. Payne, M. Kristensen, and H. Madsen (2004), An evaluation of the impact of model structure on hydrological modelling uncertainty for streamflow simulation, *Journal of Hydrology*, *298*(1–4), 242-266.

CCES (2008), Approved workplan of the project ADAPT, Unpublished report.

Cohen Liechti, T., J. P. Matos, J. L. Boillat, and A. J. Schleiss (2012), Comparison and evaluation of satellite derived precipitation products for hydrological modeling of the Zambezi River Basin, *Hydrology and Earth System Sciences*, *16*(2), 489-500.

Confesor Jr, R. B., and G. W. Whittaker (2007), Automatic calibration of hydrologic models with multi-objective evolutionary algorithm and Pareto optimization, *Journal of the American Water Resources Association*, *43*(4), 981-989.

Cukier, R. I., C. M. Fortuin, K. E. Shuler, A. G. Petschek, and J. H. Schaibly (1973), Study of the sensitivity of coupled reaction systems to uncertainties in rate coefficients. I Theory, *The Journal of Chemical Physics*, *59*(8), 3873-3878.

Daren Harmel, R., and P. K. Smith (2007), Consideration of measurement uncertainty in the evaluation of goodness-of-fit in hydrologic and water quality modeling, *Journal of Hydrology*, *337*(3-4), 326-336.

De Wit, M., and J. Stankiewicz (2006), Changes in surface water supply across Africa with predicted climate change, *Science*, *311*(5769), 1917-1921.

Deb, K., A. Pratap, S. Agarwal, and T. Meyarivan (2002), A fast and elitist multiobjective genetic algorithm: NSGA-II, *IEEE Transactions on Evolutionary Computation*, *6*(2), 182-197.

Decharme, B., R. Alkama, F. Papa, S. Faroux, H. Douville, and C. Prigent (2012), Global off-line evaluation of the ISBA-TRIP flood model, *Climate Dynamics*, *38*(7-8), 1389-1412.

Delworth, T. L., et al. (2006), GFDL's CM2 global coupled climate models. Part I: Formulation and simulation characteristics, *Journal of Climate*, *19*(5), 643-674.

Denconsult (1998), Sector Studies under ZACPLAN. Introductory Volume. Final Report, Zambezi River Authorities, Lusaka, Zambia.

Dessu, S. B., and A. M. Melesse (2012), Modelling the rainfall-runoff process of the Mara River basin using the Soil and Water Assessment Tool, *Hydrological Processes*, *26*(26), 4038-4049.

Di Baldassarre, G., and A. Montanari (2009), Uncertainty in river discharge observations: A quantitative analysis, *Hydrology and Earth System Sciences*, *13*(6), 913-921.

Dincer, T., S. Child, and B. Khupe (1987), A simple mathematical model of a complex hydrologic system - Okavango Swamp, Botswana, *Journal of Hydrology*, *93*(1-2), 41-65.

Dinku, T., P. Ceccato, E. Grover-Kopec, M. Lemma, S. J. Connor, and C. F. Ropelewski (2007), Validation of satellite rainfall products over East Africa's complex topography, *International Journal of Remote Sensing*, *28*(7), 1503-1526.

Ebert, E. E., J. E. Janowiak, and C. Kidd (2007), Comparison of near-real-time precipitation estimates from satellite observations and numerical models, *Bulletin of the American Meteorological Society*, *88*(1), 47-64.

Euroconsult Mott MacDonald (2007), Integrated water resources management stategy for the Zambezi River Basin - Rapid assessment report, Unpublished report.

FAO (1995), Digital soil map of the world and derived soil properties version 3.5 [CD-ROM], in *Land and Water Digital Media Series*, Rome, Italy.

FAO/IIASA/ISRIC/ISSCAS/JRC (2012), Harmonized World Soil Database (version 1.2), FAO, Rome, Italy and IIASA, Laxenburg, Austria.

Farquharson, F. A. K., and J. V. Sutcliffe (1998), Regional variations of African river flows, *IAHS-AISH Publication*(252), 161-169.

Fekete, B. M., C. J. Vörösmarty, and W. Grabs (1999), Global, composite runoff fields based on observed river discharge and simulated water balances, GRDC Report 22, Koblenz, Germany.

Gandolfi, C., and K. A. Salewicz (1991), Water resources management in the Zambezi valley. Analysis of the Kariba operation, Proc. of Hydrology for the Water Management of Largs River Basins - Vienna Symposium, IAHS publication 201, August 1991, 13-24.

Gandolfi, C., G. Guariso, and D. Togni (1997), Optimal flow allocation in the Zambezi River system, *Water Resources Management*, *11*(5), 377-393.

Garcia Hernandez, J., J. Dubois, and J.-L. Boillat (2007), Routing System II - Flow modelling in hydraulic system, Prof Dr A. Schleiss (ed), Communication du Laboratoire des Constructions Hydrauliques n°32, Lausanne, Switzerland.

Gassman, P. W., M. R. Reyes, C. H. Green, and J. G. Arnold (2007), The soil and water assessment tool: Historical development, applications, and future research directions, *Transactions of the ASABE*, *50*(4), 1211-1250.

Gerrits, A. M. J. (2005), Hydrological modelling of the Zambezi catchment for gravity measurements, Master thesis, Techinical University Delft, Delft, The Nederlands.

Giannini, A., M. Biasutti, I. M. Held, and A. H. Sobel (2008), A global perspective on African climate, *Climatic Change*, *90*(4), 359-383.

Gieske, A. (1997), Modelling outflow from the Jao/Boro river system in the Okavango Delta, Botswana, *Journal of Hydrology*, *193*(1-4), 214-239.

Gosling, S. N., R. G. Taylor, N. W. Arnell, and M. C. Todd (2011), A comparative analysis of projected impacts of climate change on river runoff from global and catchment-scale hydrological models, *Hydrology and Earth System Sciences*, *15*(1), 279-294.

Green, W. H., and G. A. Ampt (1911), Studies on soil physics, *J. Agric. Sci.*, *4*(1), 1-24.

Gupta, H. V., S. Sorooshian, and P. O. Yapo (1998), Toward improved calibration of hydrologic models: Multiple and noncommensurable measures of information, *Water Resources Research*, *34*(4), 751-763.

Haario, H., E. Saksman, and J. Tamminen (2001), An adaptive Metropolis algorithm, *Bernoulli*, *7*(2), 223-242.

Haensler, A., S. Hagemann, and D. Jacob (2011), The role of the simulation setup in a long-term high-resolution climate change projection for the southern African region, *Theoretical and Applied Climatology*, *106*(1-2), 153-169.

Harbaugh, A. W. (2005), MODFLOW-2005, the U.S. Geological Survey modular ground-water model: The ground-water flow process. U.S, *Geological Survey Techniques and Methods*, 6-A16.

Hargreaves, G. H., and Z. A. Samani (1985), Reference crop evapotranspiration from temperature, *Applied Engineering in Agriculture*, *1*(2), 96-99.

Harrison, D., J. Opperman, and B. Richter (2007), Can hydropower be sustainable?, *International Water Power and Dam Construction*, *59*(10), 22-25.

Harrison, G. P., and H. W. Whittington (2002), Susceptibility of the Batoka Gorge hydroelectric scheme to climate change, *Journal of Hydrology*, *264*(1-4), 230-241.

Hattermann, F. F., V. Krysanova, A. Habeck, and A. Bronstert (2006), Integrating wetlands and riparian zones in river basin modelling, *Ecological Modelling*, *199*(4), 379-392.

Herman, A., V. B. Kumar, P. A. Arkin, and J. V. Kousky (1997), Objectively determined 10-day African rainfall estimates created for famine early warning systems, *International Journal of Remote Sensing*, *18*(10), 2147-2159.

Homa, E. S., R. M. Vogel, M. P. Smith, C. D. Apse, A. Huber-Lee, and J. Sieber (2005), An optimization approach for balancing human and ecological flow needs, Proc. of World Water and Environmental Resources Congress 2005: Impacts of Global Climate Change, AK, United States, 15-19 May 2005, 76.

Huffman, G. J., R. F. Adler, D. T. Bolvin, G. Gu, E. J. Nelkin, K. P. Bowman, Y. Hong, E. F. Stocker, and D. B. Wolff (2007), The TRMM Multisatellite Precipitation Analysis (TMPA): Quasi-global, multiyear, combined-sensor precipitation estimates at fine scales, *Journal of Hydrometeorology*, *8*(1), 38-55.

International Commission On Large Dams (2007), Dams and the world's water, ICOLD, Paris, France.

International Commission On Large Dams (2012), World declaration. Water storage for sustainable development.

IPCC (2001), *Climate Change 2001 - Impacts, adaptation and vulnerability, Contribution of Working Group II to the Third Assessment Report of the Intergovernmental Panel on Climate Change*, James J. McCarthy, Osvaldo F. Canziani, Neil A. Leary, David J. Dokken, Kasey S. White ed., Cambridge University Press, United Kingdom and New York, NY, USA.

IPCC (2007), *Climate Change 2007: The Physical Science Basis. Contribution of Working Group I to the Fourth Assessment Report of the Intergovernmental Panel on Climate Change,*, Solomon, S., D. Qin, M. Manning, Z. Chen, M. Marquis, K.B. Averyt, M. Tignor and H.L. Miller ed., Cambridge University Press, United Kingdom and New York, NY, USA.

Jobard, I., F. Chopin, J. C. Berges, and R. Roca (2011), An intercomparison of 10-day satellite precipitation products during West African monsoon, *International Journal of Remote Sensing*, *32*(9), 2353 - 2376.

Joyce, R. J., J. E. Janowiak, P. A. Arkin, and P. Xie (2004), CMORPH: A method that produces global precipitation estimates from passive microwave and infrared data at high spatial and temporal resolution, *Journal of Hydrometeorology*, *5*(3), 487-503.

Junk, W. J., and R. L. Welcomme (1990), *Floodplains*, 491-524, SPB Academic Publishing, The Hague, The Nederlands.

Jury, M. R. (2003), The coherent variability of African river flows: Composite climate structure and the Atlantic circulation, *Water SA*, *29*(1), 1-10.

Jury, M. R. (2013), Climate trends in southern Africa, *South African Journal of Science*, *109*(1-2), 1-11.

Kanamitsu, M., W. Ebisuzaki, J. Woollen, S.-K. Yang, J. J. Hnilo, M. Fiorino, and G. L. Potter (2002), NCEP–DOE AMIP-II Reanalysis (R-2), *Bulletin of the American Meteorological Society*, *83*(11), 1631-1643.

Karlsson, J. M., and W. Arnberg (2011), Quality analysis of SRTM and HYDRO1K: A case study of flood inundation in mozambique, *International Journal of Remote Sensing*, *32*(1), 267-285.

Kennedy, J., and R. Eberhart (1995), Particle swarm optimization, Proc. of IEEE International Conference on Neural Networks, Perth, Australia, 27 November - 1 December 1995, 1942-1948.

Khan, S. I., Y. Hong, J. Wang, K. K. Yilmaz, J. J. Gourley, R. F. Adler, G. R. Brakenridge, F. Policelli, S. Habib, and D. Irwin (2011), Satellite remote sensing and hydrologic modeling for flood inundation mapping in lake victoria basin: Implications for hydrologic prediction in ungauged basins, *IEEE Transactions on Geoscience and Remote Sensing*, *49*(1), 85-95.

Kidd, C. (2001), Satellite rainfall climatology: A review, *International Journal of Climatology*, *21*(9), 1041-1066.

Kummerow, C., W. Barnes, T. Kozu, J. Shiue, and J. Simpson (1998), The Tropical Rainfall Measuring Mission (TRMM) Sensor Package, *Journal of Atmospheric and Oceanic Technology*, *15*(3), 809-817.

Kunz, M. J., A. Wüest, B. Wehrli, J. Landert, and D. B. Senn (2011a), Impact of a large tropical reservoir on riverine transport of sediment, carbon, and nutrients to downstream wetlands, *Water Resources Research*, *47*(12), art. no. W12531.

Kunz, M. J., F. S. Anselmetti, A. West, B. Wehrli, A. Vollenweider, S. Thüring, and D. B. Senn (2011b), Sediment accumulation and carbon, nitrogen, and phosphorus deposition in the large tropical reservoir Lake Kariba (Zambia/Zimbabwe), *Journal of Geophysical Research G: Biogeosciences*, *116*(3), art. no. G03003.

Landert, J. (2008), Modeling biogeochemistry using the Soil and Water Assessment Tool in the Zambezi Ruver Basin, Master thesis, ETH, Zurich, Switzerland.

Layberry, R., D. R. Kniveton, M. C. Todd, C. Kidd, and T. J. Bellerby (2006), Daily precipitation over Southern Africa: A new resource for climate studies, *Journal of Hydrometeorology*, *7*(1), 149-159.

Liu, Y., W. Yang, and X. Wang (2008), Development of a SWAT extension module to simulate riparian wetland hydrologic processes at a watershed scale, *Hydrological Processes*, *22*(16), 2901-2915.

Loucks, D. P., E. van Beek, J. R. with contributions from Stedinger, J. P. M. Dijkman, and M. T. Villars (2005), *Water Resources Systems Planning and Management An Introduction to Methods, Models and Applications*, UNESCO, Paris.

Madsen, H. (2000), Automatic calibration of a conceptual rainfall-runoff model using multiple objectives, *Journal of Hydrology*, *235*(3-4), 276-288.

Magadza, C. H. D. (2010), Environmental state of Lake Kariba and Zambezi River Valley: Lessons learned and not learned, *Lakes and Reservoirs: Research and Management*, *15*(3), 167-192.

Mango, L. M., A. M. Melesse, M. E. McClain, D. Gann, and S. G. Setegn (2011), Land use and climate change impacts on the hydrology of the upper Mara River Basin, Kenya: Results of a modeling study to support better resource management, *Hydrology and Earth System Sciences*, *15*(7), 2245-2258.

Mason, P. J. (2013), The variability of floods and hydropower yield in Africa, Proc. of Water storage and hydropower development in Africa, Addis Ababa, Ethiopia, 16-18 April 2013.

Matondo, J. I., and P. Mortensen (1998a), Water Resource Assessment for the Zambezi River Basin, *Water International*, *23*(4), 256 - 262.

Matondo, J. I., and P. Mortensen (1998b), Water Resource Assessment for the Zambezi River Basin, *Water International*, *23*(4), 256-262.

Matos, J. P., T. Cohen, J. L. Boillat, A. J. Schleiss, and M. M. Portela (2010), Analysis of flow regime changes due to operation of large reservoirs on the Zambezi River, Proc. of 6th International Symposium on Environmental Hydraulics, Christodoulou & Stamou (eds), Taylor and Francis Group, London, Athens, Greece, 23-25 June 2010, 337-342.

Mazvimavi, D., and P. Wolski (2006), Long-term variations of annual flows of the Okavango and Zambezi Rivers, *Physics and Chemistry of the Earth*, *31*(15-16), 944-951.

McCartney, M. P., and H. A. Houghton-Carr (1998), A modelling approach to assess inter-sectoral competition for water resources in the Kafue Flats, Zambia, *Journal of the Chartered Institution of Water and Environmental Management*, *12*(2), 101-106.

McCartney, M. P., J. J. Kashaigili, B. A. Lankford, and H. F. Mahoo (2008), Hydrological modelling to assist water management in the Usangu wetlands, Tanzania, *International Journal of River Basin Management*, *6*(1), 51-61.

McMillan, H., T. Krueger, and J. Freer (2012), Benchmarking observational uncertainties for hydrology: Rainfall, river discharge and water quality, *Hydrological Processes*, *26*(26), 4078-4111.

Meier, P., A. Frömelt, and W. Kinzelbach (2011), Hydrological real-time modelling in the Zambezi River Basin using satellite-based soil moisture and rainfall data, *Hydrology and Earth System Sciences*, *15*(3), 999-1008.

Meile, T., J. L. Boillat, and A. J. Schleiss (2011), Hydropeaking indicators for characterization of the Upper-Rhone River in Switzerland, *Aquatic Sciences*, *73*(1), 171-182.

Mertens, J., B. Wehrli, A. Tilmant, A. J. Schleiss, T. Cohen Liechti, and J. P. Matos (2013), Adapted reservoir management in the Zambezi river basin to meet environmental needs, *International Journal on Hydropower and Dams*, *20*(2), 80-84.

Mhlanga, S. Z., and B. Goguel (2007), Inspection in the dry of the Kariba arch dam toe, *International Journal on Hydropower and Dams*, *14*(6), 79-82.

Michailovsky, C. I. (2008), Comparing GRACE water storage observations and regional-scale hydrological models for Southern Africa, Master thesis, Technical University of Denmark, Lyngby, Denmark.

Michailovsky, C. I., S. McEnnis, P. A. M. Berry, R. Smith, and P. Bauer-Gottwein (2012), River monitoring from satellite radar altimetry in the Zambezi River Basin, *Hydrol. Earth Syst. Sci. Discuss.*, *9*, 3203-3235.

Milzow, C., L. Kgotlhang, P. Bauer-Gottwein, P. Meier, and W. Kinzelbach (2009), Regional review: The hydrology of the Okavango Delta, Botswana - Processes, data and modelling, *Hydrogeology Journal*, *17*(6), 1297-1328.

Minihane, M. R. (2012), Evaluation of streamflow estimates for the Rovuma River, *Physics and Chemistry of the Earth*, *50-52*, 14-23.

Mitsch, W. J., and J. G. Gosselink (2007), *Wetlands (4th ed.)*, John Wiley, Hoboken, New Jersey, USA.

Monteith, J. L. (1965), Evaporation and environment, *Symposia of the Society for Experimental Biology*, *19*, 205-234.

Moore, A. E., F. P. D. Cotterill, M. P. L. Main, and H. B. Williams (2007), The Zambezi River, in *Large rivers: Geomorphology and management*, Gupta A (ed), pp. 311-332, Wiley, New York, USA.

Muleta, M. K., and J. W. Nicklow (2005), Sensitivity and uncertainty analysis coupled with automatic calibration for a distributed watershed model, *Journal of Hydrology*, *306*(1-4), 127-145.

Munchak, S. J., and G. Skofronick-Jackson (2013), Evaluation of precipitation detection over various surfaces from passive microwave imagers and sounders, *Atmospheric Research*, *131*, 81-94.

Ndomba, P. M., and A. Van Griensven (2011), Suitability of swat model in sediment yields modeling, in *The Eastern Africa Chapter 13: Advances in Data Methods Models and Their Applications in Geosciences*, Dongmei Chen INTECH Open Access Publisher.

Neal, J., G. Schumann, and P. Bates (2012), A subgrid channel model for simulating river hydraulics and floodplain inundation over large and data sparse areas, *Water Resources Research*, *48*(11), art. no. W11506

Neitsch, S. L., J. G. Arnold, J. R. Kiniry, and J. R. Williams (2009), Soil and Water Assessment Tool Theoretical documentation (Version 2009), Temple, Texas.

Neitsch, S. L., J. G. Arnold, J. R. Kiniry, J. R. Williams, and K. W. King (2005), Soil and Water Assessment Tool: Theoretical Documentation (Version 2005), Temple, Texas.

Nicholson, S. E., et al. (2003), Validation of TRMM and other rainfall estimates with a high-density gauge dataset for West Africa. Part II: Validation of TRMM rainfall products, *Journal of Applied Meteorology*, *42*(10), 1355-1368.

Notter, B., H. Hurni, U. Wiesmann, and K. C. Abbaspour (2012), Modelling water provision as an ecosystem service in a large East African river basin, *Hydrology and Earth System Sciences*, *16*(1), 69-86.

Obrdlik, P., A. Mumeka, and J. M. Kasonde (1989), Regulated rivers in Zambia—The case study of the Kafue river, *Regulated Rivers: Research & Management*, *3*(1), 371-380.

Paiva, R. C. D., W. Collischonn, and C. E. M. Tucci (2011), Large scale hydrologic and hydrodynamic modeling using limited data and a GIS based approach, *Journal of Hydrology*, *406*(3-4), 170-181.

Paiva, R. C. D., W. Collischonn, and D. C. Buarque (2013), Validation of a full hydrodynamic model for large-scale hydrologic modelling in the Amazon, *Hydrological Processes*, *27*(3), 333-346.

Pedinotti, V., A. Boone, B. Decharme, J. F. Crétaux, N. Mognard, G. Panthou, F. Papa, and B. A. Tanimoun (2012), Evaluation of the ISBA-TRIP continental hydrologic system over the Niger basin using in situ and satellite derived datasets, *Hydrology and Earth System Sciences*, *16*(6), 1745-1773.

Perona, P., D. J. Dürrenmatt, and G. W. Characklis (2013), Obtaining natural-like flow releases in diverted river reaches from simple riparian benefit economic models, *Journal of Environmental Management*, *118*, 161-169.

Perrin, M. (2013), Integrated water ressources management on the Zambezi River Basin, Master Thesis, EPFL, Lausanne, Switzerland.

Person, E., M. Bieri, A. Peter, and A. J. Schleiss (2013), Mitigation measures for fish habitat improvement in Alpine rivers affected by hydropower operations, *Ecohydrology*, *Article in press*.

Pilgrim, D. H., T. G. Chapman, and D. G. Doran (1988), Problems of rainfall-runoff modelling in arid and semiarid regions, *Hydrological Sciences Journal/Journal des Sciences Hydrologiques*, *33*(4), 379-400.

Prakash, S., and R. M. Gairola (2013), Validation of TRMM-3B42 precipitation product over the tropical Indian Ocean using rain gauge data from the RAMA buoy array, *Theoretical and Applied Climatology*, *Article in press*, 1-10.

Priestley, C. H. B., and R. J. Taylor (1972), On the assessment of surface heat flux and evaporation using large-scale parameters, *Monthly Weather Review*, *100*(2), 81-92.

Rajurkar, M. P., U. C. Kothyari, and U. C. Chaube (2004), Modeling of the daily rainfall-runoff relationship with artificial neural network, *Journal of Hydrology*, *285*(1-4), 96-113.

Refsgaard, J. C., and B. Storm (1996), Construction, calibration and validation of hydrological models, *Distributed Hydrological Modelling*, *22*, 41-54.

Reusser, D. E., and E. Zehe (2011), Inferring model structural deficits by analyzing temporal dynamics of model performance and parameter sensitivity, *Water Resources Research*, *47*(7), art. no. W07550.

Reynolds, C. A., T. J. Jackson, and R. W.J. (2000), Estimating soil water-holding capacities by linking the Food and Agriculture Organization Soil map of the world with global pedon databases and continuous pedotransfer functions, *Water Resources Research*, *36* (12), 3653-3662

Richter, B. D., and G. A. Thomas (2007), Restoring environmental flows by modifying dam operations, *Ecology and Society*, *12*(1), art. no. 12

Richter, B. D., J. V. Baumgartner, R. Wigington, and D. P. Braun (1997), How much water does a river need?, *Freshwater Biology*, *37*(1), 231-249.

Richter, B. D., J. V. Baumgartner, D. P. Braun, and J. Powell (1998), A spatial assessment of hydrologic alteration within a river network, *River Research and Applications*, *14*(4), 329-340.

Romilly, T. G., and M. Gebremichael (2010), Evaluation of satellite rainfall estimates over Ethiopian river basins, *Hydrology and Earth System Sciences Discussions*, *7*(5), 7669-7694.

Schneider, U., T. Fuchs, A. Meyer-Christoffer, and B. Rudolf (2008), Global precipitation analysis products of the GPCC, Global Precipitation Climatology Centre, Germany.

Schuol, J., and K. C. Abbaspour (2006), Calibration and uncertainty issues of a hydrological model (SWAT) applied to West Africa, *Advances in Geosciences*, *9*, 137-143.

Schuol, J., K. C. Abbaspour, R. Srinivasan, and H. Yang (2008a), Estimation of freshwater availability in the West African sub-continent using the SWAT hydrologic model, *Journal of Hydrology*, *352*(1-2), 30-49.

Schuol, J., K. C. Abbaspour, H. Yang, R. Srinivasan, and A. J. B. Zehnder (2008b), Modeling blue and green water availability in Africa, *Water Resources Research*, *44*(7), art. no. W07406.

Scinocca, J. F., N. A. McFarlane, M. Lazare, J. Li, and D. Plummer (2008), Technical note: The CCCma third generation AGCM and its extension into the middle atmosphere, *Atmospheric Chemistry and Physics*, *8*(23), 7055-7074.

Shamseldin, A. Y. (1997), Application of a neural network technique to rainfall-runoff modelling, *Journal of Hydrology*, *199*(3-4), 272-294.

Shongwe, M. E., G. J. Van Oldenborgh, B. J. J. M. Van Den Hurk, B. De Boer, C. A. S. Coelho, and M. K. Van Aalst (2009), Projected changes in mean and extreme precipitation in Africa under global warming. Part I: Southern Africa, *Journal of Climate*, *22*(13), 3819-3837.

Sieck, L. C., S. J. Burges, and M. Steiner (2007), Challenges in obtaining reliable measurements of point rainfall, *Water Resources Research*, *43*(1), art. no. W01420.

Soils Incorporated (Pty) Ltd and Chalo Environmental and Sustainable Development Consultants (2000), Kariba Dam Case Study, prepared as an input for the World Commission on Dams, Cape Town, South Africa.

Stanski, H. R., L. J. Wilson, and W. R. Burrows (1989), *Survey of Common Verification Methods in Meteorology*, WMO/TD No. 358, Geneva, Switzerland.

Storn, R., and K. Price (1997), Differential Evolution - A Simple and Efficient Heuristic for Global Optimization over Continuous Spaces, *Journal of Global Optimization*, *11*(4), 341-359.

Suen, J. P., and J. W. Eheart (2006), Reservoir management to balance ecosystem and human needs: Incorporating the paradigm of the ecological flow regime, *Water Resources Research*, *42*(3), art. no. W03417.

The World Bank (2010), *The Zambezi River Basin A Multi-Sector Investment Opportunities Analysis*, The World Bank, Washington, USA.

Tilmant, A., and W. Kinzelbach (2012), The cost of noncooperation in international river basins, *Water Resources Research*, *48*(1), art. no. W01503.

Tilmant, A., L. Beevers, and B. Muyunda (2010a), Restoring a flow regime through the coordinated operation of a multireservoir system: The case of the Zambezi River basin, *Water Resources Research*, *46*(7), art. no. W07533.

Tilmant, A., W. Kinzelbach, L. Beevers, and D. Juizo (2010b), Optimal water allocation in the Zambezi basin, Proc. of 5th Biennial Conference of the International Environmental Modelling and Software Society: Modelling for Environment's Sake, IEMSs 2010, International Environmental Modelling and Software Society, Ottawa, Canada, 5-8 July 2010, 2174-2183.

Tilmant, A., W. Kinzelbach, D. Juizo, L. Beevers, D. B. Senn, and C. Casarotto (2012), Economic valuation of benefits and costs associated with the coordinated development and management of the Zambezi river basin, *Water Policy*, *14*(3), 490–508.

Tockner, K., and J. A. Stanford (2002), Riverine flood plains: Present state and future trends, *Environmental Conservation*, *29*(3), 308-330.

Tshimanga, R. M., D. A. Hughes, and E. Kapangaziwiri (2011), Initial calibration of a semi-distributed rainfall runoff model for the Congo River basin, *Physics and Chemistry of the Earth*, *36*(14-15), 761-774.

Tyson, P. D., G. R. J. Cooper, and T. S. McCarthy (2002), Millennial to multi-decadal variability in the climate of southern Africa, *International Journal of Climatology*, *22*(9), 1105-1117.

Uhlendahl, T., P. Salian, C. Casarotto, and J. Doetsch (2011), Good water governance and IWRM in Zambia: Challenges and chances, *Water Policy*, *13*(6), 845-862.

United Nations Development Programme (2006), Human Development Report, Beyond scarcity: Power, poverty and the global water crisis, UNDP, New York; USA.

USDA Soil Conservation Service (1972), *SCS National Engineering Handbook Section 4: Hydrology,*, Washington DC, USA.

Van Griensven, A., P. Ndomba, S. Yalew, and F. Kilonzo (2012), Critical review of SWAT applications in the upper Nile basin countries, *Hydrology and Earth System Sciences*, *16*(9), 3371-3381.

van Griensven, A., T. Meixner, S. Grunwald, T. Bishop, M. Diluzio, and R. Srinivasan (2006), A global sensitivity analysis tool for the parameters of multi-variable catchment models, *Journal of Hydrology*, *324*(1-4), 10-23.

Vorosmarty, C. J., B. Moore Iii, A. Grace, B. J. Peterson, E. B. Rastetter, and J. Melillo (1991), Distributed parameter models to analyze the impact of human disturbance of the surface hydrology of a large tropical drainage basin in southern Africa, Proc. of 20th General Assembly of the International Union of Geodesy and Geophysics, IAHS Publication (International Association of Hydrological Sciences), Vienna, Austria, 11-24 August 1991, 233-244.

Vörösmarty, C. J., and B. Moore III (1991), Modeling basin-scale hydrology in support of physical climate and global biogeochemical studies: An example using the Zambezi River, *Surveys in Geophysics*, *12*(1-3), 271-311.

Vrugt, J. A., and B. A. Robinson (2007), Improved evolutionary optimization from genetically adaptive multimethod search, *Proceedings of the National Academy of Sciences of the United States of America*, *104*(3), 708-711.

Vrugt, J. A., B. A. Robinson, and J. M. Hyman (2009), Self-adaptive multimethod search for global optimization in real-parameter spaces, *IEEE Transactions on Evolutionary Computation*, *13*(2), 243-259.

Wagener, T., D. P. Boyle, M. J. Lees, H. S. Wheater, H. V. Gupta, and S. Sorooshian (2001), A framework for development and application of hydrological models, *Hydrology and Earth System Sciences*, *5*(1), 13-26.

Wamulume, J., J. Landert, R. Zurbrügg, I. Nyambe, B. Wehrli, and D. B. Senn (2011), Exploring the hydrology and biogeochemistry of the dam-impacted Kafue River and Kafue Flats (Zambia), *Physics and Chemistry of the Earth*, *36*(14-15), 775-788.

Wang, J., and D. B. Wolff (2010), Evaluation of TRMM ground-validation radar-rain errors using rain gauge measurements, *Journal of Applied Meteorology and Climatology*, *49*(2), 310-324.

Wang, J., et al. (2011), The coupled routing and excess storage (CREST) distributed hydrological model, *Le modèle hydrologique distribué couplé routage et stockage des excédents (CREST)*, *56*(1), 84-98.

Wheater, H., S. Sorooshian, and K. D. Sharma (2008), *Hydrological modelling in arid and semi-arid areas*, 195, Cambrige University Press, Cambridge.

Wilheit, T. T., A. T. C. Chang, M. S. V. Rao, E. B. Rogers, and J. S. Theon (1977), Satellite technique for quantitatively mapping rainfall rates over the oceans, *Journal of Applied Meteorology*, *16*(5), 551-560.

Wilk, J., D. Kniveton, L. Andersson, R. Layberry, M. C. Todd, D. Hughes, S. Ringrose, and C. Vanderpost (2006), Estimating rainfall and water balance over the Okavango River Basin for hydrological applications, *Journal of Hydrology*, *331*(1-2), 18-29.

Winchell, M., R. Srinivasan, M. Di Luzio, and J. G. Arnold (2007), Arc-SWAT interface for SWAT2005 - User's guide, Temple, Texas.

Winchell, M., R. Srinivasan, M. Di Luzio, and J. G. Arnold (2010), Arc-SWAT interface for SWAT2009 - User's guide, Temple, Texas, USA.

Winsemius, H. C., H. H. G. Savenije, and W. G. M. Bastiaanssen (2008), Constraining model parameters on remotely sensed evaporation: Justification for distribution in ungauged basins?, *Hydrology and Earth System Sciences*, *12*(6), 1403-1413.

Winsemius, H. C., B. Schaefli, A. Montanari, and H. H. G. Savenije (2009), On the calibration of hydrological models in ungauged basins: A framework for integrating hard and soft hydrological information, *Water Resources Research*, *45*(1), art. no. W12422.

Winsemius, H. C., H. H. G. Savenije, A. M. J. Gerrits, E. A. Zapreeva, and R. Klees (2006a), Comparison of two model approaches in the Zambezi River Basin with regard to model reliability and identifiability, *Hydrology and Earth System Sciences*, *10*(3), 339-352.

Winsemius, H. C., H. H. G. Savenije, N. C. Van De Giesen, B. J. J. M. Van Den Hurk, E. A. Zapreeva, and R. Klees (2006b), Assessment of Gravity Recovery and Climate Experiment (GRACE) temporal signature over the upper Zambezi, *Water Resources Research*, *42*(12), art. no. W12201.

Wolski, P., H. H. G. Savenije, M. Murray-Hudson, and T. Gumbricht (2006), Modelling of the flooding in the Okavango Delta, Botswana, using a hybrid reservoir-GIS model, *Journal of Hydrology*, *331*(1-2), 58-72.

World Commission on Dams (2000), Dams and Development: A New Framework for Decision-Making, Earthscan Publications, London, UK.

Yamba, F. D., H. Walimwipi, S. Jain, P. Zhou, B. Cuamba, and C. Mzezewa (2011), Climate change/variability implications on hydroelectricity generation in the Zambezi River Basin, *Mitigation and Adaptation Strategies for Global Change*, *16*(6), 617-628.

Yates, D. N. (1997), Approaches to continental scale runoff for integrated assessment models, *Journal of Hydrology*, *201*(1-4), 289-310.

Yin, X. A., Z. F. Yang, and G. E. Petts (2011), Reservoir operating rules to sustain environmental flows in regulated rivers, *Water Resources Research*, *47*(8), art. no. 7206.

Yin, X. A., Z. F. Yang, and G. E. Petts (2012), Optimizing environmental flows below dams, *River Research and Applications*, *28*(6), 703-716.

Yu, M., X. Chen, L. Li, A. Bao, and M. J. de la Paix (2011), Streamflow Simulation by SWAT Using Different Precipitation Sources in Large Arid Basins with Scarce Raingauges, *Water Resources Management*, *25*(11), 2669-2681.

Zhang, X., R. Srinivasan, and D. Bosch (2009), Calibration and uncertainty analysis of the SWAT model using Genetic Algorithms and Bayesian Model Averaging, *Journal of Hydrology*, *374*(3-4), 307-317.

Zhang, X., R. Srinivasan, and M. Van Liew (2010), On the use of multi-algorithm, genetically adaptive multi-objective method for multi-site calibration of the SWAT model, *Hydrological Processes*, *24*(8), 955-969.

Zhang, X., R. Srinivasan, J. Arnold, R. C. Izaurralde, and D. Bosch (2011), Simultaneous calibration of surface flow and baseflow simulations: A revisit of the SWAT model calibration framework, *Hydrological Processes*, *25*(14), 2313-2320.

Zurbrügg, R., S. Suter, M. F. Lehmann, B. Wehrli, and D. B. Senn (2013), Organic carbon and nitrogen export from a tropical dam-impacted floodplain system, *Biogeosciences*, *10*(1), 23-38.

Acknowledgements

Curriculum vitae

Theodora COHEN LIECHTI

Date of birth 12 December 1984   Nationality Swiss, Italian

Education

Since 2008	Research assistant and PhD student Ecole Polytechnique Fédérale de Lausanne (EPFL) Laboratory of Hydraulic Constructions (LCH)
2006-2008	Master of Science (MSc) in Environmental Sciences and Engineering Ecole Polytechnique Fédérale de Lausanne (EPFL) Minor: Engineering of water, soil and ecosystems
2003-2006	Bachelor of Science (BSc) in Environmental Sciences and Engineering Ecole Polytechnique Fédérale de Lausanne (EPFL) 2005-2006 3rd year bachelor effectuated in the Indian Institute of Technology Madras, India
1999-2003	Matura (General qualification for university entrance) Cantonal School, Geneva, Focus: Latin and ancient Greek

Languages

French:	native speaker
English:	very good knowledge
German:	medium knowledge
Italian:	basic knowledge

Selected applied research projects

2011 and 2009	Transport of domestic waste by ship convoys – Reduction of the waves (laboratory and in-situ study) Industrial Services of Geneva, Switzerland
2010	Small scale hydropower plant (Boudry, Neuchâtel) - Hydraulic behavior and sediment transport at river water intake Colenco AG, Switzerland

Teaching

Involved in several teaching activities: assistant for master projects as well as numerous semester projects and exercises for undergraduates at the School of Architecture, Civil and Environmental Engineering (ENAC) of EPFL.

Selected journal papers

Matos, J. P., T. Cohen Liechti, D. Juízo, M. M. Portela and A. J. Schleiss (2013), Can satellite based pattern-oriented memory improve the interpolation of sparse historical rainfall records? *Journal of Hydrology*, *492*, 102-116.

Mertens, J., B. Wehrli, A. Tilmant, A. J. Schleiss, T. Cohen Liechti, and J. P. Matos (2013), Adapted reservoir management in the Zambezi river basin to meet environmental needs, *International Journal on Hydropower and Dams*, *20*(2), 80-84

Cohen Liechti, T., J. P. Matos, J. L. Boillat, and A. J. Schleiss (2012), Comparison and evaluation of satellite derived precipitation products for hydrological modeling of the Zambezi River Basin, *Hydrology and Earth System Sciences*, *16*(2), 489-500.

Cohen Liechti T., J.-L. Boillat and A. J. Schleiss (2010), Discussion of Design optimization of floating breakwaters with an interdisciplinary fluid-solid structural problem, *Canadian Journal of Civil Engineering*, *12*(37), 1646-1650.

Selected conference publications

Matos, J. P., T. Cohen, J. L. Boillat, A. J. Schleiss, and M. M. Portela (2010), Analysis of flow regime changes due to operation of large reservoirs on the Zambezi River, *Proc. of 6th International Symposium on Environmental Hydraulics*, Christodoulou & Stamou (eds), Taylor and Francis Group, London, Athens, Greece, 23-25 June 2010, 337-342.

Cohen T., R. Amacher and J.-L. Boillat (2010), Synergie de modélisations physique et numérique pour le développement d'atténuateurs de vagues d'un convoi fluvial / Synergy between physical and numerical modeling used for the development of ship waves attenuator, *Proc. of SimHydro 2010: Hydraulic modeling and uncertainty*, Société Hydrotechnique de France, Nice, Sophia Antipolis, France, 2-4 June 2010.

Cohen T., J. García Hernández, J. Dubois and J.-L. Boillat (2009), Influence of hydrological model complexity on the estimation of floods in an alpine catchment for PMP conditions, *Proc. of 33rd IAHR Congress "Water Engineering for a Sustainable Environment"*, Vancouver, Canada, 9-14 August 2009, 1763-1770.

Professional Experiences

2007   Ecotec Environnement SA, Geneva (Internship of 4 weeks)

2007   CERA Ingénierie SàRL, Geneva (Internship of 4 weeks)

2006   Géotechnique Appliquée Deriaz SA (Internship of 6 weeks)

2004   Rolex SA (Internship of 4 weeks)